THERMOHYDRODYNAMIC ANALYSIS OF MISALIGNED JOURNAL BEARINGS

A THESIS

Submitted in fulfillment of the requirements
for the award of the degree
of

DOCTOR OF PHILOSOPHY

By :

SUKHWANT SINGH BANWAIT

DEPARTMENT OF MECHANICAL AND INDUSTRIAL ENGINEERING
THAPAR INSTITUTE OF ENGINEERING AND TECHNOLOGY
(DEEMED UNIVERSITY)
PATIALA - 147 001 (INDIA)
July, 1998

CERTIFICATE

Certified that the thesis entitled " **THERMOHYDRODYNAMIC ANALYSIS OF MISALIGNED JOURNAL BEARINGS** " which is being submitted by **Shri Sukhwant Singh Banwait** in fulfillment of the requirements for the award of the degree of **Doctor of Philosophy in Mechanical Engineering**, to Thapar Institute of Engineering and Technology (A Deemed University), PATIALA, INDIA is a record of candidate's own work carried out by him under our supervision and guidance. The matter embodied in this thesis has not been submitted in part or full to any other University or Institute for the award of any degree.

(Dr. H.N. CHANDRAWAT)
Supervisor
Professor,
Department of Mechanical & Industrial Engg.,
Thapar Institute of Engineering & Technology,
PATIALA - 147 001

(Dr. M. ADITHAN)
Co - Supervisor
Professor & Head,
Department of Mechanical Engg.,
Vellore Engineering College,
VELLORE - 632 006

Countersigned, 13/8/98
Dean, R & D

ACKNOWLEDGMENT

The present work will remain incomplete unless I express my feelings of gratitude towards a number of persons who delightfully co-operated with me in the process of this research work.

I am highly indebted to my supervisor, Dr. H.N. Chandrawat, Professor, Department of Mechanical & Industrial Engineering, Thapar Institute of Engineering & Technology, Patiala for his constant encouragement. He treated me more like a friend than a student. Inspite of his busy schedule and pressure of academic work, he always spared time for me, and his guidance, precious and genial, always kept me on the right track, in my research work.

Dr. M. Adithan, Ex-Professor & Head, Department of Mechanical Engineering, Technical Teachers' Training Institute, Chandigarh was a great source of inspiration for me. I also expressed my indebtedness towards him for providing the necessary facilities and guidance during the course of this research work.

Dr. S.C. Laroiya, Professor, Department of Mechanical Engineering, Technical Teachers' Training Institute, Chandigarh rendered necessary guidance and encouragement from time to time. I also express my indebtedness towards him.

Some of my subordinate staff and post-graduate students at Technical Teachers' Training Institute, Chandigarh helped me immensely in the preparation of the manuscripts of my thesis and extended all necessary assistance in making my assignment a complete success.

I am also thankful to the staff in the Department of Mechanical & Industrial Engineering, Thapar Institute of Engineering & Technology, Patiala for the general assistance provided during the course of my research work in CAD laboratory.

I was thrilled and motivated whenever my friends, well-wishers, seniors and colleagues inquired about the progress of my research work.

My special thanks to the Principal, Technical Teachers' Training Institute, Chandigarh for sponsoring me for the Ph.D programme at Thapar Institute of Engineering & Technology, Patiala.

Lastly but not the least, I acknowledges my indebtedness to my wife, Mrs. Harjit Kaur, daughter Ashreen Kaur, son Harshdeep Singh and my revered mother for their patience, constant cooperation and forbearance. I dedicate this work to my father who could not see the completion of this research work.

Place : Chandigarh
Date :

(S.S. BANWAIT)

ABSTRACT

Hydrodynamic journal bearings are used to support rotating shafts of machines such as compressors, turbogenerators, pumps, etc. under imposed operating conditions which comprises speed and load. These bearings are normally designed using data developed with the assumptions that they operate with isoviscous lubricants and are aligned. Oil viscosity is a strong function of oil temperature and varies throughout the film. This, in turn, influences the prediction of various bearing performance characteristics. The temperature of the lubricant is largely controlled by the speed of the journal. Since there is a tendency to design rotors to operate at high speeds for optimum performance, the assumption of constant temperature (and hence constant viscosity) appears to be doubtful. Further, due to manufacturing tolerances, deflection of journal and bearing support, asymmetric bearing load, etc., journal bearings may quite often operate at the misaligned condition. The geometry of clearance space between the journal and the bush influences the bearing performance significantly. The clearance geometry depends largely on the amount of misalignment present between the axes of bearing and journal. Therefore, for a more accurate prediction of bearing performance, it is essential to perform a complete thermohydrodynamic (THD) analysis of misaligned journal bearings. The present study has been planned with these forethoughts.

Although the theory of thermohydrodynamic (THD) lubrication developed quite significantly during the last few decades, it remained confined mainly to the problems of aligned journal bearings. The published literature on the THD investigations on misaligned journal bearings is scant. Even the isothermal literature on misaligned journal bearings is generally limited to the computation of static and dynamic performance characteristics of circular bearing geometries (i.e. plain and two-axial-groove) only. Therefore, there is a need to investigate the THD effects in misaligned circular and non-circular journal bearings with more realistic mathematical models and boundary conditions for the physical problems involved. This work is an attempt to bridge this gap present in the existing literature.

The work contained in this study is broadly divided into five parts. The first part deals with the validity of the results. In the second part, the static and dynamic performance

characteristics, isopressure curves, pressure profiles, isotherms and temperature profiles are studied for different bearing configurations viz. plain journal bearing, two-axial-groove journal bearing, elliptical journal bearing and three-lobe journal bearing respectively. The third part consist of the study of transient motion trajectories followed by the comparative study of vital parameters of journal bearings. The last part deals with the effect of operating parameters on static and dynamic characteristics.

The generalised Reynolds equation is used to represent the flow of lubricant in the clearance space of journal bearings. The clearance space geometry between bearing pads/lobes and journal is expressed by including the effect of bi-planar misalignment. In the thermal (THD) analysis, the temperature distributions in the fluid-flow field and the bush-housing assembly are computed using the three-dimensional energy and Fourier heat conduction equation, respectively. A one-dimensional heat conduction equation for journal has been solved. Viscosity of the lubricant has been expressed as function of temperature using conventional exponential form. Heat transfer between bush/journal and oil in supply grooves is considered.

Finite element method is employed for solving the Reynolds equation and finite difference method with Successive Over Relaxation is employed for solving the energy and heat conduction equations. The computational procedure used to obtain the performance characteristics is an iterative one. In the global iteration scheme, the viscosity of oil is computed using the previous iteration temperatures. The Reynolds equation is then solved to obtain the converged pressure field. The temperature field for the lubricant, bush-housing and journal is then established for the computed film pressures which, in turn, gives the modified values for lubricant viscosity for the solution of Reynolds equation in the next iteration. Suitable weighting factors have been used to improve the rates of convergence of various iteration loops.

The performance characteristics of misaligned journal bearings are reported as functions of load. These characteristics include eccentricity ratio, attitude angle, maximum fluid-film pressure, minimum fluid-film thickness, side flow, mean journal temperature, maximum bush temperature, sixteen stiffness coefficients, sixteen damping coefficients, threshold speed and whirl frequency ratio. The results for aligned and misaligned journal

bearings are given for three different values of bi-planar misalignment ratios. To examine the combined effects of misalignment and THD, isopressure curves and pressure profiles are plotted for the aligned and misaligned journal bearings. Also, the isotherms and temperature profiles are plotted for oil and bush at different locations for all bearing configurations operating with misalignment.

The analysis reveals that performance characteristics are highly influenced by the inclusion of thermal effects. The THD results for the performance characteristics of misaligned journal bearings show that these characteristics are significantly altered by misalignment, particularly, when the load is heavy and/or misalignment is large. These studies indicate appreciable reduction in the bearing load capacity by the misalignment. The minimum fluid-film thickness is reduced drastically when the bearings operate with misalignment. The effect of misalignment is to make the distribution of bearing pressure asymmetric and at the same time, it changes the maximum bearing pressure values. At higher load values, misalignment reduces the side flow. The misalignment significantly improves the stability margin of all journal bearing systems.

The journal temperature and maximum bush temperature, each, increases with the increase in misalignment. For a misaligned bearing, the journal temperature varies significantly along the axial length of the journal. Hence, the journal cannot be assumed as a lumped thermal element in the analysis of misaligned bearings. The bush-fluid interface temperature at all load values increases with the misalignment in all the journal bearings studied. There is considerable variation in bush-fluid interface temperature along the circumferential and axial direction. This variation further increases with the increase in the value of load. The isotherms indicate that the heat flows into the journal from the hot regions of oil and out of the journal in the cold regions of the oil. They also show that due to misalignment, the maximum temperature region does not remain in the central plane but shifts away from the central plane. The maximum bush temperature occurs in the vicinity of hottest region of oil-film. In the high temperature region of the bush, most of the heat transfers directly out of the bush outer surface to the surroundings. It is also observed that heat transfer takes place not only in radial direction in the bush but also in the circumferential and axial directions. Hence, a two-dimensional thermal analysis is not

sufficient for the study of misaligned journal bearings and a complete three-dimensional analysis is desired.

The study of transient motion trajectories of journal-centre show that all bearings are relatively more stable when operating under misaligned condition and the relative stability is even better when the operating load is higher.

****

CONTENTS

		PAGES
CERTIFICATE		i
ACKNOWLEDGMENT		ii
ABSTRACT		iii
CONTENTS		vii
NOMENCLATURE		xi
LIST OF FIGURES		xvii
LIST OF TABLES		xxiv
CHAPTER I :	INTRODUCTION	1
CHAPTER II :	LITERATURE REVIEW	3
	2.1 EARLY WORKS	3
	2.2 ISOTHERMAL ANALYSIS	3
	2.2.1 Aligned Journal Bearings	4
	2.2.2 Misaligned Journal Bearings	5
	2.3 THERMOHYDRODYNAMIC STUDIES	8
	2.3.1 Aligned Journal Bearings	8
	2.3.2 Misaligned Journal Bearings	15
	2.4 PRESENT WORK	16
	2.5 ORGANISATION OF THESIS	19
CHAPTER III :	MATHEMATICAL MODELLING AND ANALYSIS	20
	3.1 INTRODUCTION	20
	3.2 HYDRODYNAMIC ANALYSIS	21
	3.2.1 Generalized Reynolds Equation	21
	3.2.2 Fluid-Film Thickness	21

3.2.3 Viscosity-Temperature Relation 22
3.2.4 Boundary Conditions for Reynolds Equation 22
3.2.5 Finite Element Formulation of Reynolds Equation 22
3.3 THERMAL ANALYSIS 23
3.3.1 Energy Equation 23
3.3.1.1 Boundary Conditions for the Energy Equation 25
3.3.1.2 Finite Difference Formulation of Energy Equation 26
3.3.2 Heat Conduction Equation for Bush 27
3.3.2.1 Boundary Conditions for Heat Conduction Equation 27
3.3.2.2 Finite Difference Formulation 29
3.3.3 Heat Conduction Equation for Journal 30
3.3.3.1 Boundary Conditions for Heat Conduction Equation for Journal 30
3.3.3.2 Finite Difference Formulation 30
3.3.4 Mixing in the Oil Groove 31
3.4 PERFORMANCE CHARACTERISTICS 32
3.4.1 Static Performance Characteristics 32
3.4.2 Dynamic Performance Characteristics 33
3.5 STABILITY ANALYSIS 34
3.5.1 Linearised Equation of Motion and Stability Margin 34
3.5.2 Journal Centre-Motion Trajectory 36

CHAPTER IV: SOLUTION PROCEDURE 38
4.1 INTRODUCTION 38
4.2 SOLUTION SCHEME FOR MAIN PROGRAM 38
4.3 SOLUTION SCHEME FOR SUBROUTINE TEMP 41

4.4 SOLUTION SCHEME FOR LINEAR TRAJECTORIES 44

CHAPTER V: RESULTS AND DISCUSSION 46

5.1 INTRODUCTION 46

5.2 VALIDITY OF RESULTS 46

5.2.1 Validity of IHD Results 47

5.2.2 Validity of THD Results 47

5.2.2.1 Selection of Thermal Boundary Conditions 53

5.2.2.2 Plain Journal Bearing 53

5.2.2.3 Two-Axial-Groove Journal Bearing 58

5.2.2.4 Plain Misaligned Journal Bearing 62

5.2.3 Concluding Remarks on Validation 62

5.3 STEADY STATE THD ANALYSIS OF MISALIGNED JOURNAL BEARINGS 62

5.3.1 Static Performance Characteristics 66

5.3.1.1 Eccentricity Ratio 66

5.3.1.2 Attitude Angle 66

5.3.1.3 Maximum Fluid-Film Pressure 71

5.3.1.4 Minimum Fluid-Film Thickness 71

5.3.1.5 Side Flow 71

5.3.1.6 Mean Journal Temperature and Maximum Bush Temperature 71

5.3.2 Stiffness Coefficients 76

5.3.3 Damping Coefficients 89

5.3.4 Stability Parameters 102

5.3.5 Isopressure Curves and Pressure Profiles 107

5.3.6 Isotherms and Temperature Profiles 119

5.4 TRANSIENT MOTION TRAJECTORIES 138

5.5 COMPARATIVE STUDY OF SOME VITAL PARAMETERS OF JOURNAL BEARINGS 149
5.5.1 Minimum Fluid-Film Thickness 149
5.5.2 Stability Parameters 149
5.5.3 Bush and Journal Temperatures 152
5.6 EFFECT OF OPERATING PARAMETERS ON STATIC AND DYNAMIC CHARACTERISTICS 152
5.6.1 Static Performance Characteristics 152
5.6.1.1 Effect of Radial Clearance 152
5.6.1.2 Effect of Journal Speed 156
5.6.2 Dynamic Performance Characteristics 158
5.6.2.1 Stability Parameters 158
5.6.3 Thermal Analysis 158

CHAPTER VI: CONCLUSIONS AND CLOSURE 161
REFERENCES 164
APPENDIX - I 173

NOMENCLATURE

Note : A symbol with bar indicates a dimensionless quantity.

a	viscosity coefficient
A_1, A_2, A_3	coefficients of the heat conduction equation for journal (equ. (3.29))
$\bar{A}^e$	area of eth element of discretised flow domain
b	viscosity coefficient
B_{xx} B_{xz} B_{zx} B_{zz}	damping coefficients associated with force and displacement, (N s / m)
$\bar{B}_{xx}$ $\bar{B}_{xz}$ $\bar{B}_{zx}$ $\bar{B}_{zz}$	$(B_{xx}, B_{xz}, B_{zx}, B_{zz}) / (\mu_o R^4 / c^3)$
$B_{x\gamma_x}$ $B_{x\gamma_z}$ $B_{z\gamma_x}$ $B_{z\gamma_z}$	damping coefficients associated with force and rotation, (N s / rad)
$\bar{B}_{x\gamma_x}$ $\bar{B}_{x\gamma_z}$ $\bar{B}_{z\gamma_x}$ $\bar{B}_{z\gamma_z}$	$(B_{x\gamma_x}, B_{x\gamma_z}, B_{z\gamma_x}, B_{z\gamma_z}) / (\mu_o R^5 / c^3)$
$B_{\gamma_x\gamma_x}$, $B_{\gamma_x\gamma_z}$ $B_{\gamma_z\gamma_x}$, $B_{\gamma_z\gamma_z}$	damping coefficients associated with moment and rotation,(N-m s/ rad)
$\bar{B}_{\gamma_x\gamma_x}$, $\bar{B}_{\gamma_x\gamma_z}$ $\bar{B}_{\gamma_z\gamma_x}$, $\bar{B}_{\gamma_z\gamma_z}$	$(B_{\gamma_x\gamma_x}, B_{\gamma_x\gamma_z}, B_{\gamma_z\gamma_x}, B_{\gamma_z\gamma_z}) / (\mu_o R^6 / c^3)$
$B_{\gamma_x x}$, $B_{\gamma_x z}$ $B_{\gamma_z x}$, $B_{\gamma_z z}$	damping coefficients associated with moment and displacement, (N s)
$\bar{B}_{\gamma_x x}$, $\bar{B}_{\gamma_x z}$ $\bar{B}_{\gamma_z x}$, $\bar{B}_{\gamma_z z}$	$(B_{\gamma_x x}, B_{\gamma_x z}, B_{\gamma_z x}, B_{\gamma_z z}) / (\mu_o R^5 / c^3)$
c	radial clearance, (m)
$\bar{c}$	c / R
C_L	contraction coefficient (equ. (3.15))
C_{pair}, C_p	specific heat of air and lubricant respectively, (N.m / Kg °C)

$C_1, C_2, C_3, C_4, C_5, C_6$	coefficients of the heat conduction equation for bush-housing (equ.(3.25))
D	journal diameter, (m)
$\bar{D}_e$	non-dimensional Dissipation number, = $\mu \omega_j / (C_p \rho T_r c^2)$
e	eccentricity in aligned bearings, (m)
e_0	midplane eccentricity in misaligned bearings, (m)
ν	whirl frequency, (rad / s)
$\bar{\nu}$	whirl frequency ratio = ν / ω_j
g	acceleration due to gravity, (m/ s^2)
h	fluid-film thickness, (m)
$\bar{h}$	h / c
$\bar{h}_{min}$	minimum fluid-film thickness
h_{ab}, h_{aj}	convective heat transfer coefficient of bush-housing and journal respectively, (W / m^2 °C)
h_{fb}	convective heat transfer coefficient of bush-housing (for solid to fluid), (W / m^2 °C)
K_1, K_2, K_3, K_4, K_5	coefficients of the energy equation (equ.(3.22))
k_a, k_f, k_b, k_j	thermal conductivity of air, lubricant, bush-housing and journal respectively, (W / m °C)
L	length of the bearing, (m)
M_c	critical mass of the journal, (Kg)
$\bar{M}_c$	$M_c / (\mu_o R^4 / (\omega_j c^3))$
M, M_x, M_z	total fluid-film moment and components in x-axis and z-axis respectively, (N-m)
$\bar{M}, \bar{M}_x, \bar{M}_z$	$(M, M_x, M_z) / (\mu_o \omega_j R^5 / c^2)$

N_i	shape function for ith node of a paralinear element in discretized fluid domain
p	fluid-film pressure, (Pa)
$\bar{p}$	$p / (\omega_j \mu_o R^2 / c^2)$
$\bar{p}_{max}$	maximum fluid-film pressure
$\bar{P}_e$	non-dimensional inverse Peclet Number = $k_f / (C_p \rho \omega_j c^2)$
Q_s	side flow, (m^3/s)
$\bar{Q}_s$	$Q_s / (\omega_j c R^4)$
R	journal radius, (m)
r	radial coordinate of the bearing,
$\bar{r}$	r / R
R_1, R_2	inner and outer radii of the bush-housing, (m)
$\bar{R}_1, \bar{R}_2$	$R_1, R_2 / R$
S_{xx}, S_{xz} S_{zx}, S_{zz}	stiffness coefficients associated with force and displacement, (N / m)
$\bar{S}_{xx}, \bar{S}_{xz}$ $\bar{S}_{zx}, \bar{S}_{zz}$	$(S_{xx}, S_{xz}, S_{zx}, S_{zz}) / (\mu_o \omega_j R^4 / c^3)$
$S_{x\gamma_x}, S_{x\gamma_z}$ $S_{z\gamma_x}, S_{z\gamma_z}$	stiffness coefficients associated with force and rotation, (N / rad)
$\bar{S}_{x\gamma_x}, \bar{S}_{x\gamma_z}$ $\bar{S}_{z\gamma_x}, \bar{S}_{z\gamma_z}$	$(S_{x\gamma_x}, S_{x\gamma_z}, S_{z\gamma_x}, S_{z\gamma_z}) / (\mu_o \omega_j R^5 / c^3)$
$S_{\gamma_x\gamma_x}, S_{\gamma_x\gamma_z}$ $S_{\gamma_z\gamma_x}, S_{\gamma_z\gamma_z}$	stiffness coefficients associated with moment and rotation, (N-m / rad)
$\bar{S}_{\gamma_x\gamma_x}, \bar{S}_{\gamma_x\gamma_z}$ $\bar{S}_{\gamma_z\gamma_x}, \bar{S}_{\gamma_z\gamma_z}$	$(S_{\gamma_x\gamma_x}, S_{\gamma_x\gamma_z}, S_{\gamma_z\gamma_x}, S_{\gamma_z\gamma_z}) / (\mu_o \omega_j R^6 / c^3)$

$S_{\gamma_x x}$, $S_{\gamma_x z}$ $S_{\gamma_z x}$, $S_{\gamma_z z}$	stiffness coefficients associated with moment and displacement, (N-m / m)
$\bar{S}_{\gamma_x x}$, $\bar{S}_{\gamma_x z}$ $\bar{S}_{\gamma_z x}$, $\bar{S}_{\gamma_z z}$	$(S_{\gamma_x x}, S_{\gamma_x z}, S_{\gamma_z x}, S_{\gamma_z z}) / (\mu_o \omega_j R^5 / c^3)$
t	time, (s)
$\bar{t}$	$t . \omega_j$, non-dimensional time
T_a	ambient temperature, (°C)
T_b	bush-housing temperature, (°C)
T_f	fluid-film temperature, (°C)
T_j	journal surface temperature, (°C)
T_m	mean temperature across fluid-film thickness, (°C)
T_r	reference temperature, (°C)
T_s	supply temperature of the lubricant, (°C)
$\bar{T}_a$, $\bar{T}_b$, $\bar{T}_f$, $\bar{T}_j$, $\bar{T}_s$	$(T_a, T_b, T_f, T_j, T_s) / T_r$
u, v, w	component of lubricant velocity in circumferential, axial and radial directions respectively, (m / s)
$\bar{u}$, $\bar{v}$, $\bar{w}$	$u, v, \frac{w}{\bar{c}} / (R \omega_j)$
W_x, W_z	fluid-film reactions in x and z directions, (N)
W	$\sqrt{(W_x^2 + W_z^2)} \equiv W_z$ for an external vertical load, (N)
$\bar{W}$, $\bar{W}_x$, $\bar{W}_z$	$W, W_x, W_z / (\mu_o \omega_j R^4 / c^2)$
x y z	coordinate axis in the horizontal(circumferential), axial and vertical(radial) direction with origin at geometric centre of bearing
X, Z	horizontal and vertical components of disturbed journal centre from its steady equilibrium position, (m)

X_{jo}, Z_{jo}	(e sinϕ, - e cosϕ) coordinates of steady state equilibrium position of journal centre of aligned bearings, (m)
X_{jo}, Z_{jo}	(e_0 sinϕ_0, - e_0 cosϕ_0) coordinates of steady state equilibrium position of journal centre of misaligned bearings at bearing midplane, (m)
$\bar{X}$, $\bar{Z}$, $\bar{X}_{jo}$, $\bar{Z}_{jo}$	(X, Z, X_{jo}, Z_{jo}) / c
X_{Li}, Z_{Li}	lobe centre coordinates for i th lobe, (m)
$\bar{X}_{Li}$, $\bar{Z}_{Li}$	X_{Li}, Z_{Li} / c
$\dot{X}$, $\dot{Z}$	horizontal and vertical components of lateral velocity of disturbed journal, (m / s)
$\bar{\dot{X}}$, $\bar{\dot{Z}}$	($\dot{X}$, $\dot{Z}$) / (c ω_j)
y	axial coordinate, (m)
z	coordinates across fluid-film thickness, (m)
$\bar{z}$	z / h
α	angular coordinate
β	y / R
Γα, Γβ	boundary of eth element along α and β directions respectively
ε	e / c, eccentricity ratio
ε_0	e_0 / c, midplane eccentricity ratio at steady state equilibrium position of misaligned bearings
μ_{air}, μ	viscosity of the air and lubricant respectively, (N.s / m^2)
μ_o	reference viscosity of the lubricant, (N.s / m^2)
$\bar{\mu}$	μ / μ_o
ρ_{air}, ρ	mass density of the air and lubricant respectively, Kg / m^3
φ	attitude angle, (deg)

φ_0	midplane attitude angle at steady state equilibrium position of misaligned bearings, (deg)
λ	aspect ratio, = $\pm$ L / D
ω_j	angular speed of journal, (rad / s)
Ω	threshold speed, (rad / s)
$\bar{\Omega}$	$\Omega / \sqrt{(g / c)}$
γ_x, γ_z	misalignment parameters - angular rotation of journal axis in horizontal and vertical plane at steady state, (rad)
$\Delta\gamma_x$, $\Delta\gamma_z$	rotational perturbation of journal axis in horizontal and vertical plane respectively from its steady state position, (rad)
$\bar{\gamma}_x$, $\bar{\Delta\gamma}_x$ γ_z, $\Delta\gamma_z$	$(\gamma_x, \Delta\gamma_x, \gamma_z, \Delta\gamma_z) / \bar{c}$
$\Delta\dot{\gamma}_x$, $\Delta\dot{\gamma}_z$	angular velocity components of disturbed journal axis in horizontal and vertical planes, (rad / s)
$\bar{\Delta\dot{\gamma}}_x$, $\bar{\Delta\dot{\gamma}}_z$	$(\Delta\dot{\gamma}_x, \Delta\dot{\gamma}_z) / (\bar{c}\,\omega_j)$

MATRICES AND VECTORS

[A]	global fluidity matrix for pressure field
[B]	global right-hand side matrix for pressure field
{ $\bar{p}$ }	nodal pressure vector for discretized flow domain
{ $\bar{Q}$ }	nodal flow vector for discretized flow domain

****

LIST OF FIGURES **PAGES**

Fig. 2.1	JOURNAL BEARING GEOMETRIES	17
Fig. 3.1	NODES NOMENCLATURE FOR FLUID-FILM	27
Fig. 3.2	NODES NOMENCLATURE FOR BUSH-HOUSING	29
Fig. 3.3	NODES NOMENCLATURE FOR JOURNAL	31
Fig. 4.1	SOLUTION SCHEME FOR MAIN PROGRAM	39
Fig. 4.2	SOLUTION SCHEME FOR SUBROUTINE TEMP	42
Fig. 4.3	SOLUTION SCHEME FOR LINEAR TRAJECTORIES	45
Fig. 5.1	GEOMETRICAL PARAMETER FOR PLAIN MISALIGNED JOURNAL BEARING	49
Fig. 5.2	COMPARISON OF RESULTS FOR PLAIN JOURNAL BEARING (Maximum Bush Temperature)	55
Fig. 5.3	TEMPERATURE VARIATION IN MID-PLANE AT 4000 RPM AND UNDER 6000 N	56
Fig. 5.4	TEMPERATURE VARIATION IN MID-PLANE AT 2000 RPM AND UNDER 4000 N	56
Fig. 5.5	COMPARISON OF RESULTS FOR PLAIN JOURNAL BEARING	59
Fig. 5.6	PLAIN JOURNAL BEARING - VARIATION OF JOURNAL TEMPERATURE	59
Fig. 5.7	COMPARISON OF RESULTS FOR TWO-AXIAL-GROOVE JOURNAL BEARING	60
Fig. 5.8	LOAD Vs DEGREE OF MISALIGNMENT	63
Fig. 5.9	PLAIN JOURNAL BEARING - STATIC PERFORMANCE CHARACTERISTICS (ε, ϕ, p_{max}, h_{min}, Q_s)	67
Fig. 5.10	TWO-AXIAL-GROOVE JOURNAL BEARING - STATIC PERFORMANCE CHARACTERISTICS (ε, ϕ, p_{max}, h_{min}, Q_s)	68
Fig. 5.11	ELLIPTICAL JOURNAL BEARING - STATIC PERFORMANCE CHARACTERISTICS (ε, ϕ, p_{max}, h_{min}, Q_s)	69

Fig. 5.12 THREE-LOBE JOURNAL BEARING - STATIC PERFORMANCE CHARACTERISTICS (ε, ϕ, p_{max}, h_{min}, Q_s) 70

Fig. 5.13 PLAIN JOURNAL BEARING - STATIC PERFORMANCE CHARACTERISTICS (T_J AND T_B) 72

Fig. 5.14 TWO-AXIAL-GROOVE JOURNAL BEARING - STATIC PERFORMANCE CHARACTERISTICS (T_J AND T_B) 73

Fig. 5.15 ELLIPTICAL JOURNAL BEARING - STATIC PERFORMANCE CHARACTERISTICS (T_J AND T_B) 74

Fig. 5.16 THREE-LOBE JOURNAL BEARING - STATIC PERFORMANCE CHARACTERISTICS (T_J AND T_B) 75

Fig. 5.17 PLAIN JOURNAL BEARING - STIFFNESS COEFFICIENTS ($\bar{S}_{xx}$, $\bar{S}_{xz}$, $\bar{S}_{zx}$, $\bar{S}_{zz}$) 77

Fig. 5.18 PLAIN JOURNAL BEARING - STIFFNESS COEFFICIENTS ($\bar{S}_{x\gamma_x}$, $\bar{S}_{x\gamma_z}$, $\bar{S}_{z\gamma_x}$, $\bar{S}_{z\gamma_z}$, $\bar{S}_{\gamma_x x}$, $\bar{S}_{\gamma_x z}$) 78

Fig. 5.19 PLAIN JOURNAL BEARING - STIFFNESS COEFFICIENTS ($\bar{S}_{\gamma_z x}$, $\bar{S}_{\gamma_z z}$, $\bar{S}_{\gamma_x \gamma_x}$, $\bar{S}_{\gamma_x \gamma_z}$, $\bar{S}_{\gamma_z \gamma_x}$, $\bar{S}_{\gamma_z \gamma_z}$) 79

Fig. 5.20 TWO-AXIAL-GROOVE JOURNAL BEARING - STIFFNESS COEFFICIENTS ($\bar{S}_{xx}$, $\bar{S}_{xz}$, $\bar{S}_{zx}$, $\bar{S}_{zz}$) 80

Fig. 5.21 TWO-AXIAL-GROOVE JOURNAL BEARING - STIFFNESS COEFFICIENTS ($\bar{S}_{x\gamma_x}$, $\bar{S}_{x\gamma_z}$, $\bar{S}_{z\gamma_x}$, $\bar{S}_{z\gamma_z}$, $\bar{S}_{\gamma_x x}$, $\bar{S}_{\gamma_x z}$) 81

Fig. 5.22 TWO-AXIAL-GROOVE JOURNAL BEARING - STIFFNESS COEFFICIENTS ($\bar{S}_{\gamma_z x}$, $\bar{S}_{\gamma_z z}$, $\bar{S}_{\gamma_x \gamma_x}$, $\bar{S}_{\gamma_x \gamma_z}$, $\bar{S}_{\gamma_z \gamma_x}$, $\bar{S}_{\gamma_z \gamma_z}$) 82

Fig. 5.23 ELLIPTICAL JOURNAL BEARING - STIFFNESS COEFFICIENTS ($\bar{S}_{xx}$, $\bar{S}_{xz}$, $\bar{S}_{zx}$, $\bar{S}_{zz}$) 83

Fig. 5.24 ELLIPTICAL JOURNAL BEARING - STIFFNESS COEFFICIENTS ($\bar{S}_{x\gamma_x}$, $\bar{S}_{x\gamma_z}$, $\bar{S}_{z\gamma_x}$, $\bar{S}_{z\gamma_z}$, $\bar{S}_{\gamma_x x}$, $\bar{S}_{\gamma_x z}$) 84

Fig. 5.25 ELLIPTICAL JOURNAL BEARING - STIFFNESS COEFFICIENTS ($\bar{S}_{\gamma_z x}$, $\bar{S}_{\gamma_z z}$, $\bar{S}_{\gamma_x \gamma_x}$, $\bar{S}_{\gamma_x \gamma_z}$, $\bar{S}_{\gamma_z \gamma_x}$, $\bar{S}_{\gamma_z \gamma_z}$) 85

Fig. 5.26 THREE-LOBE JOURNAL BEARING - STIFFNESS COEFFICIENTS ($\bar{S}_{xx}$, $\bar{S}_{xz}$, $\bar{S}_{zx}$, $\bar{S}_{zz}$) 86

Fig. 5.27 THREE-LOBE JOURNAL BEARING - STIFFNESS COEFFICIENTS ($\bar{S}_{x\gamma_x}$, $\bar{S}_{x\gamma_z}$, $\bar{S}_{z\gamma_x}$, $\bar{S}_{z\gamma_z}$, $\bar{S}_{\gamma_x x}$, $\bar{S}_{\gamma_x z}$) 87

Fig. 5.28 THREE-LOBE JOURNAL BEARING - STIFFNESS COEFFICIENTS ($\bar{S}_{\gamma_z x}$, $\bar{S}_{\gamma_z z}$, $\bar{S}_{\gamma_x \gamma_x}$, $\bar{S}_{\gamma_x \gamma_z}$, $\bar{S}_{\gamma_z \gamma_x}$, $\bar{S}_{\gamma_z \gamma_z}$) 88

Fig. 5.29 PLAIN JOURNAL BEARING - DAMPING COEFFICIENTS ($\bar{B}_{xx}$, $\bar{B}_{xz}$, $\bar{B}_{zx}$, $\bar{B}_{zz}$) 90

Fig. 5.30 PLAIN JOURNAL BEARING - DAMPING COEFFICIENTS ($\bar{B}_{x\gamma_x}$, $\bar{B}_{x\gamma_z}$, $\bar{B}_{z\gamma_x}$, $\bar{B}_{z\gamma_z}$, $\bar{B}_{\gamma_x x}$, $\bar{B}_{\gamma_z x}$, $\bar{B}_{\gamma_x z}$, $\bar{B}_{\gamma_z z}$) 91

Fig. 5.31 PLAIN JOURNAL BEARING - DAMPING COEFFICIENTS ($\bar{B}_{\gamma_x \gamma_x}$, $\bar{B}_{\gamma_x \gamma_z}$, $\bar{B}_{\gamma_z \gamma_x}$, $\bar{B}_{\gamma_z \gamma_z}$) 92

Fig. 5.32 TWO-AXIAL-GROOVE JOURNAL BEARING - DAMPING COEFFICIENTS ($\bar{B}_{xx}$, $\bar{B}_{xz}$, $\bar{B}_{zx}$, $\bar{B}_{zz}$) 93

Fig. 5.33 TWO-AXIAL-GROOVE JOURNAL BEARING - DAMPING COEFFICIENTS ($\bar{B}_{x\gamma_x}$, $\bar{B}_{x\gamma_z}$, $\bar{B}_{z\gamma_x}$, $\bar{B}_{z\gamma_z}$, $\bar{B}_{\gamma_x x}$, $\bar{B}_{\gamma_z x}$, $\bar{B}_{\gamma_x z}$, $\bar{B}_{\gamma_z z}$) 94

Fig. 5.34 TWO-AXIAL-GROOVE JOURNAL BEARING - DAMPING COEFFICIENTS ($\bar{B}_{\gamma_x \gamma_x}$, $\bar{B}_{\gamma_x \gamma_z}$, $\bar{B}_{\gamma_z \gamma_x}$, $\bar{B}_{\gamma_z \gamma_z}$) 95

Fig. 5.35 ELLIPTICAL JOURNAL BEARING - DAMPING COEFFICIENTS ($\bar{B}_{xx}$, $\bar{B}_{xz}$, $\bar{B}_{zx}$, $\bar{B}_{zz}$) 96

Fig. 5.36 ELLIPTICAL JOURNAL BEARING - DAMPING COEFFICIENTS ($\bar{B}_{x\gamma_x}$, $\bar{B}_{x\gamma_z}$, $\bar{B}_{z\gamma_x}$, $\bar{B}_{z\gamma_z}$, $\bar{B}_{\gamma_x x}$, $\bar{B}_{\gamma_z x}$, $\bar{B}_{\gamma_x z}$, $\bar{B}_{\gamma_z z}$) 97

Fig. 5.37 ELLIPTICAL JOURNAL BEARING - DAMPING COEFFICIENTS ($\bar{B}_{\gamma_x \gamma_x}$, $\bar{B}_{\gamma_x \gamma_z}$, $\bar{B}_{\gamma_z \gamma_x}$, $\bar{B}_{\gamma_z \gamma_z}$) 98

Fig. 5.38 THREE-LOBE JOURNAL BEARING - DAMPING COEFFICIENTS ($\bar{B}_{xx}$, $\bar{B}_{xz}$, $\bar{B}_{zx}$, $\bar{B}_{zz}$) 99

Fig. 5.39 THREE-LOBE JOURNAL BEARING - DAMPING COEFFICIENTS ($\bar{B}_{x\gamma_x}$, $\bar{B}_{x\gamma_z}$, $\bar{B}_{z\gamma_x}$, $\bar{B}_{z\gamma_z}$, $\bar{B}_{\gamma_x x}$, $\bar{B}_{\gamma_z x}$, $\bar{B}_{\gamma_x z}$, $\bar{B}_{\gamma_z z}$) 100

Fig. 5.40 THREE-LOBE JOURNAL BEARING - DAMPING COEFFICIENTS ($\bar{B}_{\gamma_x\gamma_x}$, $\bar{B}_{\gamma_x\gamma_z}$, $\bar{B}_{\gamma_z\gamma_x}$, $\bar{B}_{\gamma_z\gamma_z}$) 101

Fig. 5.41 PLAIN JOURNAL BEARING - STABILITY PARAMETERS ($\bar{\Omega}$, $\bar{\nu}$) 103

Fig. 5.42 TWO-AXIAL-GROOVE JOURNAL BEARING - STABILITY PARAMETERS ($\bar{\Omega}$, $\bar{\nu}$) 104

Fig. 5.43 ELLIPTICAL JOURNAL BEARING - STABILITY PARAMETERS ($\bar{\Omega}$, $\bar{\nu}$) 105

Fig. 5.44 THREE-LOBE JOURNAL BEARING - STABILITY PARAMETERS ($\bar{\Omega}$, $\bar{\nu}$) 106

Fig. 5.45 PLAIN JOURNAL BEARING - ISOPRESSURE CURVES (LOAD = 10 kN) 108

Fig. 5.46 TWO-AXIAL-GROOVE JOURNAL BEARING - ISOPRESSURE CURVES (LOAD = 10 kN) 109

Fig. 5.47 ELLIPTICAL JOURNAL BEARING - ISOPRESSURE CURVES (LOAD = 10 kN) 110

Fig. 5.48 THREE-LOBE JOURNAL BEARING - ISOPRESSURE CURVES (LOAD = 10 kN) 111

Fig. 5.49 UNWRAPPED JOURNAL BEARING SHOWING THE COORDINATE SYSTEM AND THE POSITION OF MAXIMUM PRESSURE POINT 112

Fig. 5.50 PLAIN JOURNAL BEARING - PRESSURE PROFILES WITH $\bar{\gamma}_x = \bar{\gamma}_z = 0.2$. (Load = 2 kN and Load =10 kN) 113

Fig. 5.51 PLAIN JOURNAL BEARING - PRESSURE PROFILES WITH $\bar{\gamma}_x = \bar{\gamma}_z = 0.4$. (Load = 2 kN and Load =15 kN) 114

Fig. 5.52 TWO-AXIAL-GROOVE JOURNAL BEARING - PRESSURE PROFILES WITH $\bar{\gamma}_x = \bar{\gamma}_z = 0.2$. (Load = 2 kN and Load =10 kN) 115

Fig. 5.53 TWO-AXIAL-GROOVE JOURNAL BEARING - PRESSURE PROFILES WITH $\bar{\gamma}_x = \bar{\gamma}_z = 0.4$. (Load = 2 kN and Load =10 kN) 116

Fig. 5.54 ELLIPTICAL JOURNAL BEARING - PRESSURE PROFILES WITH $\bar{\gamma}_x = \bar{\gamma}_z = 0.2$. (Load = 2 kN and Load =10 kN) 117

Fig. 5.55 THREE-LOBE JOURNAL BEARING - PRESSURE PROFILES WITH $\bar{\gamma}_x = \bar{\gamma}_z = 0.2$. (Load = 2 kN and Load =10 kN) 118

Fig. 5.56 PLAIN JOURNAL BEARING - BUSH-FLUID INTERFACE ISOTHERMS WITH $\bar{\gamma}_x = \bar{\gamma}_z = 0.2$. (Load = 2 kN and Load =10 kN) 120

Fig. 5.57 TWO-AXIAL-GROOVE JOURNAL BEARING - BUSH-FLUID INTERFACE ISOTHERMS WITH $\bar{\gamma}_x = \bar{\gamma}_z = 0.2$. (Load = 2 kN and Load =10 kN) 121

Fig. 5.58 ELLIPTICAL JOURNAL BEARING - BUSH-FLUID INTERFACE ISOTHERMS WITH $\bar{\gamma}_x = \bar{\gamma}_z = 0.2$. (Load = 2 kN and Load =10 kN) 122

Fig. 5.59 THREE-LOBE JOURNAL BEARING - BUSH-FLUID INTERFACE ISOTHERMS WITH $\bar{\gamma}_x = \bar{\gamma}_z = 0.2$. (Load = 2 kN and Load =10 kN) 123

Fig. 5.60 PLAIN JOURNAL BEARING - ISOTHERMS WITH $\bar{\gamma}_x = \bar{\gamma}_z = 0.2$. (Load =10 kN) 125

Fig. 5.61 TWO-AXIAL-GROOVE JOURNAL BEARING - ISOTHERMS WITH $\bar{\gamma}_x = \bar{\gamma}_z = 0.2$. (Load =10 kN) 126

Fig. 5.62 ELLIPTICAL JOURNAL BEARING - ISOTHERMS WITH $\bar{\gamma}_x = \bar{\gamma}_z = 0.2$. (Load =10 kN) 127

Fig. 5.63 THREE-LOBE JOURNAL BEARING - ISOTHERMS WITH $\bar{\gamma}_x = \bar{\gamma}_z = 0.2$. (Load =10 kN) 128

Fig. 5.64 UNWRAPPED JOURNAL BEARING SHOWING THE COORDINATE SYSTEM AND THE POSITION OF MAXIMUM TEMPERATURE POINT 129

Fig. 5.65 PLAIN JOURNAL BEARING - TEMPERATURE PROFILES WITH $\bar{\gamma}_x = \bar{\gamma}_z = 0.2$. (Load = 2 kN and Load =10 kN) 131

Fig. 5.66 PLAIN JOURNAL BEARING - TEMPERATURE PROFILES WITH $\bar{\gamma}_x = \bar{\gamma}_z = 0.4$. (Load = 2 kN and Load =15 kN) 132

Fig. 5.67 TWO-AXIAL-GROOVE JOURNAL BEARING - TEMPERATURE PROFILES WITH $\bar{\gamma}_x = \bar{\gamma}_z = 0.2$. (Load = 2 kN and Load =10 kN) 133

Fig. 5.68 TWO-AXIAL-GROOVE JOURNAL BEARING - TEMPERATURE PROFILES WITH $\bar{\gamma}_x = \bar{\gamma}_z = 0.4$. (Load = 2 kN and Load =10 kN) 134

Fig. 5.69 ELLIPTICAL JOURNAL BEARING - TEMPERATURE PROFILES WITH $\bar{\gamma}_x = \bar{\gamma}_z = 0.2$. (Load = 2 kN and Load =10 kN) 135

Fig. 5.70 THREE-LOBE JOURNAL BEARING - TEMPERATURE PROFILES WITH $\bar{\gamma}_x = \bar{\gamma}_z = 0.2$ (Load = 2 kN and Load =10 kN) 136

Fig. 5.71 JOURNAL TEMPERATURE PROFILES WITH $\bar{\gamma}_x = \bar{\gamma}_z = 0.2$. (Load =10 kN) 139

Fig. 5.72 LINEAR TRAJECTORIES FOR PLAIN JOURNAL BEARING WITH $\bar{\gamma}_x = \bar{\gamma}_z = 0.4$. (Load = 2 kN) 140

Fig. 5.73 LINEAR TRAJECTORIES FOR PLAIN JOURNAL BEARING WITH $\bar{\gamma}_x = \bar{\gamma}_z = 0.4$. (Load = 10 kN) 141

Fig. 5.74 LINEAR TRAJECTORIES FOR TWO-AXIAL-GROOVE JOURNAL BEARING WITH $\bar{\gamma}_x = \bar{\gamma}_z = 0.4$. (Load = 2 kN) 142

Fig. 5.75 LINEAR TRAJECTORIES FOR TWO-AXIAL-GROOVE JOURNAL BEARING WITH $\bar{\gamma}_x = \bar{\gamma}_z = 0.4$. (Load = 10 kN) 143

Fig. 5.76 LINEAR TRAJECTORIES FOR ELLIPTICAL JOURNAL BEARING WITH $\bar{\gamma}_x = \bar{\gamma}_z = 0.2$. (Load = 2 kN) 144

Fig. 5.77 LINEAR TRAJECTORIES FOR ELLIPTICAL JOURNAL BEARING WITH $\bar{\gamma}_x = \bar{\gamma}_z = 0.2$. (Load = 10 kN) 145

Fig. 5.78 LINEAR TRAJECTORIES FOR THREE-LOBE JOURNAL BEARING WITH $\bar{\gamma}_x = \bar{\gamma}_z = 0.2$. (Load = 2 kN) 146

Fig. 5.79 LINEAR TRAJECTORIES FOR THREE-LOBE JOURNAL BEARING WITH $\bar{\gamma}_x = \bar{\gamma}_z = 0.2$. (Load = 10 kN) 147

Fig. 5.80 PLAIN JOURNAL BEARING - STATIC PERFORMANCE CHARACTERISTICS WITH DIFFERENT $\bar{c}$ VALUES 155

Fig. 5.81 PLAIN JOURNAL BEARING - STATIC PERFORMANCE CHARACTERISTICS WITH DIFFERENT JOURNAL SPEEDS 157

Fig. 5.82 PLAIN JOURNAL BEARING - STABILITY PARAMETERS WITH DIFFERENT $\bar{c}$ VALUES 159

Fig. 5.83 PLAIN JOURNAL BEARING - STABILITY PARAMETERS WITH DIFFERENT JOURNAL SPEEDS 159

Fig. 5.84 PLAIN JOURNAL BEARING - VARIATION OF TEMPERATURES WITH DIFFERENT $\bar{c}$ VALUES 160

Fig. 5.85 PLAIN JOURNAL BEARING - VARIATION OF TEMPERATURES WITH DIFFERENT JOURNAL SPEEDS 160

****

LIST OF TABLES PAGES

TABLE 5.1 COMPARISON OF STATIC AND DYNAMIC PERFORMANCE CHARACTERISTICS OF TWO-AXIAL-GROOVE, ELLIPTICAL AND THREE-LOBE BEARINGS 48

TABLE 5.2 COMPARISON OF DIMENSIONLESS OIL-FILM PARAMETERS OF A MISALIGNED PLAIN JOURNAL BEARING - IHD ANALYSIS 50

TABLE 5.3 COMPARISON OF STATIC PERFORMANCE CHARACTERISTICS OF TWO-AXIAL- GROOVE JOURNAL BEARING - IHD ANALYSIS 51

TABLE 5.4 COMPARISON OF STABILITY PARAMETERS OF TWO-AXIAL-GROOVE JOURNAL BEARING - IHD ANALYSIS 51

TABLE 5.5 COMPARISON OF DYNAMIC PERFORMANCE CHARACTERISTICS OF TWO-AXIAL- GROOVE JOURNAL BEARING - IHD ANALYSIS 52
(i) STIFFNESS COEFFICIENTS
(ii) DAMPING COEFFICIENTS

TABLE 5.6 OPERATING CONDITIONS 54

TABLE 5.7 DATA FOR CALCULATION 61

TABLE 5.8 OPERATING CONDITIONS 64

TABLE 5.9 OPERATING CHARACTERISTICS 65

TABLE 5.10 SUMMARY OF BUSH-FLUID INTERFACE ISOTHERMS 124

TABLE 5.11 SUMMARY OF TEMPERATURE PROFILES 137

TABLE 5.12 COMPARISON OF TIME UNITS REQUIRED FOR REACHING A STABLE POSITION 148

TABLE 5.13 COMPARATIVE STUDY OF MINIMUM FILM THICKNESS IN JOURNAL BEARINGS 150

TABLE 5.14 COMPARATIVE STUDY OF STABILITY PARAMETERS IN JOURNAL BEARINGS 151
(a) THRESHOLD SPEED
(b) WHIRL FREQUENCY RATIO

TABLE 5.15 COMPARATIVE STUDY OF TEMPERATURE VARIATION IN DIFFERENT BEARINGS 153
(a) BUSH
(b) JOURNAL

TABLE 5.16 OPERATING CONDITIONS 154

****

CHAPTER-I

INTRODUCTION

Although the theory of hydrodynamic lubrication was developed in the late nineteenth century, the hydrodynamic journal bearings have been used to support rotating or stationary shafts since early ages. These bearings find their use in most of the high speed rotating machines such as turbogenerators, grinders, pumps, turbines and engines. If designed properly, they possess long life and excellent damping capabilities. Satisfactory operation of the rotating machine depends a great deal on the performance of the bearing systems supporting their rotating parts. It has often been noticed that the rotating machines fail due to malfunctioning of their bearings. Therefore, the design of hydrodynamic bearing systems is vital for the safe running of the rotating machines.

In general, the hydrodynamic journal bearings are designed using empirical relations and design data developed under simplifying assumptions. Amongst the most common assumptions used for the development of design data of journal bearings are (i) viscosity of the lubricant is constant throughout, i.e. the journal bearing operate under isothermal condition, and (ii) there is no misalignment between the journal and the bearing axes. Modern bearings are required to operate at high speeds and/or under heavy load conditions. This leads to substantial variation of lubricant temperature in the circumferential, axial and radial directions. Besides, heavy load on shaft may result in misalignment. Manufacturing or installation errors may also cause some degree of misalignment. Under these conditions, the above said assumptions are questionable. Failure of several bearings also points in this direction. Therefore, it is desirable to include the thermal and misalignment effects in the analysis and design of journal bearings. The present work has been undertaken with these forethoughts.

Ever since, O. Reynolds proposed his theory of hydrodynamic lubrication, extensive theoretical investigations have been undertaken by researchers. These works may broadly be classified as :

(a) Isothermal (IHD) analysis : which is carried out considering temperature of the bearing and the lubricant to be constant. Thus, viscosity of the lubricant is assumed constant in the solution of governing Reynolds equation. This viscosity is determined using the operating temperature of the bearing. When bearing surfaces are assumed flexible, the study is referred to as Elastohydrodynamic(EHD).

(b) Thermohydrodynamic(THD) analysis : In this type of analysis, the temperature of the lubricant is assumed to vary along one, two or all the three directions, namely, circumferential, radial and axial. The viscosity, which depends largely on temperature, varies accordingly. The pressure and temperature fields are found using iterative solutions of the governing equations. The bearing surfaces are considered rigid in the THD analysis. The analysis which considers thermal and elastic effects, both, is sometimes called thermoelastohydrodynamic(TEHD) analysis.

The present work is limited to the THD analysis of aligned and misaligned journal bearings. The temperature has been assumed to vary in all the three directions and a more general bi-planar misalignment has been considered for the theoretical analysis. The study has been carried out on circular and non-circular journal bearings to investigate the thermal and misalignment effects on these geometries. Exact problem definition is given in the next chapter.

****

CHAPTER - II

LITERATURE SURVEY

A brief review of the work undertaken by various researchers / investigators for the analysis of hydrodynamic journal bearings are presented in sections 2.1 to 2.3 under the following grouping :

(i) Early Works

(ii) Isothermal (IHD) studies, and

(iii) Thermohydrodynamic (THD) studies

2.1 EARLY WORKS

The hydrodynamic film lubrication was effectively used even before it was understood fully. Hydrodynamic journal bearings are in use since the early stages of development of machinery. In 1883, the Russian engineer N. Petrov[1] was the first to establish theoretically the friction effect of viscous shearing of an intervening fluid film. He explained the functional relationship between the frictional force and the bearing parameters.

In the same year, Bouchamp Tower [2-3] reported the results of a series of experiments which eventually led to the development of hydrodynamic lubrication theory by Osborne Reynolds [4]. Nearly two decades latter in 1904, the German physicist Sommerfeld [5] provided further theoretical extensions to the journal bearing lubrication problem. In 1918, Rayleigh[6] investigated the effect of lubricant film shape on performance characteristics of a bearing using calculus of variations. In the early 50s, the Reynolds equation was solved by Ocvirk [7] for an infinitely long and narrow journal bearings.

2.2 ISOTHERMAL STUDIES

The studies made under the assumptions of constant oil viscosity are referred to as IHD studies. A brief review of the literature on aligned and misaligned journal bearings under IHD conditions are presented in the following sub-sections :

2.2.1 Aligned Journal Bearings

Based on the Reynolds equation and assumptions of rigid bush / liner and constant oil viscosity throughout the film, several studies [8-15] are available on the performance characteristics of circular and non-circular aligned bearings. These studies are devoted to the analysis of static and dynamic performance characteristics of bearings operating in laminar and turbulent flow regimes.

Malik [16] made a theoretical comparative study of performance characteristics of various forms of two-lobe journal bearings. He predicted that two-lobe configuration can provide consistently good dynamic performance over a wide range of load conditions.

Significant contributions to the literature on hydrodynamic instability were made by Flack et al. [17] and Lanes et al. [18-19]. Flack et al. [17] carried out the studies for rigid and flexible rotors following the linearised as well as the non-linear approaches considering rigid bearing surfaces.

Lanes et al. [18-19] observed discrepancies between experimental and computed values of the threshold speed for three-lobe journal bearings. They found the experimental values to be higher. It was attributed to the possible errors in the theoretical calculations.

Chandrawat and Sinhasan [20] have presented algorithms for two solution techniques, namely the Gauss-Siedel iterative scheme and the linear complementarity problem (LCP) approach, for finding the positive pressure region in a hydrodynamic journal bearing. The two techniques are compared through the results and the computer time for plain journal bearing operating in laminar flow regimes. The LCP is reported to be far superior, when closer tolerances are required on pressure (< 0.1 %), otherwise both the techniques are equally efficient.

Choy et al. [21] have performed the nonlinear transient and frequency response analysis of a hydrodynamic journal bearing.

Kostrzewsky et al. [22] performed experiments to study the steady state operating characteristics and dynamic coefficients of a two-axial groove journal bearing. The four stiffness and four damping coefficients were determined as functions of Sommerfield

number for two fixed shaft speeds, with estimated uncertainties for each. The results agreed with the uncertainty of the data for the speed, load and temperature ranges.

Taylor et al [23,24] determined the static and dynamic characteristics of a three-lobe journal bearing with a preload factor of 0.75. They tested three operating speeds. The results indicated that the maximum pressure occurred circumferentially near the point of minimum oil film. The non-dimensionalised data at all the three speeds were independent of any given Sommerfeld number; thus, the Reynolds number(which depends on speed) had little influence for the range of conditions tested.

Elrod and Vijayaraghavan [25] presented a stability analysis for liquid-lubricated journal bearings incorporating the effect of displacement perturbations of the cavitation boundaries. They reported that these displacements are of disturbance magnitude and should be included in a stability analysis.

2.2.2 Misaligned Journal Bearings

Early work on misaligned journal bearings [26-29] was mainly confined to the experimental investigation of oil-film pressure distribution in axial direction. McKee and McKee [26] experimentally observed that the pressure distribution of misaligned journal bearings loses axial symmetry. Cowlin [27] listed misalignment as one of the principal causes for deviation of bearing performance from that predicted by the hydrodynamic theory. Piggott [28] showed that misalignment can reduce load carrying capacity by as much as 40 percent. Buske [29] showed that the hydrodynamic pressure pattern in a bearing is very sensitive to misalignment.

A first analytical study for the pressure profiles of a full journal bearing with axes skew was first carried out by Walther and Sassenfeld [30]. An experimental study of misaligned bearings was pursued by Dubois, Mabie and Ocvirk [31]. They found that for characterization of a spatially misaligned bearing, three parameters are necessary : the eccentricity ratio and two angular displacements in two angular directions. This approach has some short comings. Firstly, the data cannot be interpreted in terms of a geometrical parameter and secondly, it does not specify the boundaries and boundary conditions clearly.

In a subsequent theoretical study, Khrisanova [32] derived a geometric expression for film thickness with reference to components of skew in vertical and horizontal planes

and solved the Reynolds equation assuming 180° film extent and the boundaries as straight and inclined at an angle "gamma" at the beginning and at the end of the positive pressure zone in circumferential direction. This approach suffered from many short comings. Numerical solutions of Reynolds equation for a full or half journal bearing under misaligned conditions are given by Smalley and McCallion [33] and Stockley and Donaldson [34]. Smalley and McCallion presented design charts relating to the influence of the misaligning couple. Stockley and Donaldson analysed the effect of misalignment in a 180° partial bearing in which the misalignment was restricted to an axial tilt as the result of shaft bending. These studies too, assumed complex boundary conditions to identify positive pressure region of oil-film. Moreover, these studies were carried out for short bearings only ($L/D \leq 1$) and influence of the presence of axial oil groove(s) was ignored.

Asanabe et al. [35] made an analytical and experimental attempt to study the static performance characteristics of a two-axial groove misaligned bearing but their work was restricted to misalignment in vertical plane only. Moreover, Sommerfeld boundary conditions were used for the solution of the Reynolds equation.

Bannister [36] reported theoretical and experimental investigations into the influence of non-linearity and misalignment on eight oil film force coefficients for a 120° partial journal bearing with a length-to-diameter ratio of one.

Several investigators [37-42] solved the Reynolds equation by employing the Gauss Elimination method or Gauss-Siedel relaxation procedure to establish extent of positive pressure region. These approaches predicted a more logical boundary for the positive pressure zone.

Pinkus and Bupara [37] published considerable theoretical data of different grooved bearings, but they used the eccentricity, ε and the angle between the center line and the vertical coordinate as independent variables. Their load direction is a variable dependent on eccentricity and the misalignment ratio. Their vertical misalignment does not mean that the journal axis is tilted in the plane parallel with the load, and their horizontal grooves are not in the plane perpendicular to the load. This variable load direction makes their data's application and comparison rather difficult.

Pafelias and Broniarek [38] computed a set of sixteen stiffness and sixteen damping coefficients to study the bearing-system dynamics with general misalignment in the journal bearings. Reason and Siew [39] presented a numerical solution for the three-dimensional pressure distribution effects on the performance of a journal bearing with spatial misalignment.

Ikeuchi et al. [40] fixed the load direction and solved the attitude angles at different eccentricities for a circumferentially grooved bearings. They only presented the misalignment effects on load capacities and attitude angles. Buckholz and Lin [41] studied the misalignment effect on load for Non-Newtonian lubricants.

Jakeman [42] studied the performance of a misaligned journal bearing and worked out force and moment oil film dynamic coefficients for a stern tube bearings. In a subsequent study, Jakeman [43] developed a non-linear oil film response model for the dynamically misaligned stern tube bearing for the purpose of conducting lateral vibration analysis of marine propeller shafting.

Abdel-Latif and Mokhtar [44] explored the effects of both bearing roughness in the longitudinal and transverse directions together with journal misalignment on the bearing behavior, especially if the bearing runs at the limit of full film lubrication.

Vijayaraghavan and Keith [45, 46] modified the method of Pinkus and Bupara [37] by considering the mass continuity at both start and end edges of oil film and published considerable data on static characteristics of the grooved and ungrooved bearings. They incorporated grid transformation and adaptation techniques into a finite difference method to consider cavitation and starvation effects.

Choy et al. [47] have depicted the misalignment effect on one stiffness coefficient and critical mass of an ungrooved bearing at one set of misalignment parameters under some load conditions. They [48] further studied the nonlinear effects in a hydrodynamic journal bearing with special attention to the effects of journal axial misalignment. The study predicted that at light loads, journal axial misalignment results in a double hump in the fluid film pressure distribution and disappears as the load increases. At higher load condition, the peak fluid film pressure decreases with misalignment at a lightly misaligned condition and increases with misalignment at a highly misaligned condition.

Sharda et al. [49] reported the EHD performance characteristics of a misaligned journal bearing. They observed that the bush flexibility improves the bearing load capacity and the stability of the bearing.

Yu and Keith [50] developed a boundary element cavitation algorithm to predict cavitation in journal bearings with axially variable clearance. The results for aligned and misaligned journal bearings are compared with those obtained using the finite difference method.

Qiu and Tieu [51] presented all static and dynamic characteristics of a horizontally grooved bearing under different eccentricity and misalignment conditions and compared them with the available experimental data. The effect of misalignment on all bearing characteristics and on the stability of the rotor-bearing system are analyzed.

2.3 THERMOHYDRODYNAMIC STUDIES

The study of thermal effects in journal bearings has received considerable attention in last few decades. A large number of investigations on the thermal effects in journal bearings have been reported in literature. A brief review of the thermal literature on hydrodynamic journal bearing are reviewed in the following sub-sections under the heading of aligned and misaligned journal bearings :

2.3.1 Aligned Journal Bearings

One of the earliest analytical works is reported by Kingsbury [52] who outlined a graphical solution method for solving three equations : Newton's law of viscous shear across the fluid film, a viscosity-temperature relation; and equation for heat generation and heat flow in the fluid film.

One of the earliest experimental works is that of Musket and Morgan[53] who performed heat balance experiments for a journal bearing. They reported that it takes a long time (4 to 6 hours in some cases) to reach temperature equilibrium in a journal bearing.

Hagg [54] studied the influence of speed and viscosity on the shear stress of a journal bearing. He provided a graph for estimating frictional power losses in a journal bearing operating under high-speed conditions.

Clayton and Wilkie [55] experimentally obtained temperature profile in both radial and circumferential directions along with the temperature gradient in the bush under steady-state condition. Other early experimental work was performed by Hamilton et al. [56] who investigated a method of predicting heat dissipation in journal bearings.

Cole [57] measured bush temperature distribution in radial and circumferential directions and reported discrepancies between actual operating conditions and results of the constant viscosity assumption. He showed that only about one-half of the heat generated in the lubricant film of the bearing was carried away by the lubricant flow. Burr[58] continued this work and concluded that heat dissipated from a rotating shaft may be much more than from a stationary shaft and from the bearing housings.

The significance of including variation of viscosity across the film thickness was first reported by Zienkiewicz [59] in the year 1958, who discovered that it is responsible for an appreciable change in load-carrying capacity in bearings and therefore, should not be neglected in theoretical studies.

Tipei and Nica [60] conducted experiments to study the influence of viscosity variation on the operating conditions of finite journal bearing.

Dowson et al. [61], conducted a major experimental work and found that heat flow patterns in the bush are a combination of both radial flow and a significant amount of circumferential flow traveling from the hot region in the vicinity of minimum film thickness to the cooler region near the oil inlet. Dowson's test results also showed that cyclic variation in shaft surface temperature is small and shaft can, therefore, be treated as an isothermal component. They also inferred that shaft temperature remains within a few degrees of the mean temperature of bush inner surface. Lastly, the experiments indicated that the axial temperature gradients within the bush are negligible.

Much more sophisticated analytical work was done by Nica [62] who obtained a temperature distribution for a finite journal bearing considering viscosity variation. He presented the results for film temperature for some specific cases which compared well with the earlier experimental results of Tipei and Nica [60]. The short comings of this work was the assumption of constant viscosity across the film and the half-Sommerfeld condition used.

McCallion et al. [63] suggested decoupling of the energy equation from that of the Reynolds equation by neglecting pressure gradients in the film. Appropriate equations were derived and solved numerically by the finite difference method. The results compared favourably with the experimental work of Dowson [61].

Majumdar and Saha [64] also assumed a constant viscosity across film thickness and experimented with a bearing of length-to-diameter ratio of one and compared the load capacity with isothermal solution of Raimondi et al. [8]. They found a 35 % reduction in the load capacity at eccentricity ratio = 0.4.

Gardner and Ulshmid [65] carried out an experimental work under turbulent conditions and determined the journal temperatures under various operating conditions for two journal bearing applications.

Safar and Szeri [66] extended the thermohydrodynamic theory for the bearing from laminar to turbulent regime. Assuming that the heat transfer in the bush is in the radial direction only, they integrated the Laplace heat-conduction equation in the solid and applied the boundary condition of matching the temperature and heat flux at that interface. This boundary condition significantly simplifies the computations since it removes the necessity of iteration on that boundary. However, the method has limitation in determining the location and magnitude of the maximum bush temperature.

Following the earlier experimental work of Majumdar and Saha [64], Majumdar[67] numerically solved the Energy and Reynolds equations by neglecting heat conduction in the bush. It was reported that the extent of the film and also the load capacity decreases if one includes the density and viscosity variation in the lubricant as a function of temperature.

Sugnami and Szeri [68] found that under laminar conditions, the shaft temperature remains constant at approximately the discharge oil temperature: whereas, under turbulent conditions, an insulated shaft assumption yielded results that were in closer agreement with the experimental work of Gardner and Ulshmid [65].

Pinkus and Bupara [69] described a method of including variable viscosity in bearing analysis by the use of a simple energy equation uncoupled from the Reynolds equation. The relevant adiabatic solutions are made independent of the specifics of the kind of lubricant used and of its initial conditions. Performance results such as load, friction, maximum

temperature, flow, etc. are given for the two-axial-groove journal bearing covering three L/D ratios. The effect of variable viscosity on the performance of misaligned bearings is also examined.

Boncompain et al. [70] considered variation of viscosity across oil film and solved the 3-D energy equation in fluid domain and 2-D heat conduction equation for bush. They analyzed dynamic characteristics of a finite journal bearing under laminar conditions. Thermal effects were found to cause a large change in stiffness and damping coefficients. Ferron et al. [71] followed a similar procedure but they solved 3-D energy equation and 3-D heat conduction equation and computed a mixing temperature by performing a simple energy balance between recirculating oil and supply oil at the inlet. Good agreement was found with measurements reported for pressure and temperature, but a large discrepancy was noted between the predicted and measured values of eccentricity ratios.

Mitsui and Yamada [72] performed a thermohydrodynamic (THD) analysis in which thermal conductivity and specific heat were assumed to be constant while viscosity was assumed to vary as a function of temperature. The transverse velocity term was neglected. The two-dimensional Laplace heat-conduction equation was solved by an infinite series approximation. The energy equation was solved using the Crank-Nicholson's method and the Reynolds equation by the successive over-relaxation method. They found that both journal velocity and lubricant viscosity have a profound effect on the temperature fields and the load-carrying capacity.

Tonnesen and Hansen [73] reported experimental study of thermal effects in hydrodynamic journal bearings operating under steady-state conditions. Both viscosity and oil inlet geometry were found to have a significant effect on the operating temperatures. The shaft temperature was found to increase with decreasing loads when a high-viscosity lubricant was used. Moreover, the oil flow governed by the inlet pressure and / or the inlet geometry was found to have a pronounced influence on the onset of instability leading to the conclusion that these factors must be considered in the design of bearings.

Knight and Barrett [74] developed an approximate solution technique for multilobe journal bearings. Their energy equation was a simple ordinary differential equation based on a constant axial temperature and constant temperature across the film. They neglected the

heat conduction in lubricant and bush and assumed that all the heat generated is removed by the side leakage. In their latter work [75] the effect of heat transfer between the fluid film and its surrounding was also included in an approximate way. The viscosity across the film was assumed to be constant and the heat exchanged in the oil supply grooves was not considered. They found that the supply pressure has pronounced effects on the operating eccentricities, temperature, flow rate and dynamic characteristics of the bearing studied.

Lund et a.l [76,77] presented an approximate analysis for solving the 3-D energy equation for journal bearing film, coupled with the heat conduction equation for the bearing sleeve. The analysis approximates the temperature profile across the film thickness by a fourth order polynomial while the circumferential temperature variation is expressed in terms of a Fourier series expansion. Heat exchange in the supply groove were considered in this work. To test the validity of the theory, experiments were performed for two-axial groove journal bearing over a range of loads and speeds. A fair agreement was reported between the theoretical and their experimental work.

Gethin and Medwell [78] experimentally investigated the thermohydrodynamic behaviour of a high speed cylindrical bore journal bearing fed by two-axial-grooves. They highlighted the complex temperature patterns which are generated in the bush.

Gethin [79] described a theoretical investigation into the effect of thermoplastic bush deformation and journal thermal expansion on the behavior of a cylindrical bore bearing fed by two-axial grooves. The main conclusion which follows from this work is that thermoelastic bush deformation is an important factor in predicting bearing performance for a given load.

Boncompain et al. [80] solved the 3-D energy equation in fluid domain and 2-D heat conduction equation for bush. They extended their earlier work [70 - 71] in order to take into account the reversed flow at the inlet and the recirculating heat flux across the cavitation zone. Thermoelastic displacements of the shaft and the bush are also taken into account. Theoretical results are then compared with the experimental data.

Khonsari and Beaman [81] investigated thermohydrodynamic effects in journal bearings operating under steady-state loading and formulated an analytical model for finite journal bearings. The model includes correction factors for the cavitation effects and the

mixing of the recirculating oil and supply oil at the inlet. They compared their results with those of Dowson et al [61]. Results show that the oil-bush interface temperature drops slightly in the vicinity of the inlet followed by a rapid rise in the circumferential direction and drop in the cavitation region. The computed mixing temperature is very close to the minimum bush temperature obtained experimentally indicating the cooling effect of the inlet oil propagating into the solid.

Heshmat and Pinkus [82] offered a conceptual and experimental investigation of the mechanism of mixing in the oil groove, in terms of the relevant flows and temperatures. Results of tests aimed at measuring the mixing inlet temperatures as a function of a range of operating conditions and bearing sizes are correlated in terms of an appropriate mixing function. Empirical equations based on the above correlation for the determination of inlet temperatures are then given for both thrust and journal bearings.

Khonsari [83,84] presents an extensive survey of the work pertaining to thermal effects in hydrodynamic bearings. It includes discussions on theoretical, computational and experimental works pertaining to heat effects in journal bearings published in various technical journals.

Braun et al. [85] coupled the Reynolds equation with the energy equation to perform a rather complete analysis for a cryogenic journal bearing. To correctly account for the changes in the fluid viscosity, the energy equation was coupled with the shaft and bearing heat conduction equations. The effects of pressure and temperature on the density, viscosity, and load-carrying capacity were further discussed.

Singh et al. [86] studied thermoelastohydrodynamic(THED) effects for an elliptical bearing. The 3-D momentum and continuity equations and 3-D elasticity equations were solved to obtain pressure in the lubricant flow field and deformation in the bearing liner. The energy equation and Fourier heat conduction equation were used to obtain the temperature distribution in the fluid film and the bearing body. They used an approach similar to the one proposed by Lund et al. [76] for thermal analysis but limited thermal solution to the positive pressure region only.

Sinhasan et al. [87] presented TEHD analysis of a two-axial-groove journal bearing using finite element method to solve the governing equations. The conventional 3-D

energy equation was modified to account for the flow of lubricant to the cavitation region but it does not consider the heat exchange in the supply grooves.

Paranjpe and Han [88] developed a THD analysis of finite journal bearings based on a fully conservative finite-volume formulation for accurate prediction of the bearing performance characteristics. Sample calculations for automotive bearing show that the oil supply pressure and supply configuration(oil feed arrangement) significantly affect the bearing performance.

Gethin and El-Deihi [89] presented a thermal model for comparison between predicted and measured performance trends of a twin axial groove journal bearing. The analysis confirms the sensitivity of global bearing performance with respect to loading direction.

Tripp and Melodick [90] presented a series of measurements taken with experimental setup using a commercially representative lubricant and a non-Newtonian lubricant. Analysis of the measurements show that the oil film thickness in the hydrodynamic regime of lubrication with non-Newtonian oils is dominated by the shear-dependent viscosity and the elastic effects of these oils do not make a significant contribution to the oil film load bearing capacity.

Sheeja and Prabhu [91] carried out a theoretical and experimental investigations for a plain journal bearing considering the influence of thermal effects on Non-Newtonian lubrication. The investigations reveal that the thermal effect is more pronounced than the non-Newtonian effect on the dynamic characteristics.

Fitzgerald and Neal [92] contributed to the stock of experimental thermal data for axial-groove journal bearings. They also discussed the consequences of neglecting the effect of bush heat transfer in the prediction of operating temperature.

Paranjpe and Han [93] developed a THD analysis of steadily loaded journal bearings that included mass conserving cavitation, 3-D energy equation in the oil film, heat conduction in the bushing and journal, and mixing of hot re-circulating oil with the supply oil. The journal temperature is assumed constant and is computed by satisfying "no-net-heat-flux" condition. Predictions of the analysis compared well with the measurements reported by Dowson et al. [61]. They [94] further developed a transient THD analysis for

dynamically loaded journal bearings that included mass conserving cavitation and 3-D energy equation in the oil film with moving grids in the oil film. The journal is treated as a lumped thermal element. They considered the thermal transients in the oil film and found that the oil film temperatures vary considerably over time and space.

Gethin [95] presented a numerical investigation into the effect of temperature boundary conditions and viscous dissipation on the behaviour of two- and three-lobe bearings. For two-lobe bearing, setting the viscous generation to zero in the cavitated film gave the best agreement with the experiment. The model was also used successfully for the three-lobe bearing confirming its general applicability.

2.3.2 Misaligned Journal Bearings

Some work has been reported in the area of misaligned thermohydrodynamic journal bearings as discussed below :

Barun et al. [96] analyzed the effects of misalignment on the energy dissipation mechanism and presented an analysis that coupled the various equations involved. The journal temperature was assumed to be constant. The effects of misalignment on pressure and fluid temperature were analyzed for isothermal, adiabatic and arbitrary(i.e. finite heat transfer coefficient) fluid film boundary conditions. Simultaneous solutions were obtained by finite difference method and the results were presented for various tilt angles. The model was found to useful in predicting hot-spots in a journal bearing.

Safar, Mokhtar and Peekent [97] undertook adiabatic analysis of a journal bearing for maximum allowable misalignment with a length-to-diameter ratio of one. The Reynolds and energy equations were solved simultaneously using finite difference method. The results showed that the bearing behaviour is significantly affected by journal misalignment.

Jang et al. [98] presented an adiabatic solution for a misaligned journal bearing operating with non-Newtonian lubricant.

Chun and Lalas [99] carried out a parametric study of the effects of oil inlet temperature and pressure in half-circumferential / axial grooved journal bearings under aligned and misaligned conditions. The effects of changes of the wall temperature and the L/D ratio have been examined. The wall temperature and heat transfer rate have been found to be of secondary importance to the mixing effectiveness at the groove and the resulting

final mixture temperature. The variability of the temperature, has been shown to smooth out the peaks of both pressure and friction during the misaligned conditions.

2.4 PRESENT WORK

The survey presented above indicates that, although the investigations on thermohydrodynamic(THD) lubrication attracted a large number of researchers during the past more than three decades, the studies remained confined mainly to the problems of aligned journal bearings. The published literature on the THD analysis of misaligned journal bearings is rather scant. Even the published literature on the isothermal studies on misaligned journal bearings is generally limited to the circular bearing geometries. Studies on the effect of misalignment in the case of noncircular bearing geometries, such as elliptical and three-lobe bearings, have also been scant. Therefore, a need has been felt to investigate the thermohydrodynamic effects in misaligned circular and noncircular bearing configurations with more realistic mathematical models and boundary conditions for the physical problems involved.

The work contained in this work pertains to four bearing configurations, namely, circular plain, circular two-axial-groove, elliptical and three-lobe. Static and dynamic performance characteristics together with temperature and pressure profiles, isotherms for liquid and solid domains and other thermal characteristics of these bearing geometries, Figs. 2.1(a) to (d) have been studied and appropriate conclusions drawn.

The generalised Reynolds equation is used to represent the flow of lubrication in the clearance space of the journal bearing. The film thickness is expressed by including bi-planar misalignment. A suitable viscosity-temperature relation has been used to express viscosity of oil as a function of temperature. For the thermal analysis, the temperature distributions in the fluid-flow field (liquid domain) and the bush-housing assembly are respectively represented by the three-dimensional energy and Fourier heat conduction equations. Because of rotation and high thermal conductivity of the material, the journal temperature distribution is assumed to vary only along its length with convective heat transfer from axial ends. Appropriate boundary conditions have been used for the solution of all governing

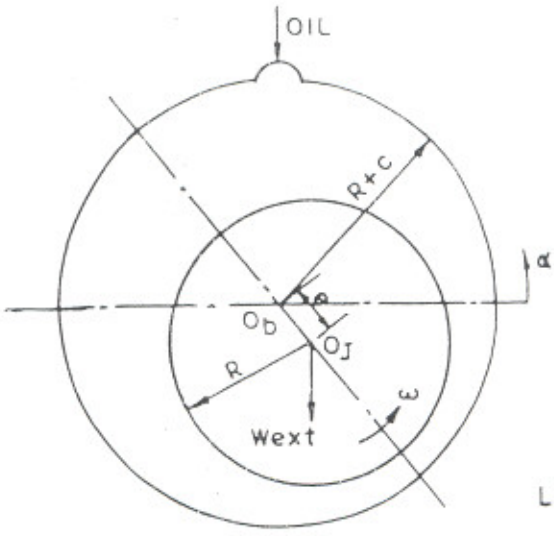

$\bar{X}_{L1} = 0.0 \qquad \bar{Z}_{L1} = 0.0$

(a) PLAIN BEARING

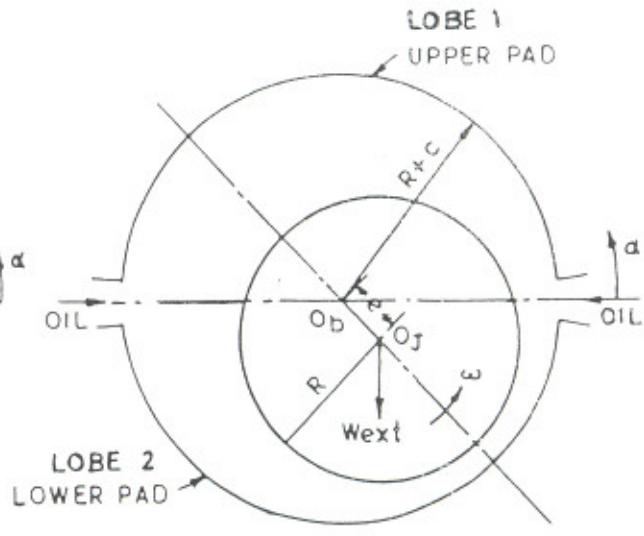

$\bar{X}_{L1} = 0.0 \qquad \bar{Z}_{L1} = 0.0$

$\bar{X}_{L2} = 0.0 \qquad \bar{Z}_{L2} = 0.0$

(b) TWO-AXIAL-GROOVE BEARING

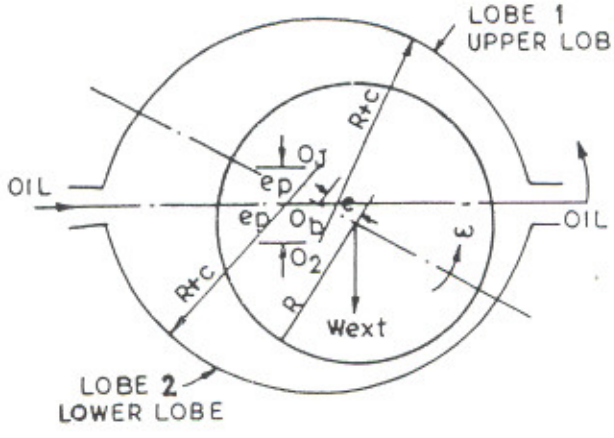

$\bar{X}_{L1} = 0.0 \qquad \bar{Z}_{L1} = -0.5$

$\bar{X}_{L2} = 0.0 \qquad \bar{Z}_{L2} = 0.5$

(c) ELLIPTICAL BEARING

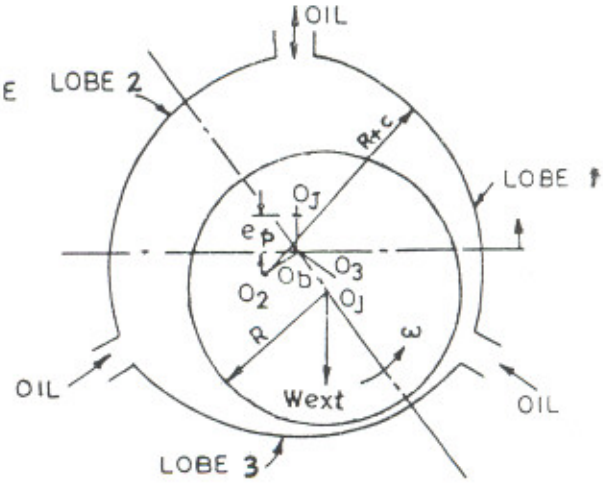

$\bar{X}_{L1} = -0.433 \qquad \bar{Z}_{L1} = -0.25$

$\bar{X}_{L2} = 0.433 \qquad \bar{Z}_{L2} = -0.25$

$\bar{X}_{L3} = 0.0 \qquad \bar{Z}_{L3} = 0.5$

(d) THREE-LOBE BEARING

Fig. 2.1 JOURNAL BEARING GEOMETRIES

equations. Mixing of recirculating hot oil with the cool supply oil has been considered. Heat transfer from solid-to-liquid and liquid-to-solid in the oil supply grooves is included.

Finite element method is employed for solving the Reynolds equation whereas finite difference method with successive over relaxation (SOR) technique has been used to obtain solution of the energy and heat conduction equations. The overall computational procedure used is an iterative one. Initially a temperature field is assumed. Viscosity obtained from this field is used to solve the Reynolds equation. The pressure field from the solution of Reynolds equation is used as input for the solution of energy equation. Converged temperature fields for the liquid and solid(bush and journal) domains are obtained from the solutions of energy and heat conduction equations in nested loops. These temperature fields are then used to modify viscosity field for the solution of Reynolds equation. Iterations are carried out until a converged solution of pressure and temperature fields are obtained. Suitable weighting factors have been used to improve the rates of convergence of various iteration loops.

Various performance characteristics of all journal bearing configurations studied in this work have been presented as functions of load. These characteristics include mid-plane eccentricity ratio, attitude angle, minimum fluid-film thickness, side flow, sixteen stiffness and sixteen damping coefficients, instability threshold speed and whirl frequency ratio. Maximum bush temperature and mean journal temperature have also been plotted as functions of load. Pressure and temperature profiles and isotherms have been presented for specified loads for all types of bearings. Results for aligned bearings have been given for ready reference. Before presenting the results, however, the analysis, the boundary conditions and the developed computer programme have been adequately validated by comparing the present results with the published experimental and the theoretical results. Linearised journal-centre motion trajectories have been drawn to carry out stability analysis.

Some of the important conclusions drawn from this study are

- Misalignment reduces the load carrying capacity and the value of minimum fluid-film thickness for all types of bearings.
- Misalignment improves the stability margin.
- Misalignment makes the bearings to run hotter.

- For the study of misaligned bearings it is essential to use a three-dimensional thermal analysis whereas a two-dimensional analysis is adequate for the study of the aligned bearings.

2.5 ORGANISATION OF THESIS

The thesis has been presented in six chapters. A brief detail of each of the six chapters are given below :

In chapter I, importance of journal bearings, introduction to various types of analyses and significance of the present work have been covered.

Chapter II presents a survey of literature starting from the earliest works. Although the survey encompasses the works on isothermal, elastohydrodynamic, thermohydrodynamic and thermoelastohydrodynamic analyses, a more emphasis has been given to the thermal studies. Research papers on aligned as well as misaligned bearings have been surveyed and the gaps in the literature are clearly brought out. In the light of the prevailing gaps in literature, the problem for the present work has been defined.

Chapter III deals with the details of mathematical modelling and analysis. In this chapter, various equations with boundary conditions are given. Mathematical relations for the computation of static and dynamic performance characteristics are also given in this chapter.

Computational experiment used in the present work is described in chapter IV. The algorithms for the solution of problem are presented in flow chart form for better understanding.

Results and discussions are given in chapter V. The chapter first deals with the validity of the present work and then the results for various types of bearings are presented and discussed.

In chapter VI main conclusions drawn from the present work are given. A brief outline of the future work is also given in this chapter.

CHAPTER - III

MATHEMATICAL MODELLING AND ANALYSIS

3.1 INTRODUCTION

In this chapter, the mathematical formulation for THD analysis of hydrodynamic journal bearings, in general, and misaligned hydrodynamic journal bearings, in particular, have been dealt with. In the succeeding sections of this chapter, representative mathematical models for the flow field, bush-housing assembly and journal with appropriate boundary conditions are described. System equations for the descretised solution domains using finite element method / finite difference method have been obtained. The analysis is presented in non-dimensional form.

In general, a thermohydrodynamic analysis involves the solutions of the following coupled equations

i) Generalised Reynolds equation for pressure field in fluid domain.

ii) Energy equation for fluid temperature field.

iii) Heat conduction equations for bush and journal temperature fields.

The solution of the Reynolds equation requires the viscosity of lubricating oil, which is computed using the temperature field obtained from the solution of energy equation. The solution of energy equation needs the pressure field established from the solution of Reynolds equation. Further, the energy equation for fluid domain and heat conduction equations for bush and journal need to be solved simultaneously to establish the temperature fields for the fluid, the bush and the journal.

Thus, the overall solution of a THD problem involves handling the above coupled equations. The converged solutions of the these equations yield the pressure field, the temperature fields for the fluid, the bush and the journal. The viscosity field is obtained using established temperature field for the fluid and a suitable viscosity-temperature relationship

In the present work, the Reynolds equation is solved using finite element method whereas, the energy and heat conduction equations are solved using finite difference

method. The expressions for static and dynamic performance characteristics of a journal bearing system are also given in this Chapter. Using the linearized approach, in which the motion of the journal centre is restricted within a close proximity of the static equilibrium position, Routh's criteria is applied to the resulting characteristic equation to derive the expressions for critical mass, instability threshold speed and whirl frequency ratio and also to trace the journal-centre motion trajectories for a free translatory whirl.

3.2 HYDRODYNAMIC ANALYSIS

3.2.1 Generalized Reynolds Equation

The flow of lubricant in the clearance space of each lobe / pad of a journal bearing is governed by the following generalized non-dimensional modified Reynolds equation :

$$\frac{\partial}{\partial \alpha}\left(\bar{h}^3 \, \bar{F}_2 \frac{\partial \bar{p}}{\partial \alpha} \right) + \frac{\partial}{\partial \beta}\left(\bar{h}^3 \, \bar{F}_2 \frac{\partial \bar{p}}{\partial \beta} \right) = \frac{\partial}{\partial \alpha}\left(\bar{h} - \bar{h} \frac{\bar{F}_1}{\bar{F}_0} \right) + \frac{\partial \bar{h}}{\partial \bar{t}} \qquad \text{----- (3.1)}$$

The non-dimensional viscosity functions $\bar{F}_0$, $\bar{F}_1$ and $\bar{F}_2$ in equations (3.1) are defined by the relations :

$$\bar{F}_0 = \int_0^1 \frac{1}{\bar{\mu}} \, d\bar{z} \; ; \quad \bar{F}_1 = \int_0^1 \frac{\bar{z}}{\bar{\mu}} \, d\bar{z} \; ; \quad \bar{F}_2 = \int_0^1 \frac{\bar{z}}{\bar{\mu}} \left(\bar{z} - \frac{\bar{F}_1}{\bar{F}_0} \right) d\bar{z} \qquad \text{------ (3.2)}$$

3.2.2 Fluid-Film Thickness

The fluid-film thickness in non-dimensional form for any lobe in equation (3.1) is given by the following relation :

$$\bar{h} = 1 - \{ \bar{X}_{j0} - \bar{X}_{Li} + \bar{X} + \beta (\bar{\gamma}_x + \Delta\bar{\gamma}_x) \} \cos\alpha - \{ \bar{Z}_{j0} - \bar{Z}_{Li} + \bar{Z} + \beta (\bar{\gamma}_z + \Delta\bar{\gamma}_z) \} \sin\alpha \qquad \text{------- (3.3)}$$

where, for an aligned bearing,

$\bar{\gamma}_x = \bar{\gamma}_z = 0$ and $\Delta\bar{\gamma}_x = \Delta\bar{\gamma}_z = 0$ and the equation reduces to :

$$\bar{h} = 1 - (\bar{X}_{j0} - \bar{X}_{Li} + \bar{X}) \cos\alpha - (\bar{Z}_{j0} - \bar{Z}_{Li} + \bar{Z}) \sin\alpha \qquad \text{------- (3.4)}$$

For a bearing operating under a steady-state condition, the perturbation coordinates $\bar{X}$, $\bar{Z}$, $\Delta\bar{\gamma}_x$ and $\Delta\bar{\gamma}_z$ are each equal to zero.

The value of $\partial \bar{h} / \partial \bar{t}$ is obtained by differentiating the expression for $\bar{h}$ partially with respect to non-dimensional time, $\bar{t}$.

3.2.3 Viscosity - Temperature Relation

In equation (3.2), the non-dimensional viscosity of the lubricant, $\bar{\mu}$ ($= \mu / \mu_o$) is obtained from the relation [77] :

$$\mu / \rho = 10^{-6} [\exp (b (T + 273.12)^{-a}) - 0.8] \qquad \text{----- (3.5)}$$

where a and b are the viscosity coefficients and are obtained by specifying values of μ at two different temperatures and ρ is the density of the lubricant. For isothermal (IHD) studies, the viscosity is assumed to be constant.

3.2.4 Boundary Conditions for Reynolds Equation

The boundary conditions used for solving the generalised Reynolds equation for pressure distribution, $\bar{p}$ are :

(i) At the bearing side boundaries i.e. (for $\beta = \pm \lambda$)

$$\bar{p} = 0 \qquad \text{------ (3.6a)}$$

(ii) On the supply groove boundaries

$$\bar{p} = \bar{p}_s = 0 \qquad \text{------ (3.6b)}$$

here, $\bar{p}_s$ is non-dimensional supply pressure (assumed 0 in the present work)

(iii) At the trailing edge of the positive pressure region : The following two conditions must be satisfied simultaneously.

$$\bar{p} = 0 \qquad \text{------ (3.6c)}$$

$$\frac{\partial \bar{p}}{\partial \alpha} = 0 \qquad \text{------ (3.6d)}$$

In the present work, these boundary conditions are satisfied by using the linear complementarity approach described by Chandrawat et al. [20].

3.2.5 Finite Element Formulation of Reynolds Equation

The entire lubricant flow domain is discretised using two-dimensional, 4-noded linear, isoparametric finite elements. For the study of a misaligned bearing, full axial length is discretised while for aligned bearings only half of the length is considered taking advantage of axial symmetry.

The pressure distribution $\bar{p}^e$ over an element is represented as :

$$\bar{p}^e = \sum N_i \, . \, \bar{p}_i, \qquad i = 1, 2, ...4 \qquad \text{------ (3.7)}$$

where N_i is the shape function for the *i th* node of an element and $\bar{p}_i$ is the corresponding nodal pressure.

Using orthogonality condition of Galerkin's method [100], equation (3.1) yields the following system equations for the discretised fluid domain.

$$[A] \{ \bar{p} \} = \{ B \} + \{ \bar{Q} \} \qquad \text{------ (3.8)}$$

where [A] is the assembled coefficient matrix, { B } is the assembled column vector consisting of static and dynamic terms and { $\bar{Q}$ } is the nodal flow vector. { $\bar{p}$ } is the nodal pressure vector.

The relations for computing the coefficients of the matrices [A], { B } and { $\bar{Q}$ } in equation (3.8) for the *e th* element are given below :

For the *m*th iteration, the equation (3.1) yields,

$$[a_{ij}^{e}]^{m} = \int_{\bar{A}e} \bar{h}^{3} \; \bar{F}_2^{m-1} \left(\frac{\partial N_i}{\partial \alpha} \frac{\partial N_j}{\partial \alpha} + \frac{\partial N_i}{\partial \beta} \frac{\partial N_j}{\partial \beta} \right) d \bar{A};$$

$$i = 1,2,.... \; 4 \qquad \text{------ (3.9a)}$$

$$\{ b_i^{e} \}^{m} = \int_{\bar{A}e} \left[\left(\bar{h} - \bar{h} \frac{\bar{F}_1^{m-1}}{\bar{F}_0^{m-1}} \frac{\partial N_i}{\partial \alpha} \right) - N_i \frac{\partial \bar{h}}{\partial \bar{t}} \right] d \bar{A};$$

$$i = 1,2,.... \; 4 \qquad \text{------ (3.9b)}$$

$$\{ \bar{q}_i^{e} \}^{m} = \int_{\Gamma\beta^e} N_i \left[\bar{h} \; \bar{F}_2^{m-1} \frac{\partial \bar{p}}{\partial \alpha} - \bar{h} \left(1 - \frac{\bar{F}_1^{m-1}}{\bar{F}_0^{m-1}} \right) \right] \partial \beta + \int_{\Gamma\alpha^e} N_i \; \bar{h} \; \bar{F}_2^{m-1} \frac{\partial \bar{p}}{\partial \beta} \partial \alpha ;$$

$$i = 1,2,.... \; 4 \qquad \text{------ (3.9c)}$$

3.3 THERMAL ANALYSIS

In this section, the energy equation for the lubricant flow field, the heat conduction equations for the bush-housing assembly and the journal with their respective boundary conditions are presented.

3.3.1 Energy Equation

The energy equation in lubrication is generally obtained by incorporating the usual thin-film approximation into the generalized energy equation. This equation is, however, valid only in the positive-pressure region. With the inception of cavitation, the fluid-film

splits into a large number of streamers which are separated by air/gas streams. In the present work it is assumed that the lubricant and gas streamers are distributed in such a manner that the lubricating film consists of the uniformly distributed streams of oil and air/gas and its properties may be represented by the effective fluid properties, defined later in this section. Thus, the three-dimensional energy equation, given below, is applied to the entire fluid domain (i.e. lubrication and cavitation regions) to obtain the lubricant temperature field :

$$\bar{h}^2 \left(\bar{u} \frac{\partial \bar{T}_f}{\partial \bar{\alpha}} + \bar{v} \frac{\partial \bar{T}_f}{\partial \beta} + \frac{\bar{w}}{\bar{h}} \frac{\partial \bar{T}_f}{\partial \bar{z}} \right) = \bar{D}_e \, \bar{\mu} \left[\left(\frac{\partial \bar{u}}{\partial \bar{z}} \right)^2 + \left(\frac{\partial \bar{v}}{\partial \bar{z}} \right)^2 \right] + \bar{P}_e \frac{\partial^2 \bar{T}_f}{\partial \bar{z}^2} \qquad \text{------ (3.10)}$$

The operator $\frac{\partial}{\partial \bar{\alpha}^*}$ is introduced to change the shape of the film into a rectangular field and is given by :

$$\frac{\partial}{\partial \bar{\alpha}^*} = \frac{\partial}{\partial \bar{\alpha}} - \frac{\bar{z}}{\bar{h}} \left(\frac{\partial \bar{h}}{\partial \bar{\alpha}} \right) \frac{\partial}{\partial \bar{z}} \qquad \text{------ (3.11)}$$

The substitution from equation (3.11) into equation (3.10) yields

$$\bar{h}^2 \left[\bar{u} \frac{\partial \bar{T}_f}{\partial \bar{\alpha}} + \bar{v} \frac{\partial \bar{T}_f}{\partial \beta} + \frac{1}{\bar{h}} \left(\bar{w} - \bar{z} \, \bar{u} \frac{\partial \bar{h}}{\partial \bar{\alpha}} \right) \frac{\partial \bar{T}_f}{\partial \bar{z}} \right] = \bar{D}_e \, \bar{\mu} \left[\left(\frac{\partial \bar{u}}{\partial \bar{z}} \right)^2 + \left(\frac{\partial \bar{v}}{\partial \bar{z}} \right)^2 \right] + \bar{P}_e \frac{\partial^2 \bar{T}_f}{\partial \bar{z}^2} \qquad \text{------ (3.12)}$$

The values of non-dimensional effective inverse Peclet number ($\bar{P}_e$) and Dissipation number ($\bar{D}_e$) are as follows :

$$\bar{P}_e = \frac{k_{fe}}{C_{pe} * \rho_e * \omega_j * c^2} \qquad \text{------ (3.13a)}$$

$$\bar{D}_e = \frac{\mu_e * \omega_j}{C_{pe} * \rho_e * T_r * c^2} \qquad \text{------ (3.13b)}$$

In computing effective inverse Peclet number ($\bar{P}_e$) and Dissipation number ($\bar{D}_e$), effective values of fluid properties (k_{fe}, C_{pe}, ρ_e and μ_e) are used, given by the following relations :

$$k_{fe} = k_f C_L + k_{air} (1 - C_L) \qquad \text{------ (3.14a)}$$

$$C_{pe} = C_p C_L + C_{pair} (1 - C_L) \qquad \text{------ (3.14b)}$$

$$\rho_e = \rho C_L + \rho_{air} (1 - C_L) \qquad \text{------ (3.14c)}$$

$$\mu_e = \mu_f \, C_L + \mu_{air} \, (1 - C_L) \qquad \text{------ (3.14d)}$$

The contraction coefficient, C_L, in the above relations is defined as follows :

$$C_L = \int_0^1 (\bar{u} \, \bar{h}) \, d\bar{z} \; / \; \int_{0}^{1} (\bar{u} \, \bar{h}) \, d\bar{z} \qquad \text{------ (3.15)}$$

The subscript *te* refers to the trailing edge of positive-pressure region of the fluid-film. C_L is unity in the positive-pressure region.

The values of the non-dimensional velocities $\bar{u}$ and $\bar{v}$ have been found using the following relations :

$$\bar{u} = \bar{h}^2 \frac{\partial \bar{p}}{\partial \alpha} \left[\int_0^{\bar{z}} \frac{\bar{z}}{\bar{\mu}} d\bar{z} - \frac{\bar{F}_1}{\bar{F}_0} \int_0^{\bar{z}} \frac{d\bar{z}}{\bar{\mu}} \right] + \frac{1}{\bar{F}_0} \int_0^{\bar{z}} \frac{d\bar{z}}{\bar{\mu}} \qquad \text{------ (3.16)}$$

$$\bar{v} = \bar{h}^2 \frac{\partial \bar{p}}{\partial \beta} \left[\int_0^{\bar{z}} \frac{\bar{z}}{\bar{\mu}} d\bar{z} - \frac{\bar{F}_1}{\bar{F}_0} \int_0^{\bar{z}} \frac{d\bar{z}}{\bar{\mu}} \right] \qquad \text{------ (3.17)}$$

The non-dimensional velocity, $\bar{w}$ is obtained by solving the following continuity equation :

$$\frac{\partial \bar{u}}{\partial \alpha} + \frac{\partial \bar{v}}{\partial \beta} + \frac{1}{\bar{h}} \frac{\partial \bar{w}}{\partial \bar{z}} = 0 \qquad \text{------- (3.18)}$$

Due to numerical uncertainties, however, direct computation of the velocities using equation (3.18) induces difficulties in the convergence process. Thus to determine the radial velocity component ($\bar{w}$), the continuity equation (3.18) is differentiated partially with respect to $\bar{z}$ which gives a second order differential equation :

$$\frac{\partial^2 \bar{w}}{\partial \bar{z}^2} + \bar{h} \frac{\partial}{\partial \bar{z}} \left(\frac{\partial \bar{u}}{\partial \alpha} + \frac{\partial \bar{v}}{\partial \beta} \right) - \frac{\partial}{\partial \bar{z}} \left(\bar{z} \frac{\partial \bar{u}}{\partial \bar{z}} \frac{\partial \bar{h}}{\partial \alpha} \right) = 0 \qquad \text{------- (3.19)}$$

This equation is then integrated using the finite differences with the following boundary conditions :

$$\bar{w} = 0 \quad \text{at} \quad \bar{z} = 0 \qquad \text{------- (3.20a)}$$

$$\bar{w} = \frac{\partial \bar{h}}{\partial \alpha} \quad \text{at} \quad \bar{z} = 1 \qquad \text{------- (3.20b)}$$

3.3.1.1 Boundary Conditions for the Energy Equation

(i) On the fluid-journal interface ($\bar{z} = 1$) :

$$\bar{T}_f = \bar{T}_j \qquad \text{------- (3.21a)}$$

(ii) On the fluid-bush interface ($\bar{z} = 0$) :

$$\bar{T}_f = \bar{T}_b \qquad \text{------- (3.21b)}$$

(iii) Temperature distribution at the inlet edge of the bearing pad :

The following two alternative boundary conditions for temperature distribution have been examined.

Boundary Conditions 1 (BC 1)

The temperature is assumed to vary quadratically with $\bar{z}$, i.e.

$$\bar{T}_f = a_0 + a_1 . \bar{z} + a_2 . \bar{z}^2 \qquad \text{------- (3.21c)}$$

The coefficients of the above equation, a_0, a_1 and a_2 are obtained by using equation (3.21a) and (3.21b) together with relation (3.30) and (3.32) given later.

Boundary Conditions 2 (BC 2)

The temperature is given by the following cubic polynomial :

$$\bar{T}_f = a_0 + a_1 . \bar{z} + a_2 . \bar{z}^2 + a_3 . \bar{z}^3 \qquad \text{------- (3.21d)}$$

In order to obtain the values of the coefficients of this equation, the conditions defined by equations (3.21a), (3.21b), (3.30) and (3.32) are employed as in the case of BC 1. But, however, $\bar{T}_b$ in equation (3.21b) is assumed to be equal to supply temperature $\bar{T}_s$ and $\frac{\partial \bar{T}_f}{\partial \bar{z}}$ is taken as zero consistent with the boundary condition at the inlet of pad for the bush, discussed later.

3.3.1.2 Finite Difference Formulation of Energy Equation

The system equations for the entire fluid-domain is obtained as follows based on the nodes nomenclature given in Fig. 3.1 :

$$\bar{T}_{fi,j,k} = K_1 \bar{T}_{fi-1,j,k} + K_2 \bar{T}_{fi,j,k-1} + K_3 \bar{T}_{fi,j,k+1} + K_4 \bar{T}_{fi,j-1,k} + K_5 \bar{T}_{fi,j+1,k} \qquad \text{------ (3.22)}$$

where K_1, K_2, K_3, K_4 and K_5 are the coefficients of the equation, the values of which are evaluated using grid geometry and values of velocity components, fluid-film thickness, $\bar{D}_e$ and $\bar{P}_e$.

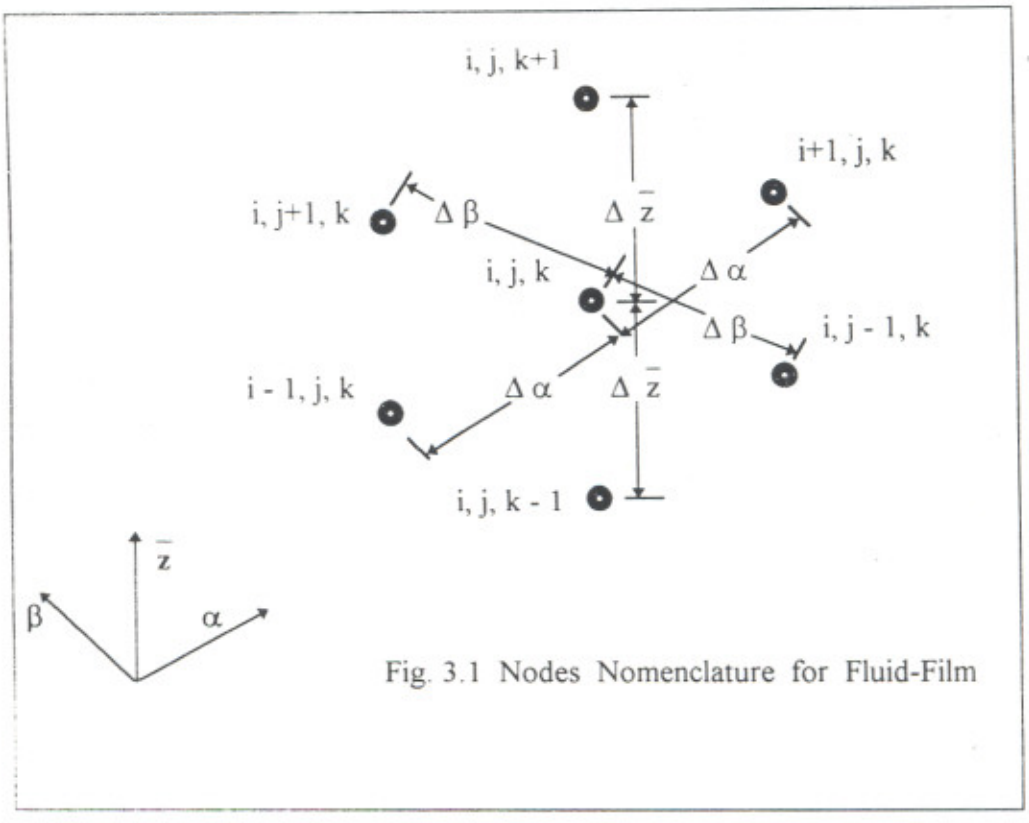

Fig. 3.1 Nodes Nomenclature for Fluid-Film

3.3.2 Heat Conduction Equation for Bush-Housing

The Fourier heat conduction equation in the non-dimensional cylindrical coordinate form, given below, has been solved for the temperature distribution in the bush and the housing, both of which have been assumed to be cylindrical and possessing the same thermal properties.

$$\frac{\partial^2 \bar{T}_b}{\partial \bar{r}^2} + \frac{1}{\bar{r}} \frac{\partial \bar{T}_b}{\partial \bar{r}} + \frac{\partial^2 \bar{T}_b}{\partial \beta^2} + \frac{1}{\bar{r}^2} \frac{\partial^2 \bar{T}_b}{\partial \alpha^2} = 0 \qquad \text{------- (3.23)}$$

3.3.2.1 Boundary Conditions for Heat Conduction Equation

The following boundary conditions have been used for the solution of heat conduction equation (3.23)

(i) On the fluid-bush interface ($\bar{z} = 0$, $\bar{r} = \bar{R}_1$) :

Continuity of heat flux gives

$$k_b \cdot \left(\frac{\partial \bar{T}_b}{\partial \bar{r}} \right)_{| \bar{r} = \bar{R}1} = - \frac{k_f}{\bar{c} \cdot \bar{h}} \left(\frac{\partial \bar{T}_f}{\partial \bar{z}} \right)_{| \bar{z} = 0} \qquad \text{------- (3.24a)}$$

(ii) On the outer part of the bush-housing ($\bar{r} = \bar{R}_2$) :

The free convection and radiation hypothesis gives

$$\left(\frac{\partial \bar{T}_b}{\partial \bar{r}} \right)_{| \bar{r} = \bar{R}2} = - \frac{h_{ab} \cdot R}{k_b} \left(\bar{T}_{b| \bar{r} = \bar{R}2} - \bar{T}_a \right) \qquad \text{------- (3. 24b)}$$

(iii) On the lateral faces of the bearing ($\beta = \pm \lambda$) :

The free convection and radiation hypothesis gives

$$\left(\frac{\partial \bar{T}_b}{\partial \beta} \right)_{| \beta = \pm \lambda} = - \frac{h_{ab} \cdot R}{k_b} \left(\bar{T}_{b| \beta = \pm \lambda} - \bar{T}_a \right) \qquad \text{------ (3. 24c)}$$

(iv) At the outlet edge of bearing pad, free convection from bush to oil in the supply groove

gives

$$\left(\frac{\partial \bar{T}_b}{\partial \alpha} \right)_{| \alpha = \alpha_e} = - \frac{h_{fb} \cdot R}{k_b} \left(\bar{T}_b - \bar{T}_s \right) \qquad \text{------ (3. 24d)}$$

where α_e = circumferential coordinate of the outlet edge of bearing pad

(v) At the inlet edge of the bearing pad ($\alpha = \alpha_i$); two alternative boundary conditions consistent with boundary conditions for fluid-film have been used.

Thus, with BC 1 : at the oil supply point on the outer surface

$$\bar{T}_{b| \bar{r} = \bar{R}2} = \bar{T}_s \qquad \text{------ (3.24e)}$$

In addition, a free convection of heat between oil and solid has been assumed giving

$$\left(\frac{\partial \bar{T}_b}{\partial \alpha} \right)_{| \alpha = \alpha_1} = - \frac{h_{fb} \cdot R}{k_b} \left(\bar{T}_b - \bar{T}_s \right) \qquad \text{------ (3. 24f)}$$

where α_i = circumferential coordinate of the inlet edge of bearing pad

with BC 2, $\bar{T}_b = \bar{T}_s$ for all values of $\bar{r}$. ------ (3.24g)

3.3.2.1 Finite Difference Formulation

The system equations for the entire discretised bush-housing assembly is formulated as below based on the nodes nomenclature given in Fig. 3.2 :

$$\bar{T}_{b\,i,j,k} = C_1\,\bar{T}_{b\,i,j,k+1} + C_2\,\bar{T}_{b\,i,j,k-1} + C_3\,\bar{T}_{b\,i,j+1,k} + C_4\,\bar{T}_{b\,i,j-1,k} + C_5\,\bar{T}_{b\,i+1,j,k} + C_6\,\bar{T}_{b\,i-1,j,k} \quad \text{------ (3.25)}$$

where C_1, C_2, C_3, C_4, C_5 and C_6 are the coefficients determined from the grid geometry in the case of all internal nodes. For nodes on the boundary, appropriate boundary conditions have been applied assuming heat transfer in all the three directions in order to compute the values of coefficients C_is.

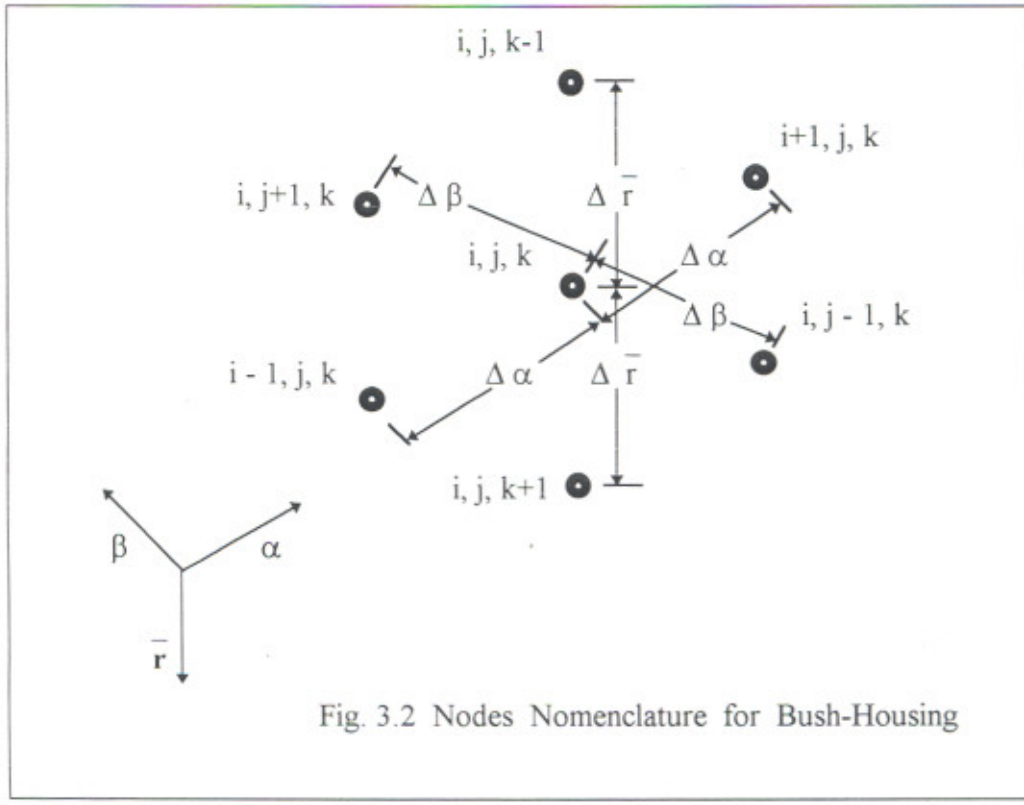

Fig. 3.2 Nodes Nomenclature for Bush-Housing

3.3.3 Heat Conduction Equation for the Journal

For the purpose of establishing the journal temperature field, the following assumptions have been made :

(i) Heat is conducted by the journal only in the axial direction.

(ii) Journal temperature does not vary in radial or circumferential direction at any section.

(iii) Heat is flowing out of the journal from its axial ends.

The steady-state unidirectional heat conduction equation used is :

$$k_J \cdot \left(\frac{\partial^2 \bar{T}_j}{\partial y^2}\right) \Delta y . A_J + \Delta q = 0 \qquad \text{------ (3.26a)}$$

where Δq = heat input to the element = $q \cdot \Delta y$

q = heat input per unit length

Δy = length of the element,

and A_J = crosectional area of the journal = $\pi \cdot R^2$

Equation (3.26a) reduces to the following non-dimensional form :

$$\pi \cdot \left(\frac{\partial^2 \bar{T}_j}{\partial \beta^2}\right) + \bar{q} = 0 \qquad \text{------ (3.26b)}$$

The non-dimensional heat input to journal, $\bar{q}$ is given by

$$\bar{q} = - \frac{k_f}{k_j \bar{c}} \left[\int_0^{2\pi} \frac{1}{\bar{h}} \left(\frac{\partial \bar{T}_f}{\partial \bar{z}}\right) d\alpha \right] - \frac{\bar{c} . h_{fj} . R}{k_j} \left(\bar{T}_j - \bar{T}_m \right) . \alpha_G \qquad \text{------ (3.27)}$$

where α_G is the groove angle in radians.

In equation (3.27), the second term on right hand side represents the heat transfer between the journal and the lubricant in oil groove.

3.3.3.1 Boundary Conditions for Heat Conduction Equation for Journal

The above equation have been solved with the following boundary condition :

At axial ends, i.e. $\beta = \pm \lambda$

$$\left(\frac{\partial \bar{T}_j}{\partial \beta}\right)_{|\beta = \pm \lambda} = - \frac{h_{aj} . R}{k_j} \left(\bar{T}_{j|\beta = \pm \lambda} - \bar{T}_a \right) \qquad \text{---- (3.28)}$$

3.3.3.1 Finite Difference Formulation

The system equation for the entire discretised journal is formulated as below based on the nodes nomenclature given in Fig. 3.3 :

$$\bar{T}_{j,i} = A_1 \bar{T}_{j,i-1} + A_2 \bar{T}_{j,i+1} + A_3 \qquad \text{------ (3.29)}$$

where A_1, A_2 and A_3 are the coefficients determined from the grid geometry in the case of all internal nodes. For nodes on the boundary, appropriate boundary conditions have been applied assuming heat transfer in two directions in order to compute the values of coefficients A_i's.

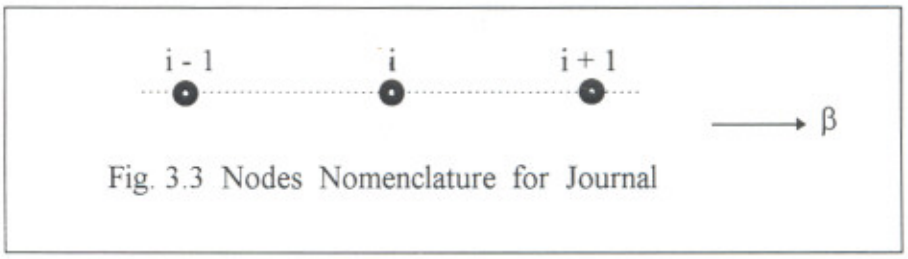

Fig. 3.3 Nodes Nomenclature for Journal

3.3.4 Mixing in the Oil Groove

Hot recirculating oil mixes with incoming cold oil from oil supply. The equation used for computing the mean temperature, $\bar{T}_m$ is based on the overall energy balance [71]. Thus

$$\bar{Q} \cdot \bar{T}_m = \bar{T}_r \cdot \bar{Q}_r + \bar{T}_s \cdot \bar{Q}_s \qquad \text{------ (3.30)}$$

and for a unit length of bearing

$$\bar{Q} = \int_0^1 (\bar{h} \cdot \bar{u}) \Big|_{\alpha_i} d\bar{z} \qquad \text{------ (3.31a)}$$

$$\bar{Q}_r = \int_0^1 (C_L \cdot \bar{h} \cdot \bar{u}) \Big|_{\alpha_e} d\bar{z} \qquad \text{------ (3.31b)}$$

$$\bar{T}_r \cdot \bar{Q}_r = \int_0^1 (C_L \cdot \bar{h} \cdot \bar{u} \cdot \bar{T}_f) \Big|_{\alpha_e} d\bar{z} \qquad \text{------ (3.31c)}$$

$$\bar{Q}_s = \bar{Q} - \bar{Q}_r \qquad \text{------ (3.31d)}$$

The mean temperature, $\bar{T}_m$ is related to the assumed temperature distribution, $\bar{T}_f(\bar{z})$ across the fluid-film at the inlet of the bearing pad as below :

$$\bar{T}_m = \int_0^1 \bar{T}_f(\bar{z}) \, d\bar{z} \qquad \text{------ (3.32)}$$

3.4 PERFORMANCE CHARACTERISTICS

The relations for computing static and dynamic performance characteristics are given as follows :

3.4.1 Static Performance Characteristics

These characteristics include mid-plane eccentricity ratio, attitude angle and side flow. Pressure and temperature fields obtained are used in the following relations to compute values of various parameters.

(a) Bearing Load and Moment

The fluid-film reaction components in the x and z directions are :

$$\begin{Bmatrix} \bar{W}_x \\ \bar{W}_z \end{Bmatrix} = \int_{-\lambda}^{\lambda} \int_{0}^{2\pi} \bar{p} . \begin{Bmatrix} \cos(\alpha) \\ \sin(\alpha) \end{Bmatrix} d\alpha . d\beta \qquad \text{------ (3.33)}$$

For a vertical load support, $\bar{W}_x = 0$ and $\bar{W}_z = \bar{W}$, load supported by the bearing.

In addition to the force components, there will be unbalance moment components about x- and z- axis in a misaligned journal bearing. The dimensionless moment components acting on the journal are given by :

$$\begin{Bmatrix} \bar{M}_x \\ \bar{M}_z \end{Bmatrix} = \int_{-\lambda}^{\lambda} \int_{0}^{2\pi} \beta . \bar{p} . \begin{Bmatrix} \cos(\alpha) \\ -\sin(\alpha) \end{Bmatrix} d\alpha . d\beta \qquad \text{------ (3.34)}$$

For an aligned bearing $\bar{M}_x = \bar{M}_z = 0$.

(b) Steady-State Equilibrium Position (Eccentricity Ratio and Attitude Angle)

The steady-state equilibrium position of a journal is usually expressed in terms of eccentricity ratio (ε_o) and attitude angle (φ). The values of eccentricity ratio and attitude angle are established during the iterative solution of a journal bearing problem satisfying the condition of vertical load support for any specified load ($\bar{W}$).

(c) Side Flow ($\bar{Q}_s$)

The side flow parameter is given by the relation :

$$Q_s = -\int_0^{2\pi} \frac{\bar{h}^3}{\bar{\mu}} \left(\frac{\partial \bar{p}}{\partial \beta} \right)_{|\beta = \lambda} d\alpha - \int_0^{2\pi} \frac{\bar{h}^3}{\bar{\mu}} \left(\frac{\partial \bar{p}}{\partial \beta} \right)_{|\beta = -\lambda} d\alpha \qquad \text{------ (3.35)}$$

3.4.2 Dynamic Performance Characteristics

For a misaligned journal bearing system, the dynamic performance characteristics are expressed in terms of sixteen stiffness and sixteen damping coefficients. The values of stiffness and damping coefficients are evaluated by assuming that the disturbed position of the journal centre remains in close proximity of its static equilibrium position so that changes in temperature, and hence, fluid viscosity are small and negligible in comparison to their steady-state values.

The dynamic coefficients are computed to account for changes in force and moment arising from lateral and angular displacement and velocity perturbations. Thus, thirty-two such coefficients are required to define the oil-film forces and moments produced by a dynamically misaligned bearing. In the case of an aligned bearing, there are no moment components, and therefore, only eight dynamic coefficients are sufficient to represent its dynamic behaviour. These coefficients are defined below.

The expressions for dynamic coefficients are given by :

$$\begin{bmatrix} \delta\bar{W}_x \\ \delta\bar{W}_z \\ \delta\bar{M}_x \\ \delta\bar{M}_z \end{bmatrix} = \begin{bmatrix} -\partial\bar{W}_x/\partial\bar{X} & -\partial\bar{W}_x/\partial\bar{Z} & -\partial\bar{W}_x/\partial\bar{\gamma}_x & -\partial\bar{W}_x/\partial\bar{\gamma}_z \\ -\partial\bar{W}_z/\partial\bar{X} & -\partial\bar{W}_z/\partial\bar{Z} & -\partial\bar{W}_z/\partial\bar{\gamma}_x & -\partial\bar{W}_z/\partial\bar{\gamma}_z \\ -\partial\bar{M}_x/\partial\bar{X} & -\partial\bar{M}_x/\partial\bar{Z} & -\partial\bar{M}_x/\partial\bar{\gamma}_x & -\partial\bar{M}_x/\partial\bar{\gamma}_z \\ -\partial\bar{M}_z/\partial\bar{X} & -\partial\bar{M}_z/\partial\bar{Z} & -\partial\bar{M}_z/\partial\bar{\gamma}_x & -\partial\bar{M}_z/\partial\bar{\gamma}_z \end{bmatrix} \begin{bmatrix} \bar{X} \\ \bar{Z} \\ \bar{\gamma}_x \\ \bar{\gamma}_z \end{bmatrix}$$

$$+ \begin{bmatrix} -\partial\bar{W}_x/\partial\dot{\bar{X}} & -\partial\bar{W}_x/\partial\dot{\bar{Z}} & -\partial\bar{W}_x/\partial\dot{\bar{\gamma}}_x & -\partial\bar{W}_x/\partial\dot{\bar{\gamma}}_z \\ -\partial\bar{W}_z/\partial\dot{\bar{X}} & -\partial\bar{W}_z/\partial\dot{\bar{Z}} & -\partial\bar{W}_z/\partial\dot{\bar{\gamma}}_x & -\partial\bar{W}_z/\partial\dot{\bar{\gamma}}_z \\ -\partial\bar{M}_x/\partial\dot{\bar{X}} & -\partial\bar{M}_x/\partial\dot{\bar{Z}} & -\partial\bar{M}_x/\partial\dot{\bar{\gamma}}_x & -\partial\bar{M}_x/\partial\dot{\bar{\gamma}}_z \\ -\partial\bar{M}_z/\partial\dot{\bar{X}} & -\partial\bar{M}_z/\partial\dot{\bar{Z}} & -\partial\bar{M}_z/\partial\dot{\bar{\gamma}}_x & -\partial\bar{M}_z/\partial\dot{\bar{\gamma}}_z \end{bmatrix} \begin{bmatrix} \dot{\bar{X}} \\ \dot{\bar{Z}} \\ \dot{\bar{\gamma}}_x \\ \dot{\bar{\gamma}}_z \end{bmatrix}$$

------ (3.36)

or,

$$\begin{bmatrix} \delta \bar{W}_x \\ \delta \bar{W}_z \\ \delta \bar{M}_x \\ \delta \bar{M}_z \end{bmatrix} = \begin{bmatrix} \bar{S}_{xx} & \bar{S}_{xz} & \bar{S}_{x\dot{\gamma}} & \bar{S}_{x\dot{\gamma}} \\ \bar{S}_{zx} & \bar{S}_{zz} & \bar{S}_{z\dot{\gamma}} & \bar{S}_{z\dot{\gamma}} \\ \bar{S}_{x\dot{\gamma}_x} & \bar{S}_{x\dot{\gamma}_z} & \bar{S}_{\dot{\gamma}_x\gamma_x} & \bar{S}_{\dot{\gamma}_x\gamma_z} \\ \bar{S}_{z\dot{\gamma}_x} & \bar{S}_{z\dot{\gamma}_z} & \bar{S}_{\dot{\gamma}_z\gamma_x} & \bar{S}_{\dot{\gamma}_z\gamma_z} \end{bmatrix} \begin{bmatrix} \bar{X} \\ \bar{Z} \\ \bar{\gamma}_x \\ \bar{\gamma}_z \end{bmatrix} + \begin{bmatrix} \bar{B}_{xx} & \bar{B}_{xz} & \bar{B}_{x\dot{\gamma}} & \bar{B}_{x\dot{\gamma}} \\ \bar{B}_{zx} & \bar{B}_{zz} & \bar{B}_{z\dot{\gamma}} & \bar{B}_{z\dot{\gamma}} \\ \bar{B}_{x\dot{\gamma}_x} & \bar{B}_{x\dot{\gamma}_z} & \bar{B}_{\dot{\gamma}_x\gamma_x} & \bar{B}_{\dot{\gamma}_x\gamma_z} \\ \bar{B}_{z\dot{\gamma}_x} & \bar{B}_{z\dot{\gamma}_z} & \bar{B}_{\dot{\gamma}_z\gamma_x} & \bar{B}_{\dot{\gamma}_z\gamma_z} \end{bmatrix} \begin{bmatrix} \dot{\bar{X}} \\ \dot{\bar{Z}} \\ \dot{\bar{\gamma}}_x \\ \dot{\bar{\gamma}}_z \end{bmatrix} \quad \text{------ (3.37)}$$

Equation (3 36) is combined with the equations (3.33) and (3.34) to convert the load and moment components into pressure derivatives for determining the values of dynamic coefficients.

3.5 STABILITY ANALYSIS

The journal of a hydrodynamic bearing, if disturbed from its static equilibrium position, experiences changes in the hydrodynamic forces and moments acting on it. This disturbs the equilibrium of the journal and induces free translatory and conical whirl in the journal. The dynamic behaviour of a journal bearing system under these conditions can be studied by integrating the resulting nonlinear equations of motion for the disturbed journal.

The technique of linearization, as described below, is found to be quite good to deal with this type of problem, especially when the disturbance is confined to close proximity of the static equilibrium position.

3.5.1 Linearized Equation of Motion and Stability Margin

The equations of disturbed motion of the journal for free translatory whirl are as follows

$$[\bar{M}_J] \begin{Bmatrix} \ddot{\bar{X}} \\ \ddot{\bar{Z}} \end{Bmatrix} = \begin{Bmatrix} \delta \bar{W}_x \ (\bar{X}, \bar{Z}, \dot{\bar{X}}, \dot{\bar{Z}}) \\ \delta \bar{W}_z \ (\bar{X}, \bar{Z}, \dot{\bar{X}}, \dot{\bar{Z}}) \end{Bmatrix} \quad \text{----- (3.38)}$$

where

$[\bar{M}_J]$ is the diagonal mass matrix;

$\ddot{\bar{X}}$, $\ddot{\bar{Z}}$ are the components of acceleration in x and z-directions;

$\delta \bar{W}_x$, $\delta \bar{W}_z$ are the components of the out of balance force on the journal in x and z-directions; respectively.

$\delta \bar{W}_x$ and $\delta \bar{W}_z$ depend on the instantaneous position and velocity of the journal centre and are usually non-linear functions of $\bar{X}$, $\bar{Z}$, $\dot{\bar{X}}$ and $\dot{\bar{Z}}$. However, within close proximity of the equilibrium position of the journal, hydrodynamic forces may be assumed to be linear functions of $\bar{X}$, $\bar{Z}$, $\dot{\bar{X}}$ and $\dot{\bar{Z}}$.

Stiffness and damping coefficients, computed using the equations (3.36 - 3.37), may now be considered invariant in the small proximity of the equilibrium position and the equation (3.36) can be written as :

$$\bar{M}_J \ddot{\bar{X}} + \bar{B}_{xx} \dot{\bar{X}} + \bar{B}_{xz} Z + \bar{S}_{xx} \bar{X} + \bar{S}_{xz} \bar{Z} = 0 \qquad \text{------ (3.39a)}$$

$$\bar{M}_J \ddot{\bar{Z}} + \bar{B}_{zx} \dot{\bar{X}} + \bar{B}_{zz} Z + \bar{S}_{zx} \bar{X} + \bar{S}_{zz} \bar{Z} = 0 \qquad \text{------ (3.39b)}$$

The characteristic equation for the linearized equation of motion is a quadratic polynomial equation of the following form :

$$\sigma^4 + A_1 \sigma^3 + A_2 \sigma^2 + A_3 \sigma + A_4 = 0 \qquad \text{------ (3.40)}$$

where σ is a complex variable, and

A_1, A_2, A_3, A_4 are functions of the journal mass, $\bar{M}_J$ and the dynamic coefficients. Using the characteristic equation (3.40) and Routh's criteria, the stability margin of the journal bearing system, in terms of critical mass $\bar{M}_C$, is obtained. The journal speed at the threshold of instability of the journal bearing system is called the instability threshold speed or simply threshold speed and is determined by :

$$\bar{\Omega} = \frac{\Omega}{\omega_n} = \sqrt{(\bar{M}_C / \bar{W})} \qquad \text{------ (3.41)}$$

and

$$\bar{M}_C = \frac{K_1}{\bar{\nu}^2} \qquad \text{------ (3.42)}$$

where $\bar{\nu}$ is defined as the whirl frequency ratio.

$$K_1 = \frac{\bar{S}_{xx} \bar{B}_{zz} + \bar{S}_{zz} \bar{B}_{xx} - \bar{S}_{xz} \bar{B}_{zx} - \bar{S}_{zx} \bar{B}_{xz}}{\bar{B}_{xx} + \bar{B}_{zz}} \qquad \text{------ (3.43)}$$

$$\bar{\nu}^2 = \frac{(\bar{S}_{xx} - K_1)(\bar{S}_{zz} - K_1) - \bar{S}_{xz}\,\bar{S}_{zx}}{\bar{B}_{xx}\,\bar{B}_{zz} - \bar{B}_{xz}\,\bar{B}_{zx}} \qquad \text{------ (3.44)}$$

and

$$\omega_n = \sqrt{(g / c)} \qquad \text{------ (3.45)}$$

ν is called whirl frequency ratio of the journal bearing system for free translatory whirl.

A journal bearing system is asymptotically stable when the journal mass $\bar{M}_J$ is less than $\bar{M}_C$. Likewise, a system is asymptotically stable when operating speed of the journal is less than the threshold speed, Ω. A negative value of $\bar{M}_C$ indicates that the journal bearing system will be stable for all the values of journal mass $\bar{M}_J$. Similarly, a negative value of $\bar{\nu}^2$ implies the absence of whirl.

3.5.2. Journal Centre-Motion Trajectory

Equations (3.39) can be integrated to give the displacement and velocity components of instantaneous journal centre position. The locus of the instantaneous journal centre position, as the bearing responds to a given initial disturbance, can be traced by repetitively integrating the governing equations of motion. This locus is known as the journal centre motion trajectory. For simplicity, it will be referred to as "linear trajectory". At any time $\bar{t}$, the equation (3.39) is written as :

$$[\,\bar{M}_J\,] \begin{Bmatrix} \ddot{\bar{X}} \\ \ddot{\bar{Z}} \end{Bmatrix}_{\bar{t}} = \begin{Bmatrix} \delta\,\bar{W}_x \\ \delta\,\bar{W}_z \end{Bmatrix}_{\bar{t}} = \begin{bmatrix} \bar{S}_{xx} & \bar{S}_{xz} & \bar{B}_{xx} & \bar{B}_{xz} \\ \bar{S}_{zx} & \bar{S}_{zz} & \bar{B}_{zx} & \bar{B}_{zz} \end{bmatrix} \begin{Bmatrix} \bar{X} \\ \bar{Z} \\ \dot{\bar{X}} \\ \dot{\bar{Z}} \end{Bmatrix}_{\bar{t}} \qquad \text{------ (3.46)}$$

where the subscript $\bar{t}$ refers to the instantaneous values and the stiffness and damping coefficients ($\bar{S}_{xx}$, $\bar{S}_{xz}$, $\bar{S}_{zx}$, $\bar{S}_{zz}$, $\bar{B}_{xx}$, $\bar{B}_{xz}$, $\bar{B}_{zx}$, $\bar{B}_{zz}$) are evaluated at the static equilibrium position of the journal centre.

The second order equations (3.46) is written in the first order form by defining $\bar{X} = \bar{X}_1$, $\bar{Z} = \bar{X}_2$, $\dot{\bar{X}} = \bar{X}_3$, $\dot{\bar{Z}} = \bar{X}_4$ as :

$$\left\{\begin{matrix}\dot{\bar{X}}_1\\ \dot{\bar{X}}_2\\ \dot{\bar{X}}_3\\ \dot{\bar{X}}_4\end{matrix}\right\}_{\bar{t}} = \left\{\begin{matrix}\bar{X}_3\\ \bar{X}_4\\ \delta\ \bar{W}_x / \bar{M}_J\\ \delta\ \bar{W}_z / \bar{M}_J\end{matrix}\right\}_{\bar{t}} = \left[\begin{matrix}0 & 0 & 1 & 0\\ 0 & 0 & 0 & 1\\ -\bar{S}_{xx}/\bar{M}_J & -\bar{S}_{xz}/\bar{M}_J & -\bar{B}_{xx}/\bar{M}_J & -\bar{B}_{xz}/\bar{M}_J\\ -\bar{S}_{zx}/\bar{M}_J & -\bar{S}_{zz}/\bar{M}_J & -\bar{B}_{zx}/\bar{M}_J & -\bar{B}_{zz}/\bar{M}_J\end{matrix}\right] \left\{\begin{matrix}\bar{X}_1\\ \bar{X}_2\\ \bar{X}_3\\ \bar{X}_4\end{matrix}\right\}_{\bar{t}}$$

------ (3.47)

Equations (3.47) are numerically integrated using the fourth order Runge-Kutta method to obtain the displacement and velocity components of the journal at time $\bar{t} + \delta\ \bar{t}$ in terms of the known values at time $\bar{t}$. This gives a linear trajectory.

****

CHAPTER - IV

SOLUTION PROCEDURE

4.1. INTRODUCTION

The governing system equations developed in the previous chapter for the thermohydrodynamic analysis of journal bearings have been solved using a personal computer of the type "Pentium PC (166 MHz)". The computer program is written in FORTRAN-77 and it requires a computer memory of about 500 kB. This chapter presents the strategy adopted to find the matched solutions of the lubrication (Reynolds), energy and heat conduction equations to establish fluid-film pressure field. Also, the solution scheme for plotting linearised journal-centre motion trajectories is discussed.

Since the solution procedure involves various iterative stages, the convergence criterion for each stage is also given in this chapter. The methods adopted to achieve a faster rate of convergence of the direct iteration schemes for the coupled problems have also been discussed

The developed program is general and can be used to obtain IHD as well as THD solutions for a specified eccentricity ratio or a given vertical load.

4.2. SOLUTION SCHEME FOR MAIN PROGRAM

The pressure field, attitude angle and components of fluid-film reaction ($\bar{W}x$, $\bar{W}z$) satisfying vertical load support for a specified eccentricity ratio/given vertical load are established using three nested loops as shown in Fig. 4.1. Outside the outer loop, all the temperatures are set equal to the reference temperature and the non-dimensional viscosity functions are then calculated. The Reynolds equation is solved and attitude angle is modified to satisfy the condition of vertical load support in the inner loop (index J). The middle loop (index K) is used to obtain thermal solution. This loop can, however, be skipped by setting the value of index NTEMP to 0. The value of the eccentricity ratio required for the given load $\bar{W}$ is found in the outer loop (index I). This loop may also be skipped by setting NWZ = 0 for solving the problem for the specified eccentricity ratio.

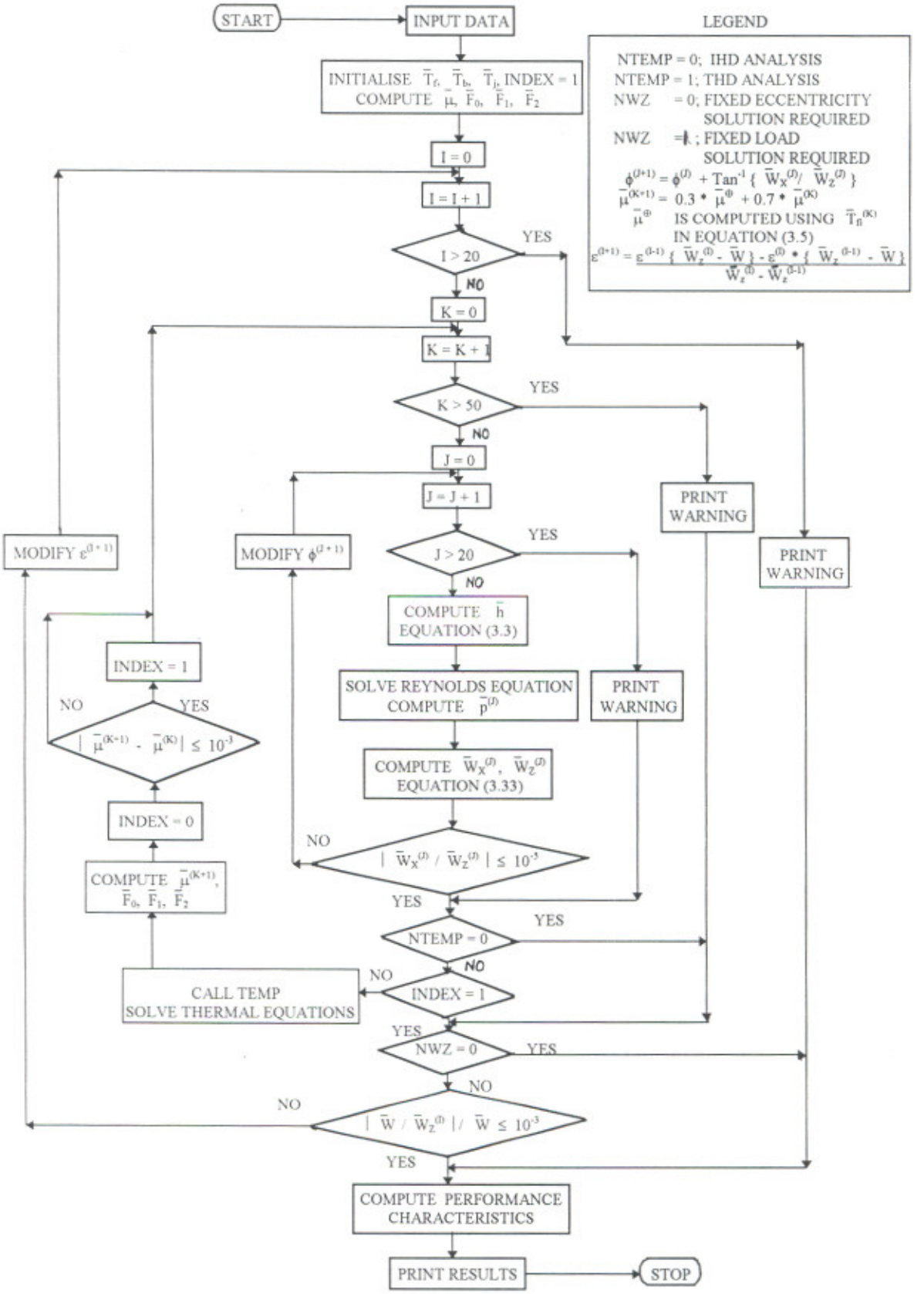

Fig. 4.1 SOLUTION SCHEME FOR MAIN PROGRAM

The solution of Reynolds equation is obtained by using Linear Complementarity Problem (LCP) approach described by Chandrawat et al.[20] in this inner loop. For termination of this inner loop, two criteria have been used. The first criterion is concerned with the convergence of solution according to which the horizontal component of film reaction must become diminishingly small in comparison with the vertical component. In the *J th* iteration, the horizontal ($\bar{W}x^{(J)}$) and vertical ($\bar{W}z^{(J)}$) components of the fluid film reactions are computed using equation (3.33). When the condition

$$| \bar{W}x^{(J)} / \bar{W}z^{(J)} | \leq 0.00001 \qquad \text{------ (4.1.)}$$

is satisfied, the solution is considered to have converged and the iterations are terminated otherwise the attitude angle, φ is modified using the equation (4.2) given below :

$$\phi^{(J+1)} = \phi^{(J)} + \tan^{-1} (\bar{W}_x^{(J)} / \bar{W}z^{(J)}) \qquad \text{------ (4.2)}$$

The loop is also terminated when the number of iterations exceeds 20.

When a thermohydrodynamic analysis is to be performed, the index NTEMP is set equal to 1. This allows the control to pass to the middle loop. For finding the solution of energy and heat conduction equations, the subroutine TEMP is called in this loop with the iteration number of the middle loop as its argument. This subroutine returns the computed temperature fields for lubricant, bush and journal. Oil viscosity is then computed using the following relation {equation (3.5)} :

$$\bar{\mu}^{(K+1)} = Wt_v \cdot \frac{e^{b.\{T_f^{(K)} + 273.12\}^{-a}}}{\mu_o} - 0.8 + (1 - Wt_v) \cdot \bar{\mu}^{(K)} \qquad \text{------ (4.3)}$$

In the above relation Wt_v is the weighting factor and its value as 0.3 is found to be quite good for the solution of all problems considered in this work. The middle loop is terminated when the following condition is satisfied at every node of the fluid-film :

$$| \bar{\mu}^{(K+1)} - \bar{\mu}^{(K)} | \leq 0.001 \qquad \text{------ (4.4)}$$

As noted earlier, the outer loop is used to modify the eccentricity ratio for getting the solution corresponding to a given load. When NWZ = 1, this loop is executed and when the following convergence criteria is satisfied, the loop is terminated.

$$| \bar{W} - \bar{W}_Z^{(I)} | / \bar{W} \leq 0.001 \qquad \text{------ (4.5)}$$

If the convergence is not achieved and the value of loop index I is less than 20, the eccentricity is modified using the following relations :

When $I \geq 2$;

$$\varepsilon^{(I+1)} = \{\varepsilon^{(I-1)} (\bar{W}_Z^{(I)} - \bar{W}) - \varepsilon^{(I)} (\bar{W}_Z^{(I-1)} - \bar{W})\} / (\bar{W}_Z^{(I)} - \bar{W}_Z^{(I-1)}) \qquad \text{------ (4.6a)}$$

When $I = 1$;

$$\varepsilon^{(2)} = \varepsilon^{(1)} + 0.01, \quad \text{for } \bar{W}_Z^{(1)} < \bar{W} \qquad \text{------ (4.6b)}$$

$$\varepsilon^{(2)} = \varepsilon^{(1)} - 0.01, \quad \text{for } \bar{W}_Z^{(1)} > \bar{W} \qquad \text{------ (4.6c)}$$

4.3 SOLUTION SCHEME FOR SUBROUTINE TEMP

The solution scheme for subroutine TEMP is shown in Fig. 4.2. In this subroutine, the solutions of the energy equation for fluid-film and heat conduction equations for the bush-housing assembly and the journal are obtain. The solution scheme is once again an iterative one using two loops. In the inner loop, the solutions of energy equation for fluid-film and heat conduction equation for the bush-housing assembly is obtained to yield temperature fields for these domains corresponding to a specified journal temperature field. Using the established fluid-film temperatures in the inner loop, the journal temperature field is computed in the outer loop. On the termination of the outer loop, the subroutine returns the established temperature fields for fluid-film, bush-housing assembly and the journal.

Pressure field established in the inner loop and the iteration number of the middle loop (called INDEX in this section) of the main program are used as input to subroutine TEMP. Using the pressure field, velocity components {equations (3.16), (3.17) and (3.18)} are computed at each node of the discretised fluid-film. Contraction coefficients, C_L are then obtained using these velocity components. These values are held constant during the execution of the two loops referred above.

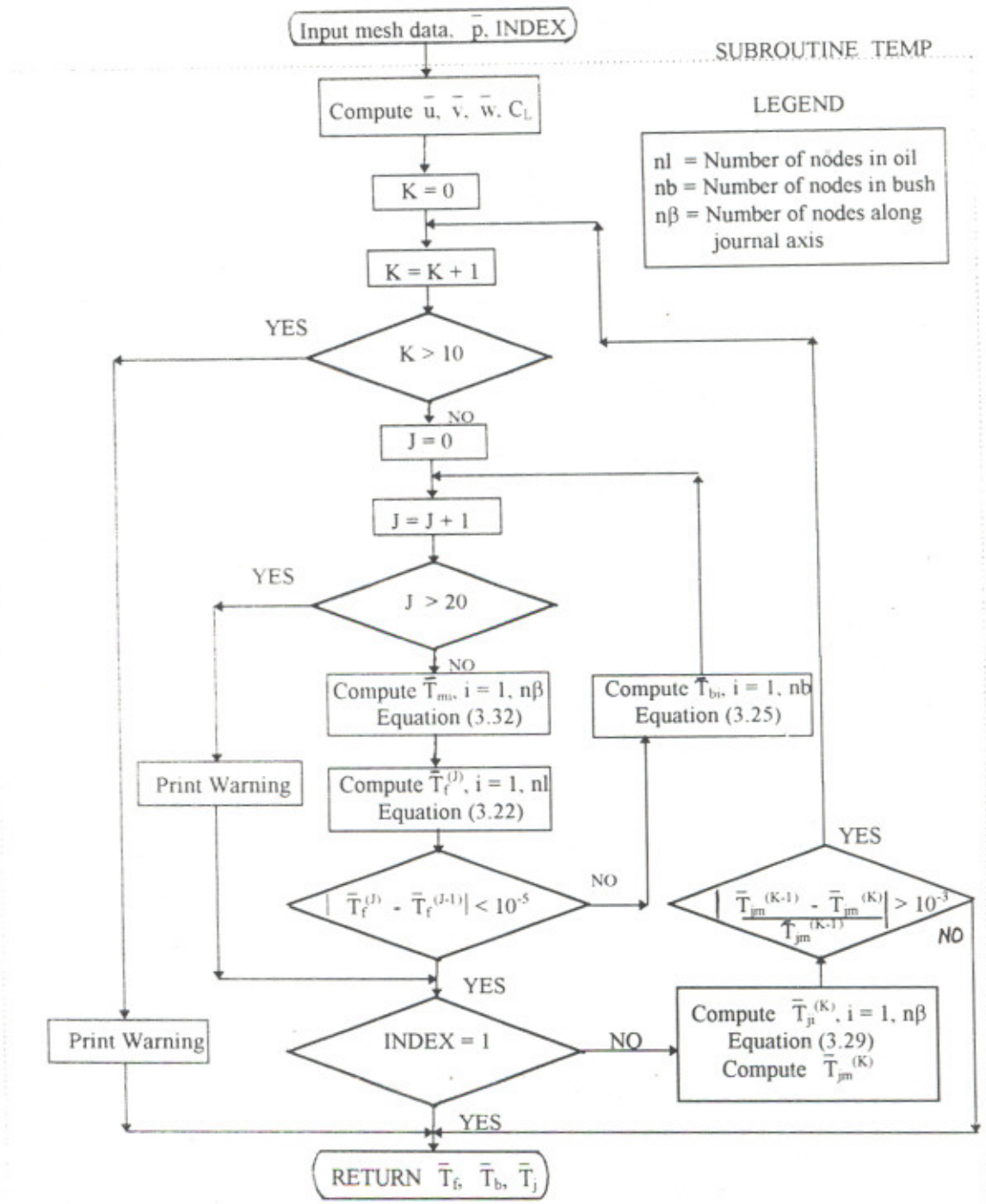

Fig. 4.2 SOLUTION SCHEME FOR SUBROUTINE TEMP

In the inner loop (index J), fluid-film temperatures are computed at every node using equation (3.22). A check is then made for convergence of the loop according to the following criterion at every node :

$$| \bar{T}_f^{(J)} - \bar{T}_f^{(J-1)} | \leq 0.00001 \qquad \text{------ (4.7)}$$

If this condition is satisfied at every node, the inner loop is terminated otherwise the heat conduction equation for the bush-housing assembly, equation (3.25), is solved using the Successive Over Relaxation approach. In the solution of heat conduction equation, the temperature in the *m th* iteration is computed using a over relaxation factor, $W_{OR} = 1.9105$ as follows :

$$\bar{T}_b^{(m)} = (1 - W_{OR}) \bar{T}_b^{(m-1)} + W_{OR} \bar{T}_b^{(m)} \qquad \text{------ (4.8)}$$

where $\bar{T}_b^{(m)}$ on the right hand side is computed using equation (3.25).

Since the temperature gradient of the fluid-film at the bush-fluid interface acts as an input for the solution of heat conduction equation, its weighted value, defined below, is used to obtain a converged solution :

$$\left(\frac{\partial \bar{T}_f^{(J)}}{\partial \bar{z}}\right)_{\text{weighted}} = Wt_I \left(\frac{\partial \bar{T}_f^{(J)}}{\partial \bar{z}}\right) + (1 - Wt_I) \left(\frac{\partial \bar{T}_f^{(J-1)}}{\partial \bar{z}}\right)_{\text{weighted}} \qquad \text{------ (4.9)}$$

The value of weight $Wt_I = 0.2$ was used and $\left(\frac{\partial \bar{T}_f^{(0)}}{\partial \bar{z}}\right)$ was assumed zero at every node on the interface.

The modified bush temperature field, $\bar{T}_b^{(J)}$ was then used to recompute the fluid-film temperatures in the *(J + 1) th* iteration and the iterations were continued till, either the converged solution was obtained as per criterion {equation (4.7)} or value of J exceeds 20.

On the termination of the inner loop, the control enters the outer loop (index K). In this loop, a check is first made for the value of INDEX. If the INDEX = 1, the outer loop is skipped i.e. journal temperature is not modified. This step greatly improves the overall convergence of the scheme for the THD solution. When INDEX > 1, the journal temperature distribution is computed using equation (3.29) with a over relaxation factor of 1.9105, same as used for the bush-housing assembly. For the convergence of this loop, a criterion based on the mean journal temperature is used as below :

$$\left| \frac{\bar{T}_{jm}^{(K)} - \bar{T}_{jm}^{(K-1)}}{\bar{T}_{jm}^{(K-1)}} \right| \leq 0.001 \qquad \text{------ (4.10)}$$

where

$$\bar{T}_{jm}^{(K)} = \sum_{i=1}^{n\beta+1} \bar{T}_{ji}^{(K)} / (n\beta + 1)$$

$$\bar{T}_{jm}^{(K-1)} = \sum_{i=1}^{n\beta+1} \bar{T}_{ji}^{(K-1)} / (n\beta + 1)$$

This loop is also terminated when the value of K exceeds 10 in the event the solution is not converged.

4.4 SOLUTION SCHEME FOR LINEAR TRAJECTORIES

A trajectory of a journal centre motion can be obtained for a given initial disturbance by numerically integrating the governing equations of motion using fourth-order Runge-Kutta method. This particular method is preferred for the present investigation owing to its accuracy and self starting nature. The scheme for the trajectories is shown in Fig. 4.3.

For a given external load, the values of stiffness coefficients ($\bar{S}_{xx}$, $\bar{S}_{xz}$, $\bar{S}_{zx}$, $\bar{S}_{zz}$), and damping coefficients ($\bar{B}_{xx}$, $\bar{B}_{xz}$, $\bar{B}_{zx}$, $\bar{B}_{zz}$) and critical mass ($\bar{M}_C$) are first determined after establishing the static equilibrium position and pressure field by using the scheme for main program, Fig. 4.1. These values are given as input for the determination of trajectories. In addition, the journal mass, $\bar{M}_J$, the time interval $\delta \bar{t}$ and the initial values of disturbance ($\bar{X}_o$, $\bar{Z}_o$, $\dot{\bar{X}}_o$, $\dot{\bar{Z}}_o$), denoted respectively by $\bar{X}_1$, $\bar{X}_2$, $\bar{X}_3$, and $\bar{X}_4$, are also given as input. The solution of equation (3.47) then yields the point on the trajectory.

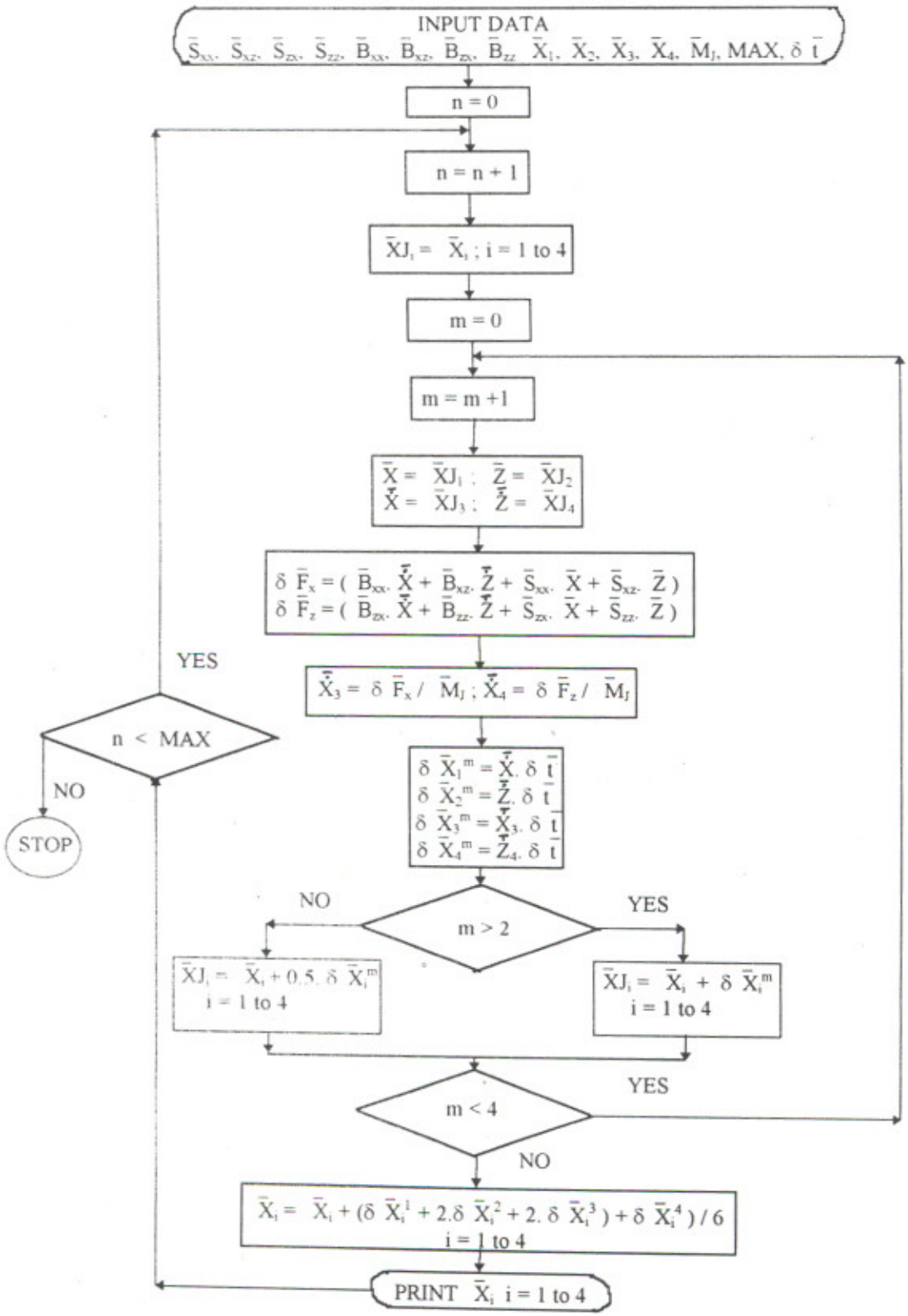

Fig. 4.3 SOLUTION SCHEME FOR LINEAR TRAJECTORIES

CHAPTER - V

RESULTS AND DISCUSSION

5.1 INTRODUCTION

This chapter presents the results obtained using the analysis and solution algorithms discussed in the previous chapters. The chapter has been organized in the following manner: first of all the analysis and computer programs have been validated by comparing the present results with the published theoretical / experimental results; then the results for four journal bearing configurations, namely, plain, two-axial-groove, elliptical, and three-lobe, are presented and discussed; next the journal center trajectories for transient response of some bearing configurations obtained from the linearized analysis have been presented; and in the end some parametric studies have been presented. In general, the presented results consist of (i) static performance characteristics (ii) Stiffness coeffcients (iii) Damping coeffcients (iv) Stability parameters (v) iso-pressure curves and pressure profiles and (vi) isotherms and temperature profiles. In the analysis, the lubricant has been assumed to be thermo-viscous and the bearings are considered to be operating in the laminar-flow regime. As the present work concerns mainly with the study of the effect of misalignment on the performance of the above types of journal bearings operating under thermohydrodynamic lubrication conditions, the results have been presented in such a manner so as to bring out this effect clearly. However, for ready reference results for aligned bearings have also been given.

5.2 VALIDITY OF RESULTS

It is already mentioned in Chapter II that the THD analyses of misaligned bearings has been scantly reported in literature. Therefore, to establish the validity of the approach of present study following strategy has been adopted :

- IHD performance characteristics of aligned two-axial-groove, elliptical and three-lobe journal bearings have been compared with the published results.
- IHD performance characteristics of misaligned plain and two-axial-groove journal bearings have been compared with the published results.

- The THD performance characteristics of aligned plain journal bearing and two-axial-groove journal bearing have been compared with the published experimental / theoretical results.
- Some parameters from the THD analysis of misaligned plain journal bearing have been compared with the available published results.

These comparisons are presented and discussed in the following sub-sections.

5.2.1 Validity of IHD Results

The static and dynamic performance characteristics of three bearing configurations, namely, two-axial-groove, elliptical and three-lobe, operating with iso-viscous lubricant have been obtained and compared with the published results of Lund and Thomsen [15] in Table 5.1. The comparison of results is quite good.

For the validity of results of misaligned journal bearings, the results for plain journal bearing with three different set of values of misalignment parameters (defined in Fig. 5.1) are compared with the published data of Jakeman [42] in Table 5.2. Likewise, the results for a two-axial-groove journal bearing are compared with the published data of Qiu and Tieu[51] in Tables 5.3 to 5.5. These results indicate very good agreement.

5.2.2 Validity of THD Results [1]

As noted earlier, the main objective of the present work is to carry out THD analyses of various types of bearing configurations operating under misaligned conditions. Therefore, to validate the present work a more appropriate approach would have been to conduct experimental investigations on these bearings and use the experimental results for validating the theoretical results from the present analysis. Since the experimental work was outside the scope of the present work, a detailed comparison has been made of the THD results for aligned plain and two-axial-groove journal bearings and that for the misaligned plain journal bearing. As a complete three-dimensional analysis has been carried out, it is expected that this approach will adequately validate the thermal analysis for aligned as well as misaligned journal bearings.

In the following, these comparisons are presented and discussed. However, before a detailed analysis of these comparisons is presented, it is considered necessary to discuss the two different thermal boundary conditions examined in this work.

---

[1] Paper given at ref.[102] was published from this part of the work.

Table 5.1 Comparison of Static and Dynamic Performance Characteristics of Two-Axial-Groove, Elliptical and Three-Lobe Journal Bearings
L/D = 1

	Two-Axial-Groove		Elliptical		Three-Lobe	
	1*	2*	1*	2*	1*	2*
ε	0.650	0.650	0.250	0.250	0.246	0.246
ϕ	39.6	39.720	88.4	88.28	59.5	59.460
$\bar{W}$	5.8084	5.895	2.8095	2.842	3.4743	3.517
$\bar{S}_{xx}$	7.61	8.489	2.27	2.330	7.10	7.351
$\bar{S}_{xz}$	1.86	1.356	9.53	9.748	9.37	9.637
$\bar{S}_{zx}$	- 20.78	-19.689	- 12.26	- 12.817	- 15.29	- 15.792
$\bar{S}_{zz}$	20.64	20.338	19.62	19.752	18.89	19.028
$\bar{B}_{xx}$	9.27	8.430	10.61	10.970	16.18	16.636
$\bar{B}_{xz} = \bar{B}_{zx}$	- 8.33	- 10.139	7.29	7.247	- 2.24	- 2.568
$\bar{B}_{zz}$	42.77	40.617	37.66	39.049	38.16	39.393

1* : Present Work
2* : Reference [15]

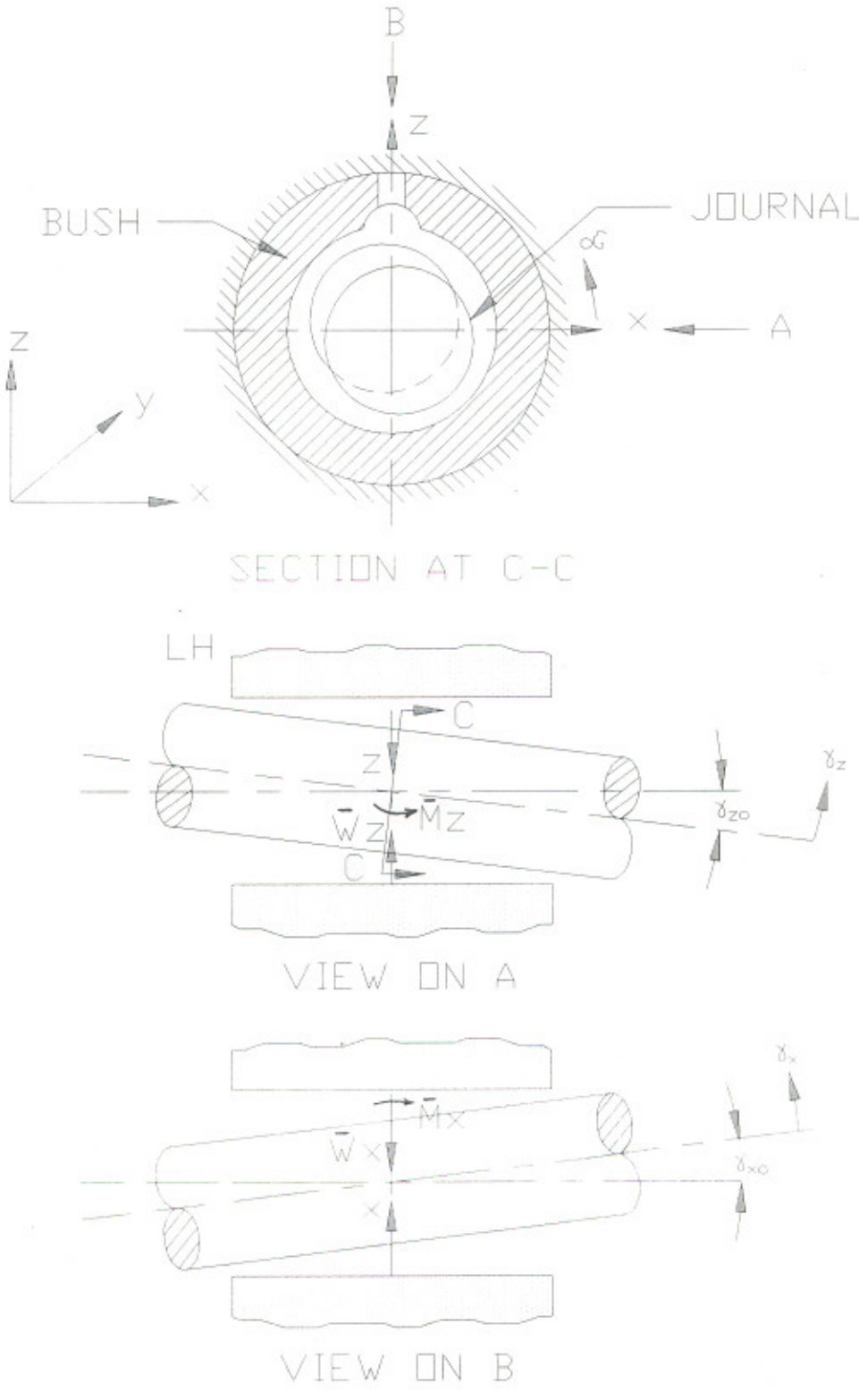

Fig. 5.1 GEOMETRICAL PARAMETER FOR PLAIN MISALIGNED JOURNAL BEARING

Table 5.2 Comparison of dimensionless oil-film parameters of a misaligned plain journal bearing - IHD analysis

Bearing 150° Partial arc and L / D = 0.5

ε	0.9		0.8		0.6	
γ_x	0.0		0.5		0.5	
γ_z	0.0		0.0		-0.5	
	1*	2*	1*	2*	1*	2*
$\bar{W}$	9.99	10.05	3.88	3.97	1.32	1.42
ϕ deg	22.10	22.10	25.70	25.29	34.70	32.83
$\bar{S}_{xx}$	15.15	15.52	7.48	7.92	2.27	2.81
$\bar{S}_{xz}$	-11.08	-11.10	-3.04	-3.51	-0.47	-0.94
$\bar{S}_{zx}$	-54.74	-55.76	-19.81	-20.84	-5.76	-6.97
$\bar{S}_{zz}$	137.59	139.14	33.71	35.53	7.67	9.43
$\bar{S}_{x\gamma_x}$	0.0	0.0	1.36	1.56	0.48	0.74
$\bar{S}_{x\gamma_z}$	0.0	0.0	-1.37	-1.66	-0.26	-0.58
$\bar{S}_{z\gamma_x}$	0.0	0.0	-2.98	-3.31	-1.07	-1.60
$\bar{S}_{z\gamma_z}$	0.0	0.0	4.11	4.19	1.34	2.21
$\bar{S}_{\gamma_x x}$	0.0	0.0	1.41	1.59	0.52	0.72
$\bar{S}_{\gamma_x z}$	0.0	0.0	-1.45	-1.69	-0.35	-0.53
$\bar{S}_{\gamma_z x}$	0.0	0.0	-2.98	-3.45	-1.14	-1.60
$\bar{S}_{\gamma_z z}$	0.0	0.0	3.70	4.86	1.54	2.15
$\bar{S}_{\gamma_x \gamma_x}$	0.68	0.68	0.50	0.59	0.17	0.27
$\bar{S}_{\gamma_x \gamma_z}$	-0.58	-0.58	-0.34	-0.44	-0.09	-0.20
$\bar{S}_{\gamma_z \gamma_x}$	-2.17	-2.16	-1.04	-1.21	-0.35	-0.56
$\bar{S}_{\gamma_z \gamma_z}$	6.39	6.43	1.85	2.12	0.51	0.82
$\bar{B}_{xx}$	6.68	7.08	4.55	4.62	1.75	2.01
$\bar{B}_{xz}$	-16.44	-18.08	-7.33	-7.36	-2.19	-2.62
$\bar{B}_{zx}$	-16.44	-17.38	-7.33	-7.40	-2.19	-2.60
$\bar{B}_{zz}$	99.40	103.47	33.57	34.33	9.65	10.99
$\bar{B}_{x\gamma_x}$	0.0	0.0	0.75	0.77	0.30	0.38
$\bar{B}_{x\gamma_z}$	0.0	0.0	-1.47	-1.64	-0.53	-0.73
$\bar{B}_{z\gamma_x}$	0.0	0.0	-1.61	-1.54	-0.56	-0.70
$\bar{B}_{z\gamma_z}$	0.0	0.0	2.82	1.67	1.43	0.76
$\bar{B}_{\gamma_x x}$	0.0	0.0	0.75	0.76	0.30	0.40
$\bar{B}_{\gamma_x z}$	0.0	0.0	-1.61	-1.55	-0.56	-0.72
$\bar{B}_{\gamma_z x}$	0.0	0.0	-1.47	-1.67	-0.53	-0.76
$\bar{B}_{\gamma_z z}$	0.0	0.0	2.82	3.0	1.43	1.88
$\bar{B}_{\gamma_x \gamma_x}$	0.27	0.27	0.27	0.28	0.11	0.15
$\bar{B}_{\gamma_x \gamma_z}$	-0.68	-0.70	-0.44	-0.46	-0.16	-0.24
$\bar{B}_{\gamma_z \gamma_x}$	-0.68	-0.68	-0.44	-0.46	-0.16	-0.24
$\bar{B}_{\gamma_z \gamma_z}$	3.35	3.38	1.27	1.34	0.45	0.61

1* : Present Work

2* : Reference [42]; data from this reference has been converted into present non-dimensional form.

Table 5.3 Comparison of Static Performance Characteristics of Two- Axial-Groove Journal Bearing - IHD analysis
L / D = 1 with 20° grooves

Load, $\bar{W}$	Minimum film thickness, $\bar{h}_{min}$				Attitude Angle, ϕ (Degrees)				Side Flow, $\bar{Q}_s$			
	$\bar{\gamma}_x = 0.0$ $\bar{\gamma}_z = 0.0$		$\bar{\gamma}_x = 0.2$ $\bar{\gamma}_z = 0.0$		$\bar{\gamma}_x = 0.0$ $\bar{\gamma}_z = 0.0$		$\bar{\gamma}_x = 0.2$ $\bar{\gamma}_z = 0.0$		$\bar{\gamma}_x = 0.0$ $\bar{\gamma}_z = 0.0$		$\bar{\gamma}_x = 0.2$ $\bar{\gamma}_z = 0.0$	
	1*	2*	1*	2*	1*	2*	1*	2*	1*	2*	1*	2*
0.45	0.89	0.89	0.695	0.70	75.4	75.0	70.1	68.5	0.125	0.13	0.133	0.13
0.64	0.85	0.85	0.656	0.66	70.5	70.0	66.5	65.5	0.171	0.18	0.172	0.18
1.27	0.72	0.73	0.546	0.54	59.7	60.0	57.3	57.0	0.290	0.30	0.285	0.28
2.55	0.55	0.55	0.395	0.40	50.1	50.0	48.3	49.0	0.435	0.44	0.425	0.42
3.82	0.45	0.45	0.305	0.30	44.9	45.0	43.2	43.0	0.515	0.48	0.503	0.48
6.37	0.33	0.34	0.204	0.21	38.9	40.0	37.1	37.0	0.603	0.52	0.585	0.50
12.73	0.20	0.21	0.102	0.10	31.6	32.0	29.4	30.0	0.691	0.55	0.666	0.53
19.10	0.15	0.16	0.062	-	27.9	27.5	25.3	26.0	0.727	0.56	0.696	0.55

Table 5.4 Comparison of Stability Parameters of Two-Axial-Groove Journal Bearing - IHD analysis
L / D = 1 with 20° grooves

Load, $\bar{W}$	Whirl Frequency Ratio, $\bar{\nu}$				Threshold Speed, $\bar{\Omega}$			
	$\bar{\gamma}_x = 0.0$ $\bar{\gamma}_z = 0.0$		$\bar{\gamma}_x = 0.2$ $\bar{\gamma}_z = 0.0$		$\bar{\gamma}_x = 0.0$ $\bar{\gamma}_z = 0.0$		$\bar{\gamma}_x = 0.2$ $\bar{\gamma}_z = 0.0$	
	1*	2*	1*	2*	1*	2*	1*	2*
0.45	0.500	0.50	0.497	0.50	2.091	2.10	2.191	2.2
0.64	0.501	0.50	0.499	0.50	2.097	2.10	2.163	2.2
1.27	0.506	0.505	0.502	0.50	2.108	2.10	2.169	2.2
2.55	0.508	0.51	0.495	0.49	2.110	2.10	2.211	2.3
3.82	0.495	0.49	0.472	0.48	2.162	2.15	2.327	2.4
6.37	0.445	0.45	0.394	0.40	2.406	2.40	2.838	2.8

1* : Present Work
2* : Reference [51]; results from this reference has been converted into present non-dimensional form.

Table 5.5 : Comparison of Dynamic Performance Characteristics of Two-Axial-Groove Journal Bearing - IHD analysis
L / D = 1 with 20° grooves

(i) Stiffness Coefficients

Load, $\bar{W}$	$\bar{S}_{xx}$				$\bar{S}_{xz}$				$\bar{S}_{zx}$				$\bar{S}_{zz}$			
	$\bar{\gamma}_x = 0.0$ $\bar{\gamma}_z = 0.0$		$\bar{\gamma}_x = 0.2$ $\bar{\gamma}_z = 0.0$		$\bar{\gamma}_x = 0.0$ $\bar{\gamma}_z = 0.0$		$\bar{\gamma}_x = 0.2$ $\bar{\gamma}_z = 0.0$		$\bar{\gamma}_x = 0.0$ $\bar{\gamma}_z = 0.0$		$\bar{\gamma}_x = 0.2$ $\bar{\gamma}_z = 0.0$		$\bar{\gamma}_x = 0.0$ $\bar{\gamma}_z = 0.0$		$\bar{\gamma}_x = 0.2$ $\bar{\gamma}_z = 0.0$	
	1*	2*	1*	2*	1*	2*	1*	2*	1*	2*	1*	2*	1*	2*	1*	2*
0.45	1.50	1.50	1.74	1.40	-2.89	-3.0	-3.14	-3.1	9.75	9.8	10.54	10.4	1.54	1.5	1.50	1.5
0.64	1.52	1.50	1.69	1.50	-2.16	-2.2	-2.31	-2.3	7.27	7.4	7.67	7.6	1.56	1.6	1.51	1.5
1.27	1.59	1.60	1.67	1.52	-1.39	-1.45	-1.42	-1.4	4.67	4.75	4.84	5.0	1.67	1.7	1.70	1.7
2.55	1.55	1.55	1.59	1.51	-0.82	-0.8	-0.79	-0.8	3.60	3.6	3.71	3.8	2.14	2.2	2.24	2.2
3.82	1.49	1.50	1.55	1.50	-0.51	-0.55	-0.47	-0.5	3.37	3.35	3.48	3.5	2.67	2.8	2.79	2.8
6.37	1.44	1.45	1.55	1.52	-0.17	-0.2	-0.10	-0.15	3.36	3.4	3.51	3.6	3.62	3.5	3.81	3.8
12.73	1.41	1.47	1.62	1.60	0.34	0.30	0.54	0.5	3.67	3.7	4.02	4.0	5.81	5.7	6.29	6.1
19.10	1.46	1.50	1.77	1.75	0.60	0.60	1.02	1.0	4.14	4.2	4.68	4.6	7.68	7.7	8.67	8.4

(ii) Damping Coefficients

Load, $\bar{W}$	$\bar{B}_{xx}$				$\bar{B}_{xz} = \bar{B}_{xz}$				$\bar{B}_{zz}$			
	$\bar{\gamma}_x = 0.0$ $\bar{\gamma}_z = 0.0$		$\bar{\gamma}_x = 0.2$ $\bar{\gamma}_z = 0.0$		$\bar{\gamma}_x = 0.0$ $\bar{\gamma}_z = 0.0$		$\bar{\gamma}_x = 0.2$ $\bar{\gamma}_z = 0.0$		$\bar{\gamma}_x = 0.0$ $\bar{\gamma}_z = 0.0$		$\bar{\gamma}_x = 0.2$ $\bar{\gamma}_z = 0.0$	
	1*	2*	1*	2*	1*	2*	1*	2*	1*	2*	1*	2*
0.45	5.90	6.15	6.57	6.5	1.53	1.50	1.85	1.5	19.57	19.50	20.98	21.0
0.64	4.50	4.60	4.91	4.9	1.59	1.55	1.82	1.6	14.63	14.70	15.34	15.1
1.27	3.11	3.00	3.24	3.1	1.82	1.75	1.86	1.75	9.50	9.70	9.78	9.9
2.55	2.22	2.30	2.25	2.3	1.86	1.80	1.82	1.8	7.41	7.50	7.53	7.6
3.82	1.78	1.80	1.81	1.8	1.78	1.75	1.75	1.75	6.95	7.00	7.05	7.0
6.37	1.39	1.40	1.46	1.5	1.72	1.65	1.71	1.7	6.90	7.05	6.99	7.0
12.73	0.96	1.05	1.05	1.1	1.55	1.60	1.58	1.65	7.32	7.50	7.52	7.5
19.10	0.87	0.85	0.95	0.9	1.64	1.65	1.63	1.7	8.14	8.10	8.28	8.3

1* : Present Work
2* : Reference [51]; results from this reference has been converted into present non-dimensional form.

5.2.2.1 Selection of Thermal Boundary Conditions : As mentioned above, two different thermal boundary conditions have been examined in this work. In the first of these boundary conditions (BC1), the temperature of lubricant at the inlet of a bearing lobe/pad is assumed to vary as a parabolic function of distance from the fluid-bush interface. The coefficients of the describing polynomial are determined by assuming fluid temperature at the fluid-bush interface to be equal to the bush temperature and that at the fluid-journal interface equal to the journal temperature. The third condition requires the determination of mean fluid temperature after accounting for mixing of re-circulating oil with the cool supply oil and then equating it to the mean of the assumed temperature distribution over the film thickness. For the determination of temperature field for the bush, heat conduction equation is solved after prescribing oil supply temperature at the bearing outer surface on the inlet edge of the lobe / pad.

The second thermal boundary conditions (BC2) assumes the bush temperature constant equal to the supply temperature at the radial inlet edge of lobe / pad, whereas the fluid temperature is assumed to vary as a cubic function of distance from the fluid-bush interface. The coefficients of the describing polynomial are obtained by assuming the temperature of the lubricant equal to that of bush at the bush-fluid interface, and that of the journal at the fluid-journal interface. The third condition assumes the continuity of heat flux at the bush-fluid interface and for the fourth condition, a mean temperature is obtained as in the case of BC1.

Fig. 5.2 shows the variation of maximum bush temperature obtained using the two boundary conditions with eccentricity ratio for two speeds (2000 and 4000 r.p.m.). It is seen from this figure that with BC2, the bush temperature distribution has a cup shape which is quite inconsistent when compared with the experimental results for the range of eccentricity ratio considered. Results from the first boundary conditions (BC1) do not show this trend. Also, the experiments indicate that the bush temperature at the inlet of the pad is higher than the supply temperature (Fig. 5.3), which is not possible with BC2. Therefore, the first boundary conditions (BC1) are more appropriate and have been used in this work throughout.

5.2.2.2 Plain Journal Bearing : Results obtained for a plain journal bearing are compared with the published experimental and theoretical works of Ferron et al [71], Figs. 5.2 to 5.5. The present results were obtained for two sets of data for thermal properties of bush-housing assembly. The operating conditions shown in Table 5.6 and the viscosity-temperature relation

Table 5.6 Operating Conditions

Journal Radius, R		= 0.05	m
External Bearing Radius, R_2		= 0.10	m
Bearing Length, L		= 0.08	m
Radial Clearance, c / R		= 0.0029	
Lubricant Viscosity at 40 °C		= 0.0277	Pa.s
Viscosity Coeffcients,	k_0	= 3.287	
	k_1	= 3.064	
	k_2	= 0.777	
Lubricant Density, ρ		= 860	Kg / m^3
Lubricant Specific Heat, C_p		= 2000	J / Kg. °C
Thermal Conductivity, k_f		= 0.13	W / m °C
Bush-Housing Thermal Conductivity, k_b		= 250	W / m °C
Journal Thermal Conductivity, k_j		= 50	W / m °C
Convection Heat Transfer Coefficient, h_{fb}		= 80	W / m °C
Inlet Lubricant Temperature, T_s		= 40	°C
Ambient Temperature, T_a		= 40	°C
Reference Temperature, T_r		= 40	°C
Oil Groove Angle		= 18^0	

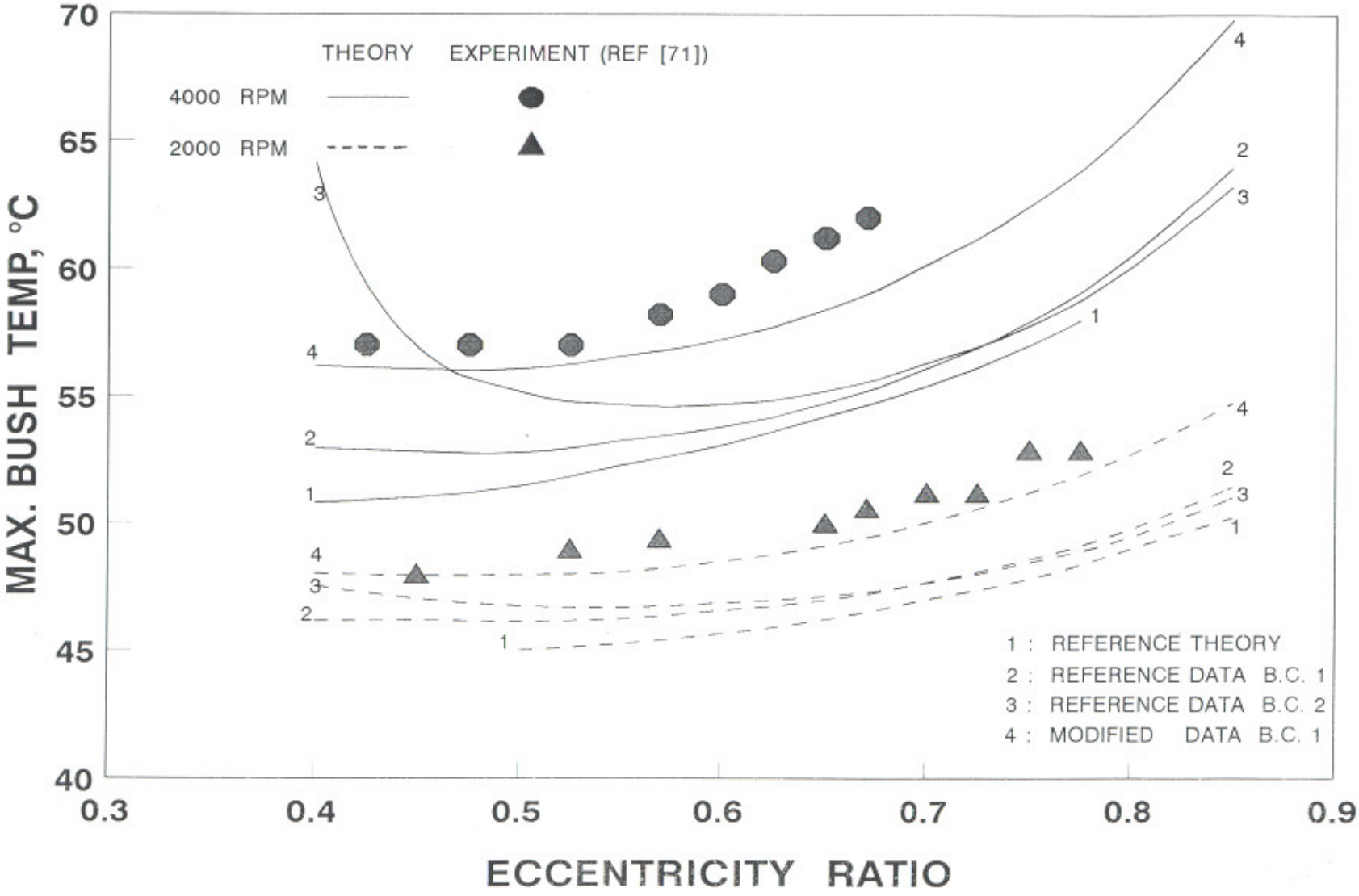

Fig. 5.2 COMPARISON OF RESULTS FOR PLAIN JOURNAL BEARING
(MAXIMUM BUSH TEMPERATURE)

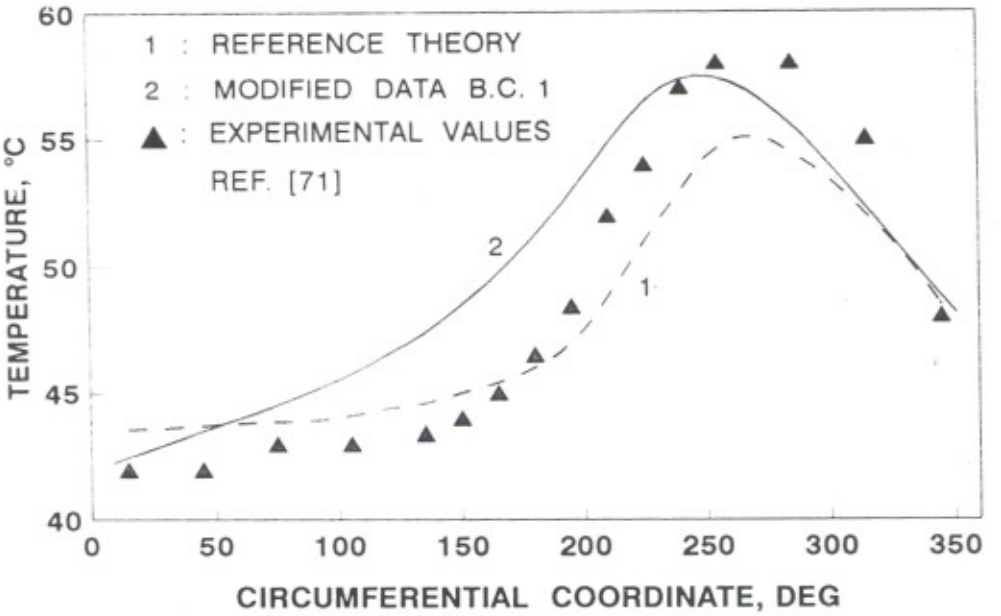

Fig. 5.3 TEMPERATURE VARIATION IN MID-PLANE AT 4000 RPM AND UNDER 6000 N

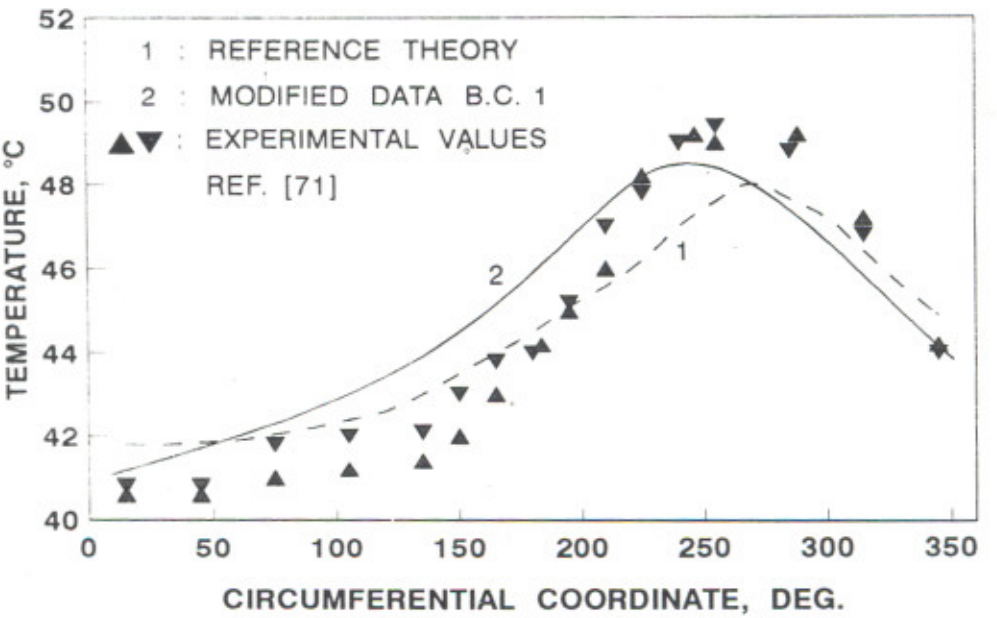

Fig. 5.4 TEMPERATURE VARIATIONS IN MID-PLANE AT 2000 RPM AND UNDER 4000 N

used in taking the present results were chosen identical to those employed by Ferron et al. in their theoretical work. These figures indicate that

- The present results are closer to the published experimental data with reference data as well as the modified data. With the modified data, however, the difference between bush temperatures as predicted by the experiment and from the present work is significantly less, Figs. 5.2 to 5.4. It may be noted here that the modified thermal properties are quite possible as several other researchers have used these properties closer to the chosen ones.
- The bearing load capacity at a given eccentricity ratio as indicated by theory is on the higher side, Fig. 5.5. Boncompain et al [80] also obtained similar results but their values being still higher.
- The computed maximum bush temperature is lower for both speeds considered, Fig.5.2. It may be noted that the modified data give very close values of the maximum bush temperature when compared with the experimental results at both the speeds. Similar trend was also observed at other speeds but not presented here.
- The affect of free convection of heat from the bush at outlet of pad to fluid in the supply groove is quite important. A value of h_{fb} = 1500 W / m^2 °C have been used in the present work which is found to be quite appropriate. This value of h_{fb} has been chosen by an iterative method by simulating the experimental conditions. The effect of h_{fb} is found to be more pronounced in the cavitation zone i.e. after the location of maximum bush temperature and a higher value of h_{fb}, as expected, gives more drop in the bush temperature near the trailing edge of the pad / lobe.
- It has been observed that the maximum bush temperature occurs at / or near the trailing edge of the positive-pressure region. The experimental results also indicate this trend.
- Although results for maximum pressures as well as pressure distribution are not presented here, the values of pressure and the extent of positive-pressure region were found to be very close to the respective experimental values given in the reference for all values of eccentricity ratio, speeds and loads. Infact, the difference was so small that the experimental and theoretical values nearly overlapped and primarily that is the reason for not presenting these results here.
- The journal temperature distribution has been obtained along the axial length by neglecting the radial variation of the temperature. This assumption is quite satisfactory because of high

thermal conductivity of the journal material. The computed journal temperature along the length of the journal varies by about one degree for an aligned bearing as seen in the course of the present work. For misaligned bearings this variation is much higher, especially in the case of an elliptical or a three-lobe bearing. Therefore, for the sake of convenience, the journal temperature has been presented by taking a mean over the length. Fig. 5.6 shows the variation of mean journal temperature against load for two speeds (2000 r.p.m. and 4000 r.p.m.) and the two sets of bush thermal properties. As expected, the journal temperature at higher speed is higher at a given load. Also, the journal temperature is higher when the bush thermal conductivity (k_b) is lesser as the journal has to transfer more amount of heat now.

5.2.2.3 Two-Axial-Groove Journal Bearing : A two-axial-groove bearing differs from a plain bearing in the manner of oil supply. Two supply grooves are provided in this case as against only one in a plain bearing. Thus for the purpose of thermal studies, a two-axial-groove bearing will represent a multi-lobe configuration and the comparison obtained for such a bearing can easily be extended for a multi-lobe configuration. Accordingly, the THD results obtained for a two-axial-groove journal bearing are compared with those published by Lund and Tonnesen [77] in Figs. 5.7(a) to (d). Table 5.7 gives the data used in the present work as well as in the above reference. For numerical discretization, 37 divisions in the circumferential direction in each lobe, 10 divisions each in the axial and across the thickness of the oil film have been used. The first boundary conditions (BC1) are used here.

Fig. 5.7(a) shows the variation of mean journal temperature as a function of load for two values of speed. It is seen from this figure that the mean journal temperatures obtained in the present work are slightly on higher side when compared with the experimental results. In comparison, the theoretical results of Lund et al. are on the lower side and differ significantly at the higher speed.

Fig. 5.7(b) shows the results for the maximum bush temperature versus load for two speeds. The results with the present analysis are quite comparable with the referred experimental values. In fact these results are more consistent as compared to the theoretical results from the reference.

The circumferential temperature profile for the bush temperature at two different speeds (3500 r.p.m. and 5000 r.p.m.) for a given load of 5600 N are shown in Fig. 5.7(c) and Fig. 5.7(d). The theoretical results from the reference show large discrepancies in the upper lobe,

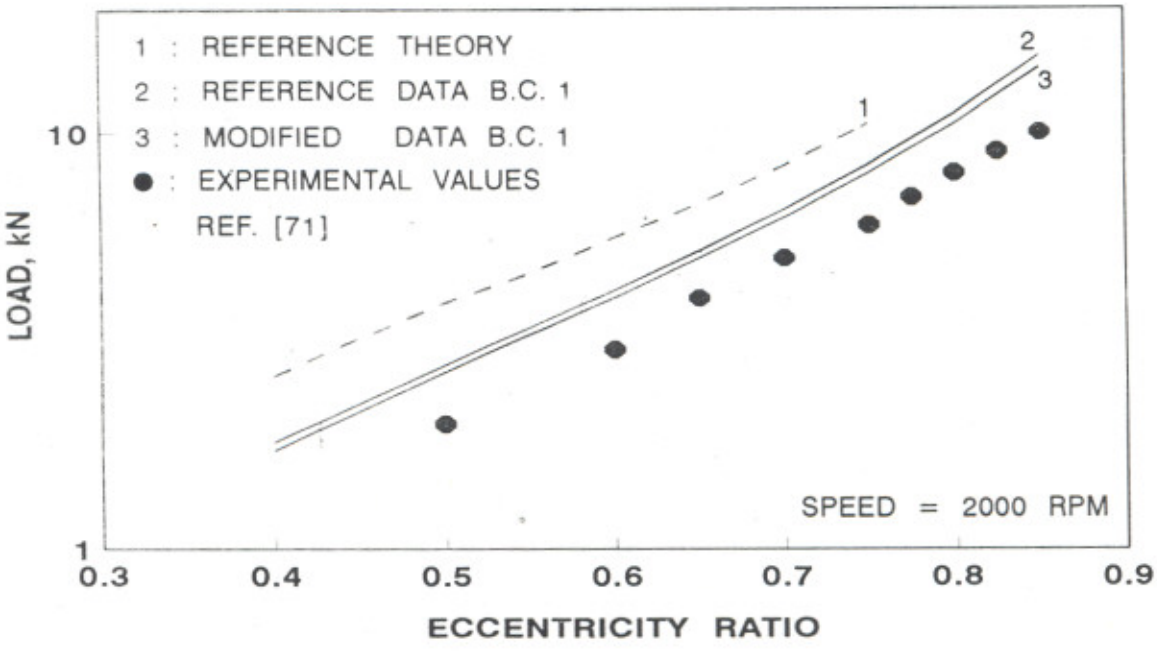

Fig. 5.5 COMPARISON OF RESULTS FOR PLAIN JOURNAL BEARING

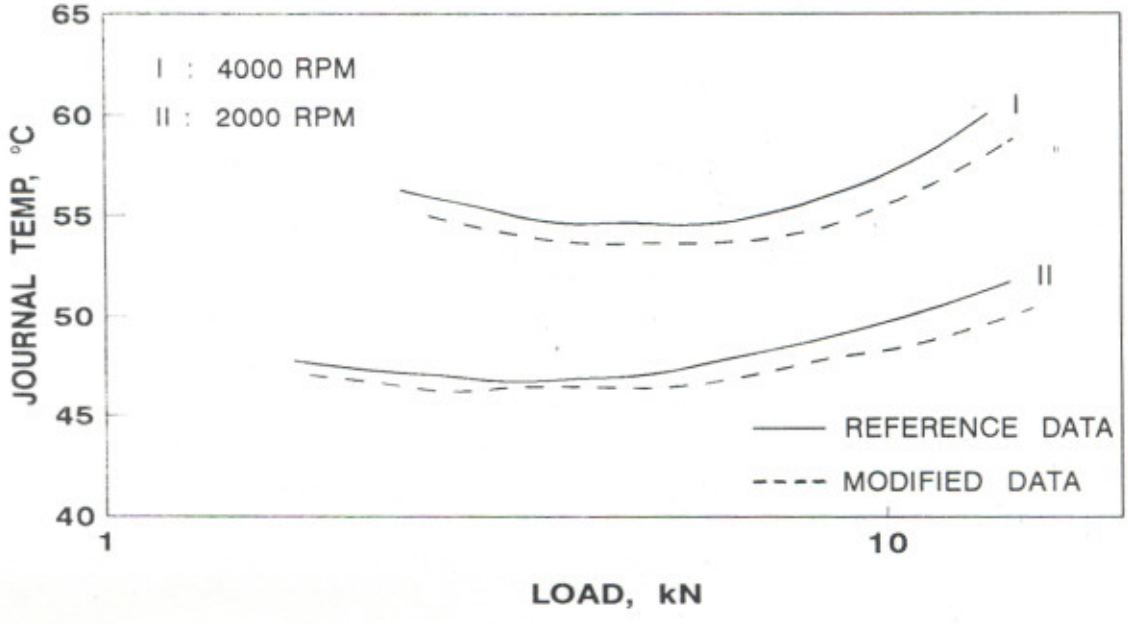

Fig. 5.6 PLAIN JOURNAL BEARING - VARIATION OF JOURNAL TEMPERATURE

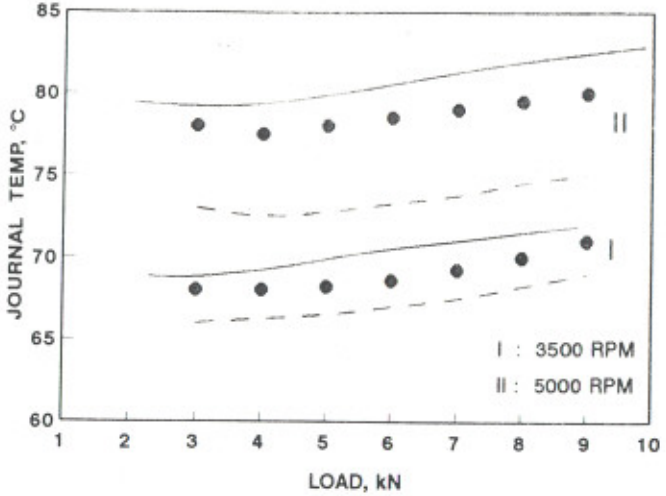

(a)

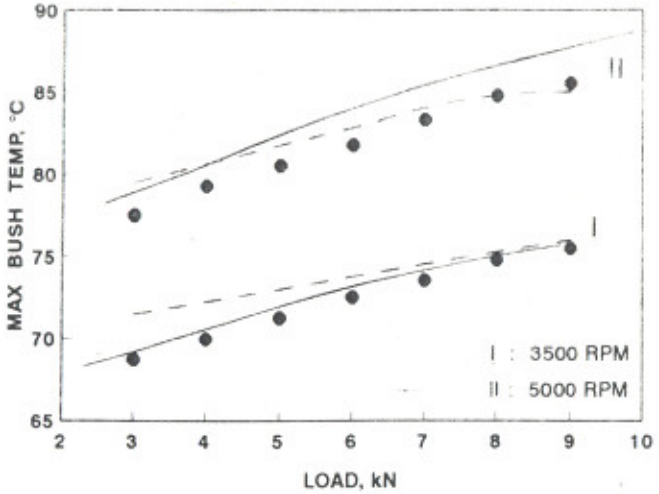

(b)

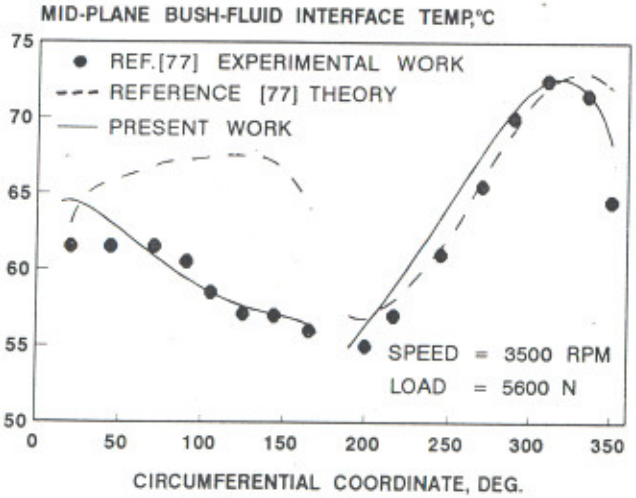

(c)

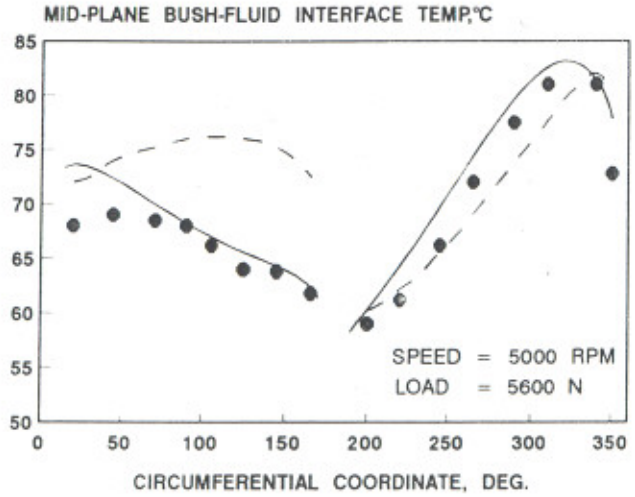

(d)

Fig. 5.7 COMPARISON OF RESULTS FOR TWO-AXIAL GROOVE JOURNAL BEARING

Table 5.7 Data for Calculation

Bearing Dimensions :	Diameter, D = 0.1 m Length, L = 0.05 m
	Radial Clearance, c = 68.6 μm at 3500 RPM
	66.8 μm at 5000 RPM
	Groove Angle = 20 °
Oil Properties :	Kinematic Viscosity, = $21.5 * 10^{-6}$ m^2 / s at 50 °C
	$6.6 * 10^{-6}$ m^2 / s at 90 °C
	Mass Density, ρ = 850 Kg / m^3
	Specific Heat, C_p = 2000 J / Kg °C
	Thermal Conductivity, k = 0.15 W / m °C
	Oil Supply Temperature, T_s = 50 °C
	Oil Supply Pressure : 0.12 MPa (α = 90 °)
	0.15 MPa (α = 270 °)
Bearing Sleeve :	Outer Radius = 0.1 m
	Thermal Conductivity, k_b = 50 W / m °C
	Ambient Temperature, T_a = 20 °C
	Outer Surface Heat Transfer Coeffcient = 50 W / m^2 °C
	Groove Wall Heat Transfer Coeffcient = 100 W / m^2 °C
Shaft :	Diameter = 0.1 m
	Thermal Conductivity, k_j = 50 W / m °C
	Surface Heat Transfer Coeffcient = 50 W / m^2 °C
	Ambient Temperature, T_a = 20 °C

where the measured and computed temperatures differ by more than 12 °C. The present results are very close to the experimental results over both the lobes except a small region near the inlet edge of the upper lobe. The bush temperature distribution in the positive pressure region in the lower lobe shows very good agreement between the calculated values and measured values, the maximum deviation being only about 2.5 °C.

5.2.2.4 Plain Misaligned Journal Bearing : The available THD results for a misaligned plain journal bearing are scant. Chun and Lalas[99] published a few results of misaligned plain journal bearing which were obtained using an approximation for the heat transfer in journal and bush. A comparison of some results have been made with their results in Figs. 5.8(a) to 5.8(b). The operating conditions shown in table 5.8, the viscosity-temperature relation and the degree of misalignment used in taking the present results were chosen identical to those employed by Chun and Lalas in their theoretical work. For the purpose of this comparison, the expression for fluid-film thickness was modified to account for misalignment in the plane of the eccentricity vector as employed by Chun and Lalas. The results of the computations are compared for isothermal and THD conditions, as shown in Figs. 5.8(a) to 5.8(b). A good agreement is seen between the present and published theoretical results. The difference in the present and published results may be attributed to the approximate thermal analysis for the bush and the journal employed by Chun and Lalas.

5.2.3 Concluding Remarks on Validation

Based on the comparisons provided in this section, it may be said that the analysis and the developed programs are adequately validated for the study of misaligned journal bearings operating under thermohydrodynamic lubrication conditions.

5.3. STEADY STATE THD ANALYSIS OF MISALIGNED JOURNAL BEARINGS

A three-dimensional thermal analysis has been carried out in the present work as it is expected to give more accurate results especially when the bearings operate under misalignment conditions. Studies of performance characteristics of plain, two-axial-groove, elliptical and three-lobe journal bearings have been performed by using geometry and operating characteristics shown in Table 5.9.

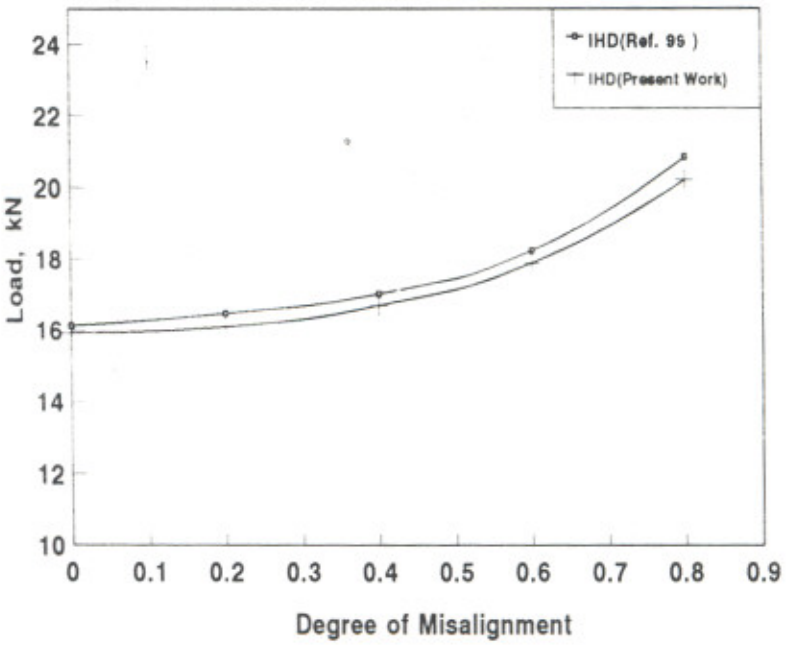

(a)

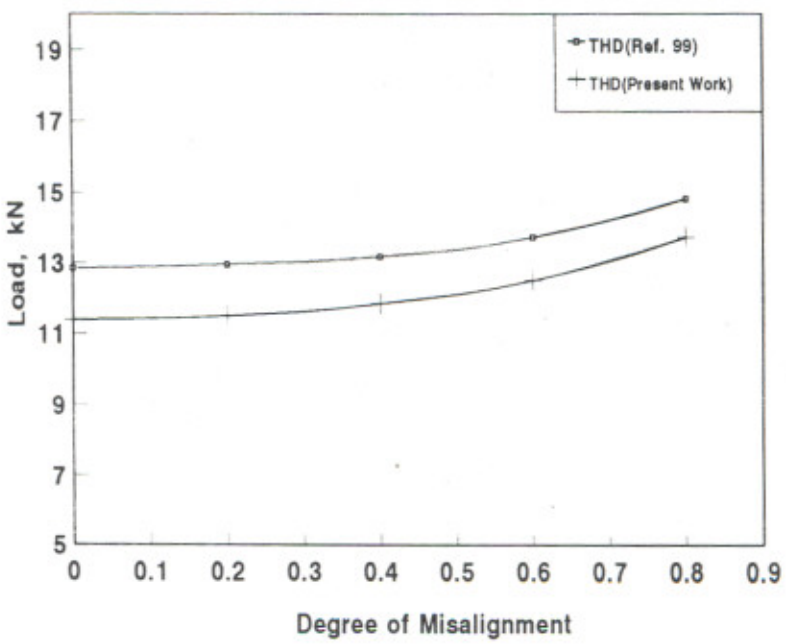

(b)

Ref. [99]; results from this reference has been converted into dimensional form.

Fig. 5.8 Load Vs. Degree of Misalignment

Table 5.8 Operating Conditions

Bearing Diameter, 2R	= 0.10	m
Bearing Length, L	= 0.08	m
Radial Clearance, c / R	= 0.0029	
Eccentricity Ratio	= 0.80	
Speed of the Journal, N	= 2000	R.P.M.
Lubricant Viscosity at 40 °C	= 0.0277	Pa.s
Temperature Viscosity Coefficient	= 0.0033	$°C^{-1}$
Lubricant Density, ρ	= 860	Kg / m^3
Lubricant Specific Heat, C_p	= 2000	J / Kg. °C
Thermal Conductivity, k_f	= 0.13	W / m °C
Bush-Housing Thermal Conductivity, k_b	= 250	W / m °C
Journal Thermal Conductivity, k_j	= 50	W / m °C
Convection Heat Transfer Coefficient of Lubricant to the bush, h_{fb}	= 50	W / m °C
Convection Heat Transfer Coefficient of air to the bush, h_{ab}	= 5	W / m °C
Convection Heat Transfer Coefficient of Lubricant to the journal, h_{fj}	= 130	W / m °C
Oil Groove Angle	= 17.1^0	
Inlet Lubricant Temperature, T_s	= 40	°C
Ambient Temperature, T_a	= 45	°C
Reference Temperature, T_r	= 40	°C

TABLE 5.9 Operating Characteristics

Journal Radius, R		= 50 mm
Journal Speed, N		= 3500 r.p.m.
External Bearing Radius, R_2		= 100 mm
Bearing Length, L		= 100 mm
Radial Clearance, c/R		= 0.003
Lubricant Viscosity	at 50 °C	= $21.5 * 10^{-6}$ m^2/s
	at 90 °C	= $6.6 * 10^{-6}$ m^2/s
Lubricant Density, ρ		= 860 Kg/m^3
Lubricant Specific Heat, C_p		= 2000 J / Kg. °C
Lubricant Thermal Conductivity, k_f		= 0.13 W / m °C
Bush-Housing Thermal Conductivity, k_b		= 250 W / m °C
Journal Thermal Conductivity, k_j		= 50 W / m °C
Convection Heat Transfer Coefficient, h_{ab} (from bush to air)		= 50 W / m °C
Convection Heat Transfer Coefficient, h_{fb} (from bush to oil)		= 1500 W / m °C
Inlet Lubricant Temperature, T_s		= 40 °C
Ambient Temperature, T_a		= 30 °C
Reference Temperature, T_r		= 40 °C
Groove Angle		= 20 °

The static and dynamic performance characteristics of misaligned journal bearing are presented and discussed in this section. For ready reference, however, the performance characteristics of aligned bearings have also been given. In general, these characterisitics have been presented as functions of load. All static performance characteristics except eccentricity ratio are presented in dimensional form where as the dynamic performance characteristics have been given in the non-dimensional form. A conversion table from non-dimensional to dimensional form is given as Appendix I.

The static performance characteristics include eccentricity ratio (ε_o), attitude angle (φ), maximum pressure (p_{max}), minimum fluid-film thickness (h_{min}), side flow (Q_s), mean journal temperature and maximum bush temperature. Dynamic performance characteristics are presented in terms of sixteen stiffness coefficients ($\bar{S}_{xx}$, $\bar{S}_{xz}$, $\bar{S}_{zx}$, $\bar{S}_{zz}$, $\bar{S}_{x\gamma_x}$, $\bar{S}_{x\gamma_z}$, $\bar{S}_{z\gamma_x}$, $\bar{S}_{z\gamma_z}$, $\bar{S}_{\gamma_x x}$, $\bar{S}_{\gamma_x z}$, $\bar{S}_{\gamma_z x}$, $\bar{S}_{\gamma_z z}$, $\bar{S}_{\gamma_x \gamma_x}$, $\bar{S}_{\gamma_x \gamma_z}$, $\bar{S}_{\gamma_z \gamma_x}$, $\bar{S}_{\gamma_z \gamma_z}$), sixteen damping coefficients ($\bar{B}_{xx}$, $\bar{B}_{xz}$, $\bar{B}_{zx}$, $\bar{B}_{zz}$, $\bar{B}_{x\gamma_x}$, $\bar{B}_{x\gamma_z}$, $\bar{B}_{z\gamma_x}$, $\bar{B}_{z\gamma_z}$, $\bar{B}_{\gamma_x x}$, $\bar{B}_{\gamma_z x}$, $\bar{B}_{\gamma_x z}$, $\bar{B}_{\gamma_z z}$, $\bar{B}_{\gamma_x \gamma_x}$, $\bar{B}_{\gamma_x \gamma_z}$, $\bar{B}_{\gamma_z \gamma_x}$, $\bar{B}_{\gamma_z \gamma_z}$), instability threshold speed and whirl frequency ratio. To facilitate logical conclusions from this analysis, the results are presented for two different values of bi-planar misalignment ratios. In addition to these characteristics, isopressure curves, pressure profiles, isotherms and temperature profiles for liquid and solid domains have also been presented. In the present work, a pre-load factor of 0.5 has been used in the study of elliptical and three-lobe journal bearings.

5.3.1 Static Performance Characteristics

Various static performance characteristics of a plain, two-axial-groove, elliptical and three-lobe journal bearing are shown in Figs. 5.9 to 5.12. In the following, salient features of these characteristics are discussed.

5.3.1.1 Eccentricity Ratio : It is observed from the results presented in Figs. 5.9(a), 5.10(a), 5.11(a) and 5.12(a) that the eccentricity ratio (ε_o) shows a decreasing trend as misalignment is increased in all the bearing systems. This effect is mainly caused due to the decrease in the film thickness caused by misalignment on one side of the mid-plane which results in the increase in fluid-film pressure substantially and hence increase in load at a given eccentricity.

5.3.1.2 Attitude Angle : Figs. 5.9(b), 5.10(b), 5.11(b) and 5.12(b) shows that for all the bearing systems, the attitude angle (φ) decreases with the increase in misalignment. The effect is more pronounced at higher values of misalignment ratio. For a vertical load support, this trend is expected to improve the stability of the journal bearing system.

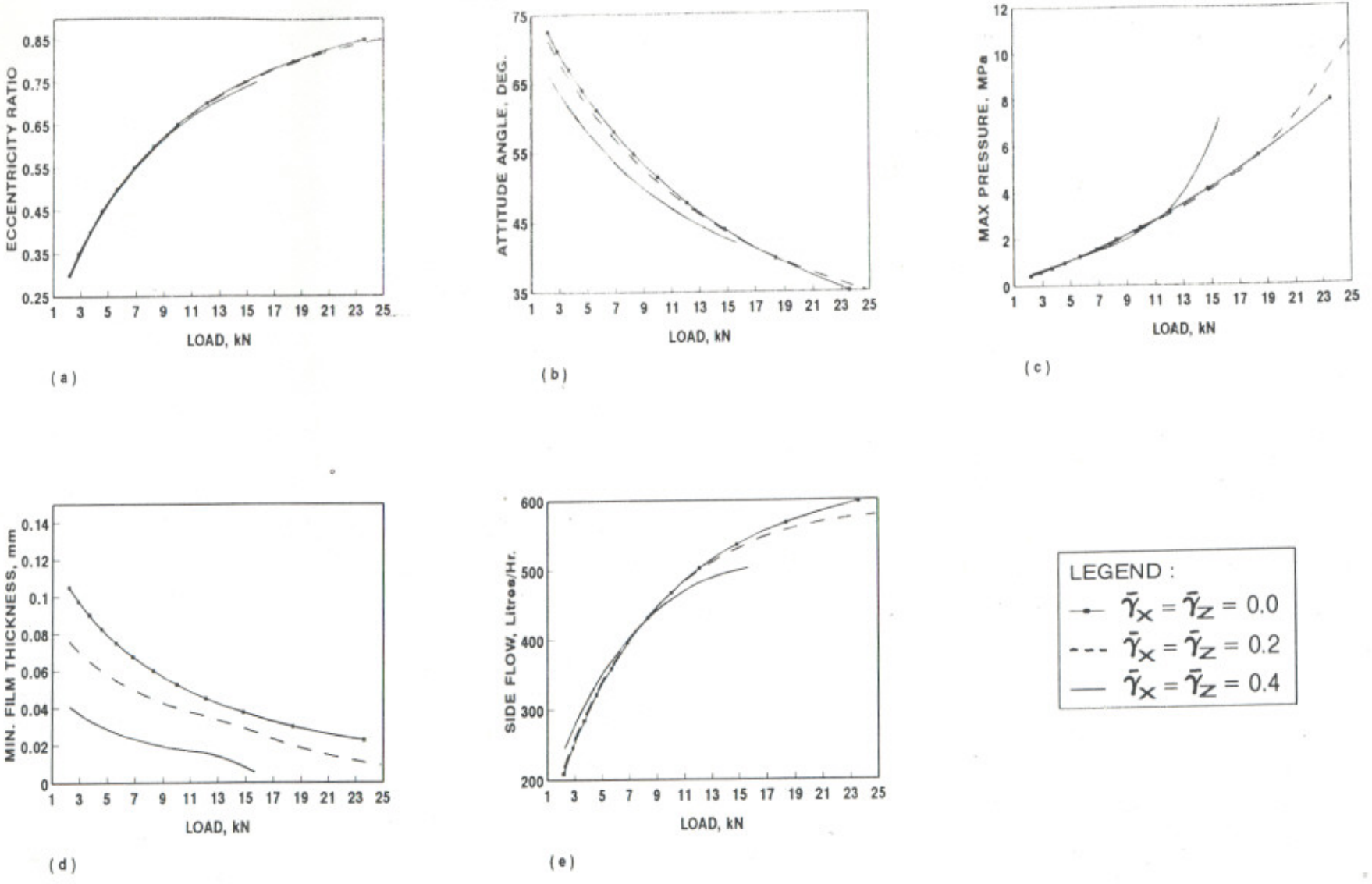

Fig. 5.9 PLAIN JOURNAL BEARING - STATIC PERFORMANCE CHARACTERISTICS
(ε_0, φ, p_{max}, h_{min}, Q_s)

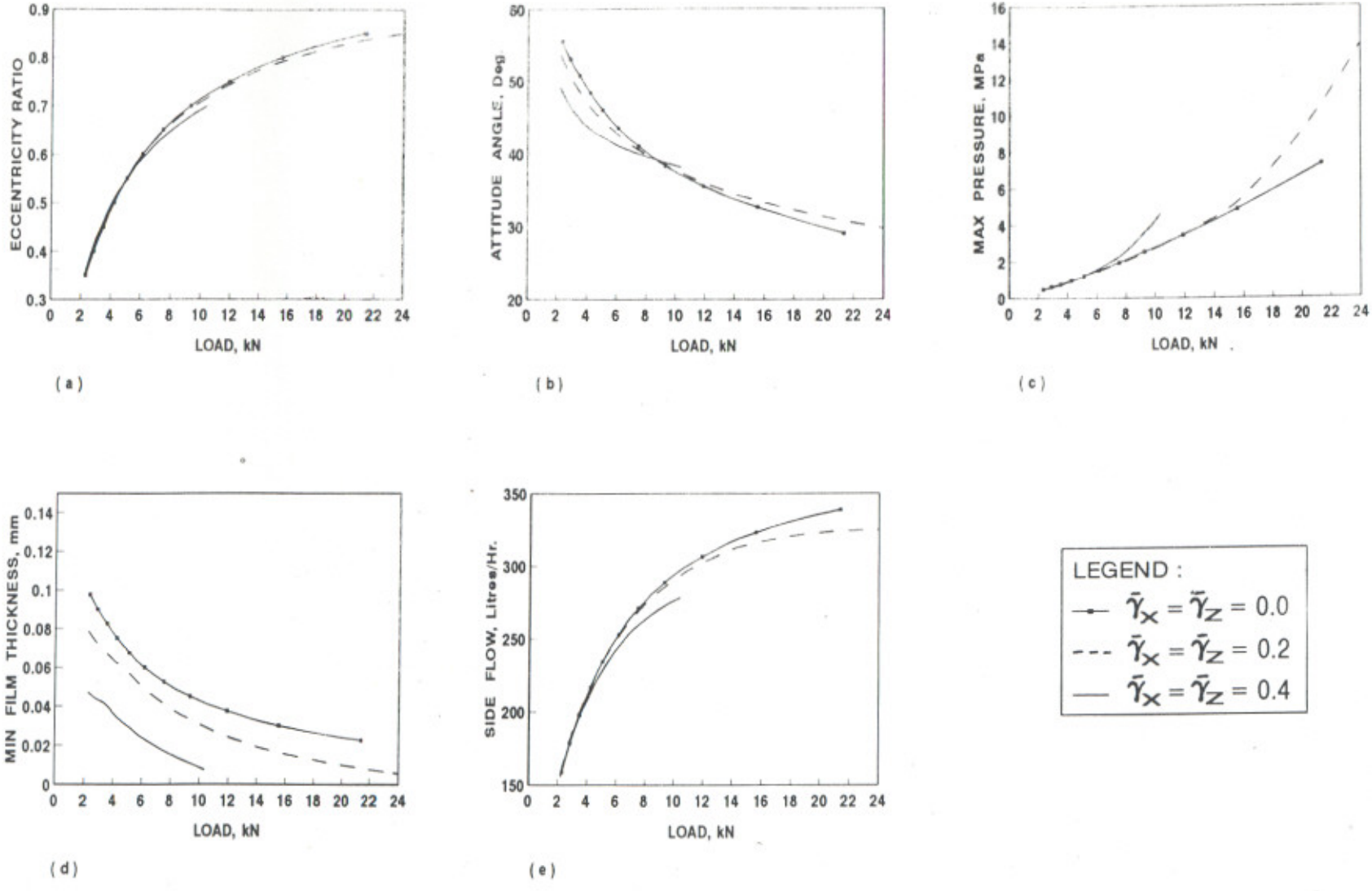

Fig. 5.10 TWO-AXIAL-GROOVE JOURNAL BEARING - STATIC PERFORMANCE CHARACTERISTICS (ε_0, φ, p_{max}, h_{min}, Q_s)

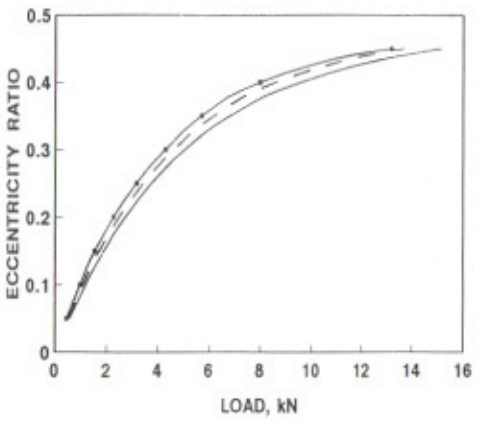

(a)

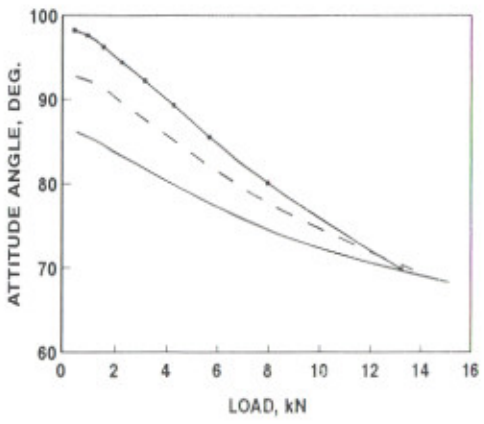

(b)

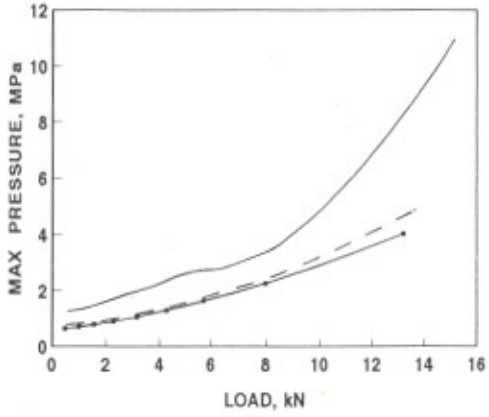

(c)

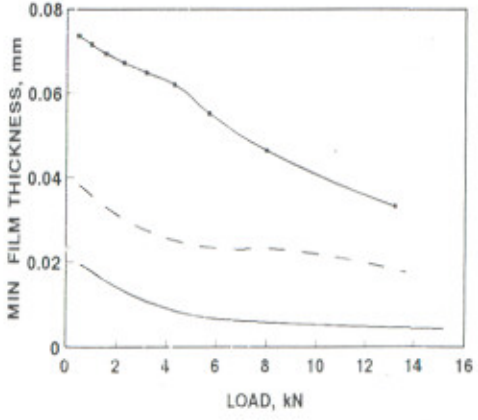

(d)

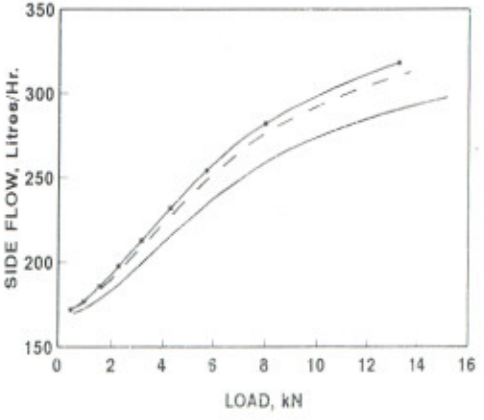

(e)

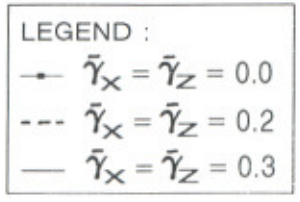

Fig. 5.11 ELLIPTICAL JOURNAL BEARING - STATIC PERFORMANCE CHARACTERISTICS (ε_0, φ, p_{max}, h_{min}, Q_s)

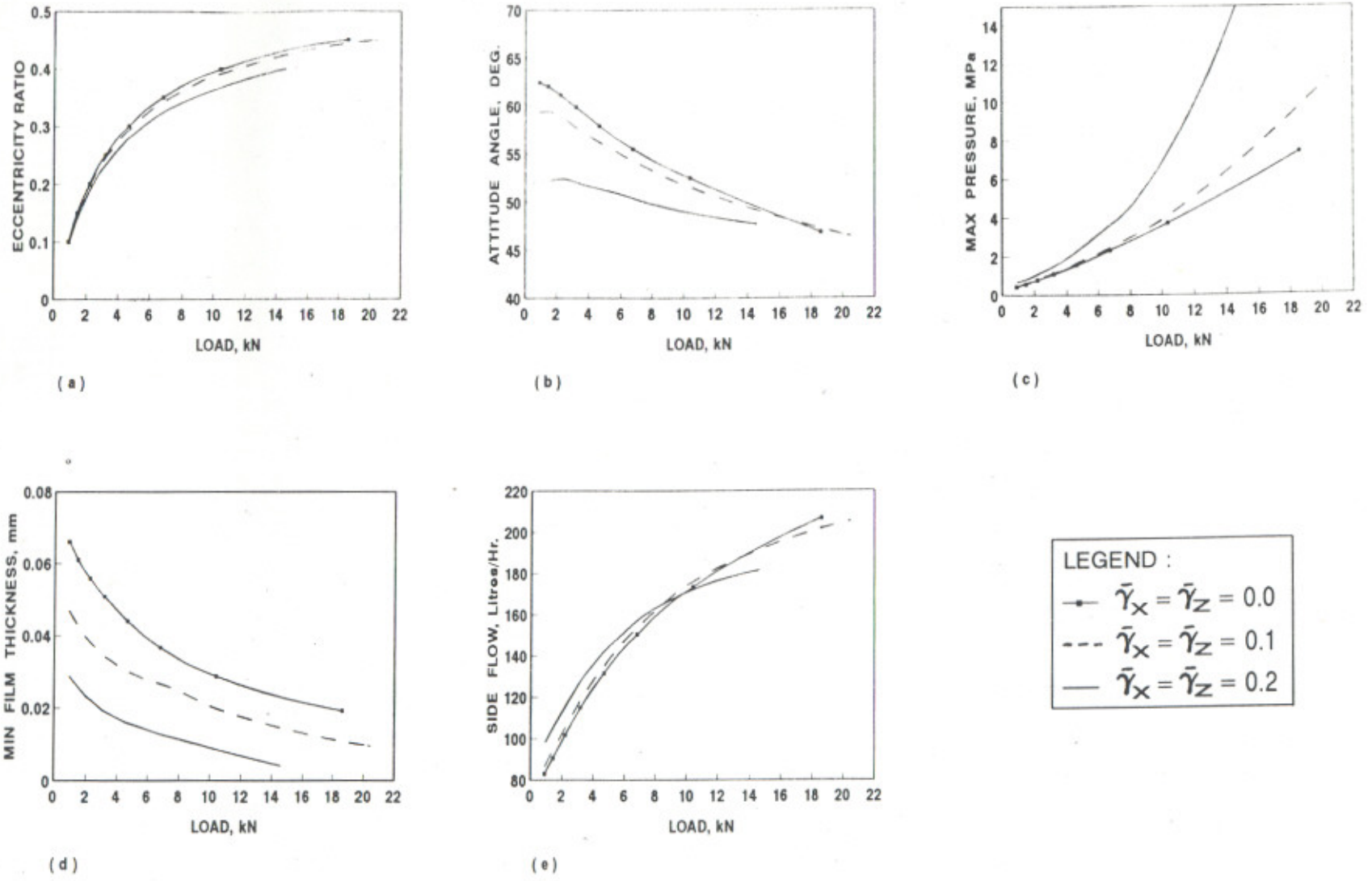

Fig. 5.12 THREE-LOBE JOURNAL BEARING - STATIC PERFORMANCE CHARACTERISTICS
(ε_0, φ, p_{max}, h_{min}, Q_s)

5.3.1.3 Maximum Fluid-Film Pressure: At higher load values, the values of maximum fluid-film pressures are significantly higher in a misaligned plain and two-axial-groove bearing as compared to an aligned bearing, Figs. 5.9(c) and 5.10(c). At moderate loads, however, the maximum fluid-film pressures are slightly lower than the corresponding values for an aligned bearing.

For elliptical and three-lobe bearings, it is observed from Figs. 5.11(c) and 5.12(c) that the maximum pressure (p_{max}) increases significantly with the increase in misalignment for all values of load.

5.3.1.4 Minimum Fluid-film Thickness : The effect of misalignment is quite adverse on fluid-film thickness. It is seen that for all the bearing systems, as the misalignment increases, the minimum fluid-film thickness decreases for all values of load, Figs. 5.9(d), 5.10(d), 5.11(d) and 5.12(d). This may lead to eventual failure of the journal bearing system due to metal-to-metal contact and resulting wear.

5.3.1.5 Side Flow : Figs. 5.9(e), 5.10(e) and 5.12(e) reveals that at light loads, the effect of increasing misalignment leads to increased side flow (Q_s) whereas at higher load values, the trend is reversed for all bearings except elliptical journal bearing where increased misalignment leads to increased side flow (Q_s) at all load values, Fig. 5.11(e).

5.3.1.6 Mean Journal Temperature and Maximum Bush Temperature : The mean journal temperature and the maximum bush temperature both, are shown in Figs. 5.13 to 5.16. Figs. 5.13(a), 5.14(a), 5.15(a) and 5.16(a) reveals that at heavy load, an increase in the misalignment leads to higher mean journal temperature which is probably caused by the reduction in side flow requiring greater amount of heat generated due to viscous friction now being transferred out of the bearing by the solids. Figs. 5.13(b) and 5.14(b) which shows the maximum bush temperatures, also confirms this observation.

It is a well known fact that the bearing load capacity is limited by a specified value of the minimum fluid-film thickness and / or a maximum allowable bush temperature. The bearing is expected to fail whenever these limits are violated. With reference to the present work, if we limit the maximum bush temperature at 70 °C (say) in case of plain journal bearing, the load capacity reduces from 23.6 kN for an aligned bearing to only 15.2 kN for a misaligned bearing with $\bar{\gamma}_x = \bar{\gamma}_z = 0.4$, Fig. 5.13(b). This shows a decrease of about 35.6 % in the load capacity due to misalignment. Likewise, if the value of minimum fluid-film thickness should not reduce

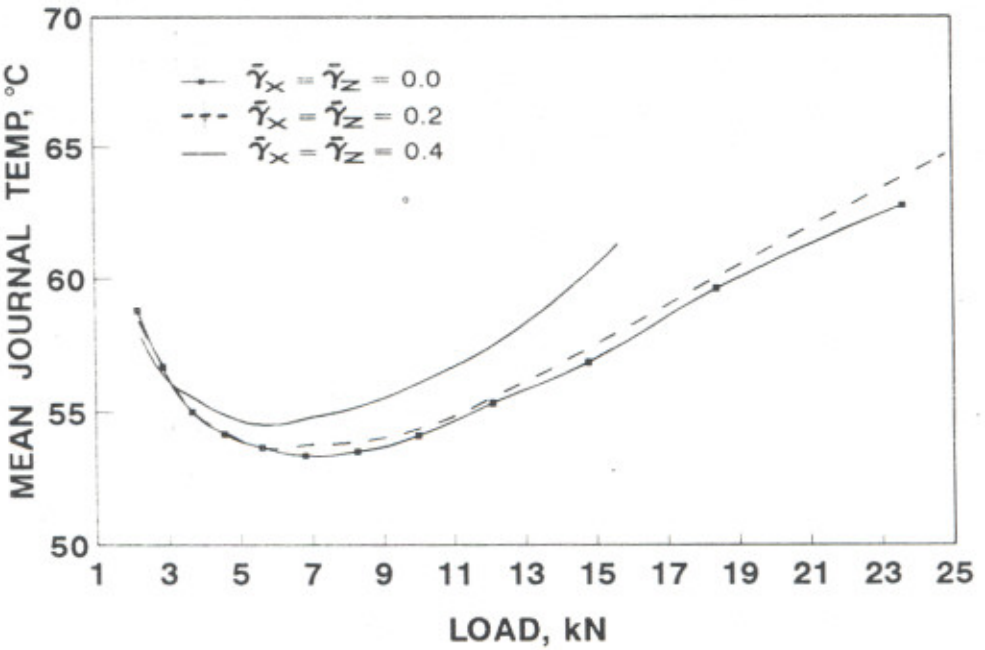

(a)

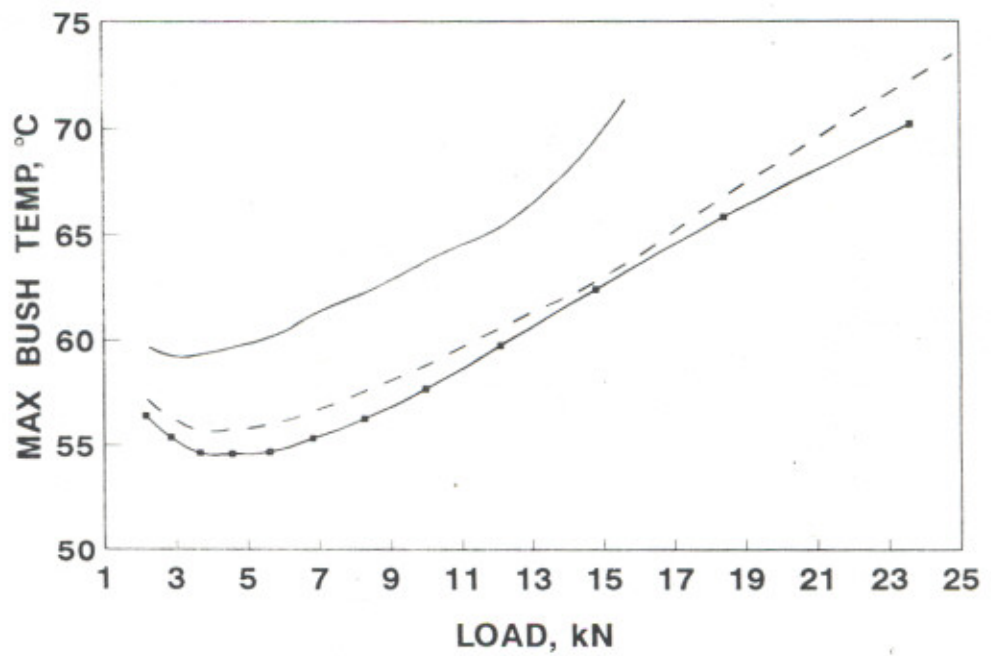

(b)

Fig. 5.13 PLAIN JOURNAL BEARING - STATIC PERFORMANCE CHARACTERISTICS (T_J AND T_B)

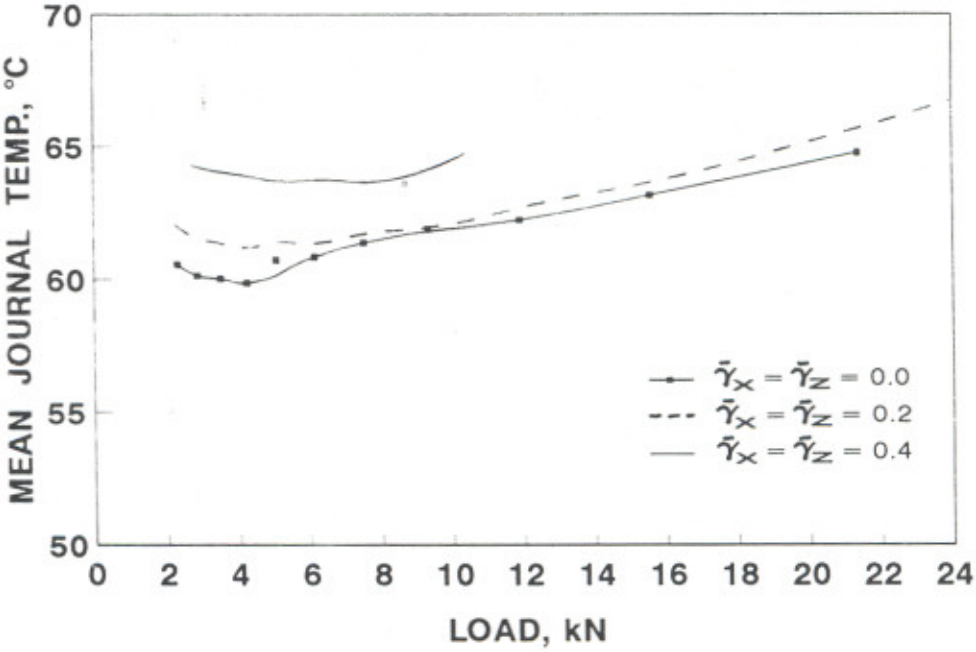

(a)

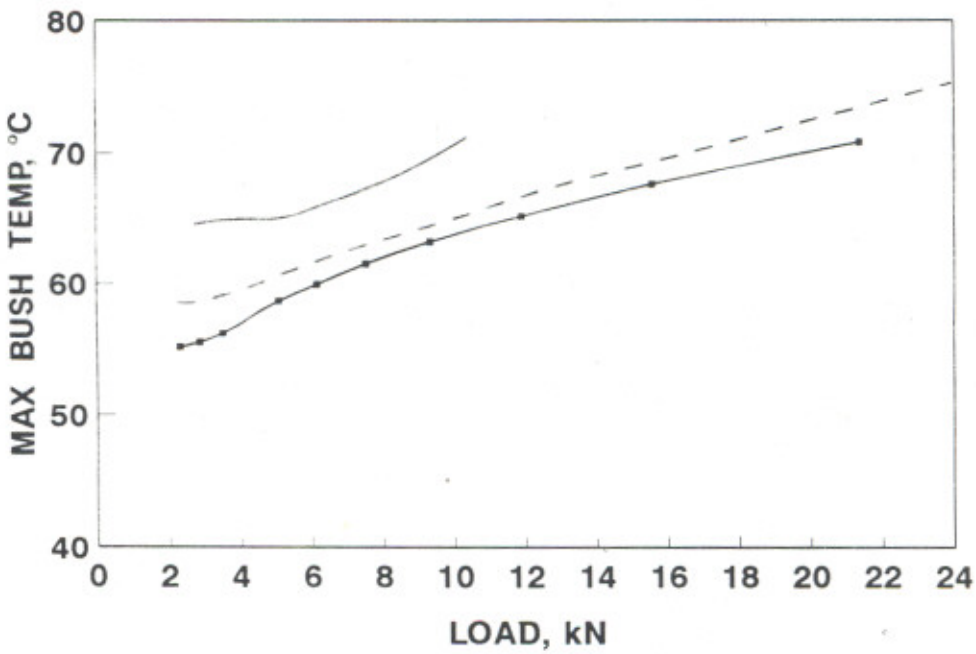

(b)

Fig. 5.14 TWO-AXIAL-GROOVE JOURNAL BEARING - STATIC PERFORMANCE CHARACTERISTICS (T_J AND T_B)

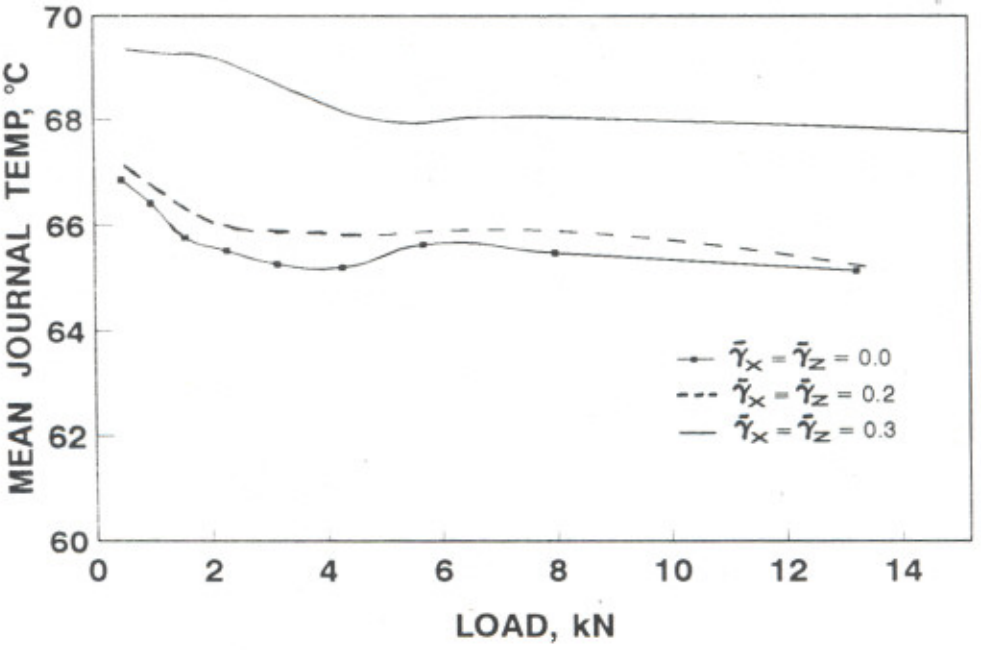

(a)

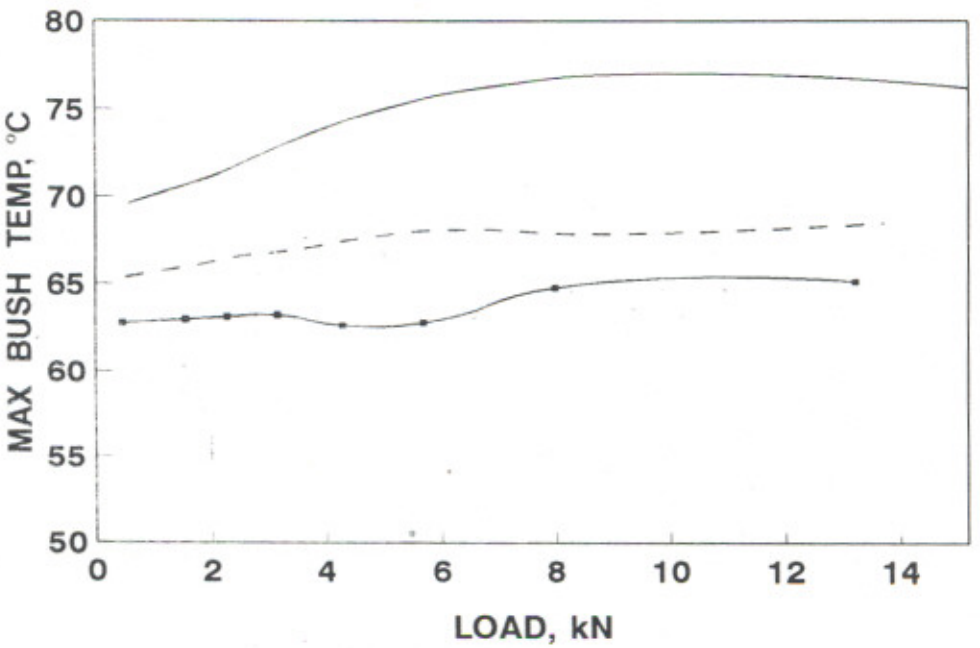

(b)

Fig. 5.15 ELLIPTICAL JOURNAL BEARING - STATIC PERFORMANCE CHARACTERISTICS (T_J AND T_B)

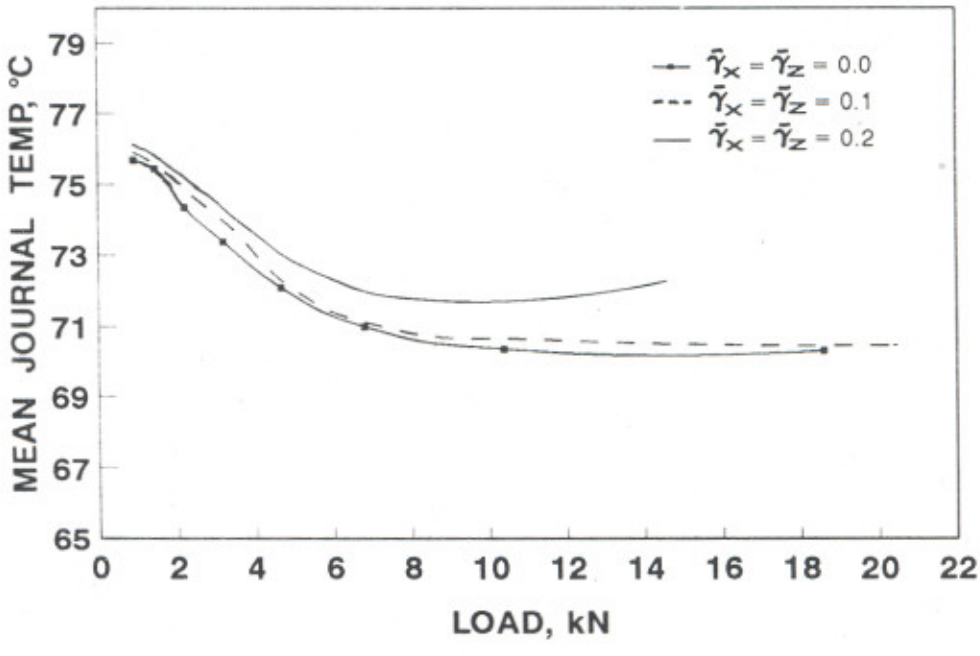

(a)

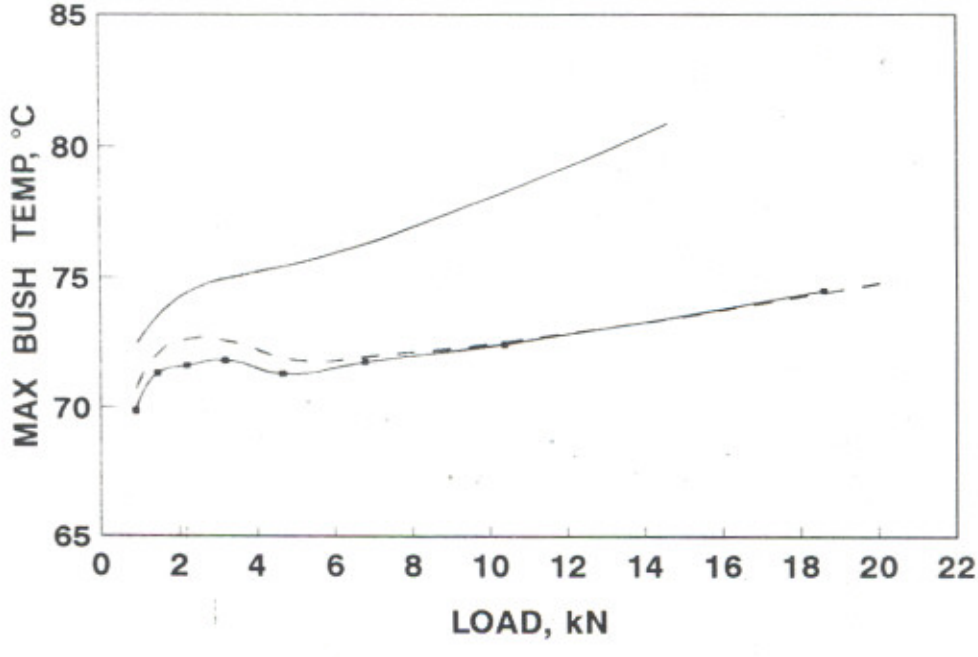

(b)

Fig. 5.16 THREE-LOBE JOURNAL BEARING - STATIC PERFORMANCE CHARACTERISTICS (T_J AND T_B)

below 0.02 mm (say), the bearing load capacity reduces from nearly 27 kN to 9 kN in the misaligned bearing showing a reduction of 66.7 % in the load capacity of the plain journal bearing, Fig. 5.9(d).

Figs. 5.15(a) and 5.16(a) indicates that for elliptical and three-lobe bearings, the mean journal temperature slightly reduces as the load supported by the bearing increases and the trend is similar for aligned and misaligned bearings.

The maximum bush temperature, however, increases with the increase in load. For example, at a load value of 10 kN, the maximum bush temperature is 65.6 °C in case of an aligned elliptical journal bearing whereas for bearing running with a misalignment of $\bar{\gamma}_x = \bar{\gamma}_z =$ 0.2, it is approximately 68 °C and rises to 77 °C for a misalignment of $\bar{\gamma}_x = \bar{\gamma}_z = 0.3$, Fig. 5.15(b).

5.3.2 Stiffness Coefficients

The stiffness coefficients for the four bearing systems are plotted in Figs. 5.17 to 5.28. In general, the values of $\bar{S}_{xx}$ {Figs. 5.17(a), 5.20(a), 5.23(a), 5.26(a)}, $\bar{S}_{xz}$ {Figs. 5.17(b), 5.20(b), 5.23(b), 5.26(b)} and $\bar{S}_{zz}$ {Figs. 5.17(d), 5.20(d), 5.23(d), 5.26(d)} at any load are found to increase with misalignment for all the bearing systems studied. The stiffness coefficient, $\bar{S}_{zx}$ {Figs. 5.17(c), 5.20(c)} shows no significant change due to misalignment in case of circular bearings where as in case of non-circular bearings, $\bar{S}_{zx}$ {Figs. 5.23(c), 5.26(c)} increases with misalignment at any load value. The stiffness coeffcients, $\bar{S}_{xx}$ {Figs. 5.17(a), 5.20(a), 5.23(a), 5.26(a)} and $\bar{S}_{zz}$ {Figs. 5.17(d), 5.20(d), 5.23(d), 5.26(d)} increases with the increase in load values where as the stiffness coeffcients, $\bar{S}_{xz}$ {Figs. 5.17(b), 5.20(b), 5.23(b), 5.26(b)} and $\bar{S}_{zx}$ {Figs. 5.17(c), 5.20(c), 5.23(c), 5.26(c)} decreases with the increase in the load values.

Likewise, the figures show that the values of stiffness coefficients, $\bar{S}_{x\gamma_x}$ {Figs. 5.18(a), 5.21(a), 5.24(a), 5.27(a)}, $\bar{S}_{\gamma_x x}$ {Figs. 5.18(e), 5.21(e), 5.24(e), 5.27(e)}, $\bar{S}_{\gamma_x\gamma_x}$ {Figs. 5.19(c), 5.22(c), 5.25(c), 5.28(c)}, $\bar{S}_{\gamma_x\gamma_z}$ {Figs. 5.19(d), 5.22(d), 5.25(d), 5.28(d)}, $\bar{S}_{\gamma_z\gamma_z}$ {Figs. 5.19(f), 5.22(f), 5.25(f), 5.28(f)}, increase with the increase in misalignment. In all these cases, the effect is more pronounced at higher values of misalignment ratio. Figures reveal that the values of stiffness coefficients $\bar{S}_{x\gamma_z}$ {Figs. 5.18(b), 5.21(b), 5.27(b)}, $\bar{S}_{z\gamma_z}$ {Figs. 5.18(d), 5.21(d), 5.24(d), 5.27(d)}, $\bar{S}_{\gamma_x z}$ {Figs. 5.18(f), 5.21(f), 5.27(f)}, $\bar{S}_{\gamma_z x}$ {Figs. 5.19(a), 5.22(a)}, $\bar{S}_{\gamma_z z}$ {Figs.

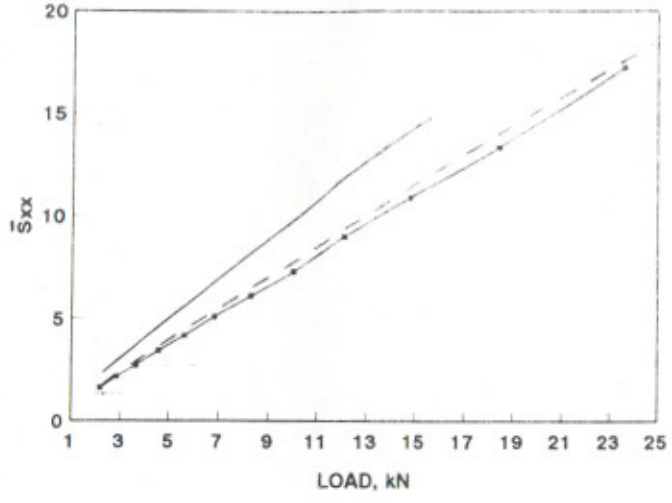

(a)

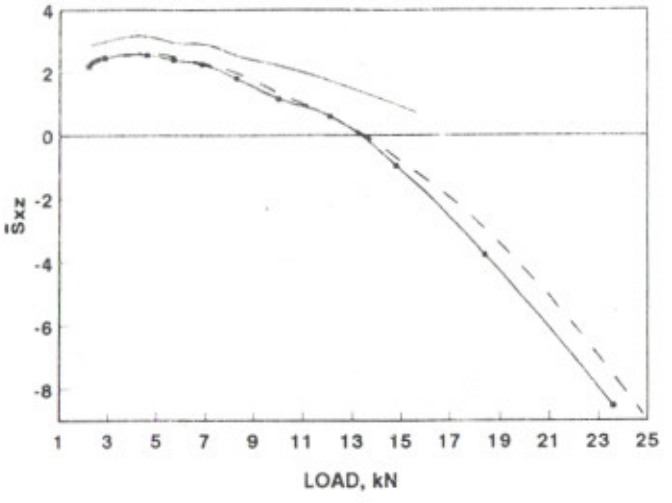

(b)

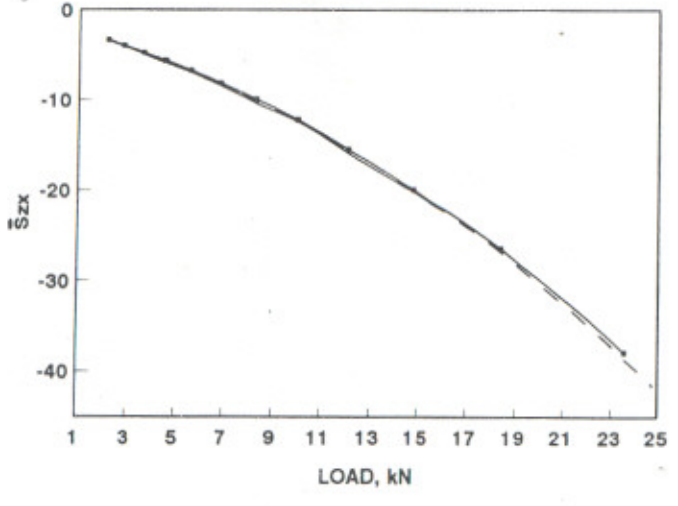

(c)

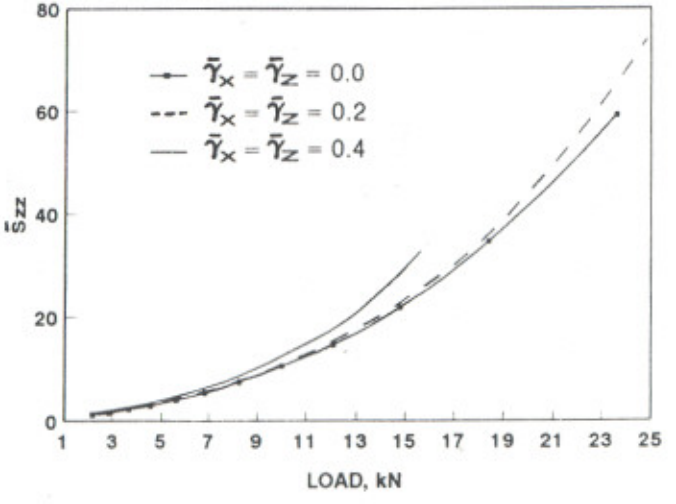

(d)

Fig. 5.17 PLAIN JOURNAL BEARING - STIFFNESS COEFFICIENTS ($\bar{S}xx$, $\bar{S}xz$, $\bar{S}zx$, $\bar{S}zz$)

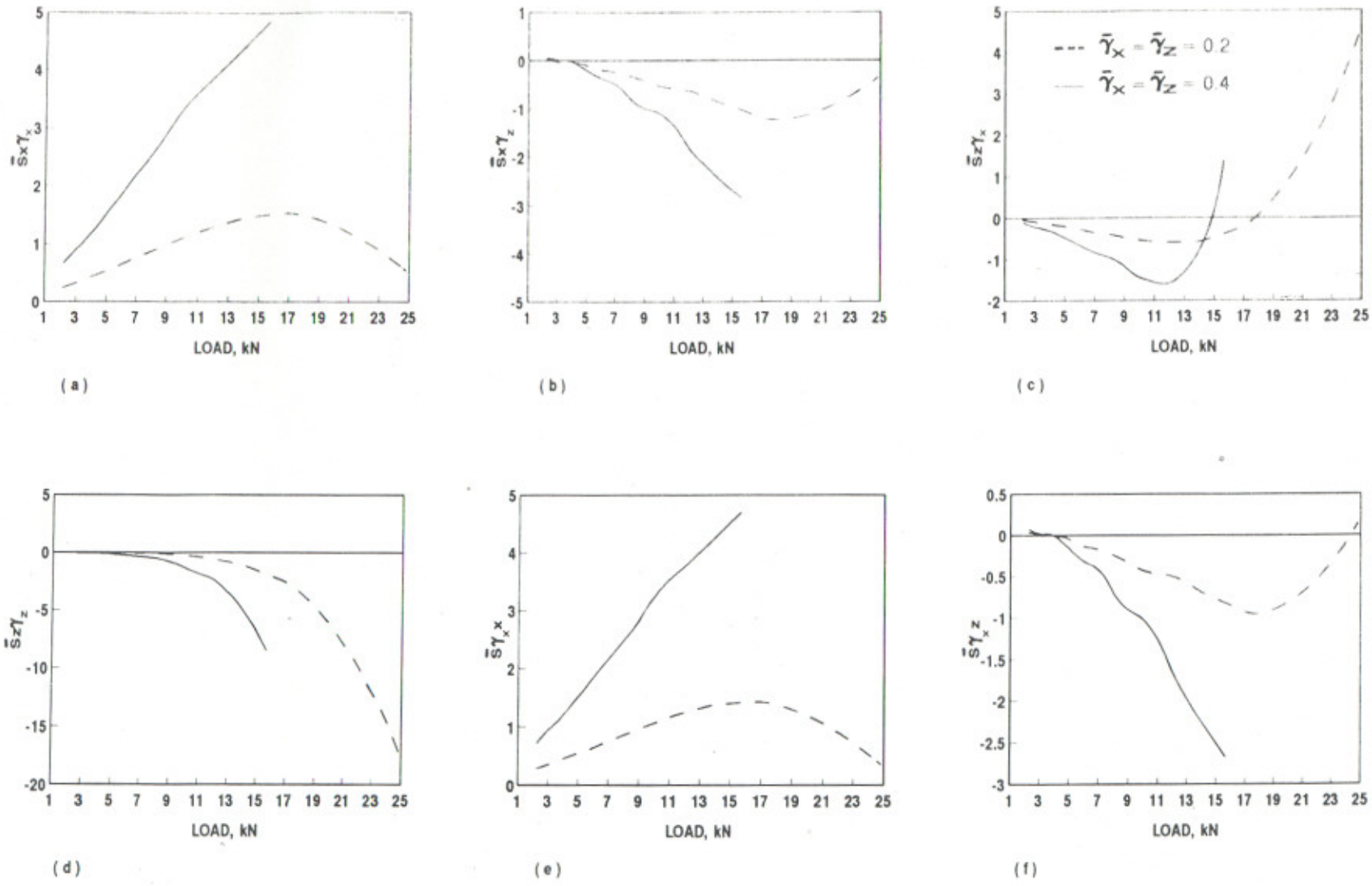

Fig. 5.18 PLAIN JOURNAL BEARING - STIFFNESS COEFFICIENTS
($\bar{S}x\gamma_x$, $\bar{S}x\gamma_z$, $\bar{S}z\gamma_x$, $\bar{S}z\gamma_z$, $\bar{S}\gamma_x x$, $\bar{S}\gamma_x z$)

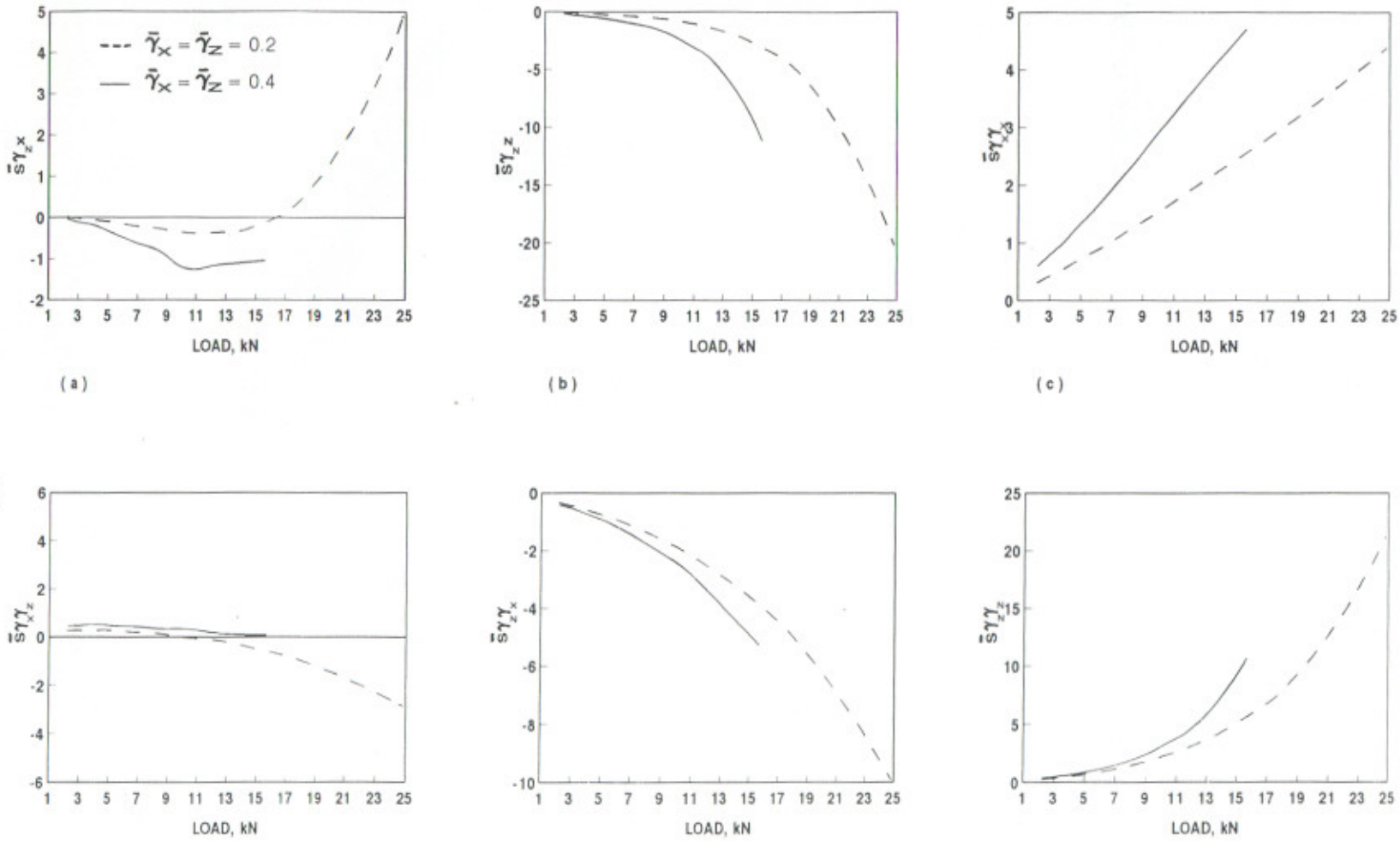

Fig. 5.19 PLAIN JOURNAL BEARING - STIFFNESS COEFFICIENTS
($\bar{S}\gamma_z x$, $\bar{S}\gamma_z z$, $\bar{S}\gamma_x \gamma_x$, $\bar{S}\gamma_x \gamma_z$, $\bar{S}\gamma_z \gamma_x$, $\bar{S}\gamma_z \gamma_z$)

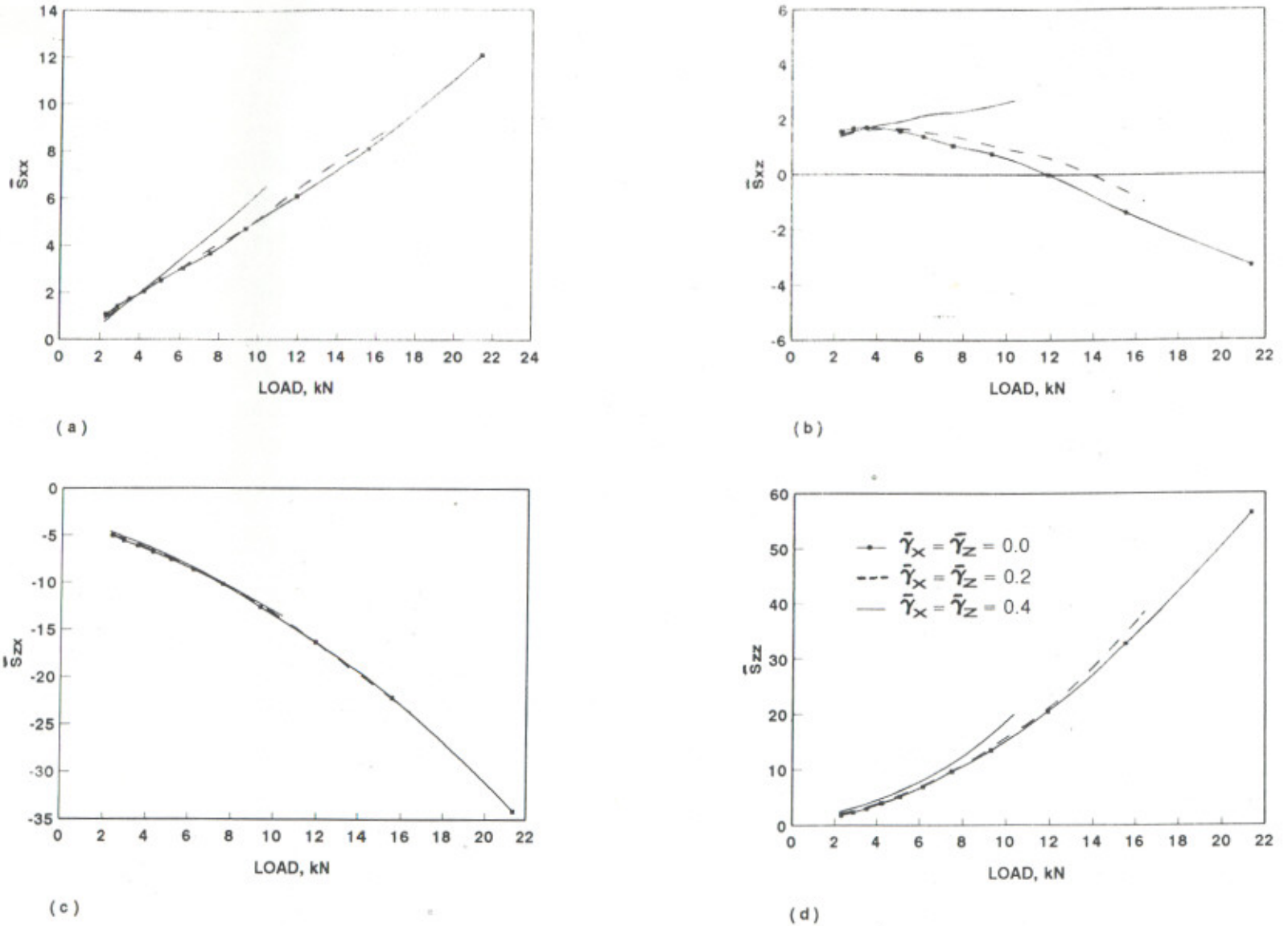

Fig. 5.20 TWO-AXIAL-GROOVE JOURNAL BEARING - STIFFNESS COEFFICIENTS ($\bar{S}_{xx}$, $\bar{S}_{xz}$, $\bar{S}_{zx}$, $\bar{S}_{zz}$)

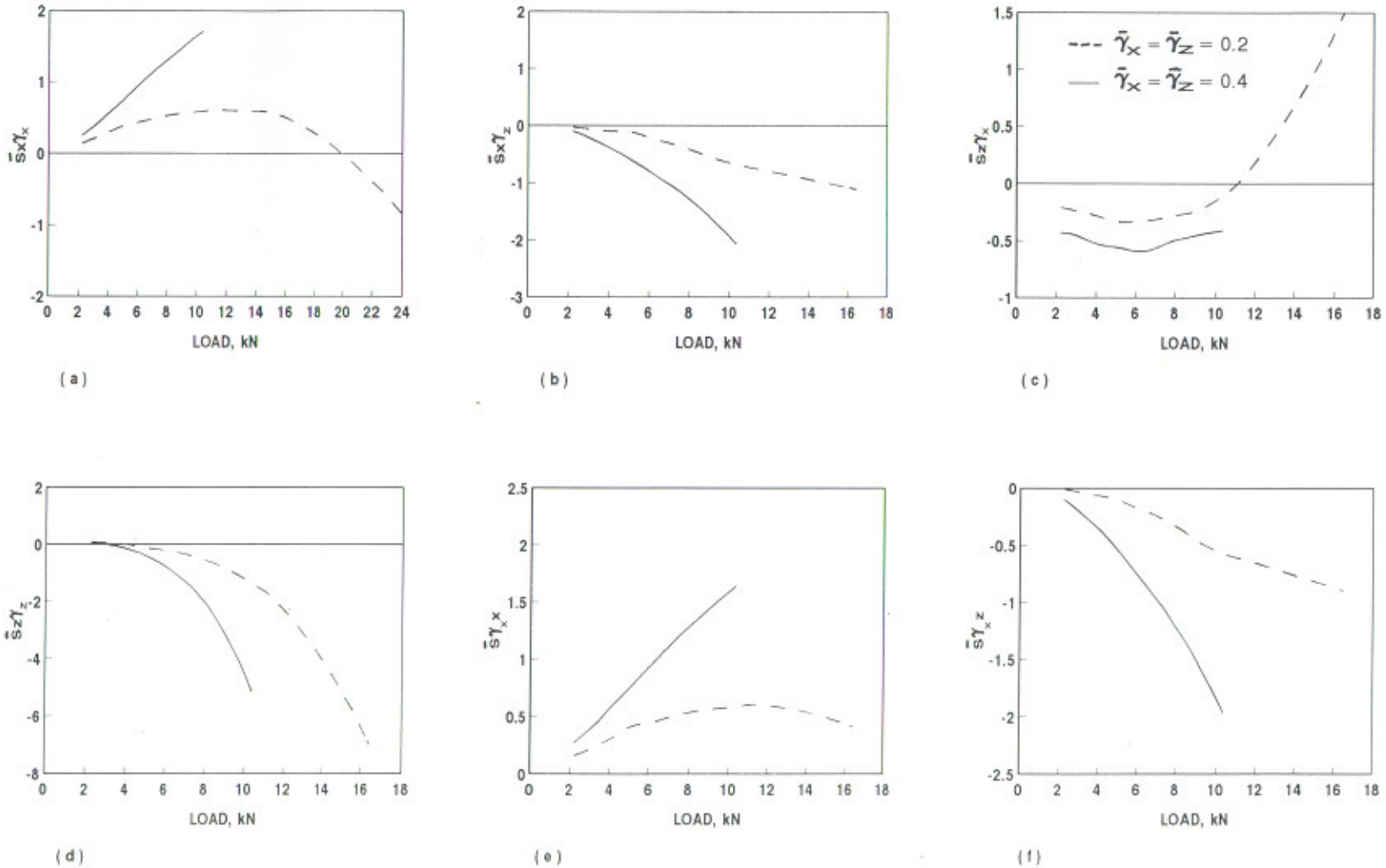

Fig. 5.21 TWO-AXIAL-GROOVE JOURNAL BEARING - STIFFNESS COEFFICIENTS

($\bar{S}x\gamma_x$, $\bar{S}x\gamma_z$, $\bar{S}z\gamma_x$, $\bar{S}z\gamma_z$, $\bar{S}\gamma_x x$, $\bar{S}\gamma_x z$)

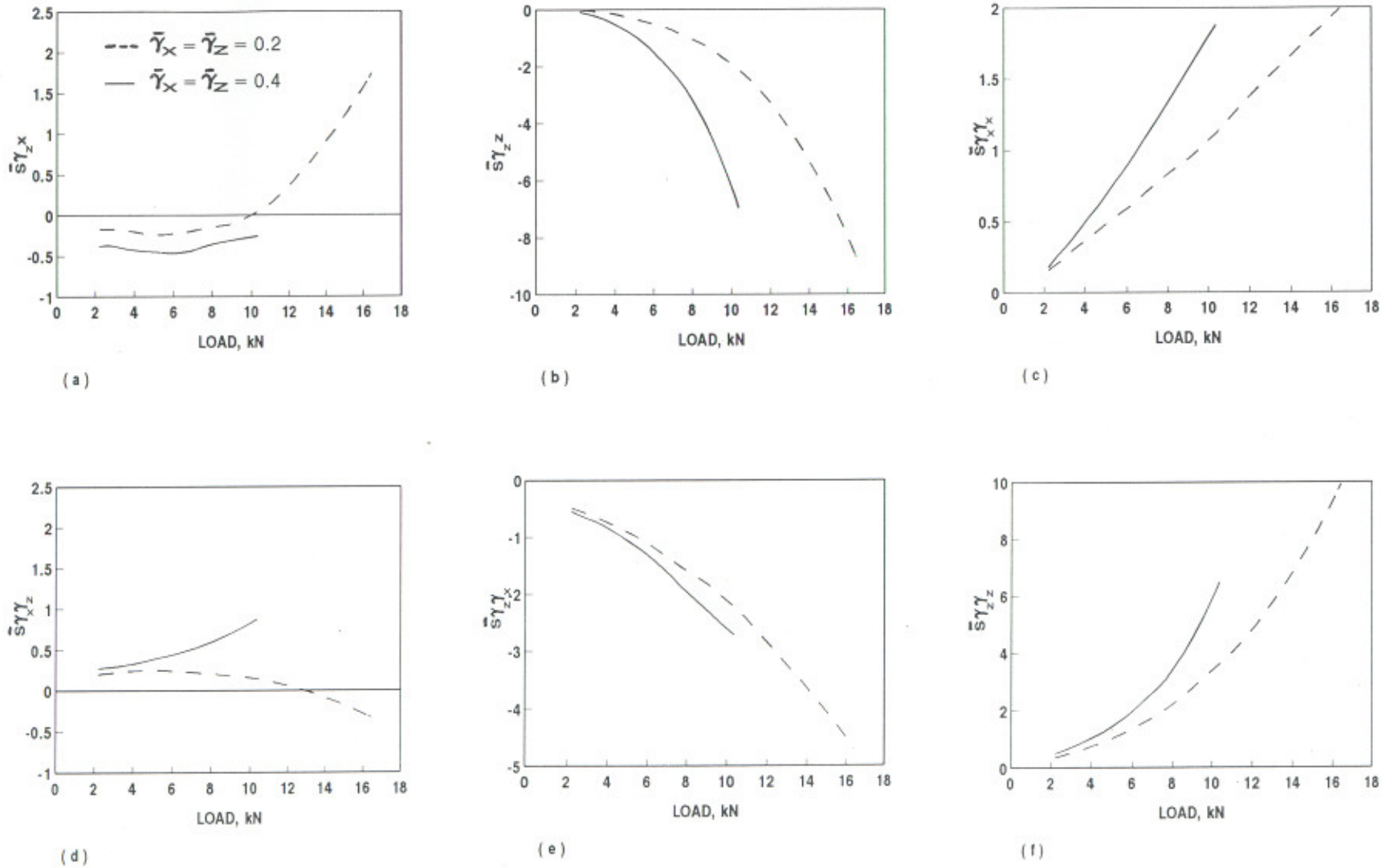

Fig. 5.22 TWO-AXIAL-GROOVE JOURNAL BEARING - STIFFNESS COEFFICIENTS ($\bar{S}\gamma_z x$, $\bar{S}\gamma_z z$, $\bar{S}\gamma_x\gamma_x$, $\bar{S}\gamma_x\gamma_z$, $\bar{S}\gamma_z\gamma_x$, $\bar{S}\gamma_z\gamma_z$)

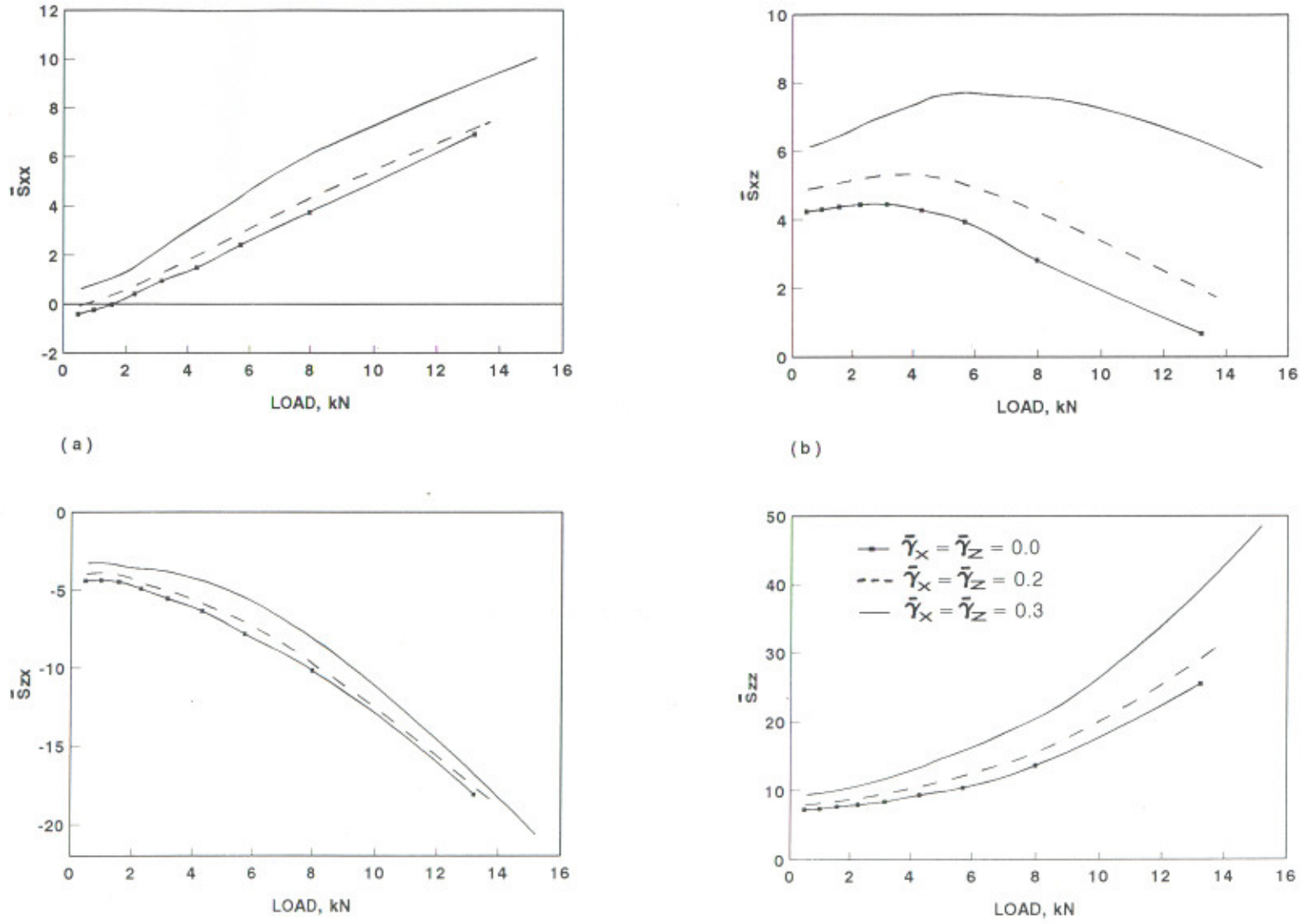

Fig. 5.23 ELLIPTICAL JOURNAL BEARING - STIFFNESS COEFFICIENTS ($\bar{S}_{xx}$, $\bar{S}_{xz}$, $\bar{S}_{zx}$, $\bar{S}_{zz}$)

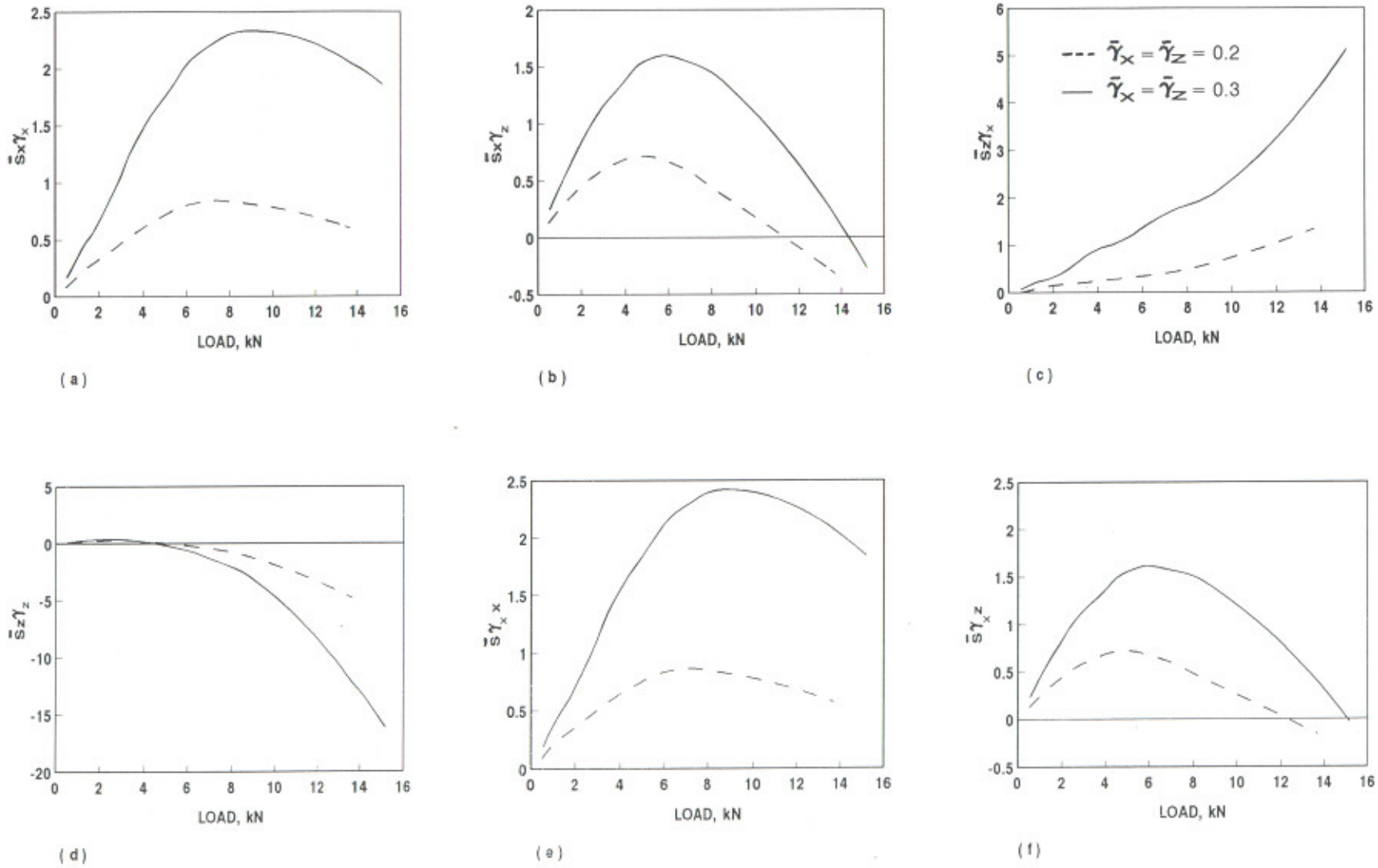

Fig. 5.24 ELLIPTICAL JOURNAL BEARING - STIFFNESS COEFFICIENTS
($\bar{S}x\gamma_x$, $\bar{S}x\gamma_z$, $\bar{S}z\gamma_x$, $\bar{S}z\gamma_z$, $\bar{S}\gamma_x x$, $\bar{S}\gamma_x z$)

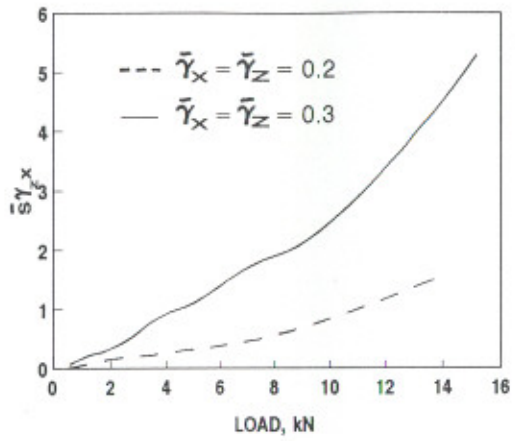

(a)

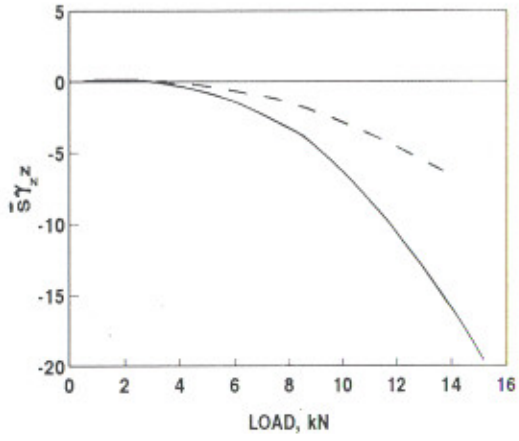

(b)

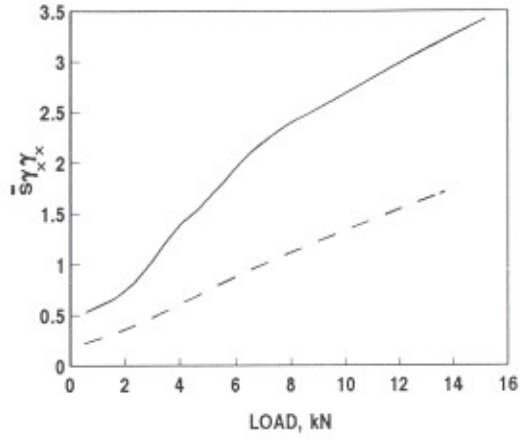

(c)

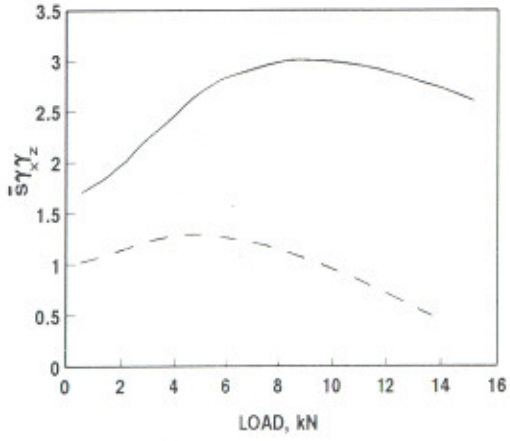

(d)

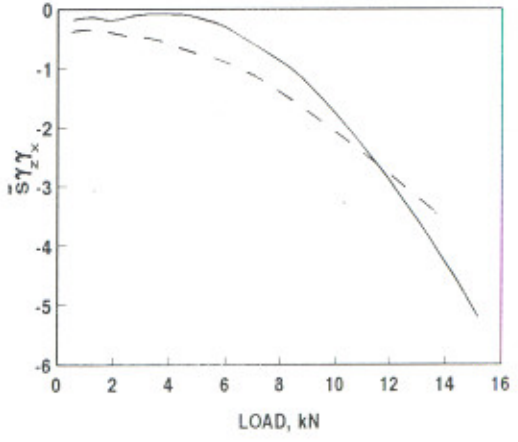

(e)

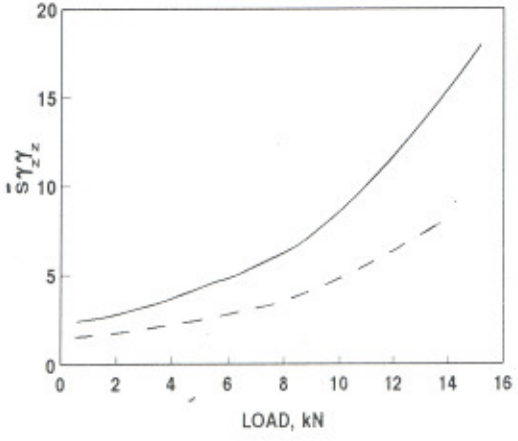

(f)

Fig. 5.25 ELLIPTICAL JOURNAL BEARING - STIFFNESS COEFFICIENTS

($\bar{S}\gamma_z x$, $\bar{S}\gamma_z z$, $\bar{S}\gamma_x\gamma_x$, $\bar{S}\gamma_x\gamma_z$, $\bar{S}\gamma_z\gamma_x$, $\bar{S}\gamma_z\gamma_z$)

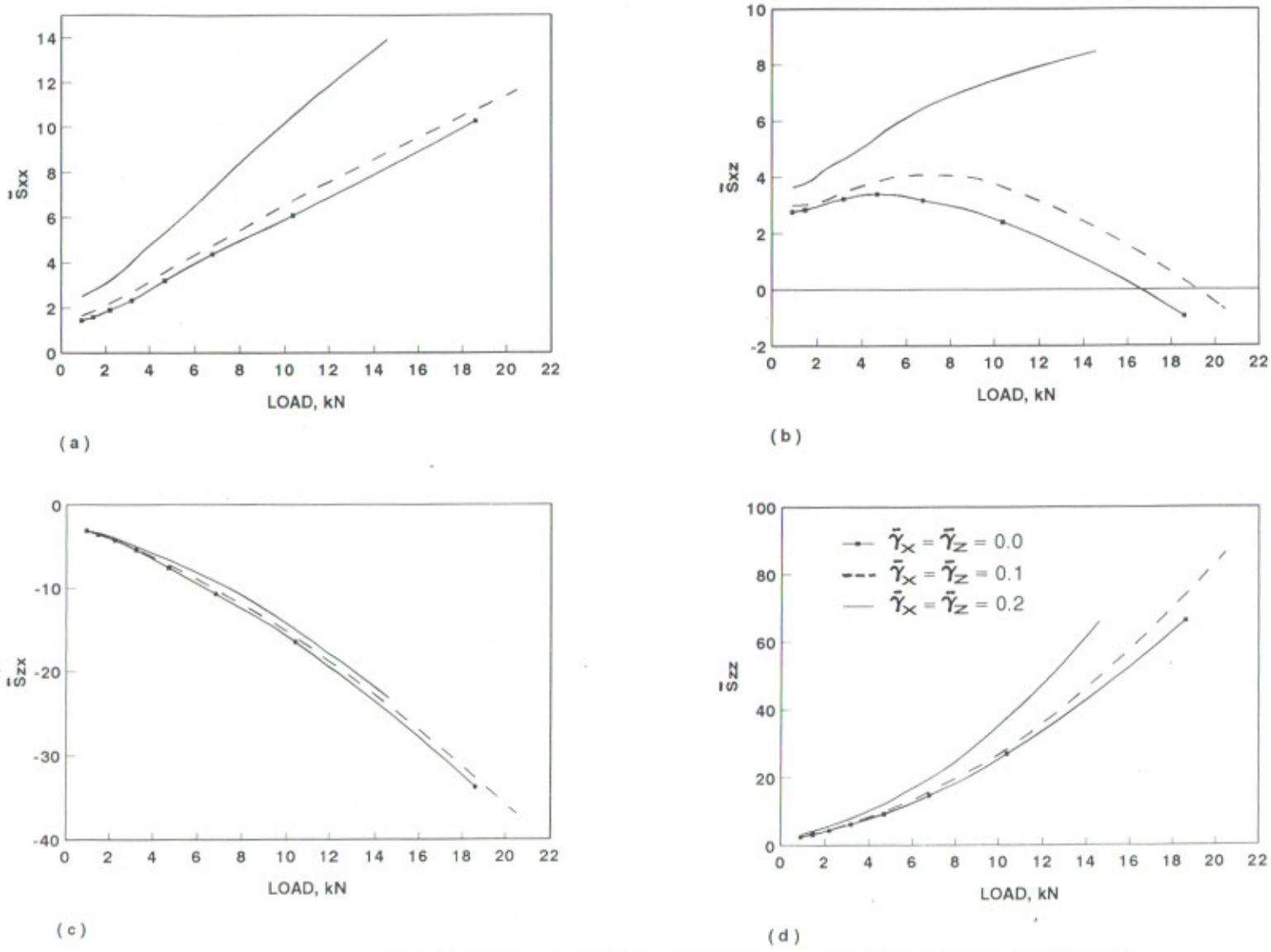

Fig. 5.26 THREE-LOBE JOURNAL BEARING - STIFFNESS COEFFICIENTS
($\bar{S}_{XX}$ $\bar{S}_{XZ}$ $\bar{S}_{ZX}$ $\bar{S}_{ZZ}$)

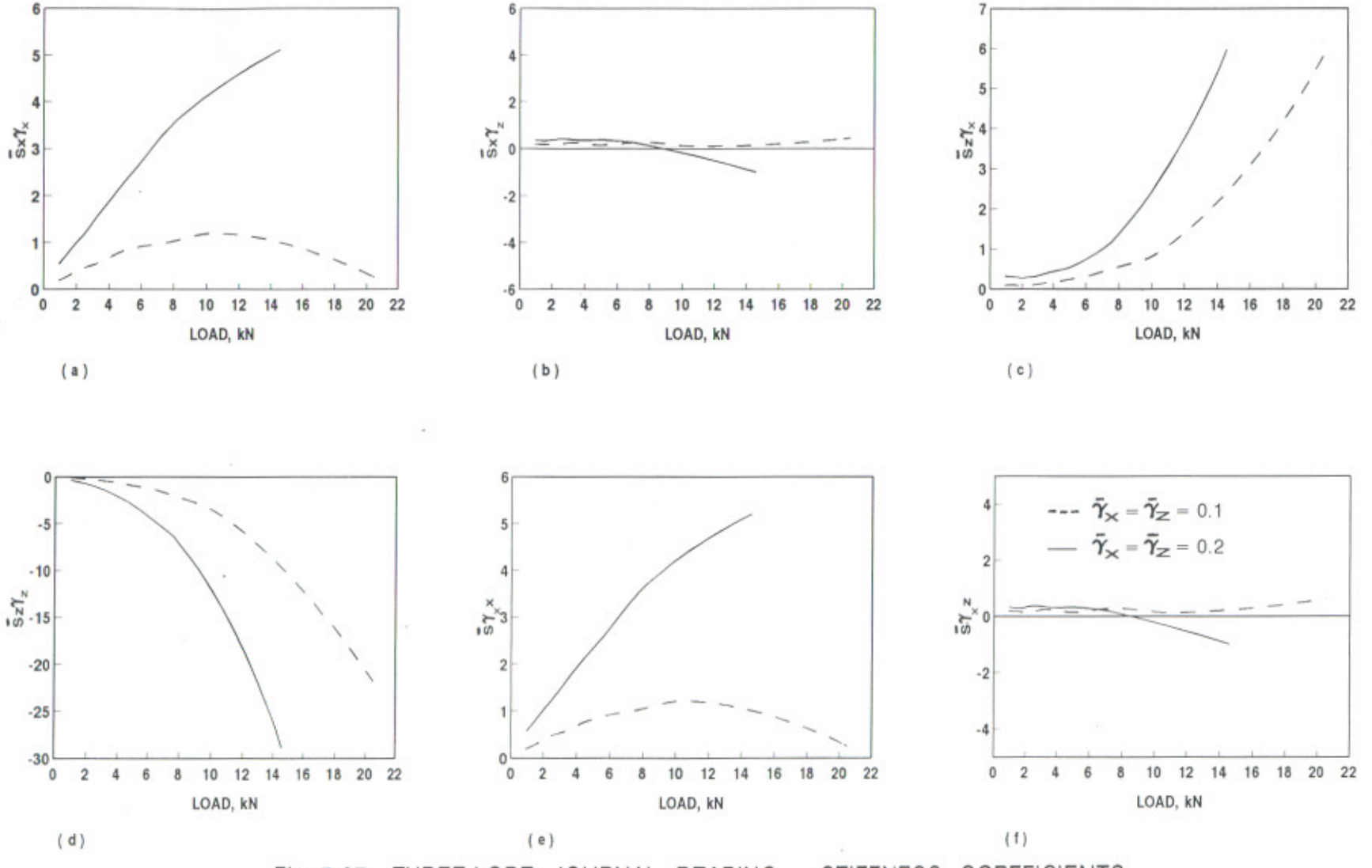

Fig. 5.27 THREE-LOBE JOURNAL BEARING - STIFFNESS COEFFICIENTS
($\bar{S}x\gamma_x$, $\bar{S}x\gamma_z$, $\bar{S}z\gamma_x$, $\bar{S}z\gamma_z$, $\bar{S}\gamma_x x$, $\bar{S}\gamma_x z$)

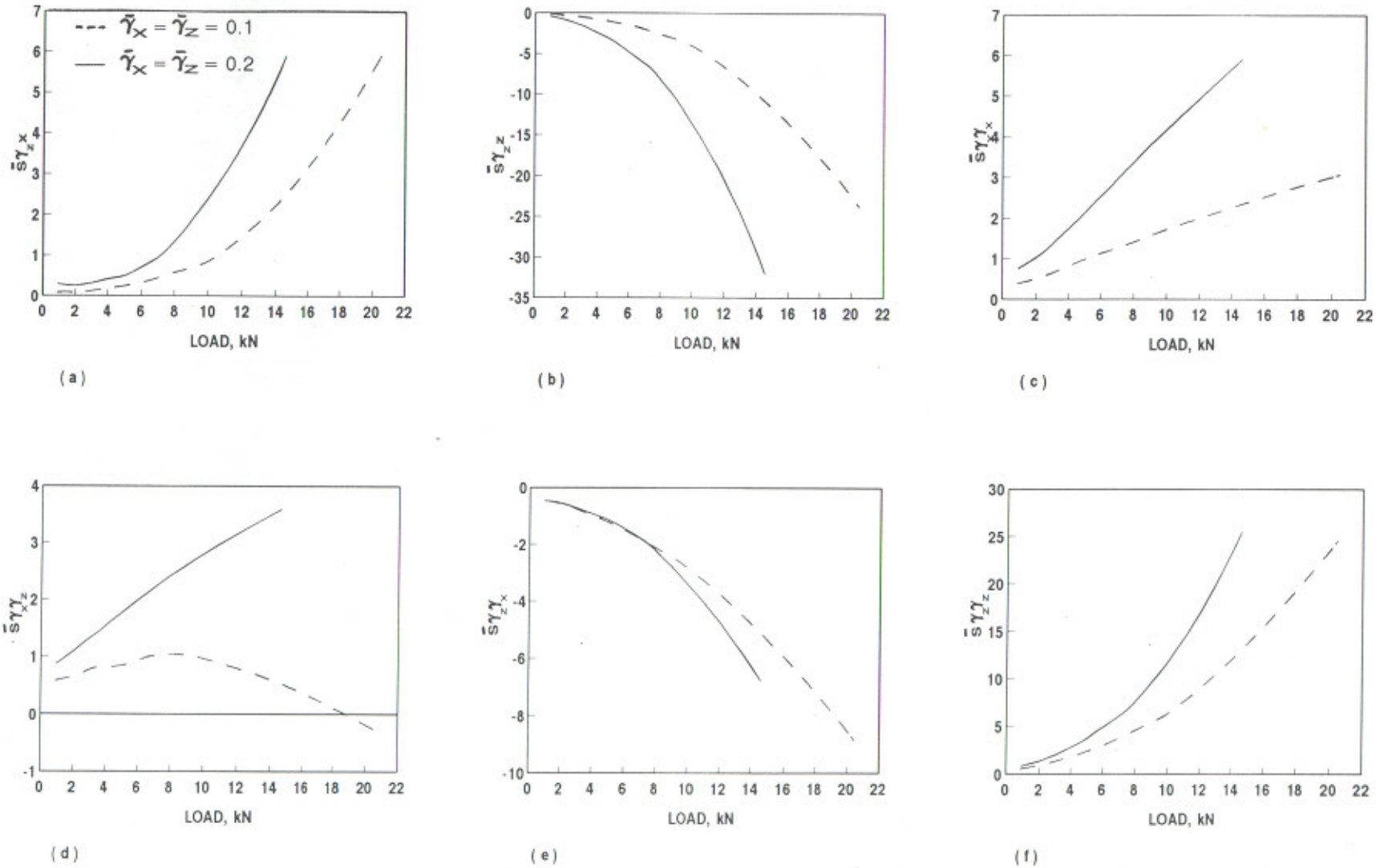

Fig. 5.28 THREE-LOBE JOURNAL BEARING - STIFFNESS COEFFICIENTS

($\bar{S}\gamma_z x$, $\bar{S}\gamma_z z$, $\bar{S}\gamma_x \gamma_x$, $\bar{S}\gamma_x \gamma_z$, $\bar{S}\gamma_z \gamma_x$, $\bar{S}\gamma_z \gamma_z$)

5.19(b), 5.22(b), 5.25(b), 5.28(b)}, and $\bar{S}_{\gamma_z\gamma_x}$ {Figs. 5.19(e), 5.22(e)}, decrease with the increase in misalignment. In the case of plain journal bearing and two-axial-groove journal bearing, the stiffness coefficients $\bar{S}_{x\gamma_z}$, $\bar{S}_{z\gamma_z}$, $\bar{S}_{\gamma_x z}$, $\bar{S}_{\gamma_z z}$ and $\bar{S}_{\gamma_z\gamma_x}$ have negative values in the entire range of load and their absolute values are increased by the misalignment. Figs. 5.18(c) and 5.21(c) reveal that as the misalignment increases, $\bar{S}_{z\gamma_x}$ decreases at light loads but increases at higher load values for plain and two-axial-groove journal bearings whereas for elliptical and three-lobe journal bearings, the stiffness coeffcient, $\bar{S}_{z\gamma_x}$ increases with the increase in misalignment, {Figs. 5.24(c) and 5.27(c)}.

It has been noticed that in the case of non-circular bearings, $\bar{S}_{\gamma_z x}$ {Figs. 5.25(a), 5.28(a)} and $\bar{S}_{\gamma_z\gamma_x}$ {Figs. 5.25(e), 5.28(e)} increase with the increase in the value of misalignment. In the case of elliptical journal bearing, $\bar{S}_{x\gamma_z}$ {Fig. 5.24(b)} and $\bar{S}_{\gamma_x z}$ {Fig. 5.24(f)} show a rising trend with the increase in value of misalignment.

5.3.3 Damping Coefficients

The damping coefficients are presented for all the bearing systems in Figs. 5.29 to 5.40. It is observed from the figures that the damping coefficients $\bar{B}_{xx}$ {Figs. 5.29(a), 5.32(a), 5.35(a), 5.38(a)}, $\bar{B}_{xz}$ (= $\bar{B}_{zx}$) {Figs. 5.29(b), 5.32(b), 5.35(b), 5.38(b)}, $\bar{B}_{zz}$ {Figs. 5.29(c), 5.32(c), 5.35(c), 5.38(c)}, $\bar{B}_{x\gamma_x}$ (= $\bar{B}_{\gamma_x x}$) {Figs. 5.30(a), 5.33(a), 5.36(a), 5.39(a)}, $\bar{B}_{\gamma_x\gamma_x}$ {Figs. 5.31(a), 5.34(a), 5.37(a), 5.40(a)}, $\bar{B}_{\gamma_x\gamma_z}$ (= $\bar{B}_{\gamma_z\gamma_x}$) {Figs. 5.31(b), 5.34(b), 5.37(b), 5.40(b)} and $\bar{B}_{\gamma_z\gamma_z}$ {Figs. 5.31(c), 5.34(c), 5.37(c), 5.40(c)} for all the bearing systems increase with the increase in misalignment. This increase is more at higher value of misalignment ratio. The damping coefficients $\bar{B}_{x\gamma_z}$ (= $\bar{B}_{\gamma_z x}$) {Figs. 5.30(b), 5.33(b), 5.39(b)}, $\bar{B}_{z\gamma_x}$ (= $\bar{B}_{\gamma_x z}$) {Figs. 5.30(c), 5.33(c), 5.39(c)} and $\bar{B}_{z\gamma_z}$ (= $\bar{B}_{\gamma_z z}$) {Figs. 5.30(d), 5.33(d), 5.36(d), 5.39(d)} are reduced with the increase in misalignment.

In the case of elliptical journal bearing, the damping coefficient $\bar{B}_{x\gamma_z}$ (= $\bar{B}_{\gamma_z x}$) {Fig. 5.36(b)} and $\bar{B}_{z\gamma_x}$ (= $\bar{B}_{\gamma_x z}$) {Fig. 5.36(c)} show a rising trend with the increase in misalignment.

The damping coefficients, $\bar{B}_{xx}$ {Figs. 5.29(a), 5.32(a), 5.35(a), 5.38(a)}, $\bar{B}_{zz}$ {Figs. 5.29(c), 5.32(c), 5.35(c), 5.38(c)}, $\bar{B}_{x\gamma_x}$ (= $\bar{B}_{\gamma_x x}$) {Figs. 5.30(a), 5.33(a), 5.36(a), 5.39(a)}, $\bar{B}_{\gamma_x\gamma_x}$ {Figs. 5.31(a), 5.34(a), 5.37(a), 5.40(a)} and $\bar{B}_{\gamma_z\gamma_z}$ {Figs. 5.31(c), 5.34(c), 5.37(c), 5.40(c)} increase with the rise in load values. Whereas $\bar{B}_{xz}$ (= $\bar{B}_{zx}$) {Figs. 5.29(b), 5.32(b), 5.35(b),

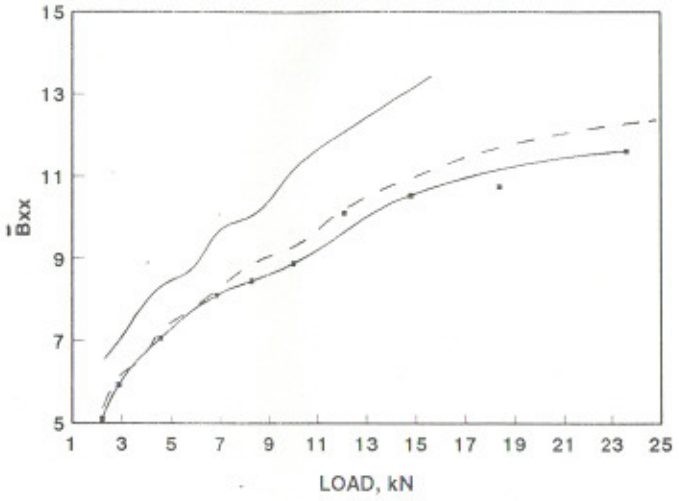

(a)

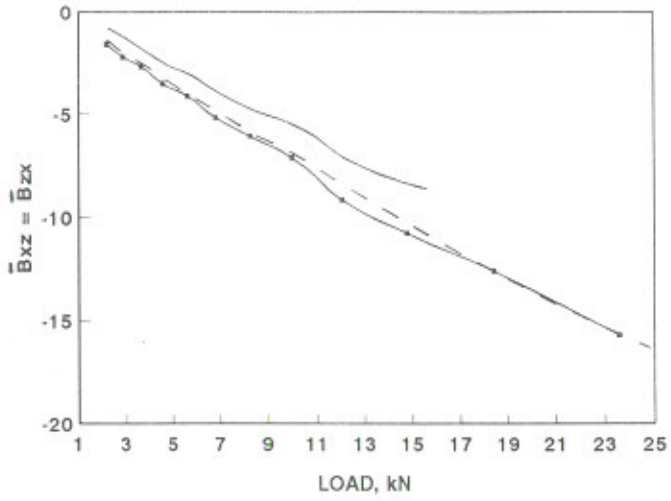

(b)

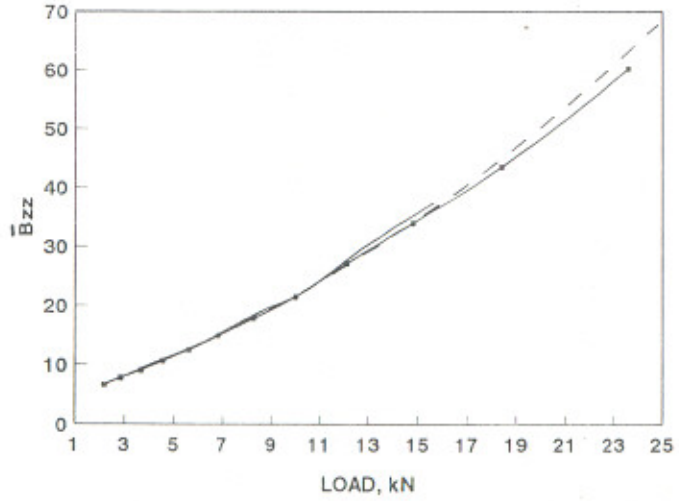

(c)

LEGEND :

$\bar{\gamma}_x = \bar{\gamma}_z = 0.0$

$\bar{\gamma}_x = \bar{\gamma}_z = 0.2$

$\bar{\gamma}_x = \bar{\gamma}_z = 0.4$

Fig. 5.29 PLAIN JOURNAL BEARING - DAMPING COEFFICIENTS
($\bar{B}xx$, $\bar{B}xz$, $\bar{B}zx$, $\bar{B}zz$)

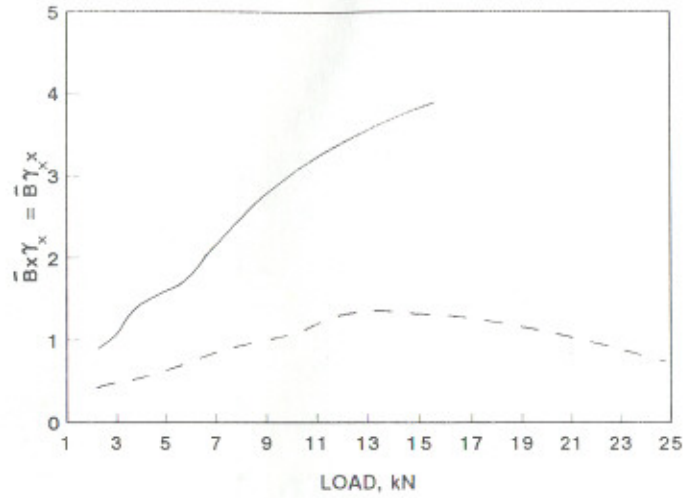

(a)

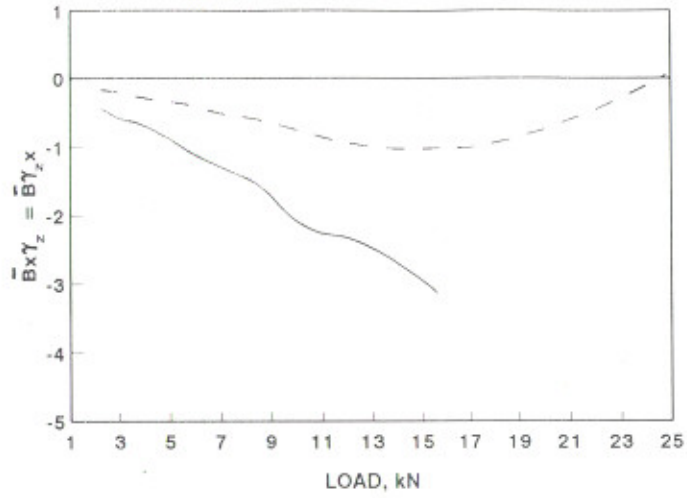

(b)

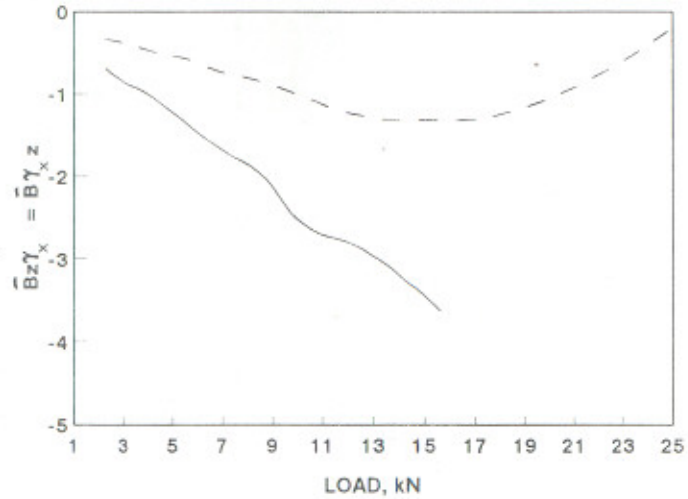

(c)

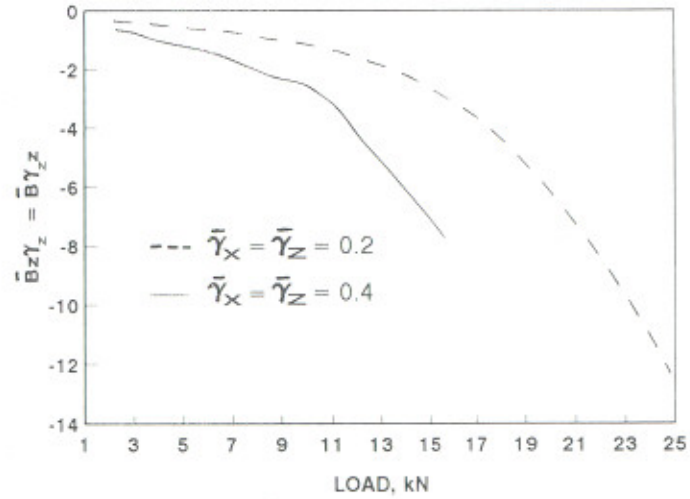

(d)

Fig. 5.30 PLAIN JOURNAL BEARING - DAMPING COEFFICIENTS

($\bar{B}x\bar{\gamma}_x$, $\bar{B}x\bar{\gamma}_z$, $\bar{B}z\bar{\gamma}_x$, $\bar{B}z\bar{\gamma}_z$, $\bar{B}\bar{\gamma}_x x$, $\bar{B}\bar{\gamma}_z x$, $\bar{B}\bar{\gamma}_x z$, $\bar{B}\bar{\gamma}_z z$)

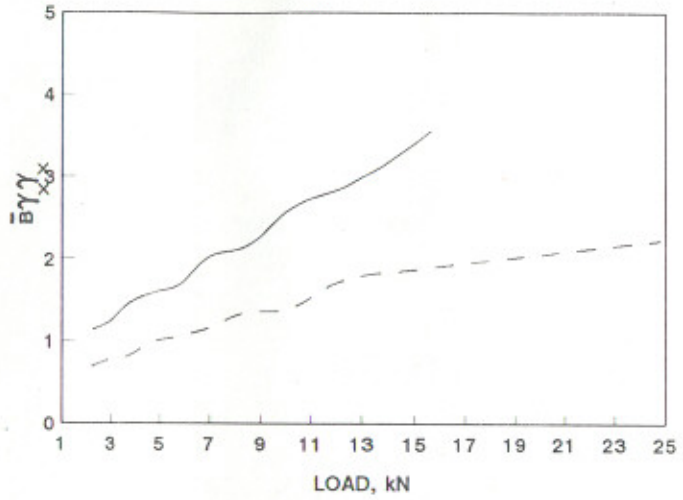

(a)

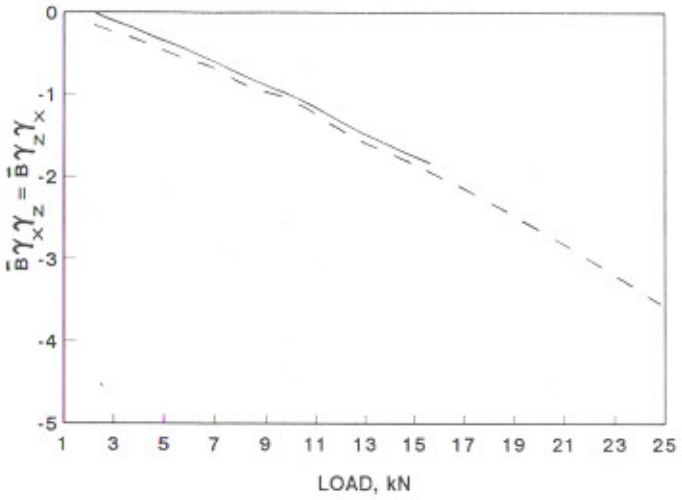

(b)

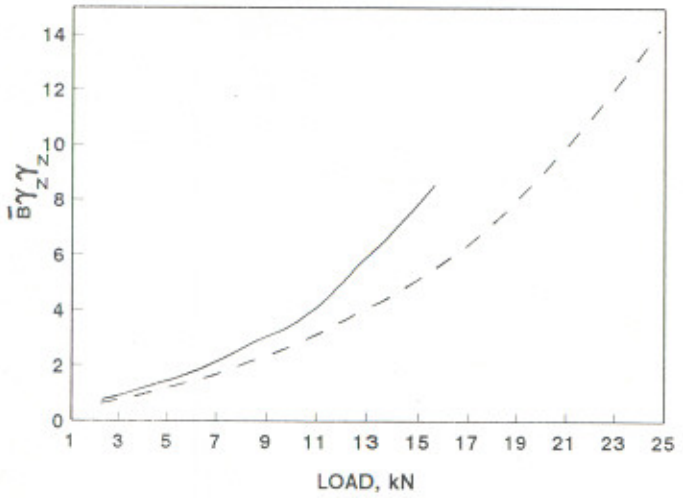

(c)

LEGEND :

--- $\bar{\gamma}_x = \bar{\gamma}_z = 0.2$

—— $\bar{\gamma}_x = \bar{\gamma}_z = 0.4$

Fig. 5.31 PLAIN JOURNAL BEARING - DAMPING COEFFICIENTS ($\bar{B}\bar{\gamma}_x\bar{\gamma}_x$, $\bar{B}\bar{\gamma}_x\bar{\gamma}_z$, $\bar{B}\bar{\gamma}_z\bar{\gamma}_x$, $\bar{B}\bar{\gamma}_z\bar{\gamma}_z$)

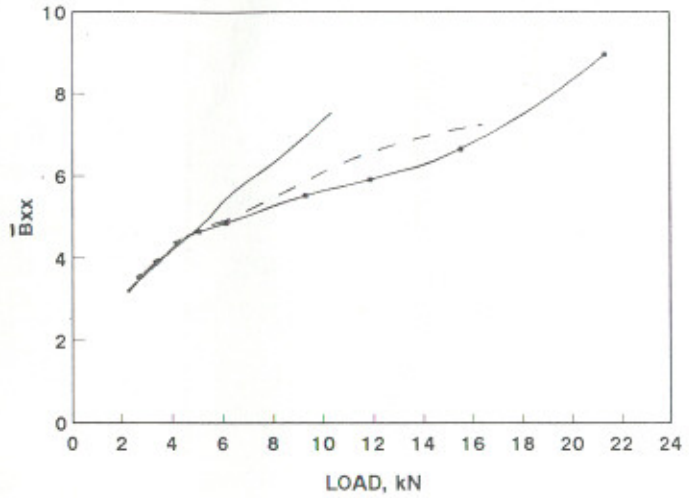

(a)

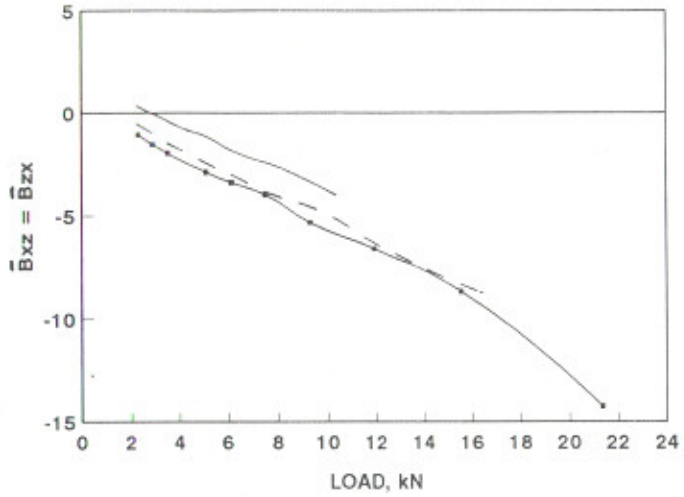

(b)

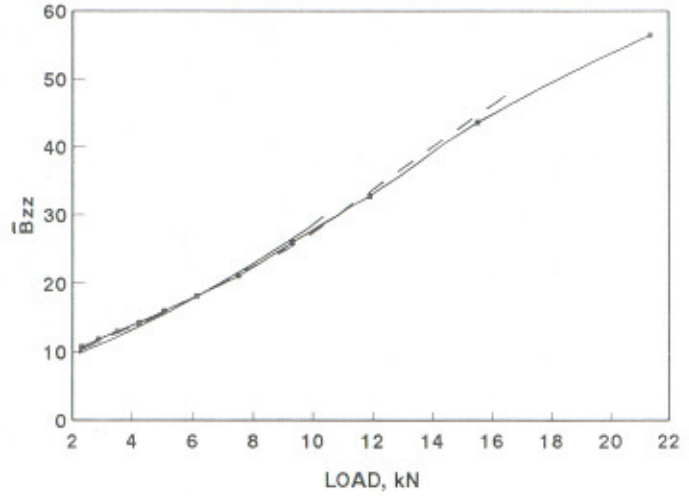

(c)

LEGEND :

$\bar{\gamma}_x = \bar{\gamma}_z = 0.0$

$\bar{\gamma}_x = \bar{\gamma}_z = 0.2$

$\bar{\gamma}_x = \bar{\gamma}_z = 0.4$

Fig. 5.32 TWO-AXIAL-GROOVE JOURNAL BEARING - DAMPING COEFFICIENTS ($\bar{B}_{xx}$, $\bar{B}_{xz}$, $\bar{B}_{zx}$, $\bar{B}_{zz}$)

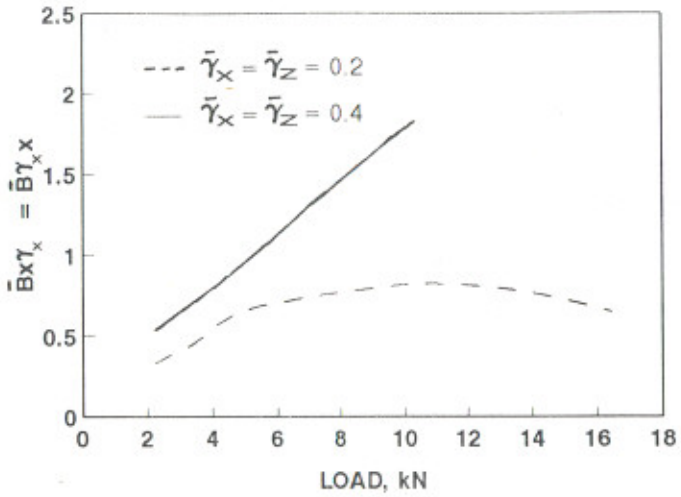

(a)

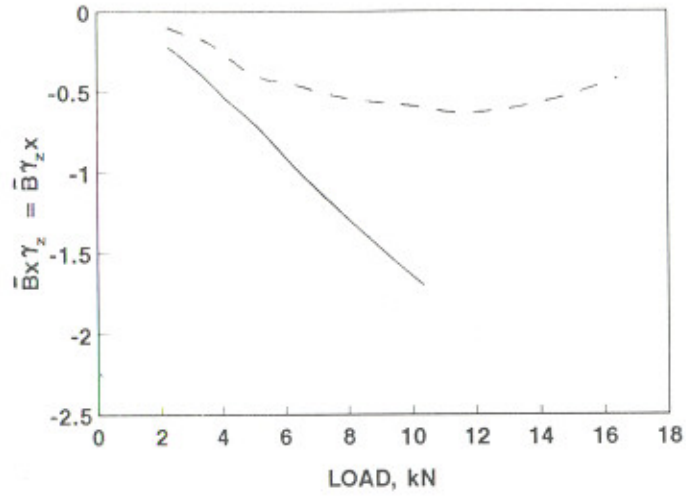

(b)

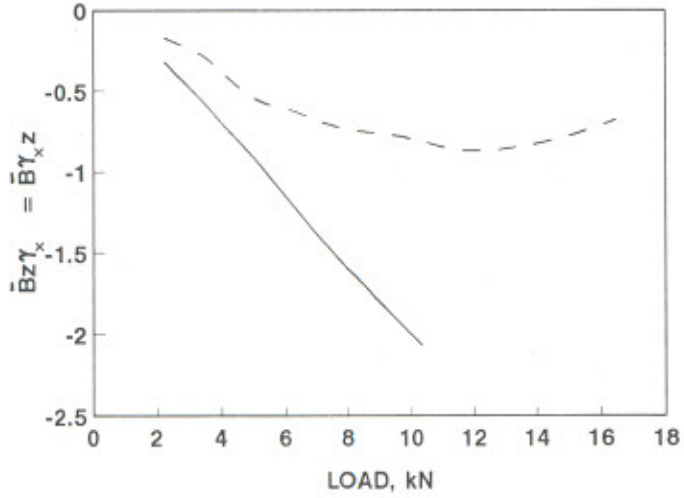

(c)

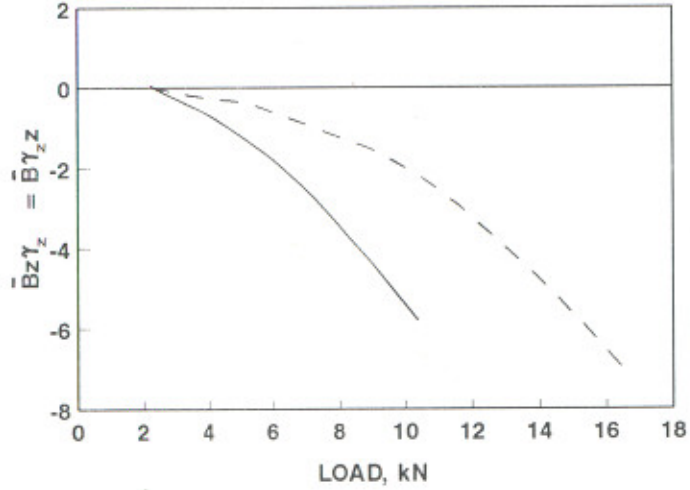

(d)

Fig. 5.33 TWO-AXIAL-GROOVE JOURNAL BEARING - DAMPING COEFFICIENTS

($\bar{B}x\gamma$, $\bar{B}x\gamma$, $\bar{B}z\gamma$, $\bar{B}z\gamma$, $\bar{B}\gamma x$, $\bar{B}\gamma x$, $\bar{B}\gamma z$, $\bar{B}\gamma z$)

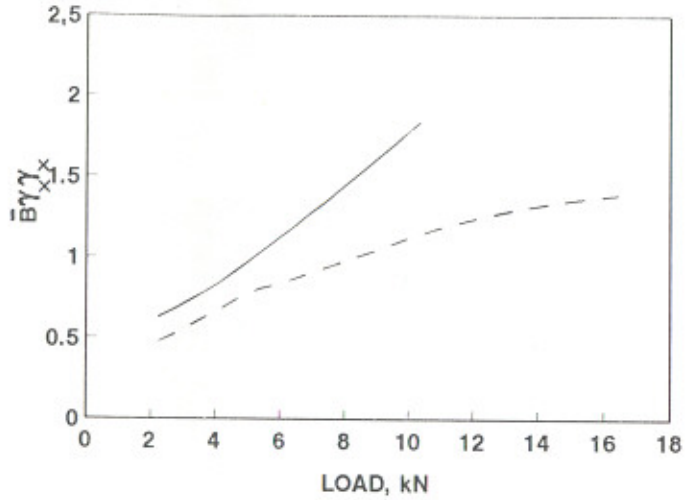

(a)

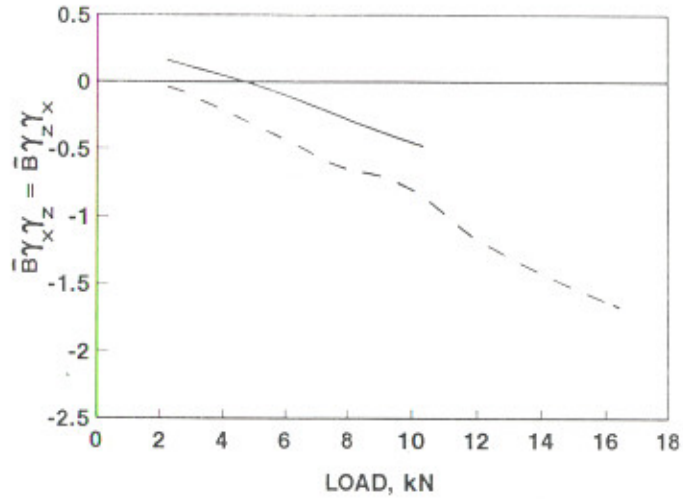

(b)

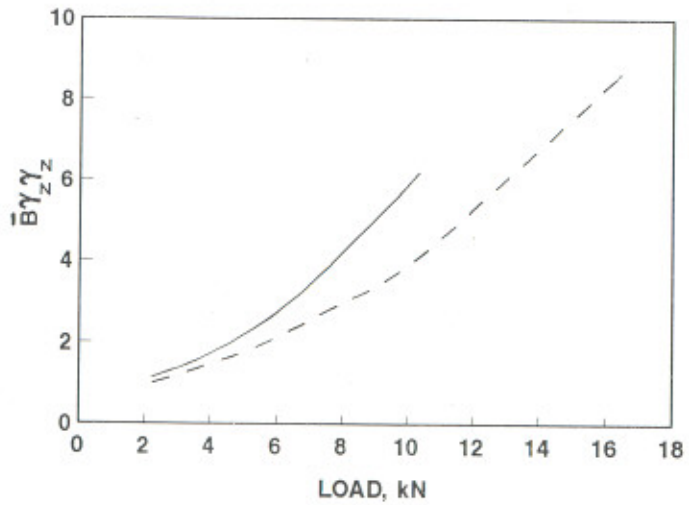

(c)

LEGEND :

--- $\bar{\gamma}_x = \bar{\gamma}_z = 0.2$

— $\bar{\gamma}_x = \bar{\gamma}_z = 0.4$

Fig. 5.34 TWO-AXIAL-GROOVE JOURNAL BEARING - DAMPING COEFFICIENTS ($\bar{B}\gamma_x\gamma_x$, $\bar{B}\gamma_x\gamma_z$, $\bar{B}\gamma_z\gamma_x$, $\bar{B}\gamma_z\gamma_z$)

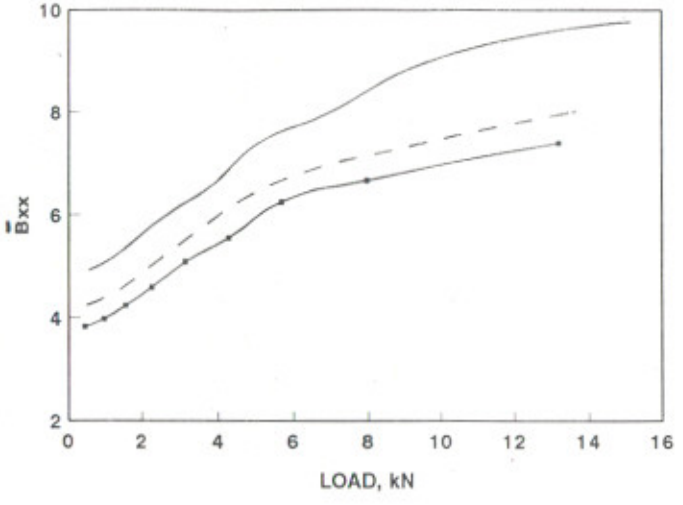

(a)

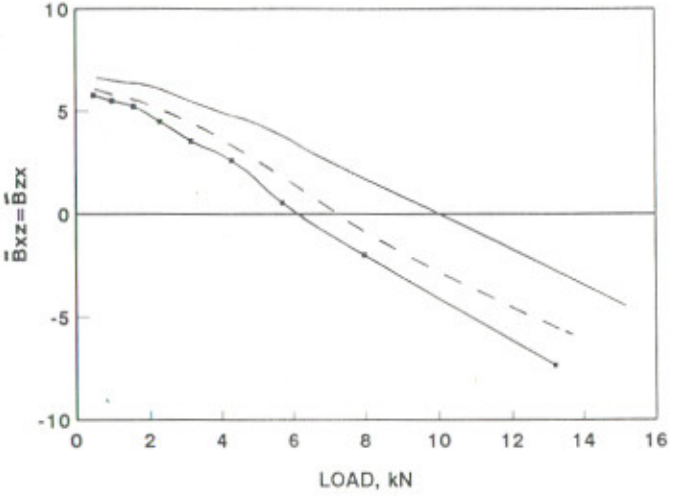

(b)

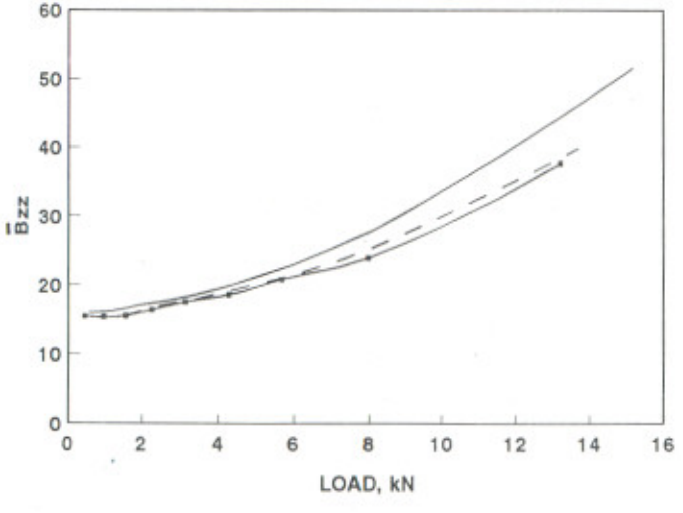

(c)

LEGEND :

$\bar{\gamma}_x = \bar{\gamma}_z = 0.0$

$\bar{\gamma}_x = \bar{\gamma}_z = 0.2$

$\bar{\gamma}_x = \bar{\gamma}_z = 0.3$

Fig. 5.35 ELLIPTICAL JOURNAL BEARING - DAMPING COEFFICIENTS
($\bar{B}xx$, $\bar{B}xz$, $\bar{B}zx$, $\bar{B}zz$)

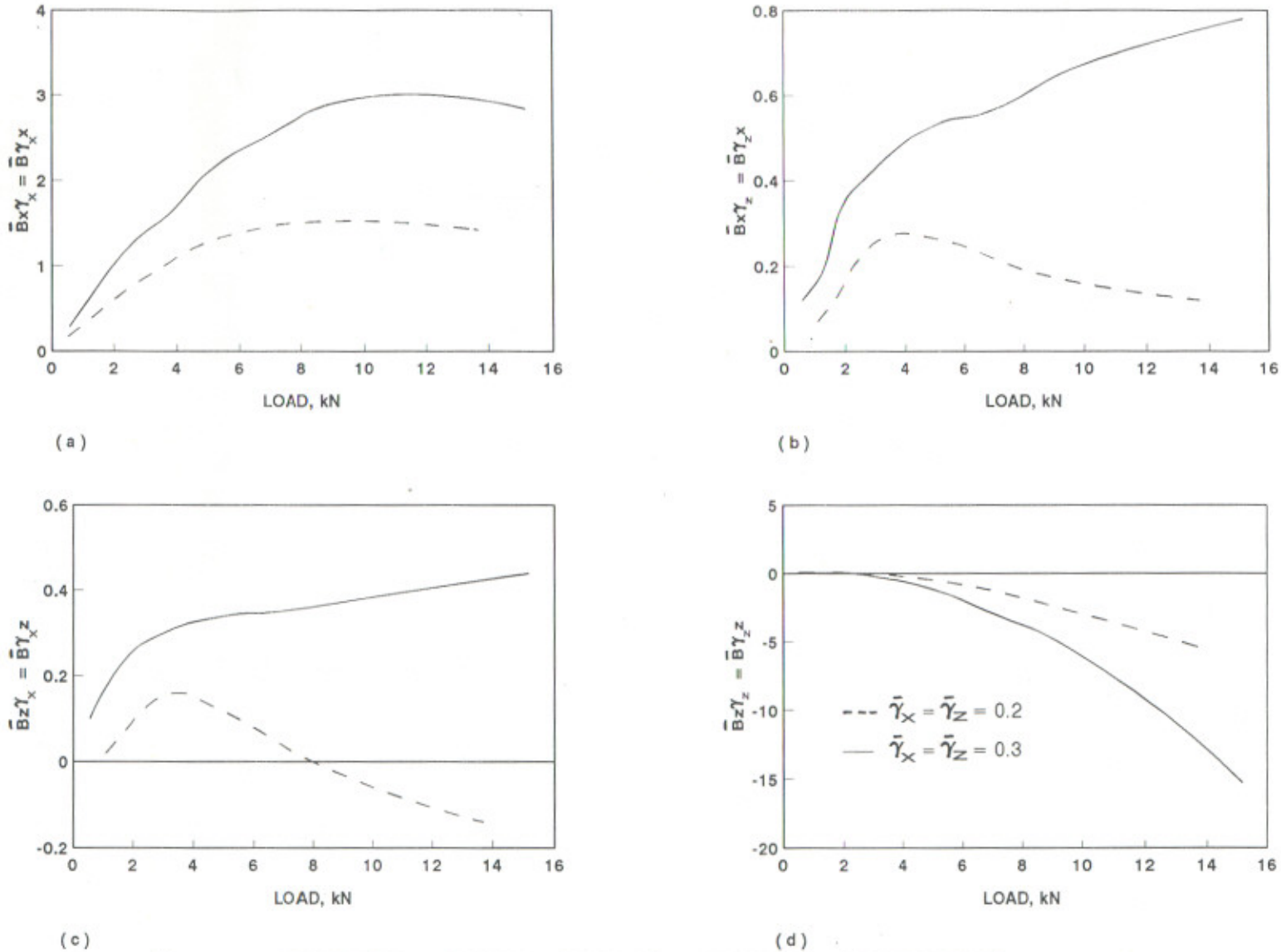

Fig. 5.36 ELLIPTICAL JOURNAL BEARING - DAMPING COEFFICIENTS

($\bar{B}x\bar{\gamma}_x$, $\bar{B}x\bar{\gamma}_z$, $\bar{B}z\bar{\gamma}_x$, $\bar{B}z\bar{\gamma}_z$, $\bar{B}\bar{\gamma}_x x$, $\bar{B}\bar{\gamma}_z x$, $\bar{B}\bar{\gamma}_x z$, $\bar{B}\bar{\gamma}_z z$)

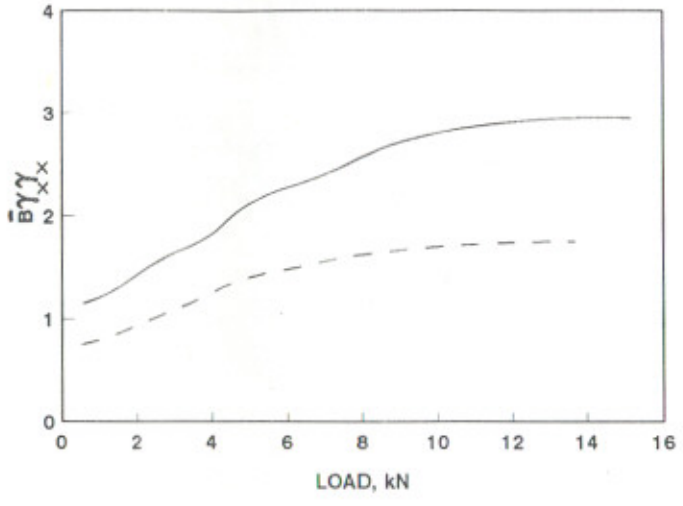

(a)

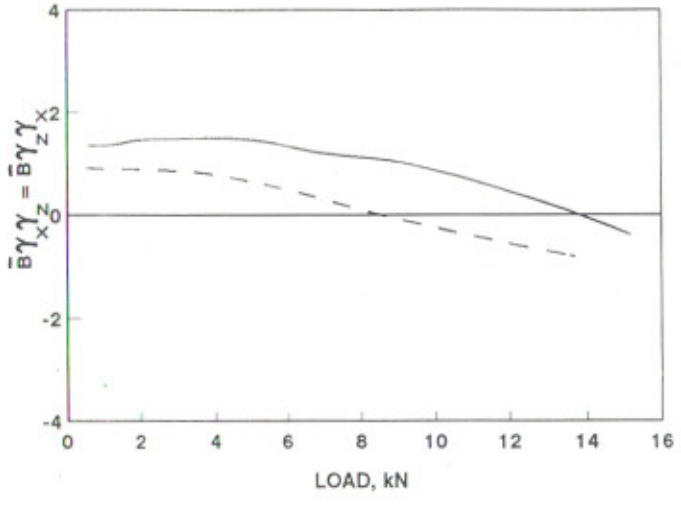

(b)

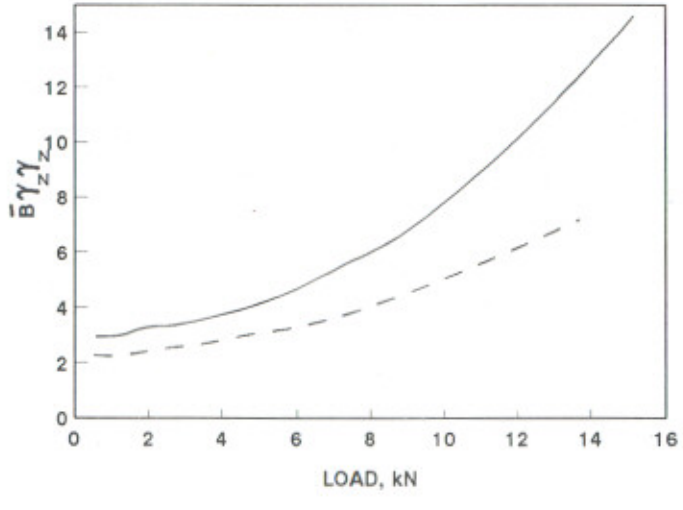

(c)

LEGEND :

--- $\bar{\gamma}_x = \bar{\gamma}_z = 0.2$

— $\bar{\gamma}_x = \bar{\gamma}_z = 0.3$

Fig. 5.37 ELLIPTICAL JOURNAL BEARING - DAMPING COEFFICIENTS ($\bar{B}\bar{\gamma}_x\bar{\gamma}_x$, $\bar{B}\bar{\gamma}_x\bar{\gamma}_z$, $\bar{B}\bar{\gamma}_z\bar{\gamma}_x$, $\bar{B}\bar{\gamma}_z\bar{\gamma}_z$)

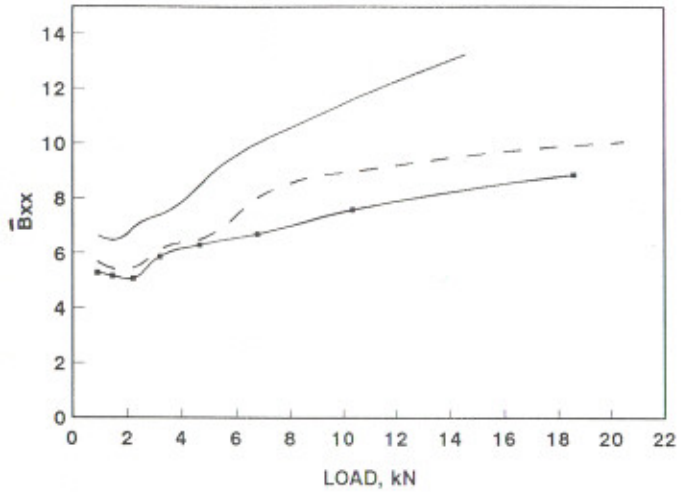

(a)

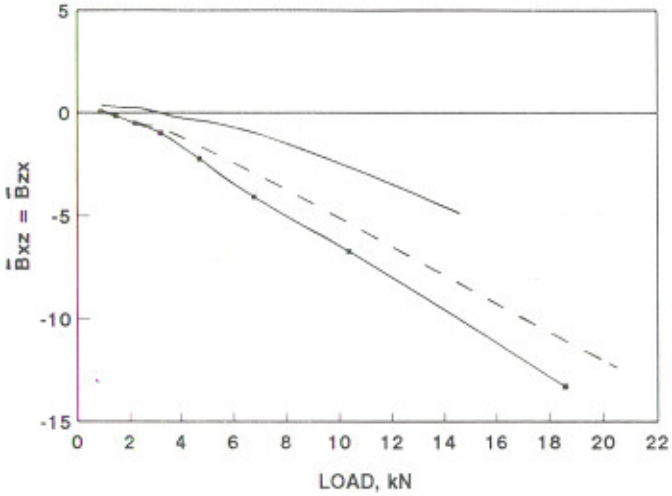

(b)

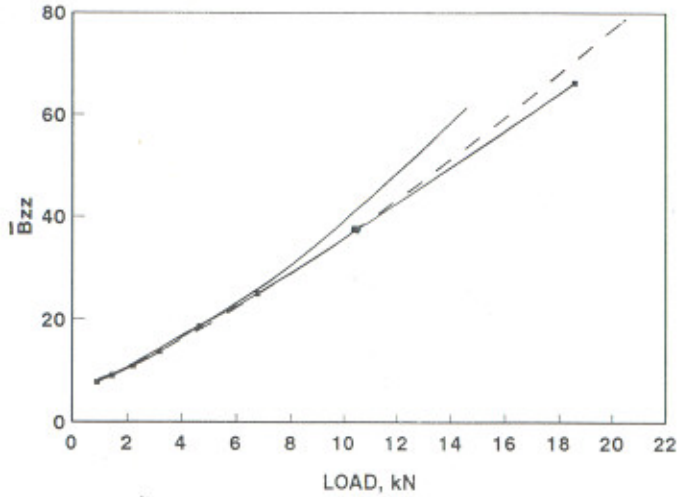

(c)

LEGEND :

$\bar{\gamma}_x = \bar{\gamma}_z = 0.0$

$\bar{\gamma}_x = \bar{\gamma}_z = 0.1$

$\bar{\gamma}_x = \bar{\gamma}_z = 0.2$

Fig. 5.38 THREE-LOBE JOURNAL BEARING - DAMPING COEFFICIENTS ($\bar{B}_{xx}$, $\bar{B}_{xz}$, $\bar{B}_{zx}$, $\bar{B}_{zz}$)

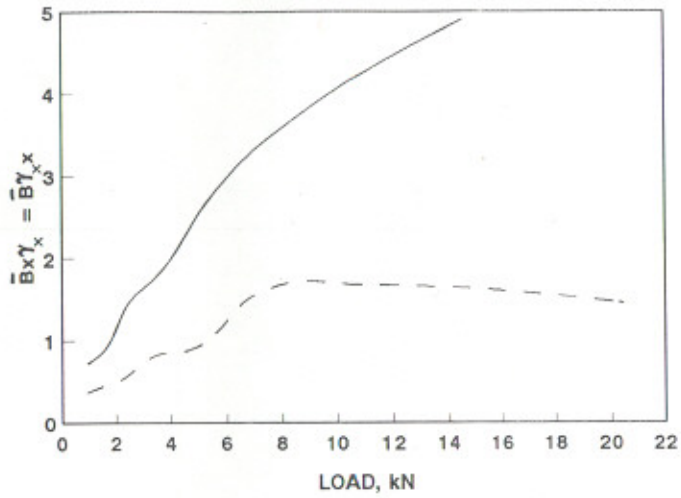

(a)

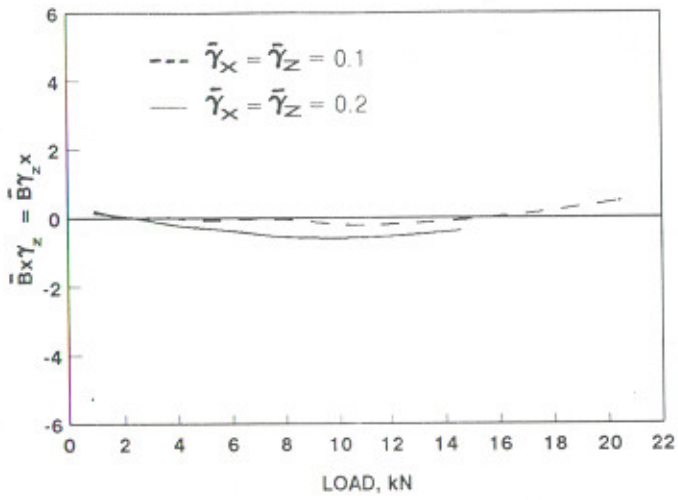

(b)

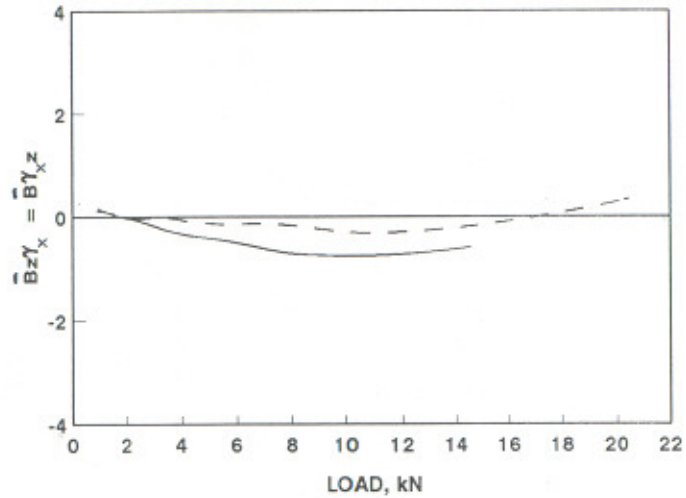

(c)

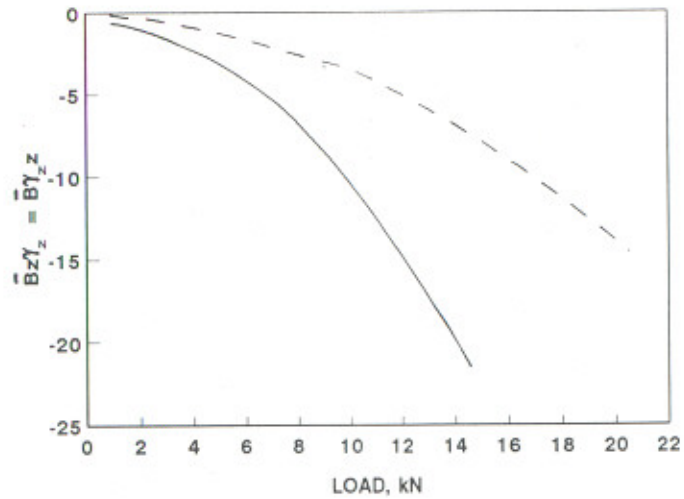

(d)

Fig. 5.39 THREE-LOBE JOURNAL BEARING - DAMPING COEFFICIENTS

($\bar{B}x\bar{\gamma}_x$, $\bar{B}x\bar{\gamma}_z$, $\bar{B}z\bar{\gamma}_x$, $\bar{B}z\bar{\gamma}_z$, $\bar{B}\bar{\gamma}_x x$, $\bar{B}\bar{\gamma}_z x$, $\bar{B}\bar{\gamma}_x z$, $\bar{B}\bar{\gamma}_z z$)

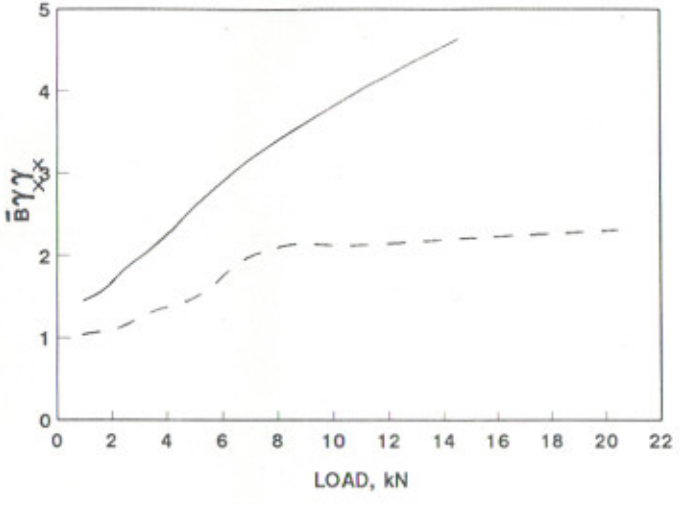

(a)

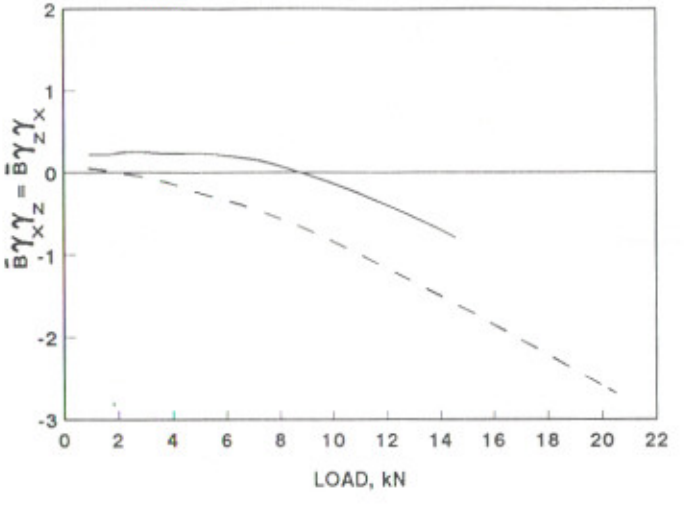

(b)

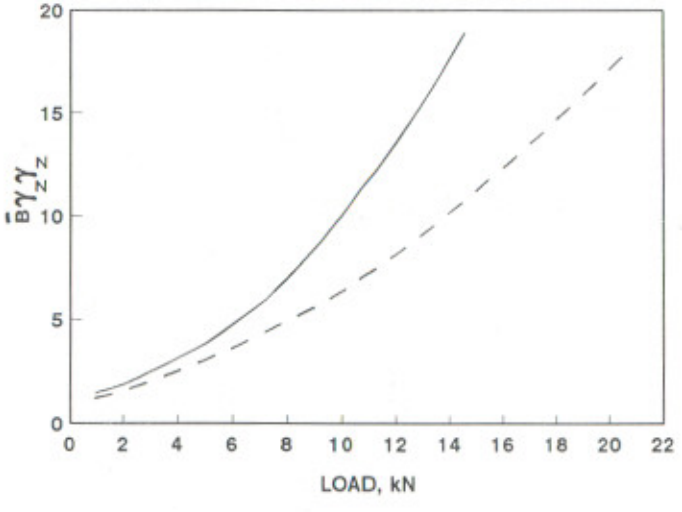

(c)

LEGEND :

--- $\bar{\gamma}_x = \bar{\gamma}_z = 0.1$

—— $\bar{\gamma}_x = \bar{\gamma}_z = 0.2$

Fig. 5.40 THREE-LOBE JOURNAL BEARING - DAMPING COEFFICIENTS ($\bar{B}\bar{\gamma}_x\bar{\gamma}_x$, $\bar{B}\bar{\gamma}_x\bar{\gamma}_z$, $\bar{B}\bar{\gamma}_z\bar{\gamma}_x$, $\bar{B}\bar{\gamma}_z\bar{\gamma}_z$)

5.38(b)}, $\bar{B}_{z\gamma_z}$ (= $\bar{B}_{\gamma_z z}$) {Figs. 5.30(d), 5.33(d), 5.36(d), 5.39(d)} and $\bar{B}_{\gamma_x \gamma_z}$ (= $\bar{B}_{\gamma_z \gamma_x}$) {Figs. 5.31(b), 5.34(b), 5.37(b), 5.40(b)} decrease with the rise in load values.

In the case of plain journal bearing and two-axial-groove journal bearing, the damping coefficients $\bar{B}_{x\gamma_z}$ (= $\bar{B}_{\gamma_z x}$) {Figs. 5.30(b) and 5.33(b)} and $\bar{B}_{z\gamma_x}$ (= $\bar{B}_{\gamma_x z}$) {Figs. 5.30(c) and 5.33(c)} decrease with the increase in load values. Whereas in case of elliptical journal bearing, at light loads, the damping coefficients $\bar{B}_{x\gamma_z}$ (= $\bar{B}_{\gamma_z x}$) {Fig. 5.36(b)} and $\bar{B}_{z\gamma_x}$ (= $\bar{B}_{\gamma_x z}$) {Fig. 5.36(c)}, increase with the increase in the load value but at lower values of misalignment and at high load values, $\bar{B}_{x\gamma_z}$ (= $\bar{B}_{\gamma_z x}$) and $\bar{B}_{z\gamma_x}$ (= $\bar{B}_{\gamma_x z}$) show a decreasing trend. The damping coefficients, $\bar{B}_{x\gamma_z}$ (= $\bar{B}_{\gamma_z x}$) {Fig. 5.39(b)} and $\bar{B}_{z\gamma_x}$(= $\bar{B}_{\gamma_x z}$) {Fig. 5.39(c)} are almost constant in the entire range of load values, in case of both aligned and misaligned three-lobe journal bearing.

5.3.4 Stability Parameters

The values of instability threshold speed ($\bar{\Omega}$) and whirl frequency ratio ($\bar{\nu}$) are shown in Figs. 5.41 to 5.44 for all the bearing systems. The figures show that an increase in the misalignment significantly improves stability margin defined by $\bar{\Omega}$. The tendency to whirl after a disturbance is also reduced by misalignment. These effects are quite important at light loads where the journal bearing system has a tendency to become unstable in case of plain and two-axial-groove journal bearing. As an example, in case of plain journal bearing at 4 kN load, $\bar{\Omega}$ increases to 3.3 with the misalignment ratio of $\bar{\gamma}_x = \bar{\gamma}_z = 0.4$ from 2.65 for an aligned bearing showing an improvement in stability margin by about 23 %, Fig. 5.41(a).

For the aligned elliptical and three-lobe bearings, the values of threshold speed are first reduced and then increased as the load supported by the bearing is increased {Figs. 5.43(a) and 5.44(a)}. The both types of bearings tend to become infinitely stable for some value of load. The trends for the misaligned bearings are also same. In the later cases, however, the values of $\bar{\Omega}$ at each load are higher and the values of load at which the two journal bearing systems become infinitely stable are lower compared to the corresponding values for aligned bearings.

Whirl frequency ratio reduces with the increase in bearing load, {Figs. 5.41(b), 5.42(b), 5.43(b) and 5.44(b)}. In case of plain journal bearing and two-axial-groove bearing, whirl frequency ratio reduces with the increase in misalignment. For elliptical bearing, this

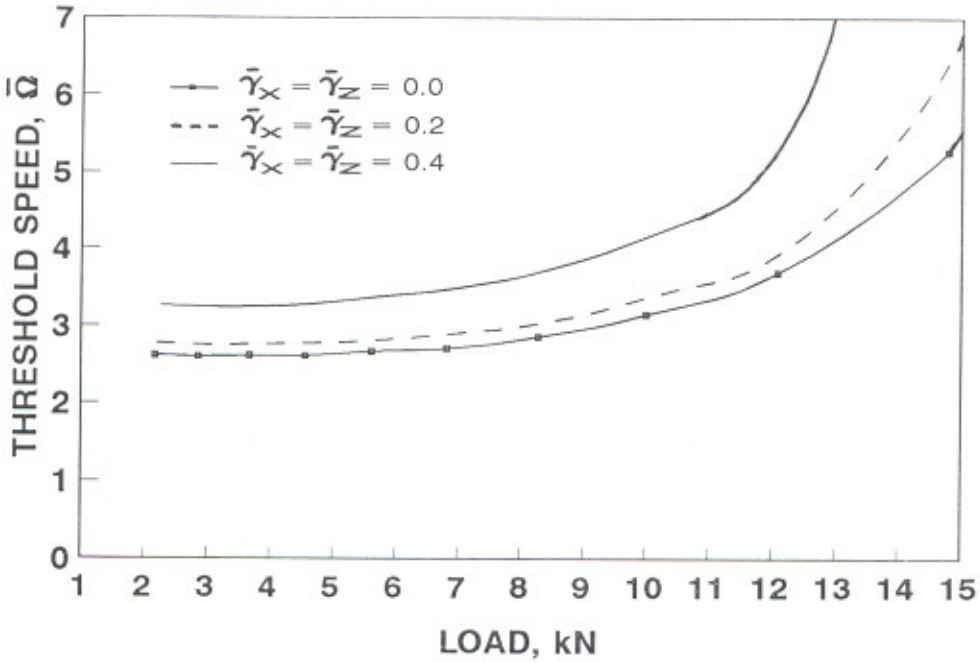

(a)

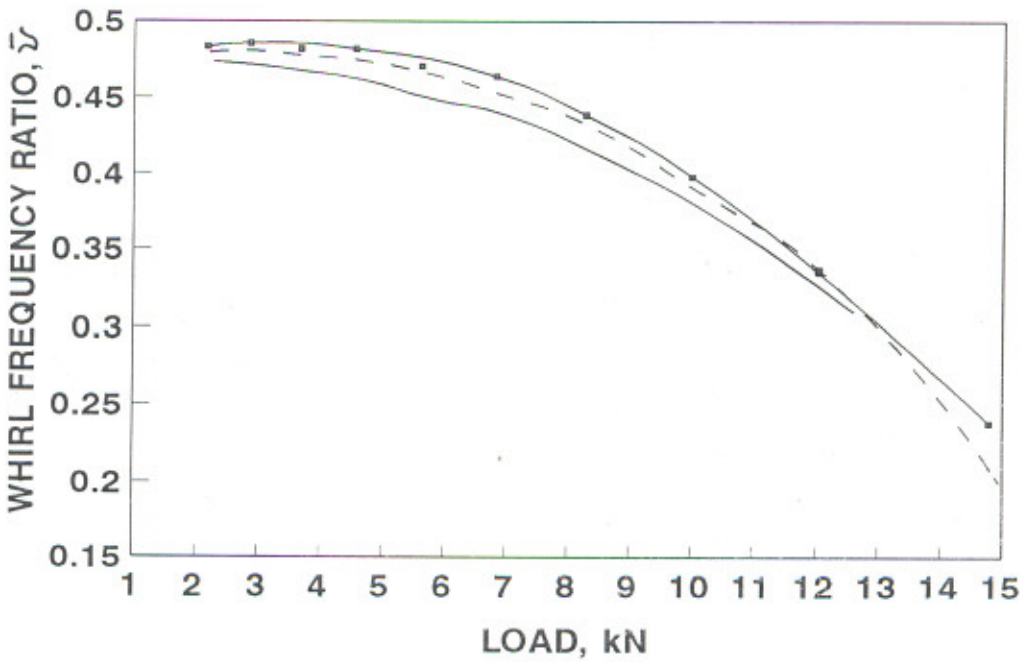

(b)

Fig. 5.41 PLAIN JOURNAL BEARING - STABILITY PARAMETERS

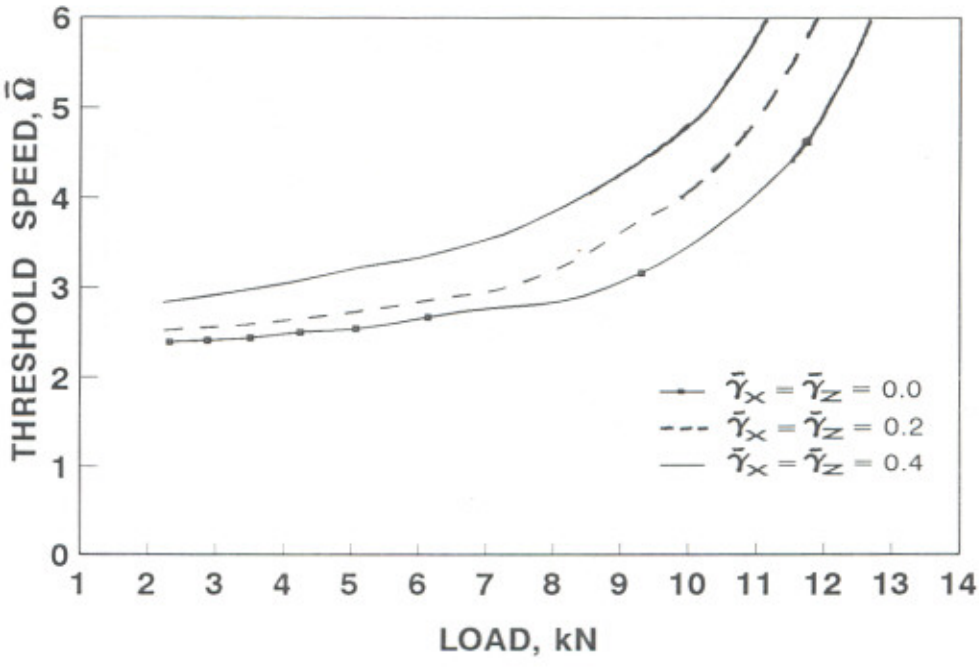

(a)

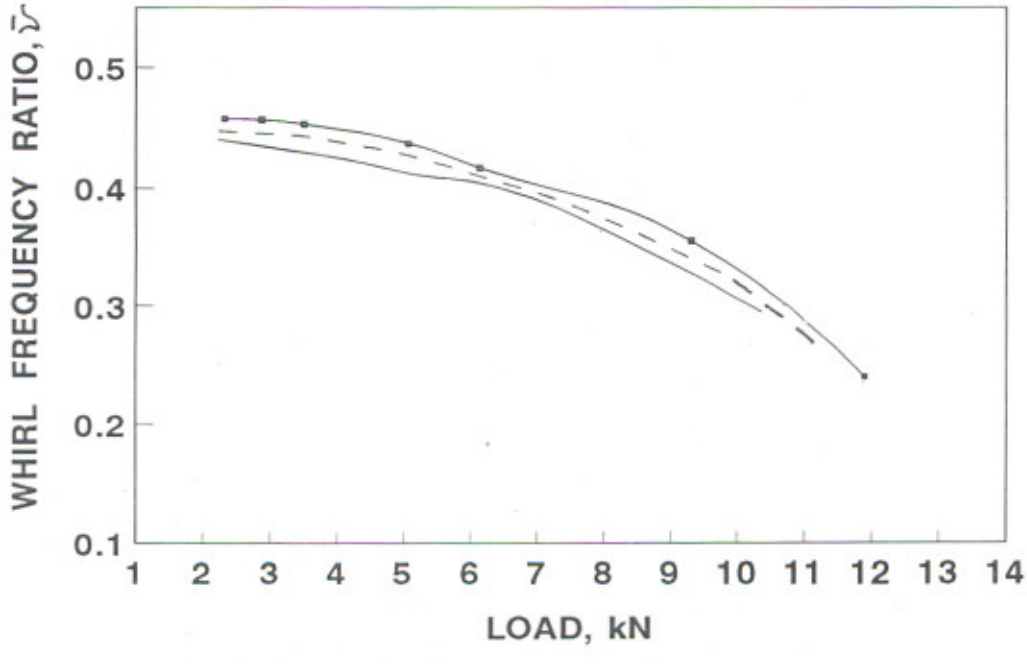

(b)

Fig. 5.42 TWO-AXIAL-GROOVE JOURNAL BEARING - STABILITY PARAMETERS

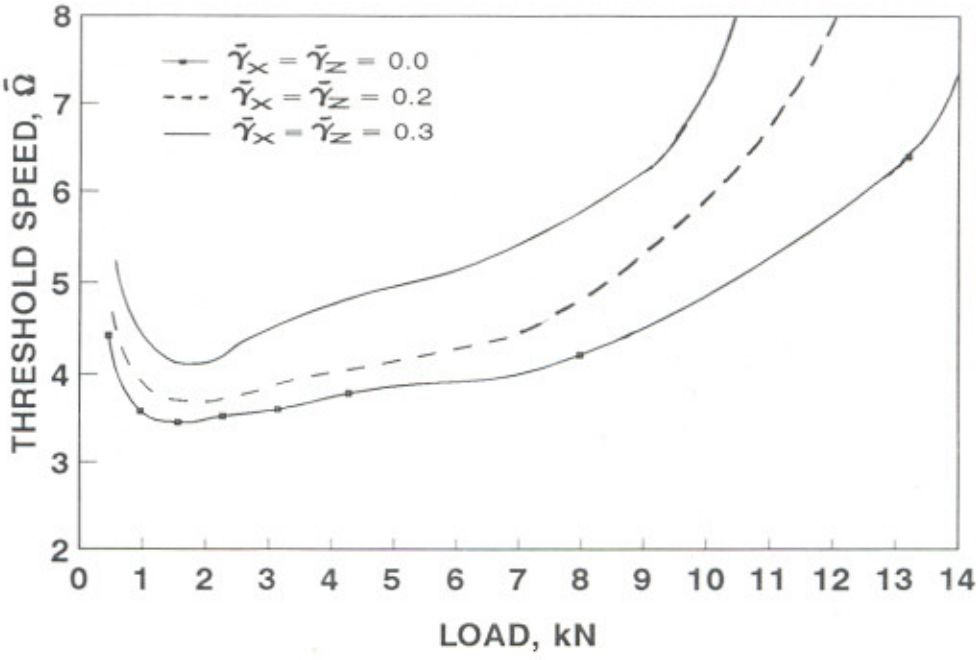

(a)

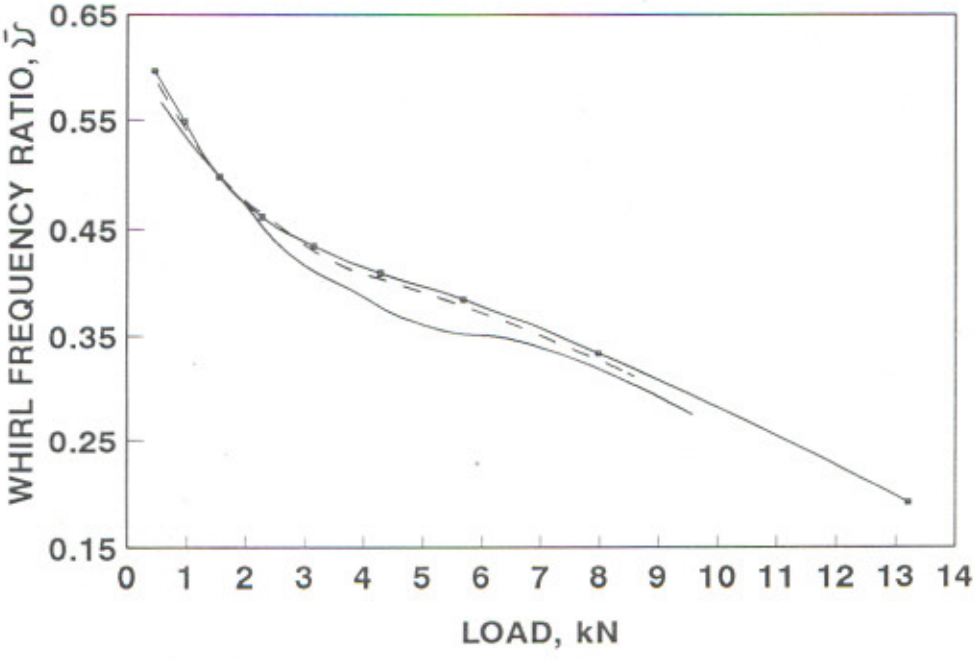

(b)

Fig. 5.43 ELLIPTICAL JOURNAL BEARING - STABILITY PARAMETERS

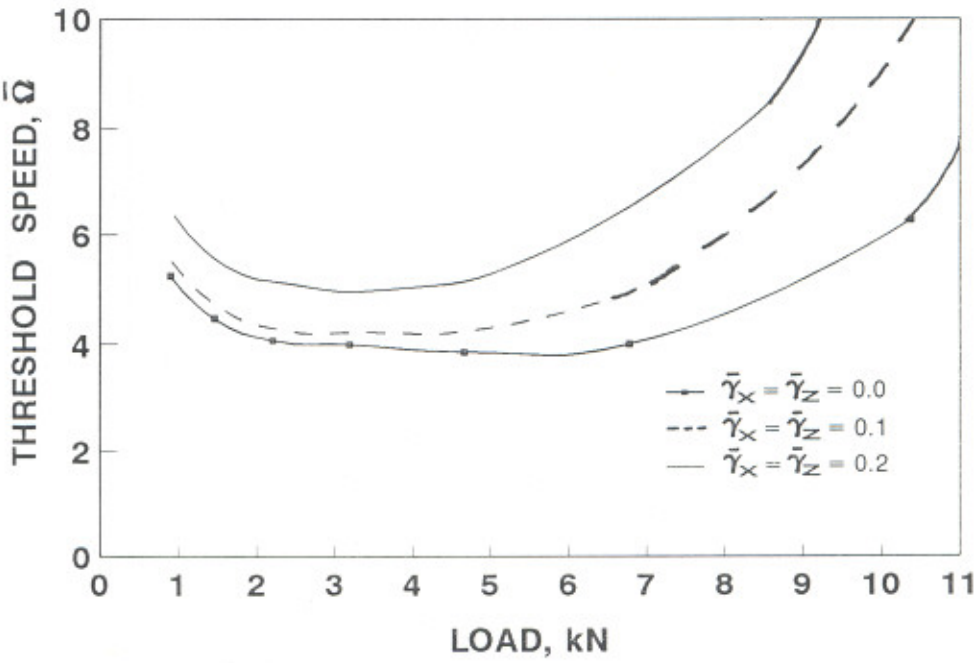

(a)

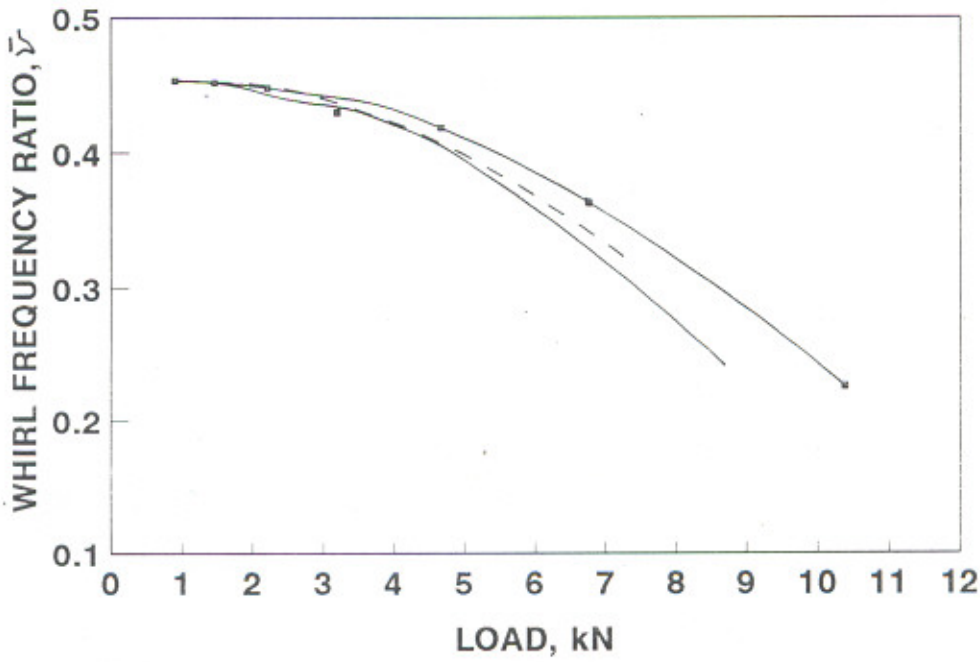

(b)

Fig. 5.44 THREE-LOBE JOURNAL BEARING - STABILITY PARAMETERS

parameter, $\bar{v}$ is not effected much by misalignment where as for three-lobe bearings, the misalignment reduces the whirl frequency ratio only at higher loads.

5.3.5 Isopressure Curves and Pressure Profiles

Figs. 5.45, 5.46, 5.47 and 5.48 shows the isopressure curves for the aligned and misaligned bearings each operating at 10 kN load. It is found that the effect of misalignment is to make the distribution of fluid-film pressure asymmetric in all bearings.

The pressure profiles have been plotted at circumferential (section A_1 - A_1) and axial (section B_1 - B_1) planes which pass through the point of maximum fluid-film pressure in respective cases, Fig. 5.49. The circumferential and the axial coordinates corresponding the maximum pressure points are expressed as α_p and β_p respectively.

The pressure profiles, in case of plain journal bearing for a light load (2 kN) and heavy loads (10 kN and 15 kN) are shown in Figs. 5.50 to 5.51 for two different values of misalignment ratios. Likewise, the Figs. 5.52 to 5.53 show the pressure profiles for two-axial-groove bearing for a light load (2 kN) and heavy load (10 kN) at two different values of misalignment ratios. It is seen from these figures that the maximum pressure in both cases is slightly reduced with the misalignment. There is not much change in the location of maximum pressure point.

Figs. 5.51 and 5.53 present the pressure profiles for plain journal bearing and two-axial-groove journal bearing with more severe misalignment, $\bar{\gamma}_x = \bar{\gamma}_z = 0.4$, again for two values of load. The maximum pressures in the cases of misaligned bearings are much higher than those for the respective pressures for the aligned bearings. Also, it is noticed that the location of maximum pressure shifts significantly with misalignment, both, circumferentially as well as axially.

The pressure profiles for elliptical and three-lobe bearings at a light (2 kN) and a heavy load (10 kN) are shown in Figs. 5.54 and 5.55 respectively. It is observed from these figures that for both values of load (i) the values of maximum fluid-film pressures are increased and (ii) location of maximum pressure does not lie in the mid-plane in the case of the misaligned bearings.

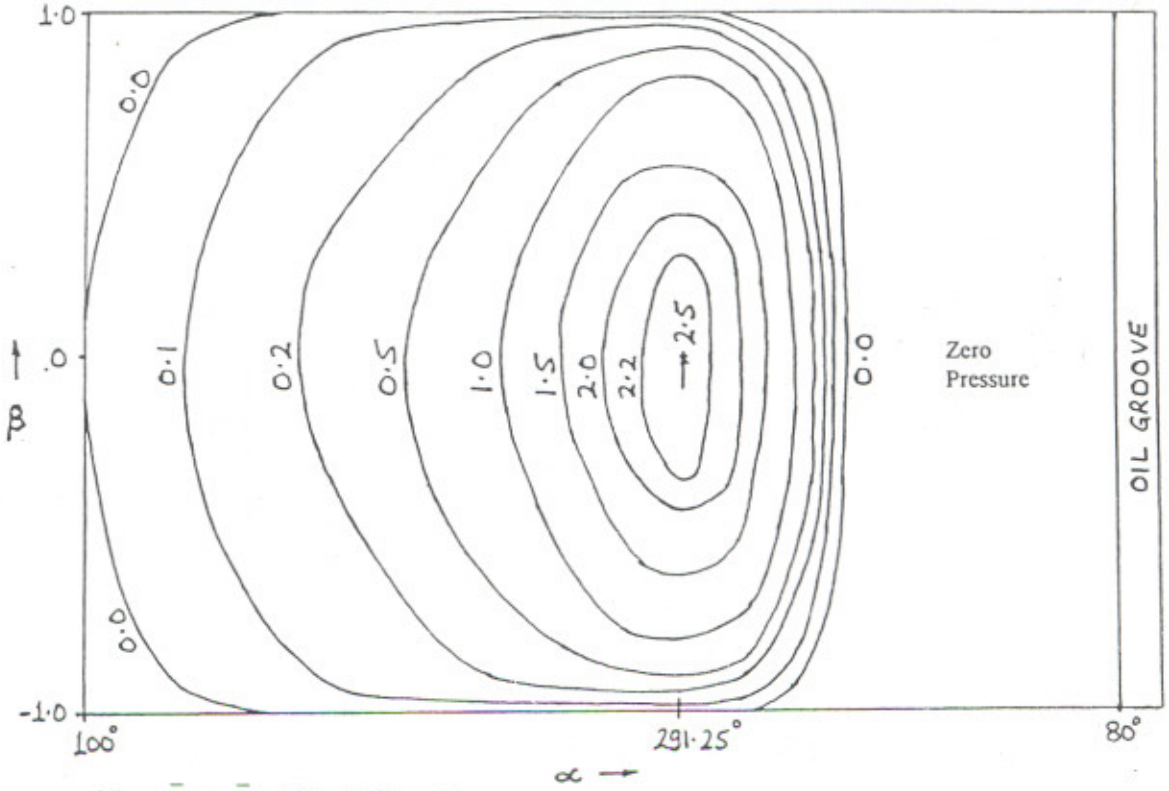

(a) $\bar{\gamma}_x = \bar{\gamma}_z = 0.0$ (Aligned)

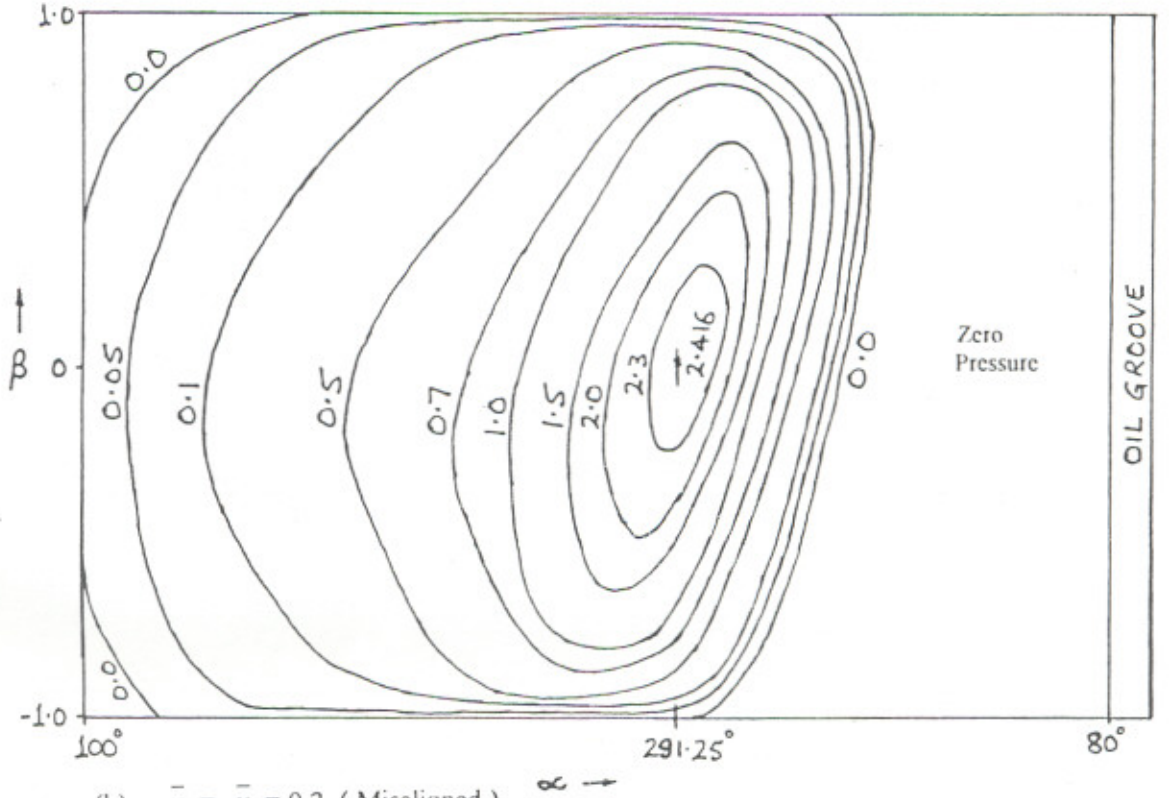

(b) $\bar{\gamma}_x = \bar{\gamma}_z = 0.2$ (Misaligned)

Fig. 5·45 PLAIN JOURNAL BEARING : ISOPRESSURE CURVES
(LOAD = 10 kN)

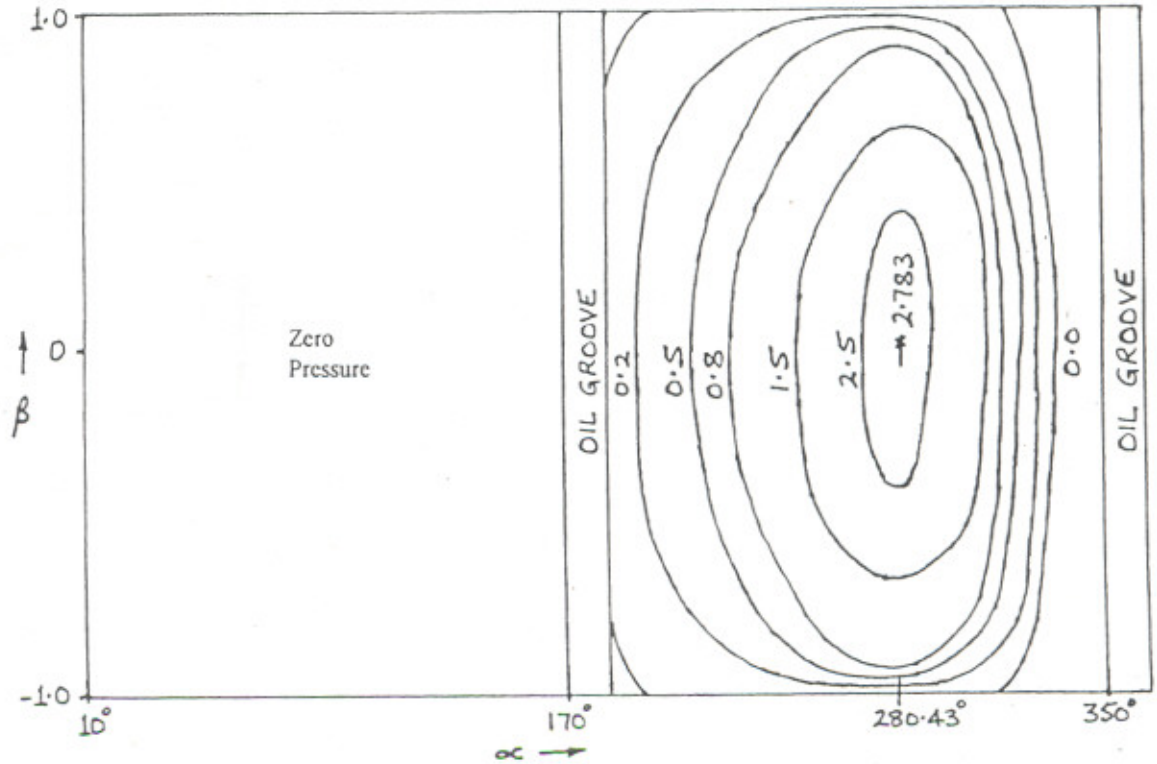

(a) $\bar{\gamma}_x = \bar{\gamma}_z = 0.0$ (Aligned)

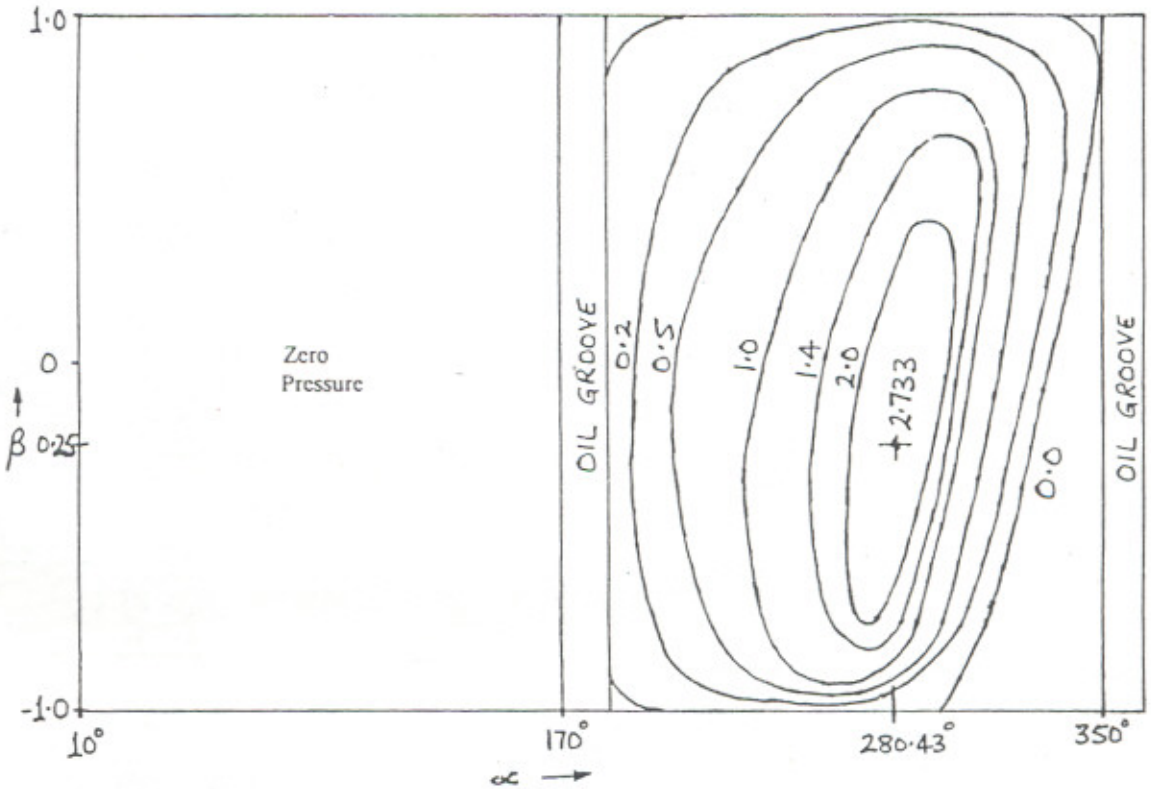

(b) $\bar{\gamma}_x = \bar{\gamma}_z = 0.2$ (Misaligned)

Fig. 5·46 TWO-AXIAL-GROOVE JOURNAL BEARING : ISOPRESSURE CURVES
(LOAD = 10 kN)

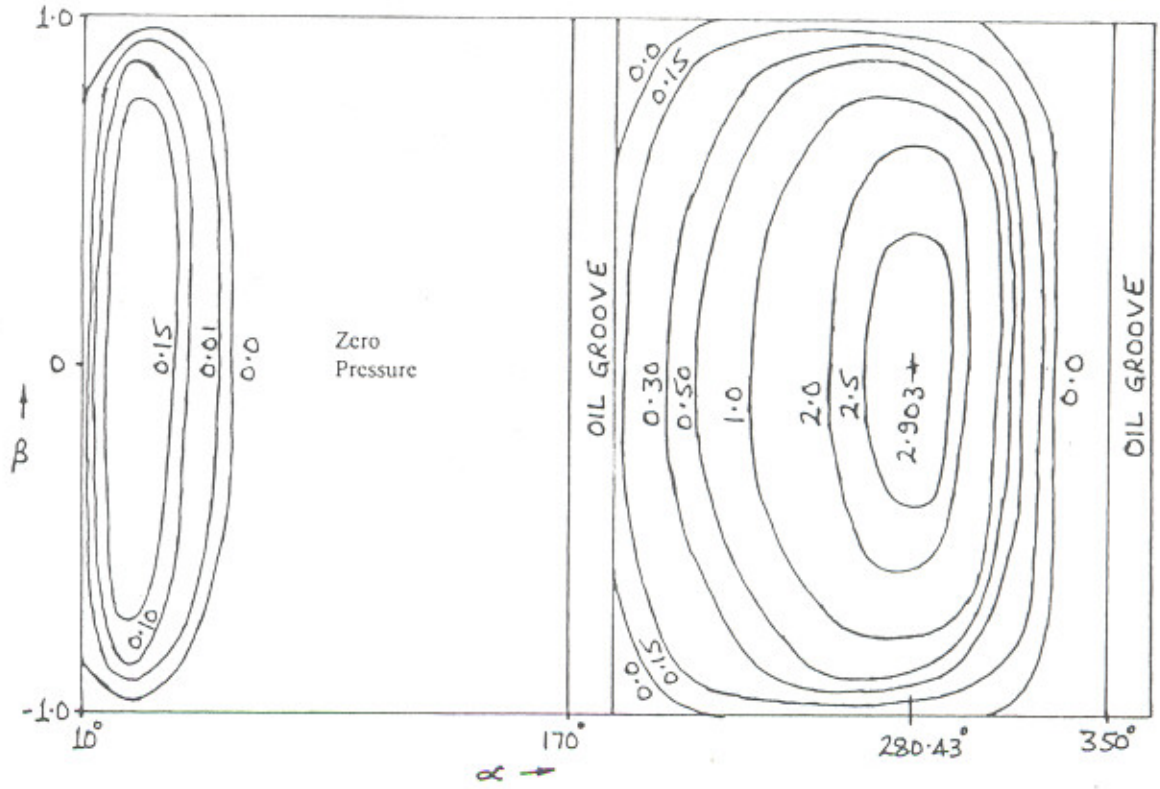

(a) $\bar{\gamma}_x = \bar{\gamma}_z = 0.0$ (Aligned)

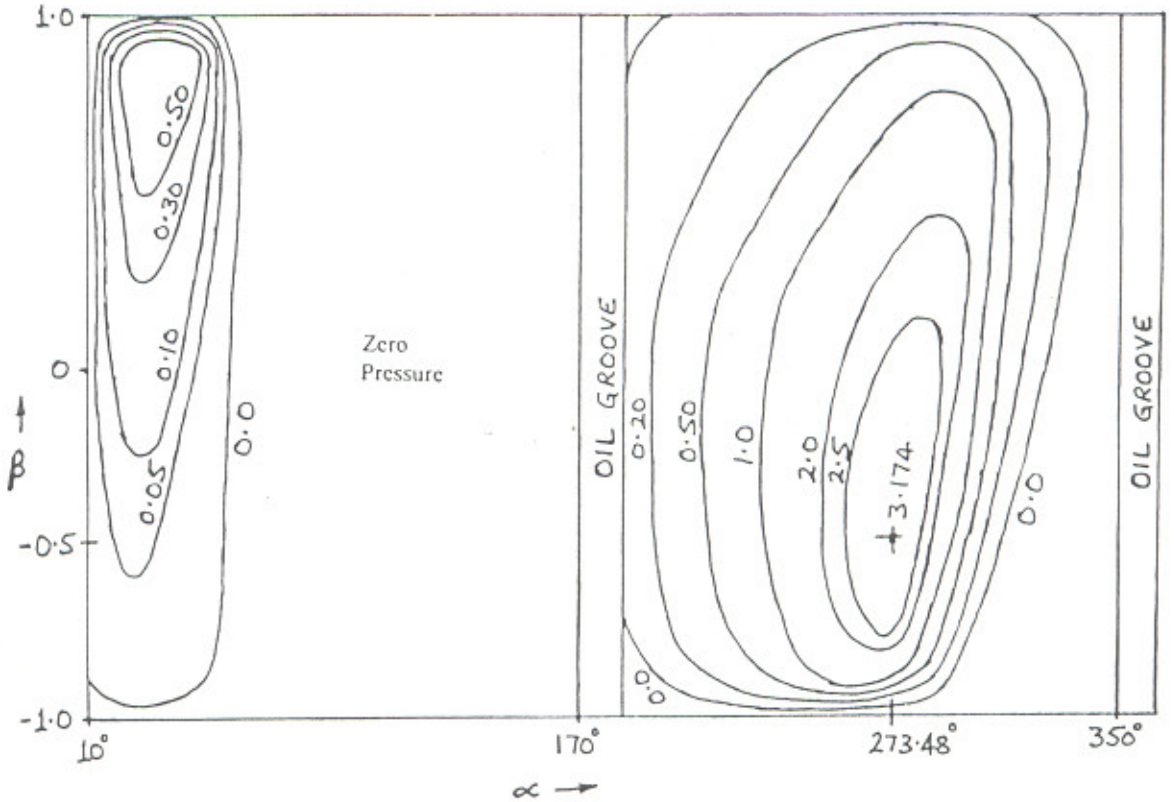

(b) $\bar{\gamma}_x = \bar{\gamma}_z = 0.2$ (Misaligned)

Fig 5·47 ELLIPTICAL JOURNAL BEARING : ISOPRESSURE CURVES
(LOAD = 10 kN)

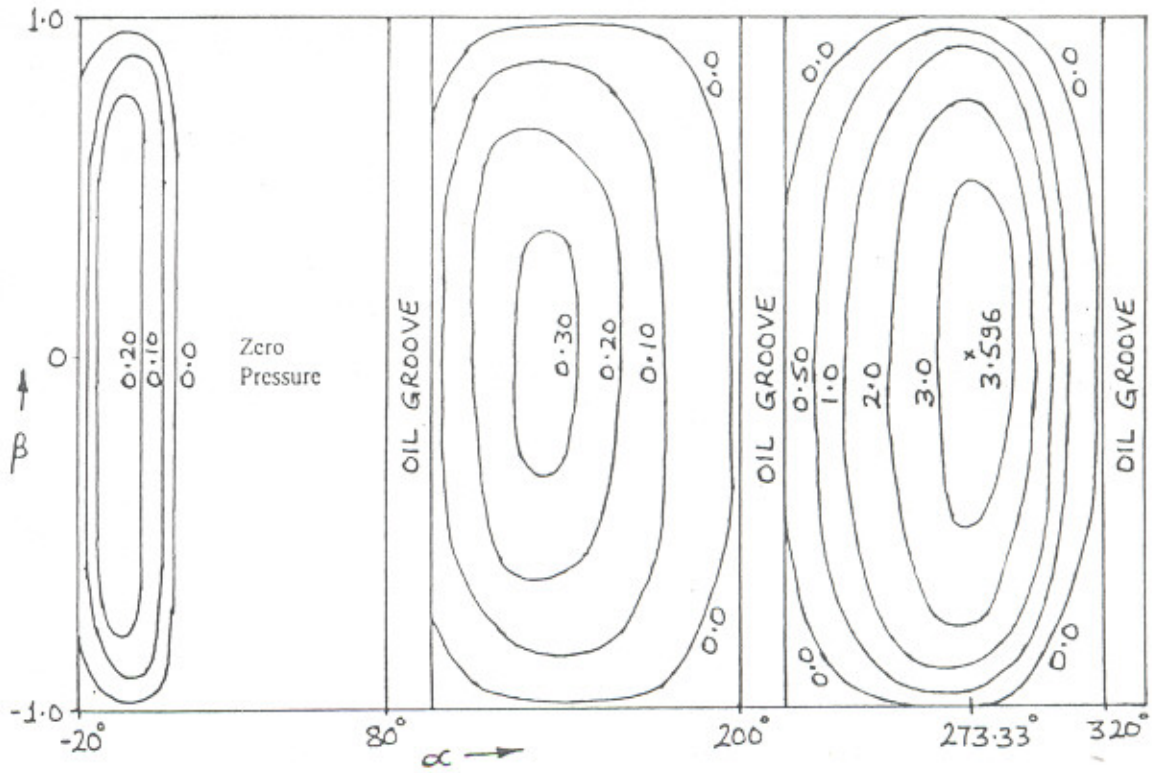

(a) $\bar{\gamma}_x = \bar{\gamma}_z = 0.0$ (Aligned)

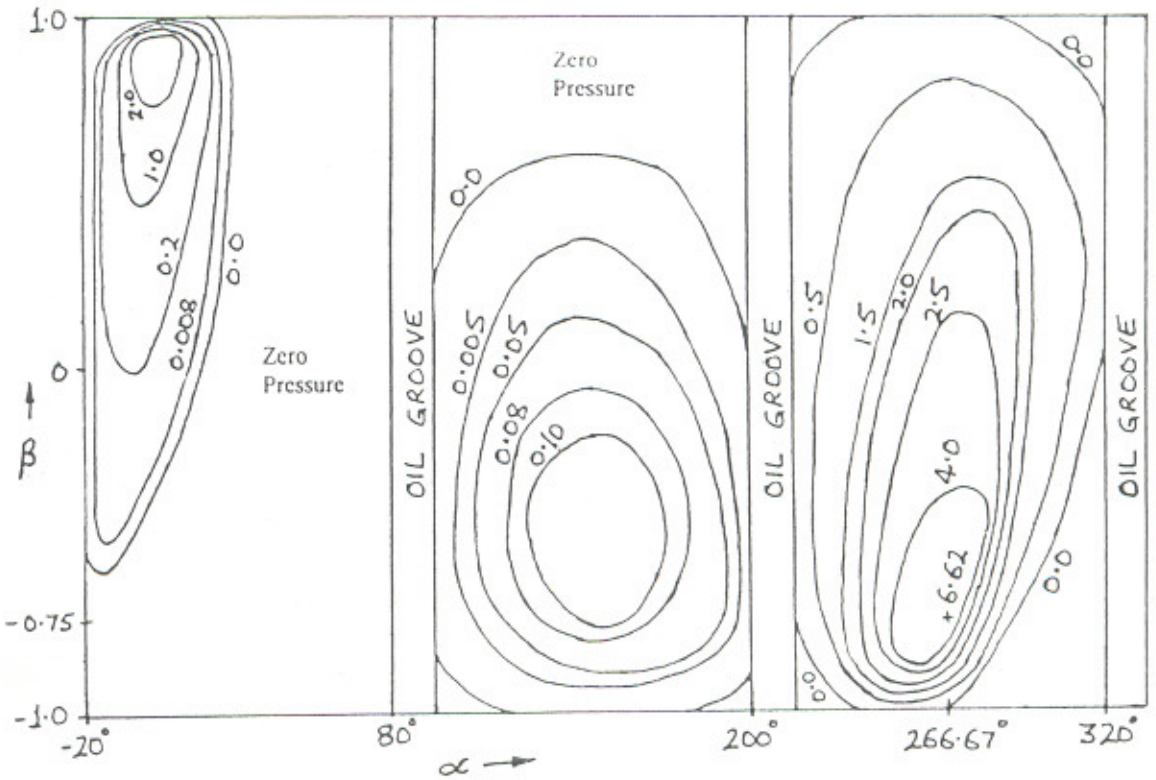

(b) $\bar{\gamma}_x = \bar{\gamma}_z = 0.2$ (Misaligned)

Fig 5·48 THREE-LOBE JOURNAL BEARING : ISOPRESSURE CURVES
(LOAD = 10 kN)

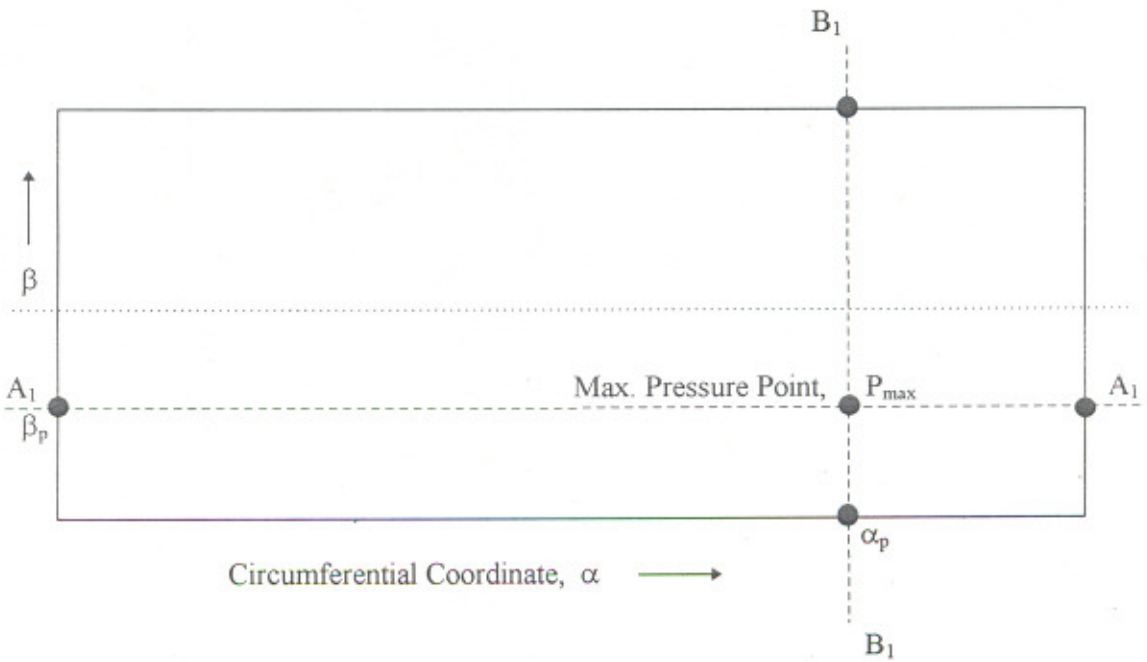

Fig. 5.49 Unwrapped Journal Bearing showing the Coordinate System and the Position of Maximum Pressure Point

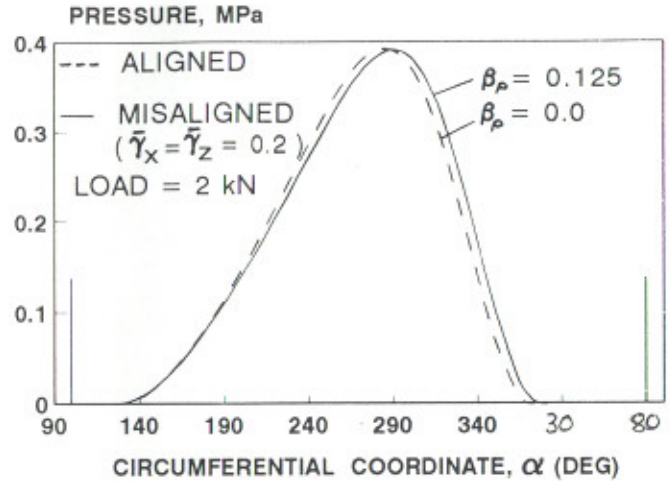

(a) SECTION AT A_1 - A_1

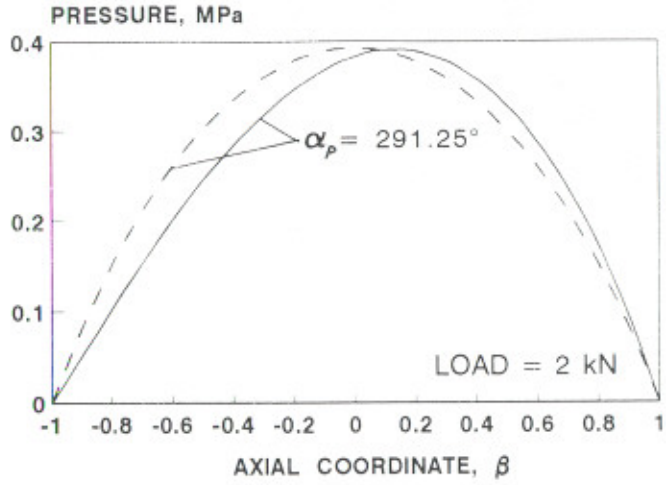

(b) SECTION AT B_1 - B_1

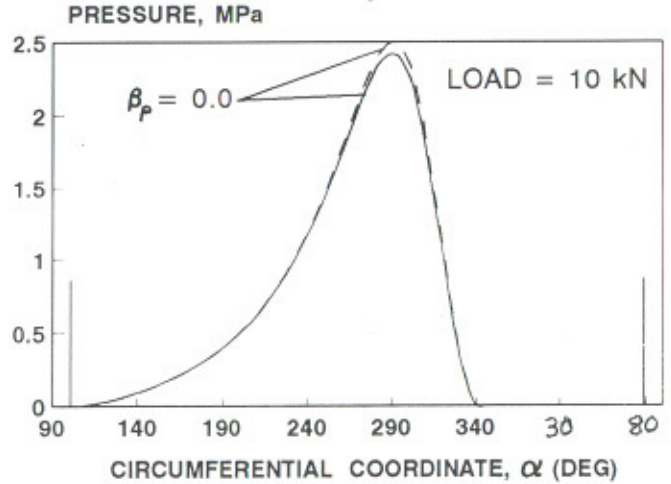

(c) SECTION AT A_1 - A_1

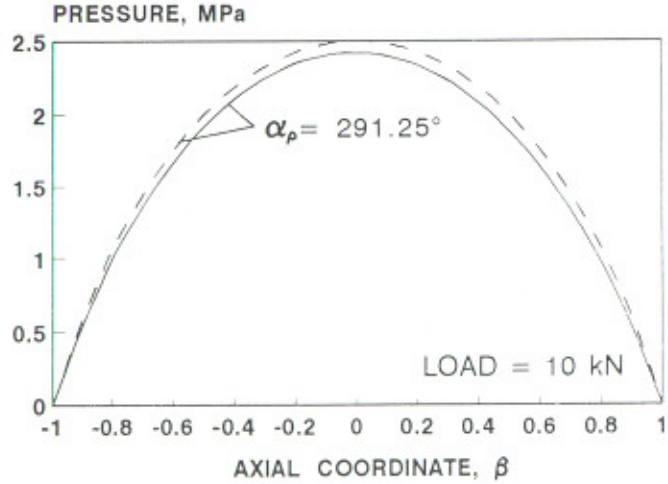

(d) SECTION AT B_1 - B_1

Fig. 5.50 PLAIN JOURNAL BEARING - PRESSURE PROFILES

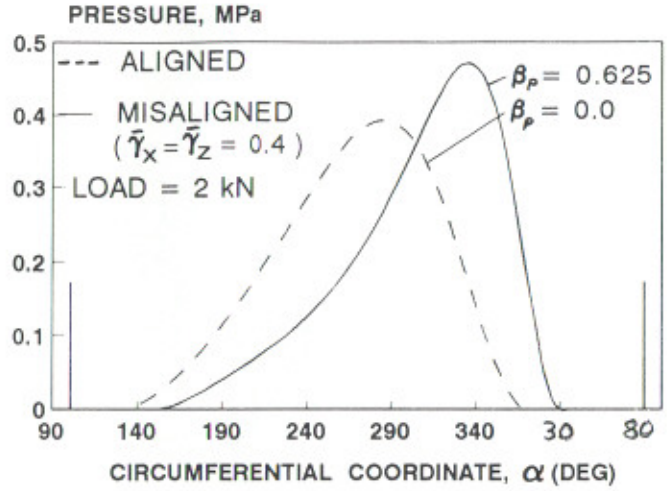

(a) SECTION AT A_1 - A_1

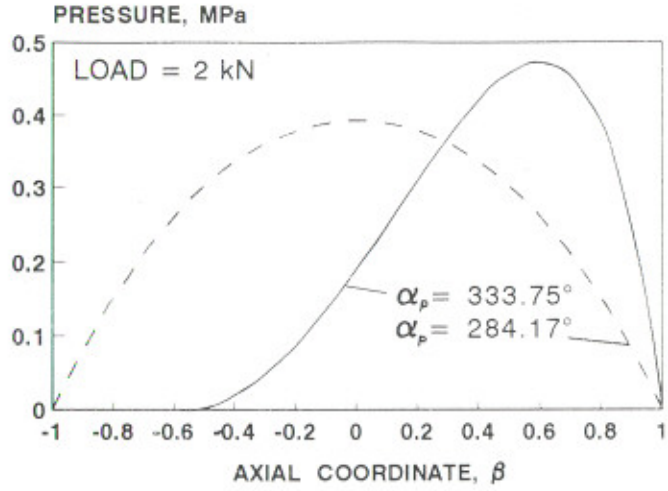

(b) SECTION AT B_1 - B_1

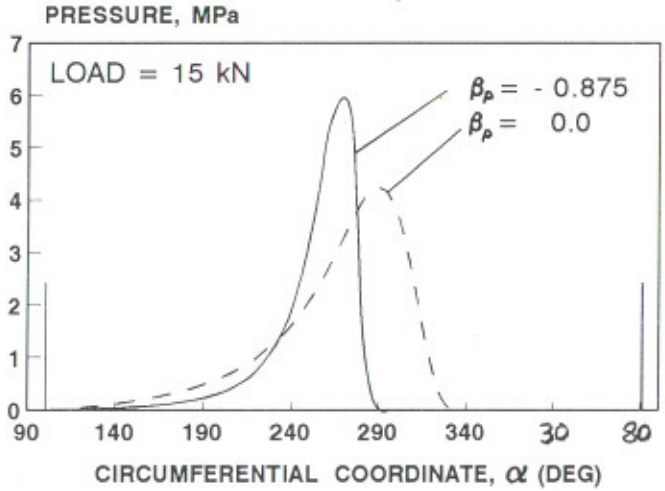

(c) SECTION AT A_1 - A_1

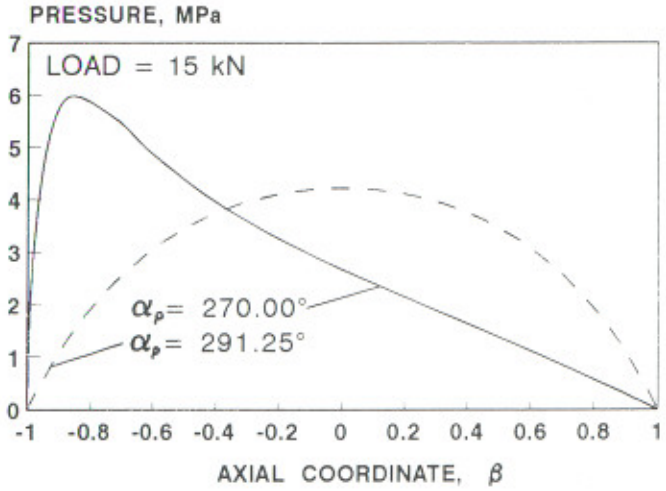

(d) SECTION AT B_1 - B_1

Fig. 5.51 PLAIN JOURNAL BEARING - PRESSURE PROFILES

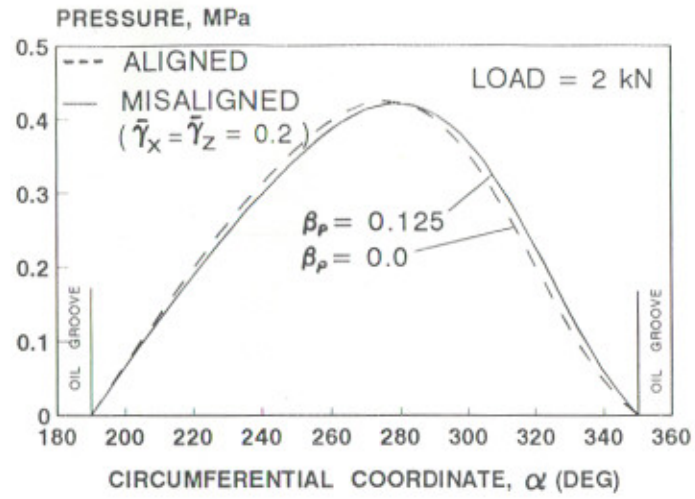

(a) SECTION AT A_1 - A_1

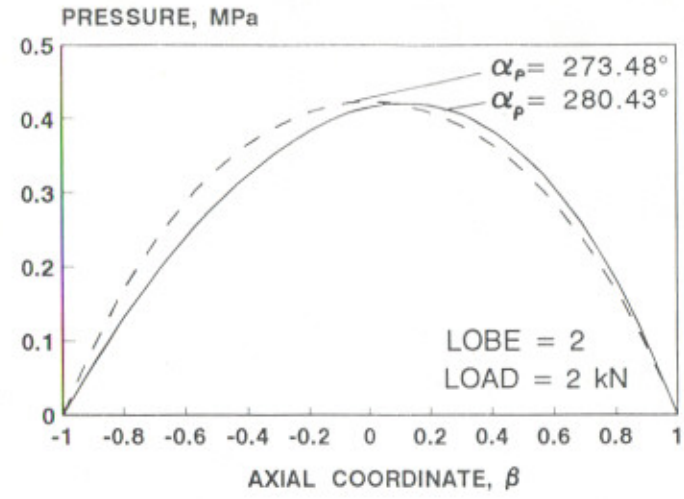

(b) SECTION AT B_1 - B_1

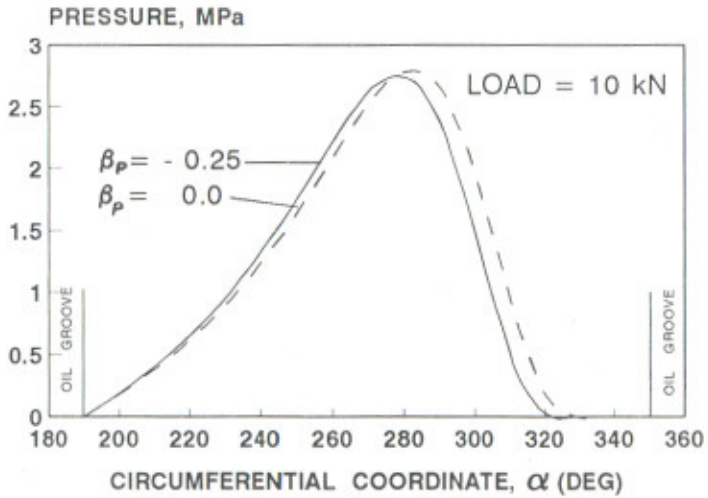

(c) SECTION AT A_1 - A_1

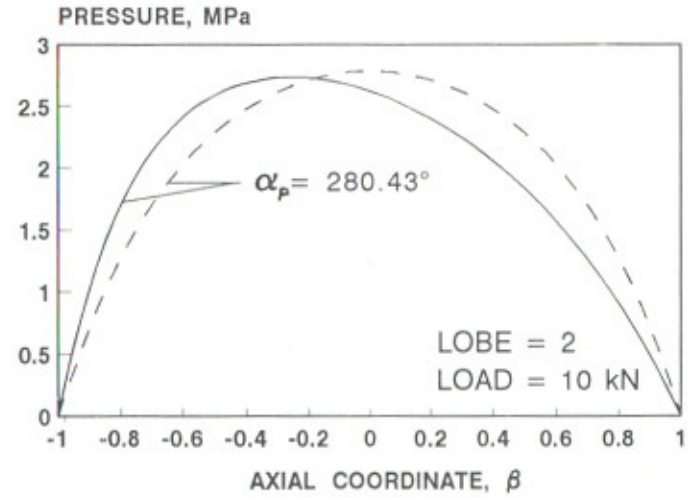

(d) SECTION AT B_1 - B_1

Fig. 5.52 TWO-AXIAL-GROOVE JOURNAL BEARING - PRESSURE PROFILES

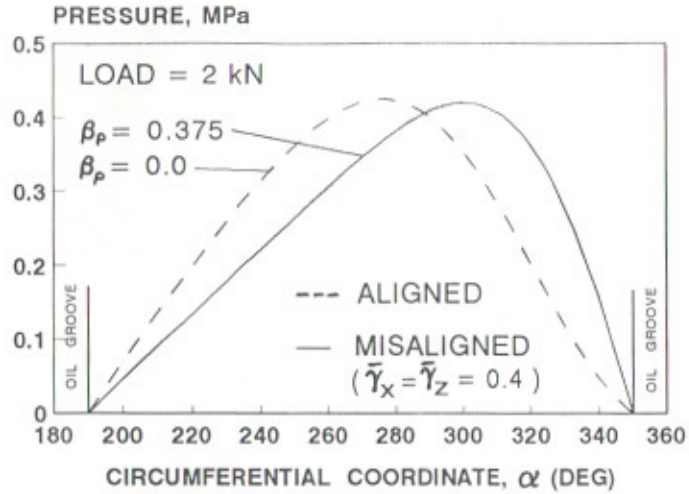

(a) SECTION AT A_1 - A_1

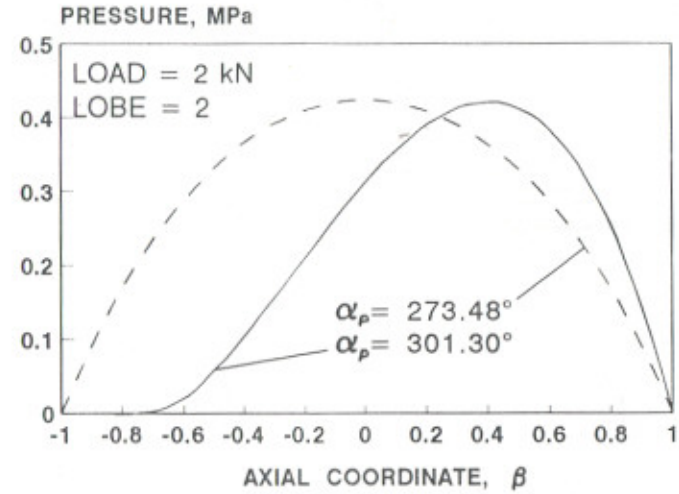

(b) SECTION AT B_1 - B_1

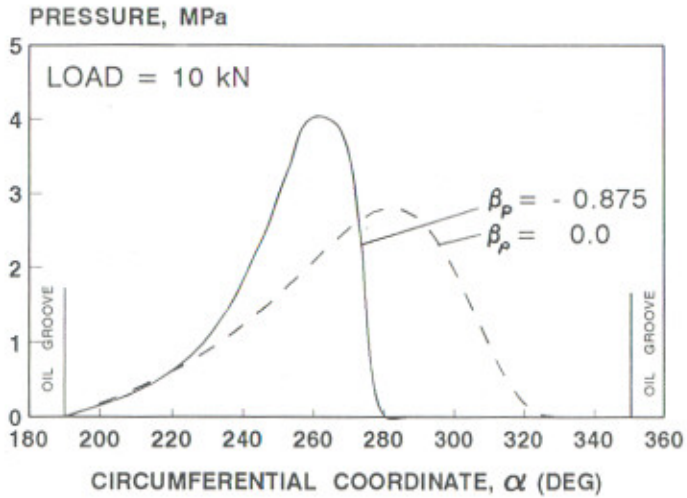

(c) SECTION AT A_1 - A_1

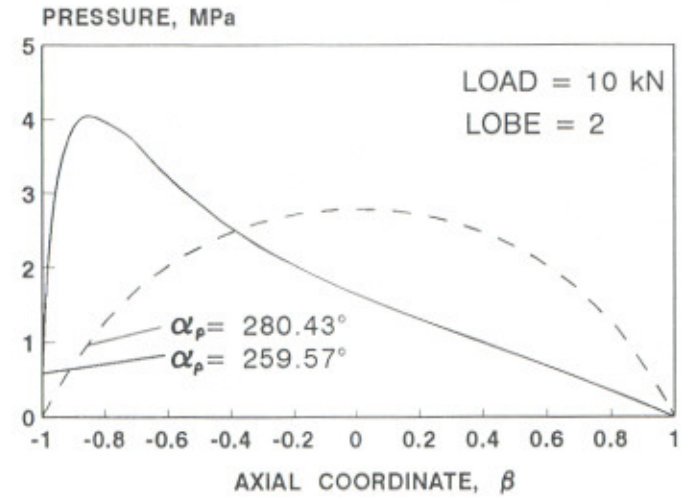

(d) SECTION AT B_1 - B_1

Fig. 5.53 TWO-AXIAL-GROOVE JOURNAL BEARING - PRESSURE PROFILES

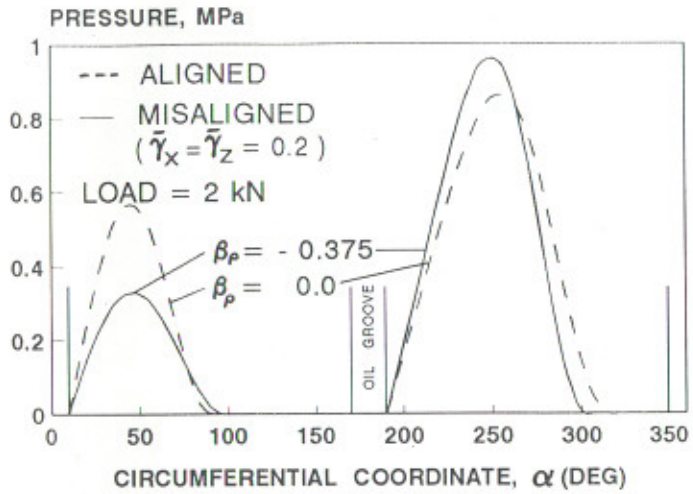

(a) SECTION AT A_1 - A_1

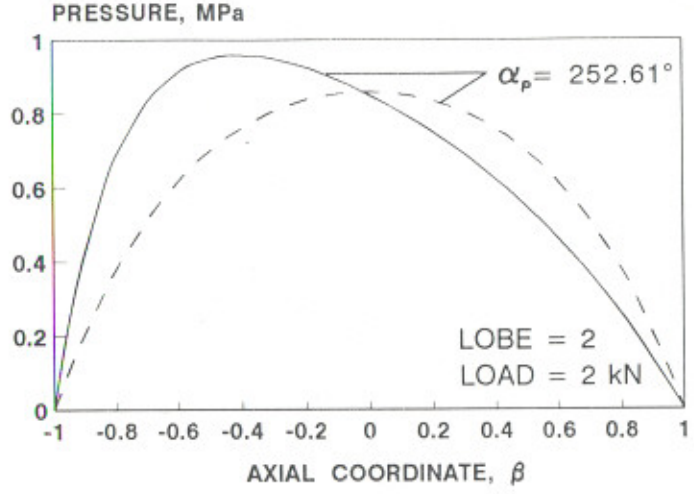

(b) SECTION AT B_1 - B_1

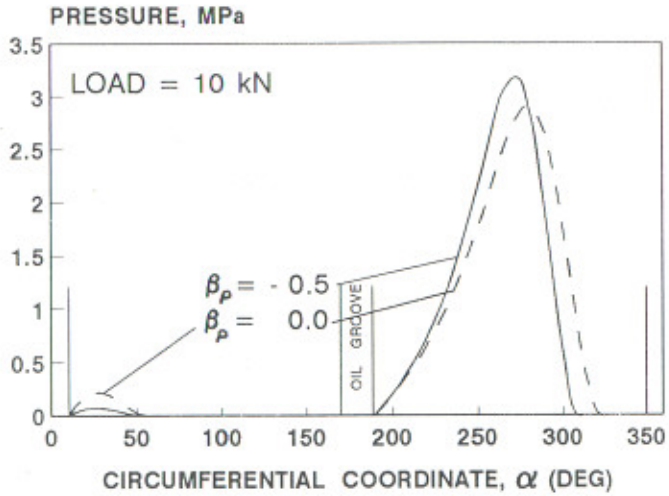

(c) SECTION AT A_1 - A_1

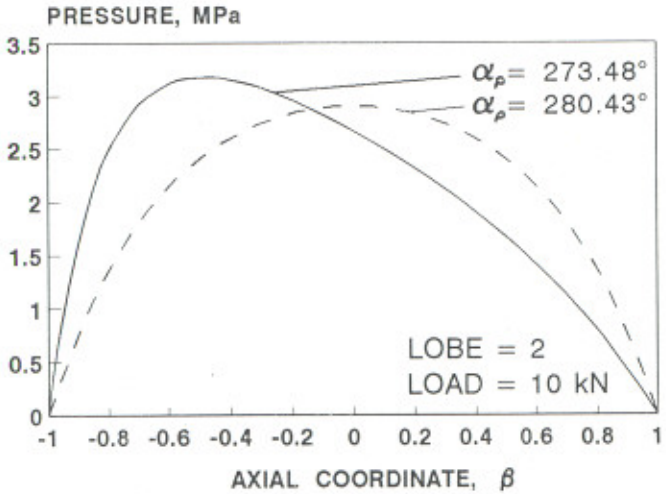

(d) SECTION AT B_1 - B_1

Fig. 5.54 ELLIPTICAL JOURNAL BEARING - PRESSURE PROFILES

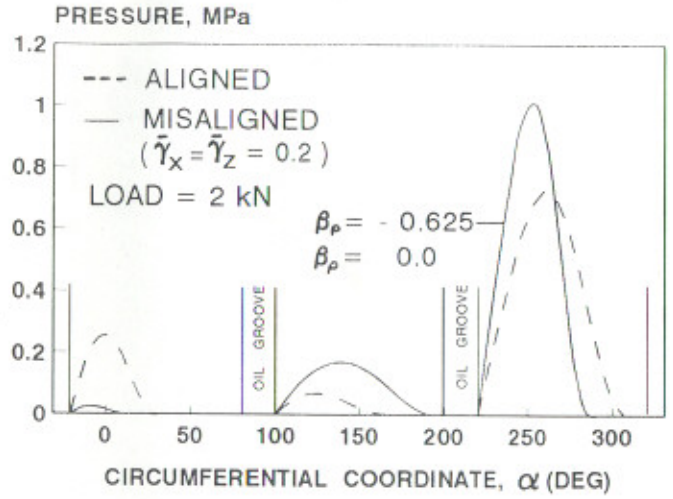

(a) SECTION AT A_1 - A_1

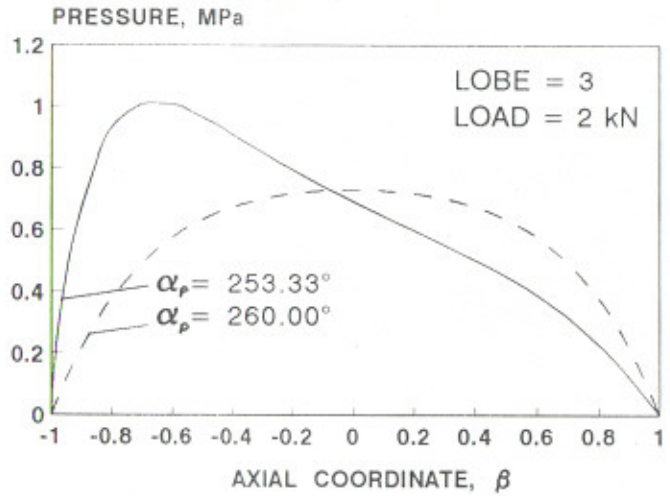

(b) SECTION AT B_1 - B_1

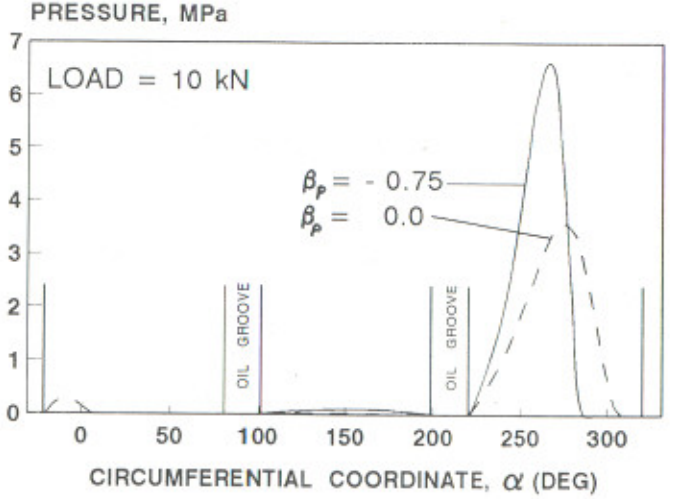

(c) SECTION AT A_1 - A_1

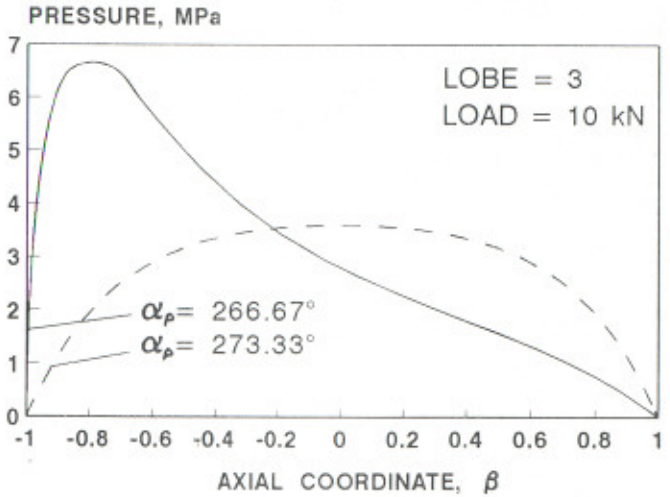

(d) SECTION AT B_1 - B_1

Fig. 5.55 THREE-LOBE JOURNAL BEARING - PRESSURE PROFILES

5.3.6 Isotherms and Temperature Profiles

Figs. 5.56, 5.57, 5.58 and 5.59 show the bush-fluid interface isotherms for the four bearing configurations at two values of load (2 kN and 10 kN) and $\bar{\gamma}_x = \bar{\gamma}_z = 0.2$. The temperature difference occuring along circumferential direction and axial direction, and the maximum temperature in the bush-fluid isotherms has been summarised in table 5.10 for all the bearing geometries. It is revealed that at both the loads, there is considerable variation in temperature along the circumferential and axial directions indicating heat transfer in these directions. The temperature variation in axial direction is more in the case of non-circular bearings as compared to the circular bearings and this variation increases with the increase in the value of load. The trend for other values of misalignment was also found to be similar, although not reported here.

The oil and bush isotherms for the bearing systems are shown in Figs. 5.60, 5.61, 5.62 and 5.63 for the four bearings each operating with a load = 10 kN and misalignment of $\bar{\gamma}_x = \bar{\gamma}_z = 0.2$. These isotherms have been plotted at three circumferential planes for each bearing. From these isotherms it is observed that heat flows into the journal from the hot region in the oil-film and out of the journal in the cold region of the oil-film. There is considerable variation in temperature across the thickness of the oil-film and the bush. The isotherms show that due to misalignment, expectedly, the maximum temperature zone does not remain in the central plane ($\beta = 0$) but shifts away from the central plane. The bush isotherms indicate that the maximum bush temperature occurs in the vicinity of the hottest region of oil-film. In the high temperature region of the bush, most of the heat transfers directly out of the bush outer surface to the surroundings. It is also observed from these figures that heat transfer takes place not only in radial direction in the bush but also in the circumferential and axial directions.

The interface temperature profiles have been plotted at circumferential (section A_2 - A_2) and axial (section B_2 - B_2) planes which pass through the point of maximum interface temperature in respective cases, Fig. 5.64. The coordinates of the maximum temperature on the interface are designated as α_t and β_t as shown in the figure.

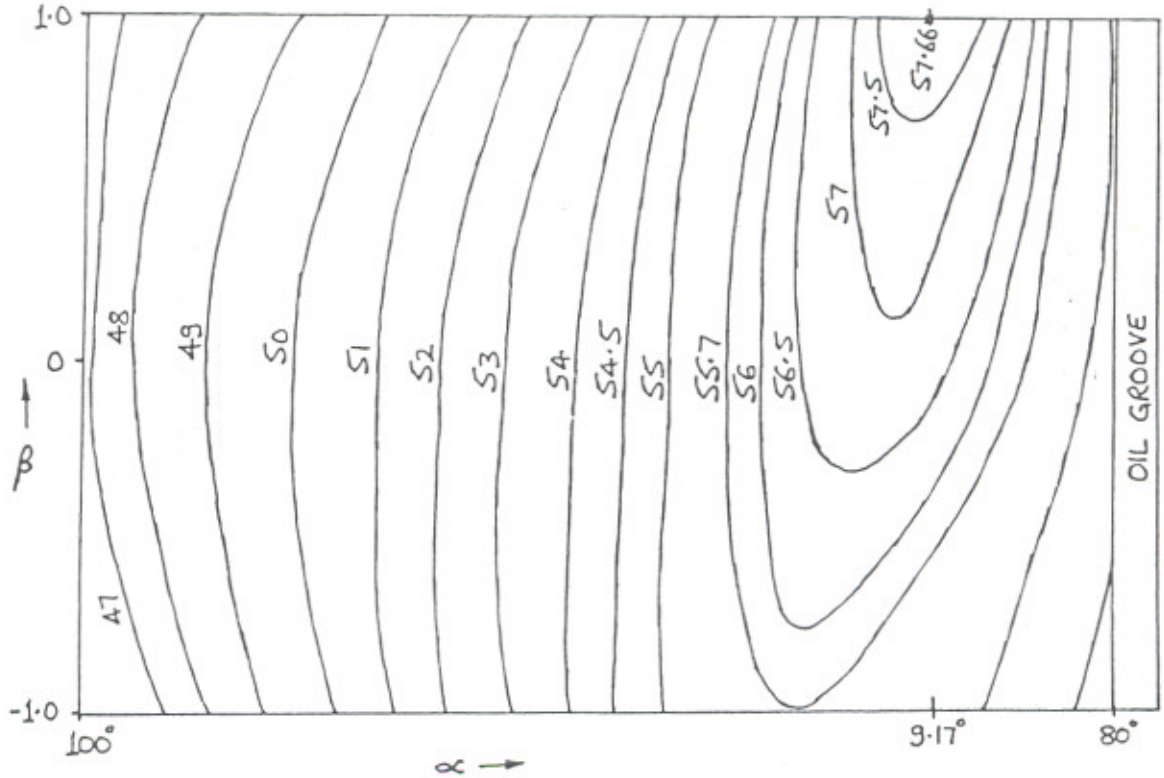

(a) LOAD = 2 kN

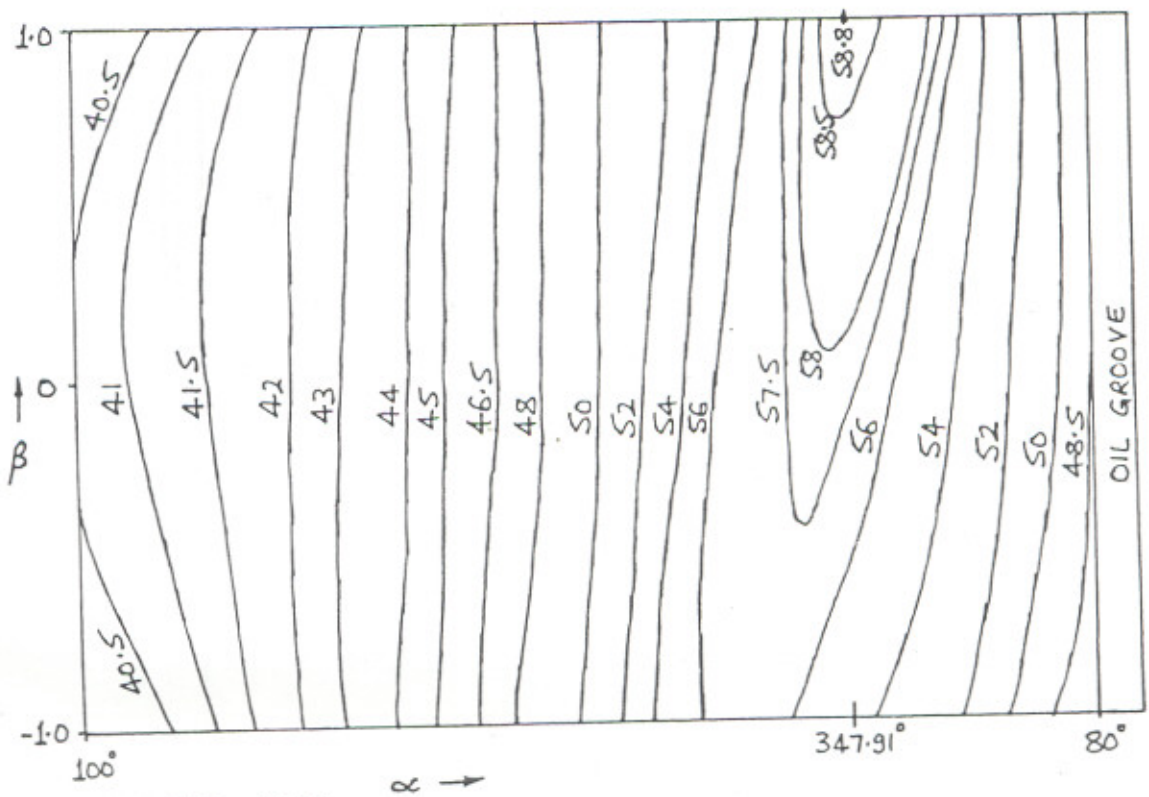

(b) LOAD = 10 kN

Fig. 5·56 PLAIN JOURNAL BEARING: BUSH-FLUID INTERFACE ISOTHERMS
($\bar{\gamma}_x = \bar{\gamma}_z = 0.2$)

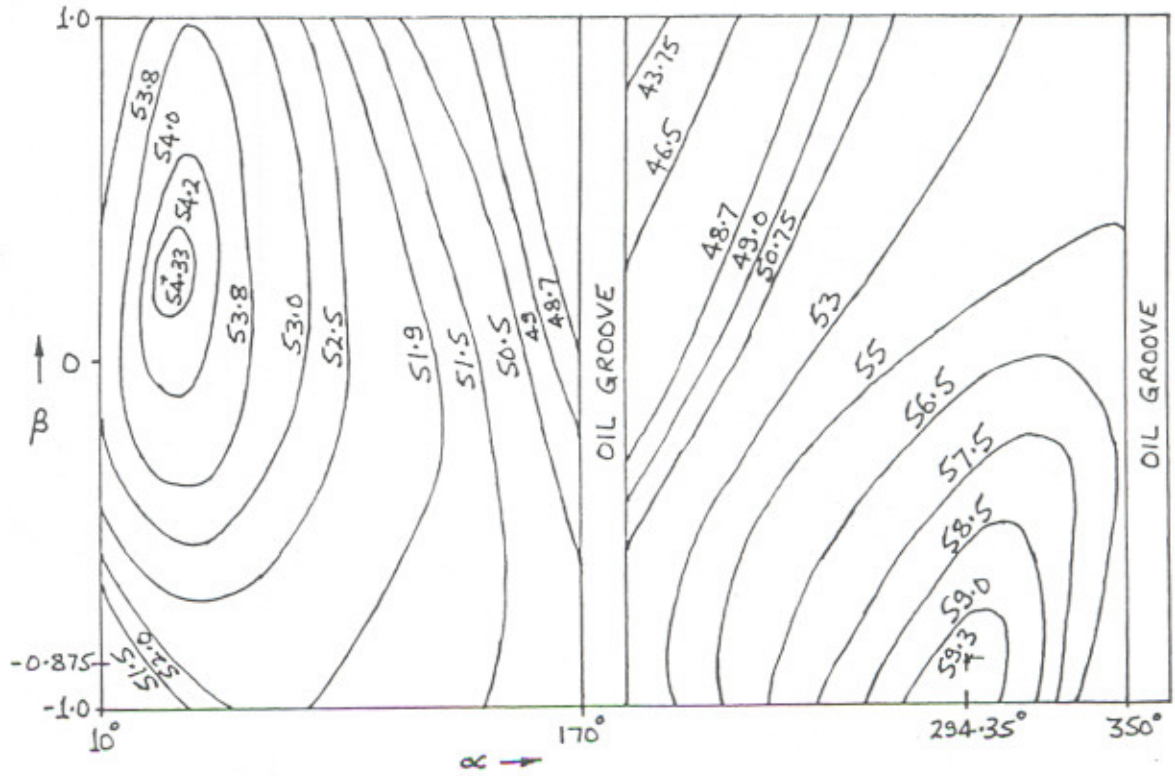

(a) LOAD = 2 kN

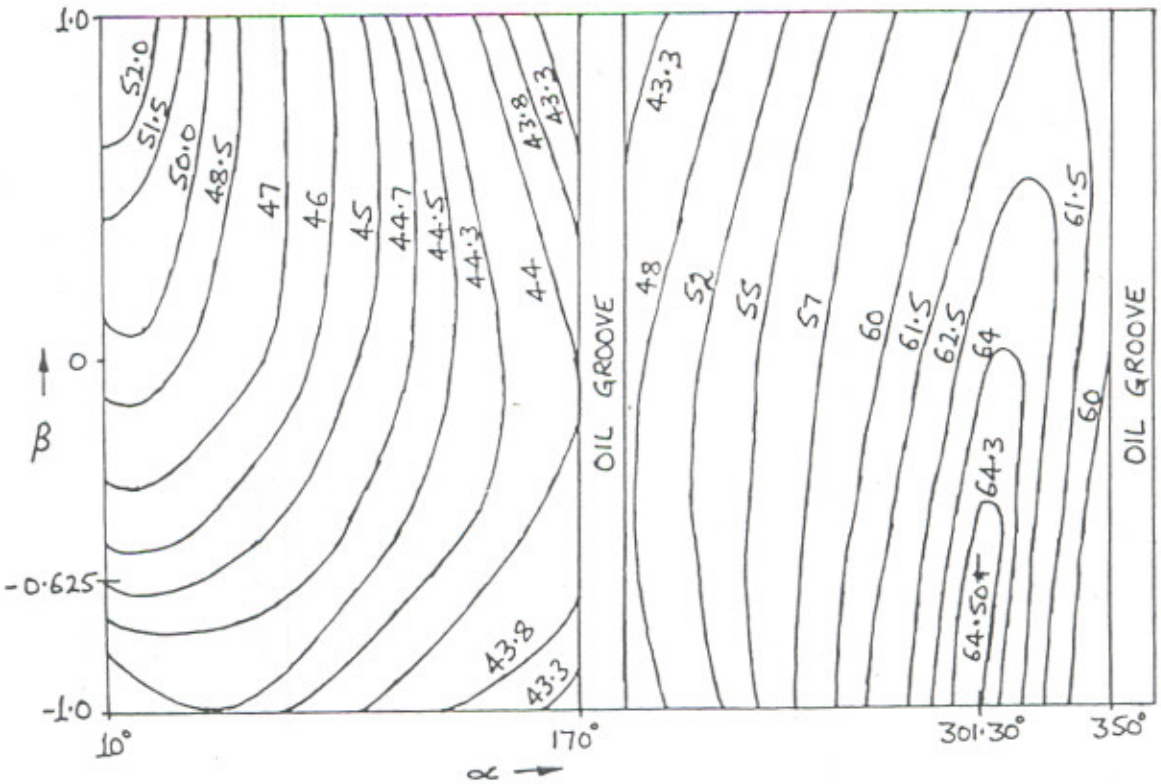

(b) LOAD = 10 kN

Fig. 5·57 TWO-AXIAL-GROOVE JOURNAL BEARING : BUSH-FLUID INTERFACE ISOTHERMS ($\bar{\gamma}_x = \bar{\gamma}_z = 0.2$)

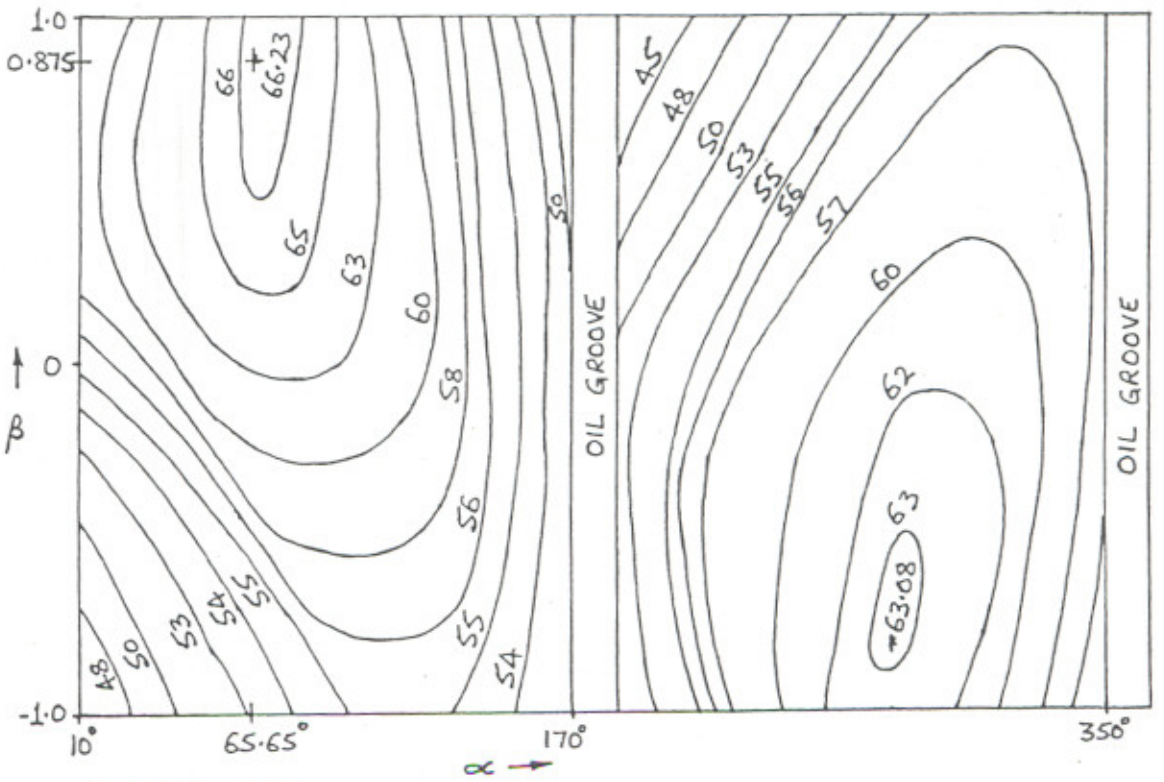

(a) LOAD = 2 kN

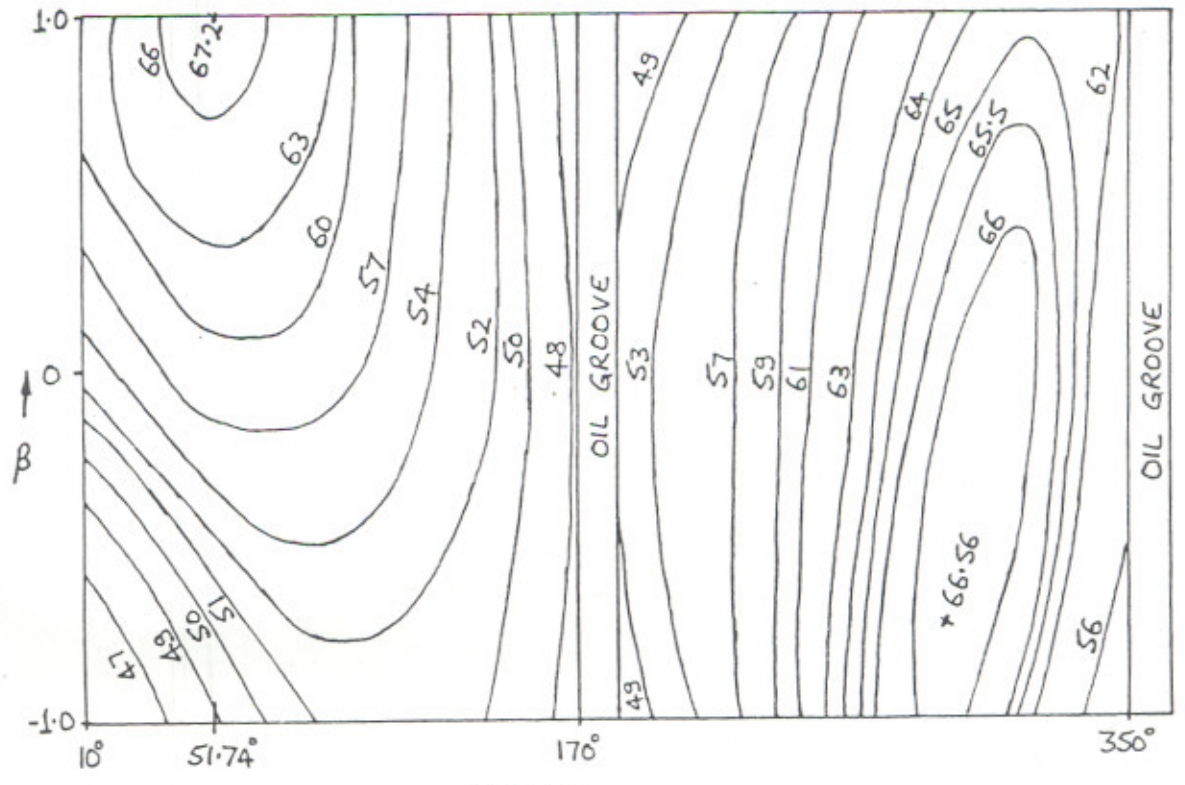

(b) LOAD = 10 kN

Fig. 5.58 ELLIPTICAL JOURNAL BEARING: BUSH-FLUID INTERFACE ISOTHERMS ($\bar{\gamma}_x = \bar{\gamma}_z = 0.2$)

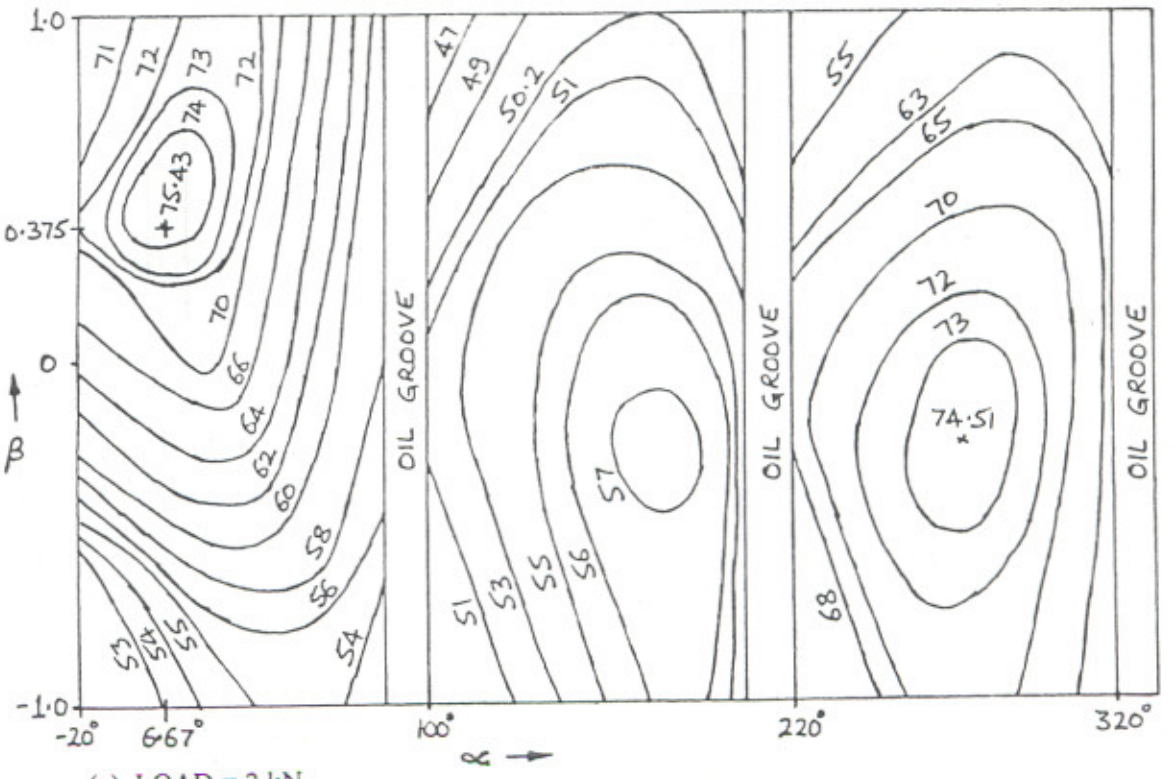

(a) LOAD = 2 kN

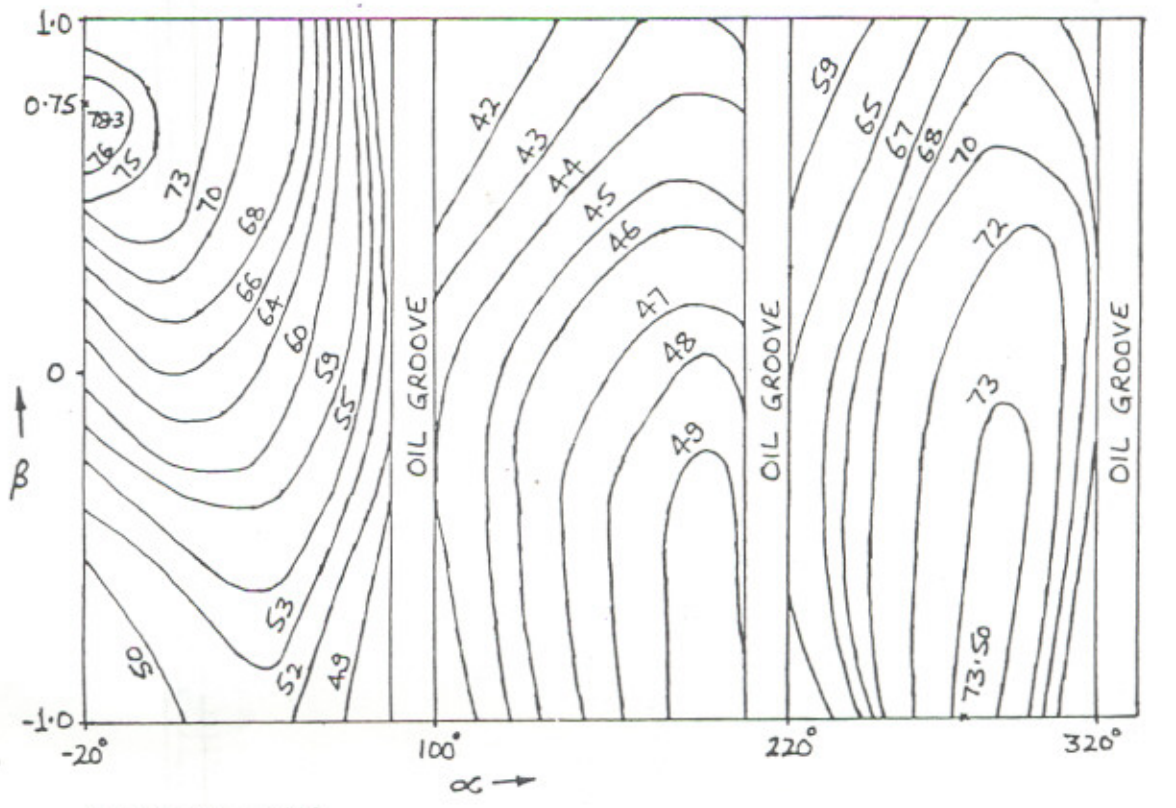

(b) LOAD = 10 kN

Fig. 5·59 THREE-LOBE JOURNAL BEARING : BUSH-FLUID INTERFACE ISOTHERMS ($\bar{\gamma}_x = \bar{\gamma}_z = 0.2$)

Table 5.10 Summary of Bush-Fluid Interface Isotherms

(Misalignment ratio, $\bar{\gamma}_x = \bar{\gamma}_z = 0.2$)

Type of Bearing	Load, kN	Lobe*	Temperature Difference, °C		Maximum Temperature, °C
			Circumferentially	Axially	
Plain	2	1	11.6	3.4	57.6
	10	1	18.8	4.3	58.8
Two-Axial-Groove	2	1	5.6	2.8	54.33
		2	10.0	6.8	59.30
	10	1	8.7	7.5	52.86
		2	18.2	4.0	64.54
Elliptical	2	1	16.0	12.2	66.23
		2	11.5	8.0	63.08
	10	1	19.2	18.2	67.20
		2	13.0	3.5	66.56
Three-Lobe	2	1	10.0	22.0	75.43
		2	6.0	7.0	57.44
		3	5.0	15.5	74.51
	10	1	20.3	29.3	78.33
		2	5.0	6.0	49.75
		3	6.0	6.5	73.50

* lobe nomenclature is given in Fig. 2.1.

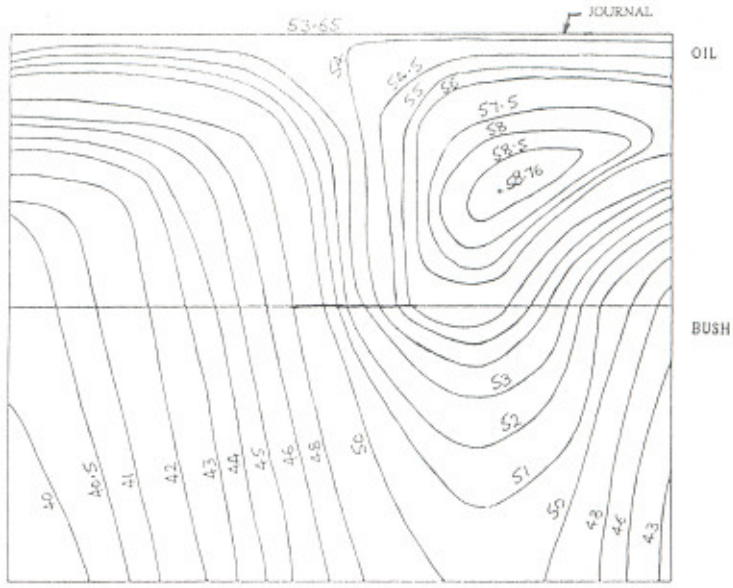

(a) β = - 1.0

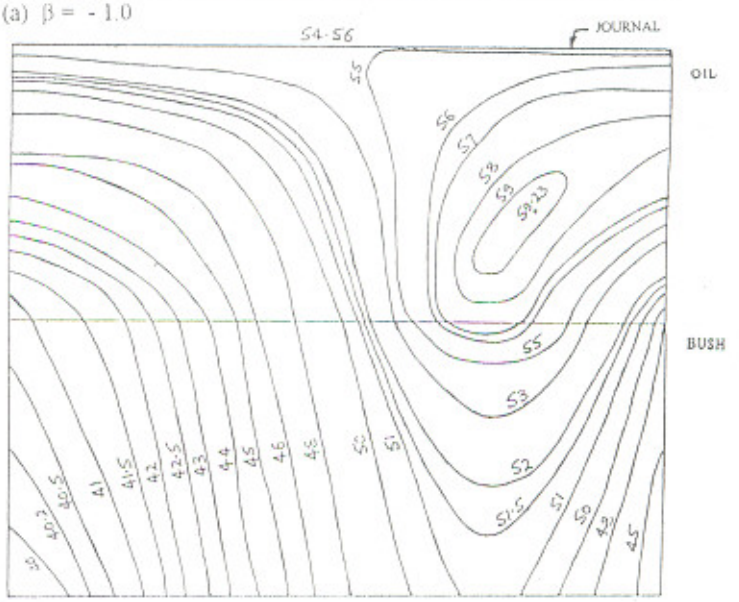

(b) β = 0.0

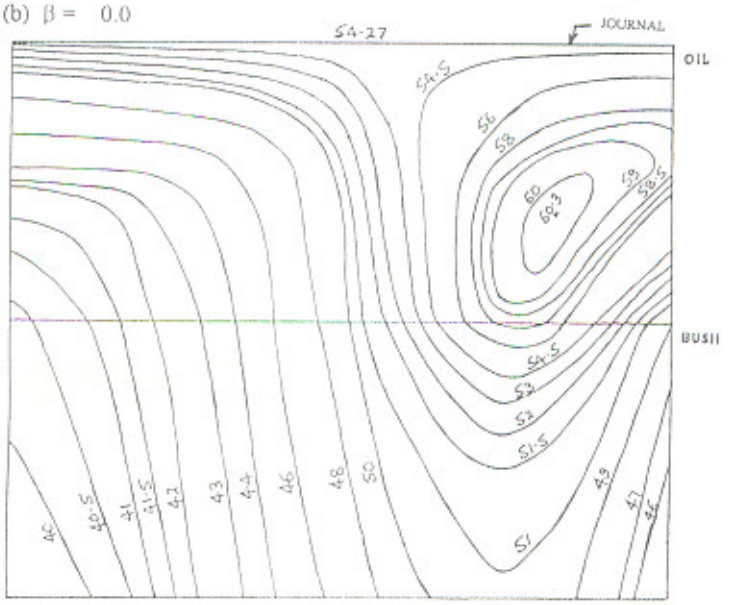

(c) β = 1.0 (MAXIMUM TEMPERATURE)

LOAD = 10 kN
($\bar{\gamma}_x = \bar{\gamma}_z = 0.2$)

Fig. 5.60 PLAIN JOURNAL BEARING ; ISOTHERMS

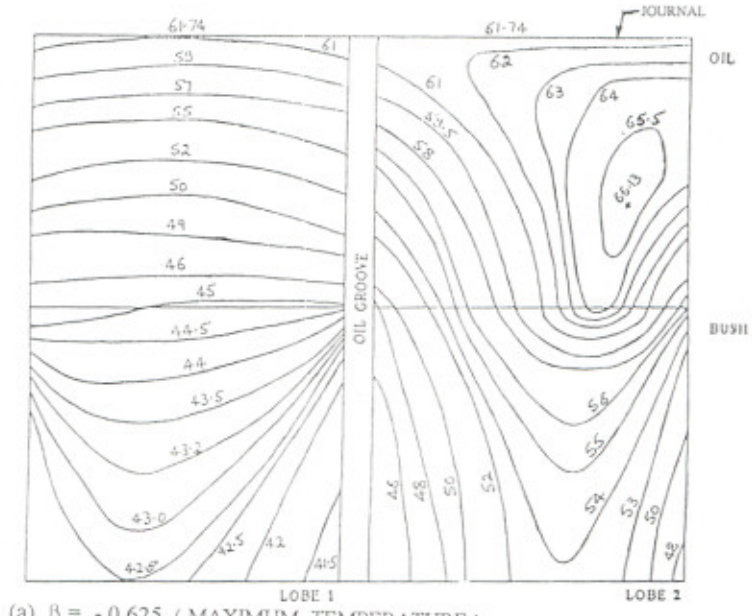

(a) β = - 0.625 (MAXIMUM TEMPERATURE)

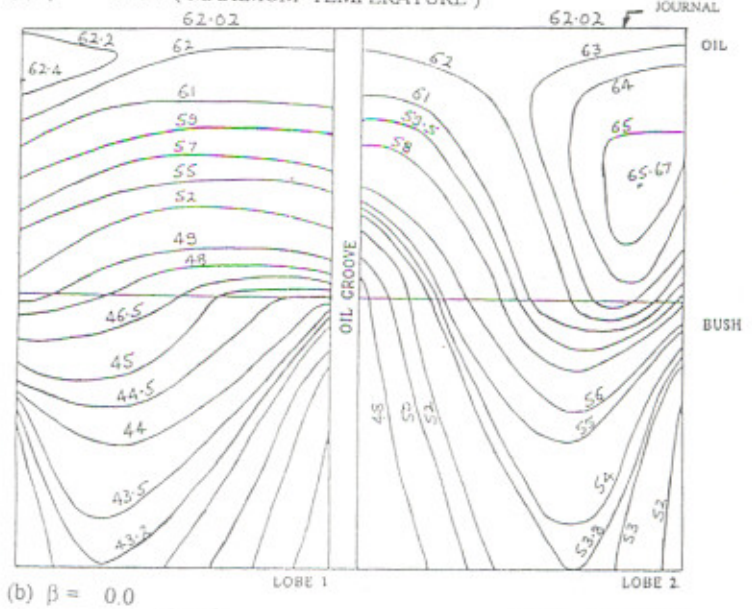

(b) β = 0.0

LOAD = 10 kN
($\bar{\gamma}_x = \bar{\gamma}_z = 0.2$)

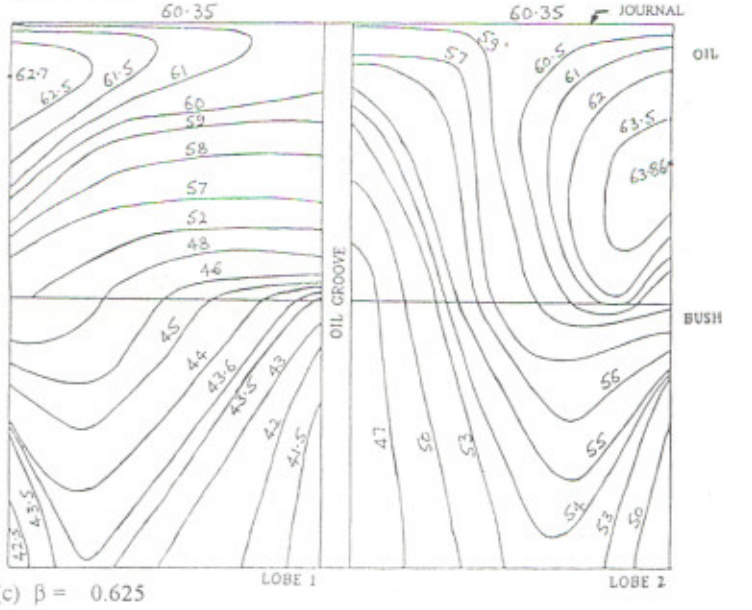

(c) β = 0.625

Fig. 5.61 TWO-AXIAL-GROOVE JOURNAL BEARING : ISOTHERMS

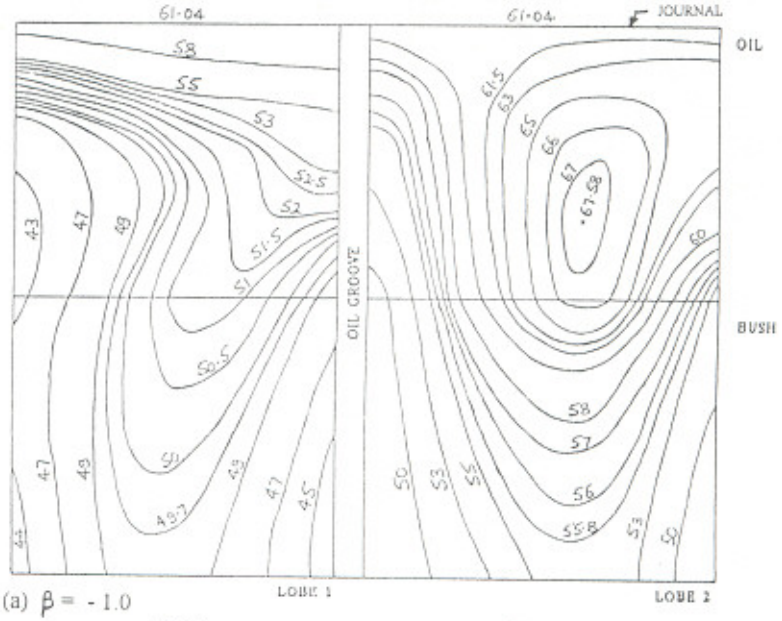

(a) β = - 1.0

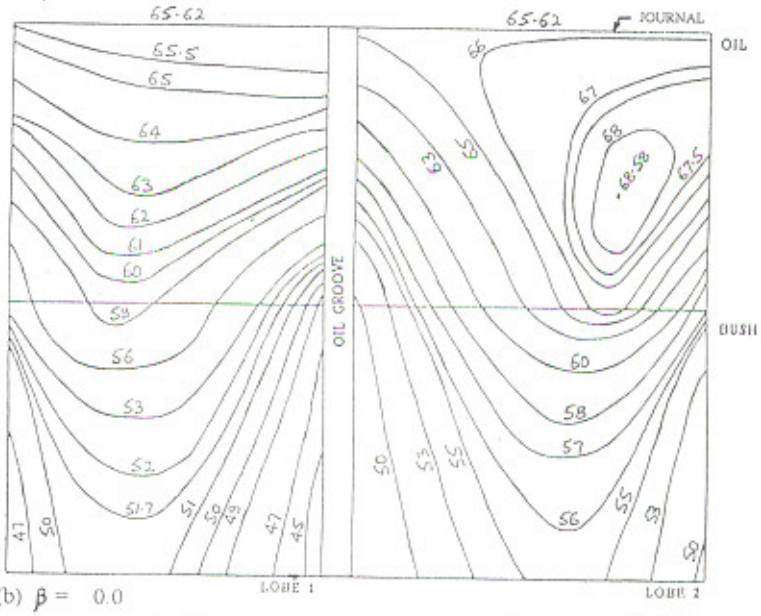

(b) β = 0.0

LOAD = 10 kN
($\bar{\gamma}_x = \bar{\gamma}_z = 0.2$)

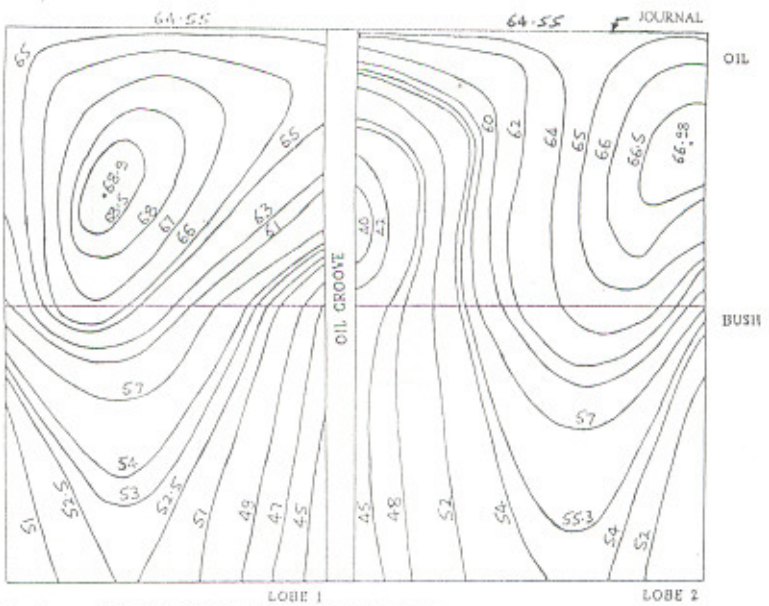

(c) β = 1.0 (MAXIMUM TEMPERATURE)

Fig. 5.62 ELLIPTICAL JOURNAL BEARING : ISOTHERMS

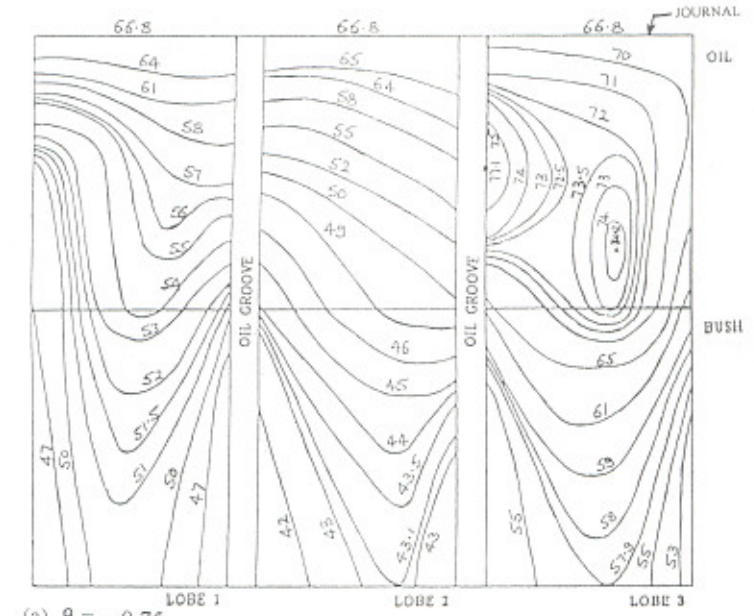

(a) β = - 0.75

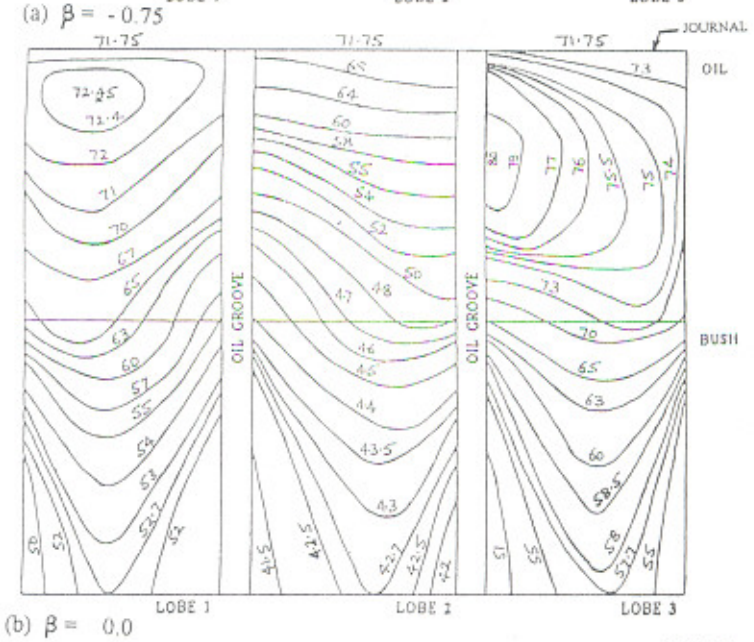

(b) β = 0.0

LOAD = 10 kN
($\bar{\gamma}_x = \bar{\gamma}_z = 0.2$)

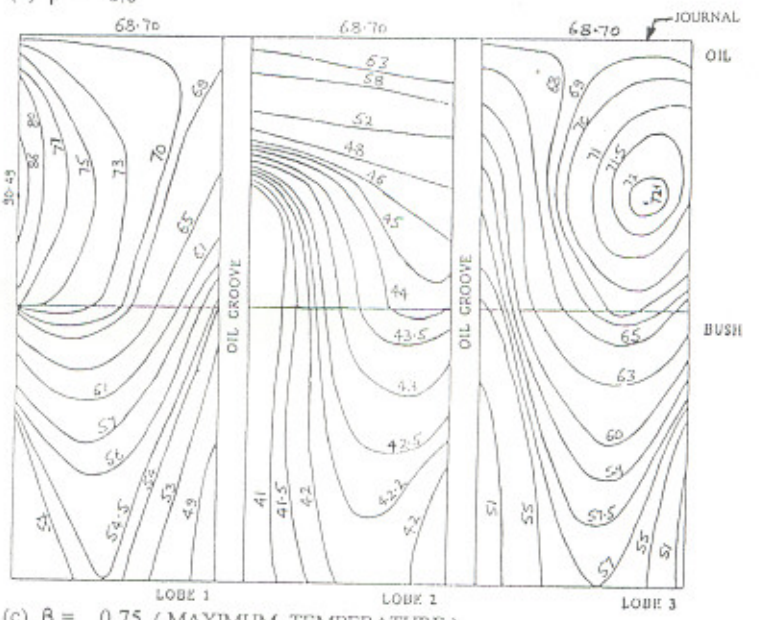

(c) β = 0.75 (MAXIMUM TEMPERATURE)

Fig. 5.63 THREE-LOBE JOURNAL BEARING : ISOTHERMS

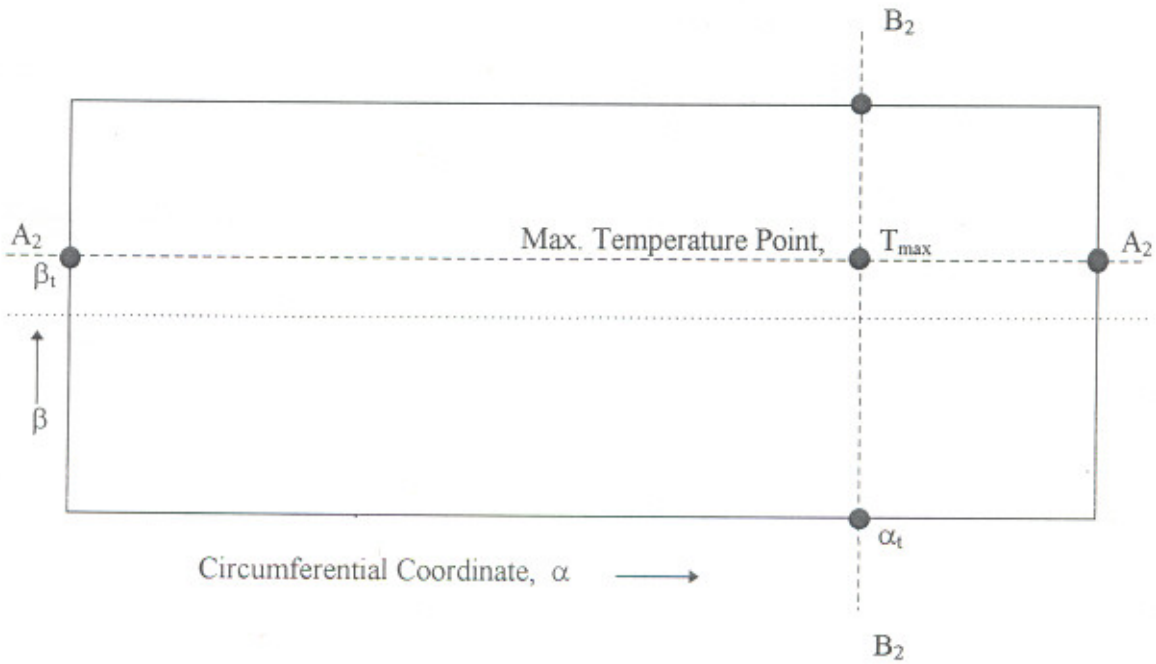

Fig. 5.64 Unwrapped Journal Bearing showing the Coordinate System and the Position of Maximum Temperature Point

The bush-fluid interface temperature profiles for aligned and misaligned journal bearings are shown in Figs. 5.65 to 5.70. These figures reveal that the maximum interface temperature is higher in the case of a misaligned bearing and the axial temperature profiles, indicate that the axial variation of temperature is quite significant in the case of misaligned bearings especially for non-circular bearing configurations.

The Figs.5.65(a), 5.66(a), 5.67(a) and 5.68(a) reveals that in the case of plain journal bearing and lobe 1 of two-axial-groove journal bearing supporting a light load (2 kN), the temperature is higher at the inlet of edge of the bearing pad, which could be the result of mixing of relatively higher amount of hot recirculating oil with the cool supply oil at lower values of eccentricity ratios. For heavy loads, the operating eccentricity is higher and hence the amount of cool supply oil will be relatively much more than the recirculating oil. Thus the temperature after mixing will be lesser.

It is observed that at the light load, the difference of temperature across the bush ends in misaligned plain journal bearing and two-axial-groove journal bearing is respectively 2.7 °C and 7 °C, {Figs. 5.65(b) and 5.67(b)} whereas for an aligned bearing it is only about 0.4 °C and 0.7 °C respectively. At heavier load, this difference is even higher and increases further with the increase in misalignment. Figs. 5.66(a) to 5.66(d) and 5.68(a) to 5.68(d) show the bush-fluid interface temperature profiles of aligned and misaligned journal bearings at the higher values of misalignment ratio ($\bar{\gamma}_x = \bar{\gamma}_z = 0.4$) for light and a heavy load. The trends in this case are also similar to those in Figs. 5.65 and 5.66 except that the difference in temperature between aligned and misaligned bearing cases is much higher.

The bush-fluid interface temperature profiles for elliptical journal bearing and three-lobe journal bearing are shown in Figs. 5.69 and 5.70. Figs. 5.69(a) and 5.70(a) reveal that at light load, misalignment leads to significant rise (7 °C) in bush-fluid interface temperature in the lobe 1. Fig. 5.69(b) shows that at light load, the axial variation of temperature increases from 3 °C to 13 °C due to misalignment in case of elliptical journal bearing where as in three-lobe journal bearing{Fig. 5.70(b)}, the axial variation of temperature increases from 5.0 to 22.3 °C.

Table 5.11 summaries the observations of temperature profiles studied. These results indicate that the assumption of negligible change in temperature across the axial length of bearing, generally used for the study of aligned bearings, is not quite valid for the analysis of misaligned bearings as it may lead to serious inaccuracies.

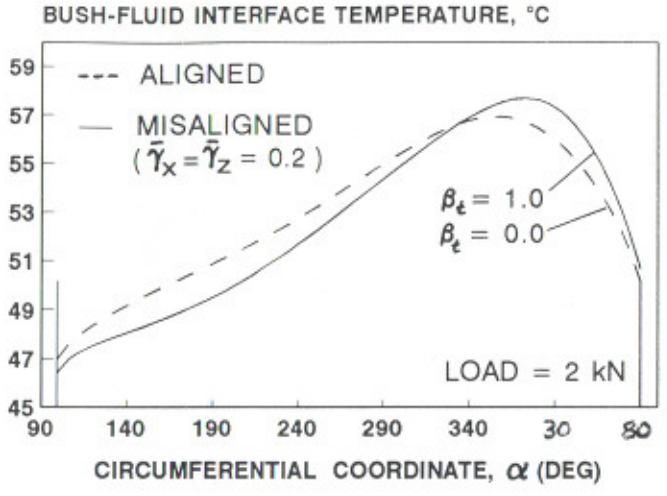

(a) SECTION AT A_2 - A_2

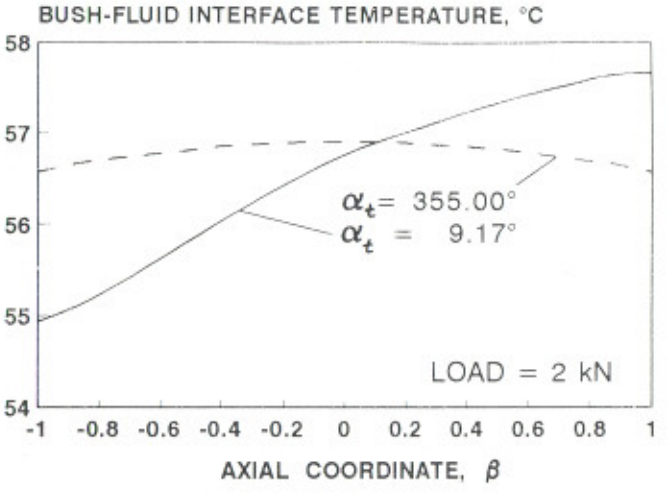

(b) SECTION AT B_2 - B_2

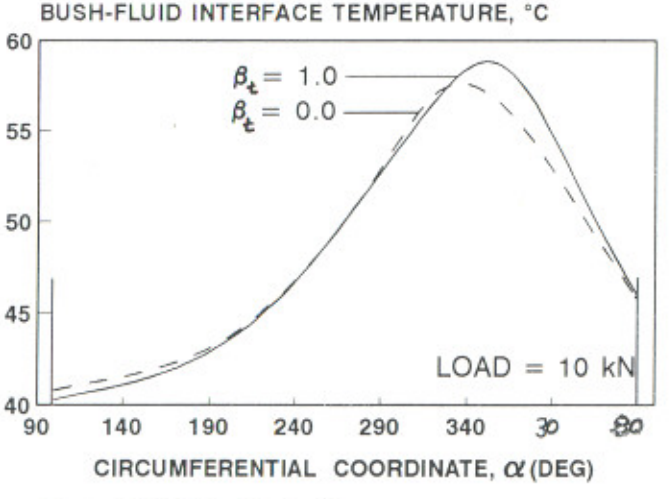

(c) SECTION AT A_2 - A_2

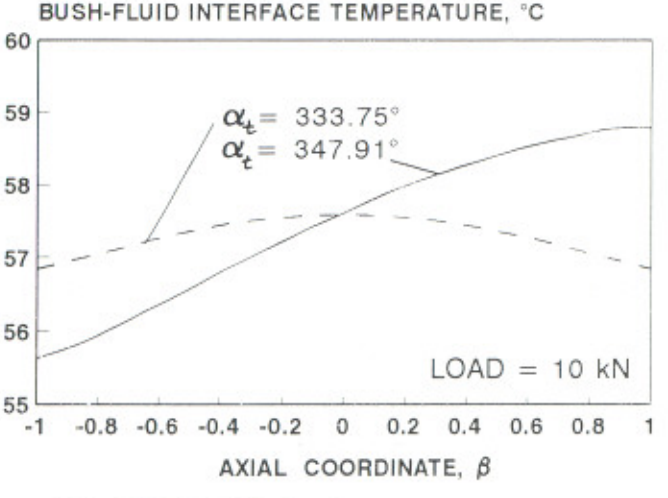

(d) SECTION AT B_2 - B_2

Fig. 5.65 PLAIN JOURNAL BEARING - TEMPERATURE PROFILES

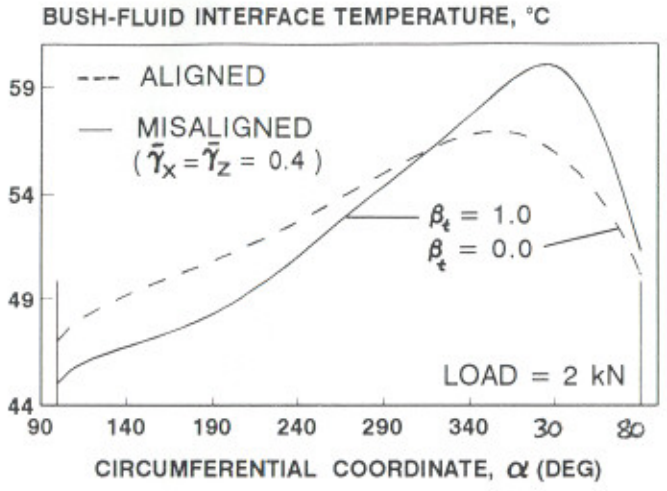

(a) SECTION AT A_2 - A_2

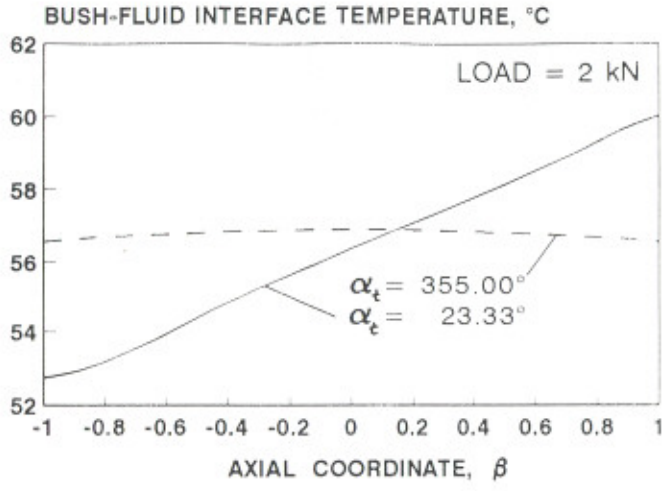

(b) SECTION AT B_2 - B_2

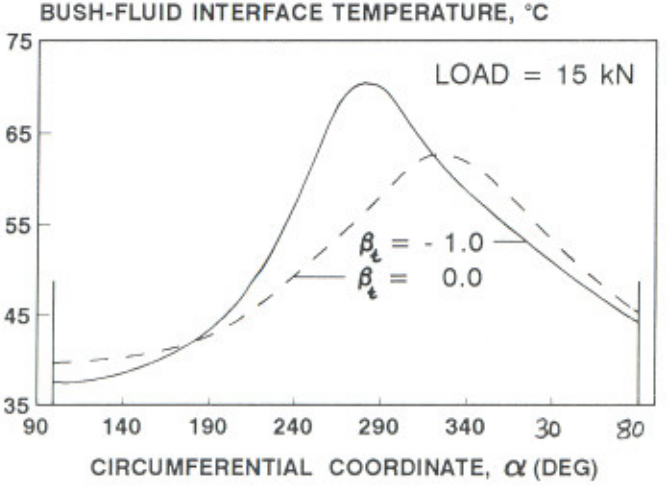

(c) SECTION AT A_2 - A_2

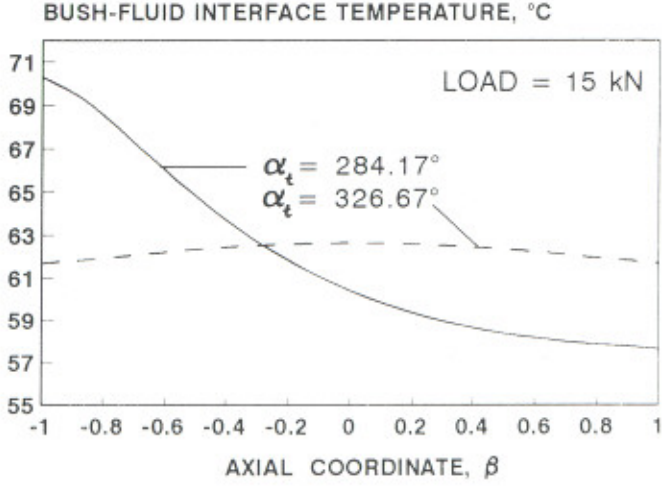

(d) SECTION AT B_2 - B_2

Fig. 5.66 PLAIN JOURNAL BEARING - TEMPERATURE PROFILES

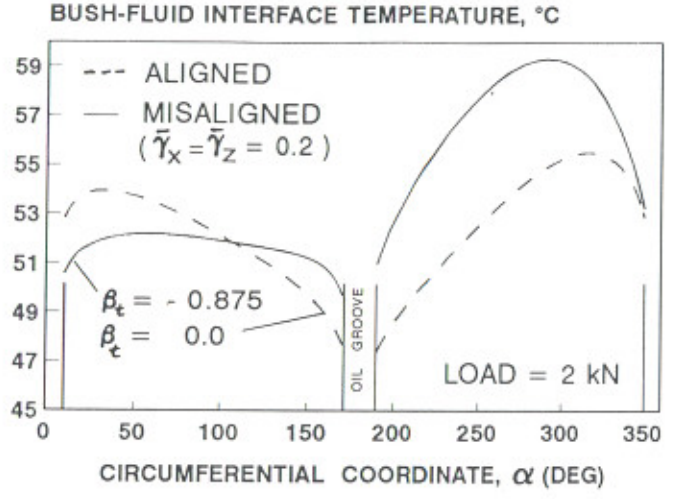

(a) SECTION AT A_2 - A_2

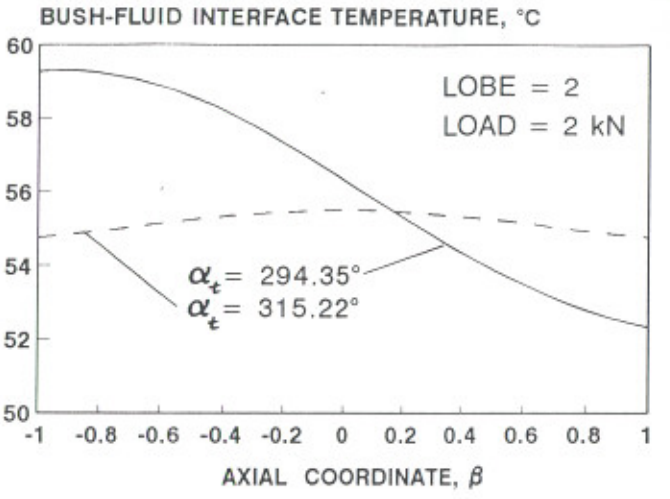

(b) SECTION AT B_2 - B_2

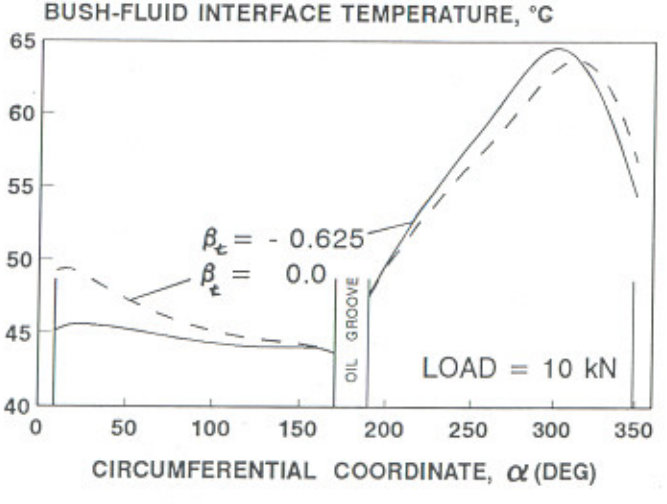

(c) SECTION AT A_2 - A_2

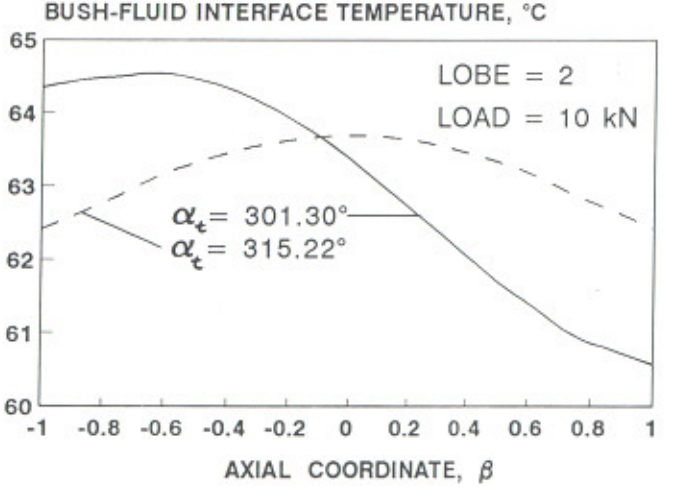

(d) SECTION AT B_2 - B_2

Fig. 5.67 TWO-AXIAL-GROOVE JOURNAL BEARING - TEMPERATURE PROFILES

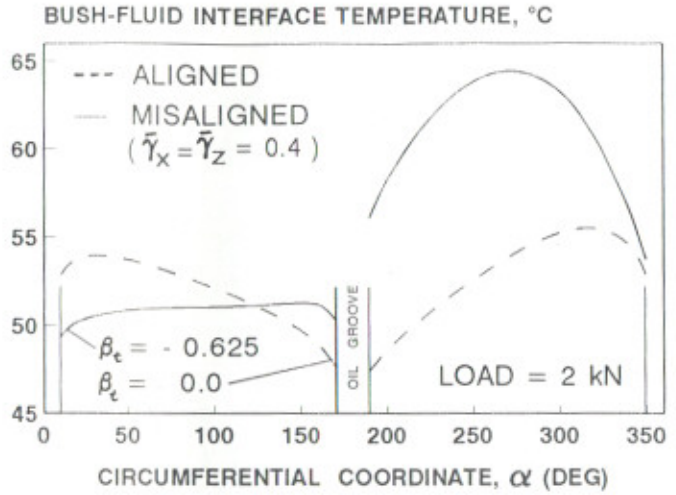

(a) SECTION AT A_2 - A_2

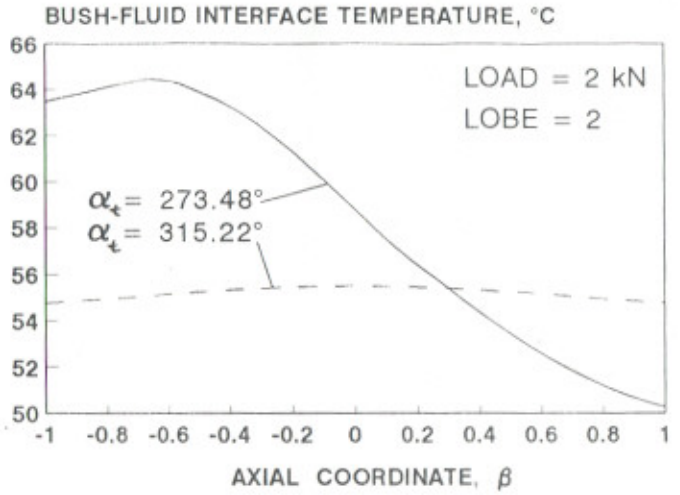

(b) SECTION AT B_2 - B_2

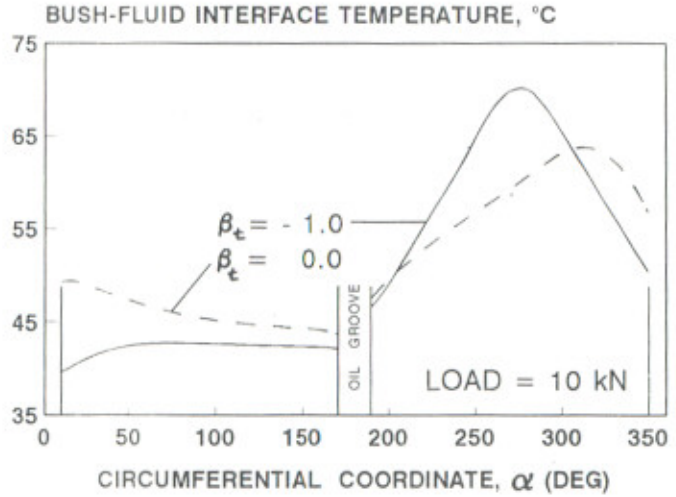

(c) SECTION AT A_2 - A_2

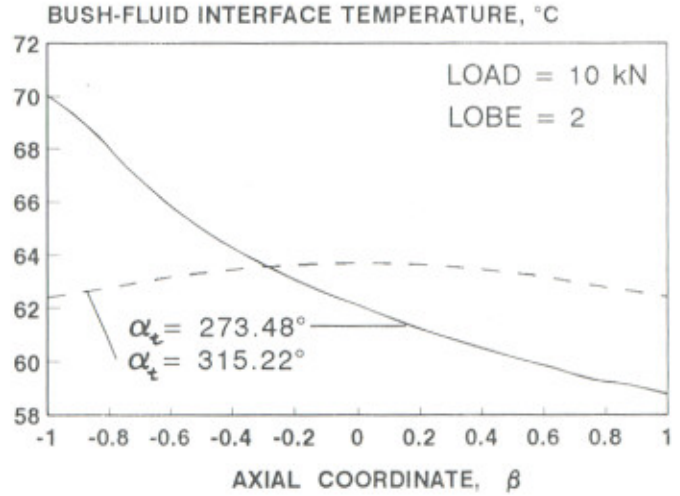

(d) SECTION AT B_2 - B_2

Fig. 5.68 TWO-AXIAL-GROOVE JOURNAL BEARING - TEMPERATURE PROFILES

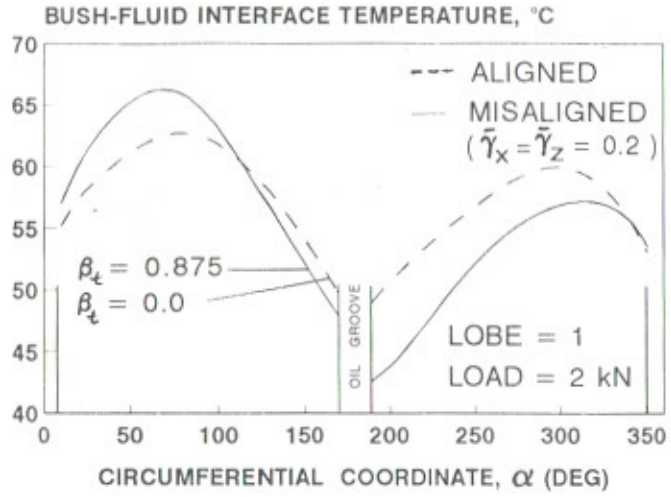

(a) SECTION AT A_2 - A_2

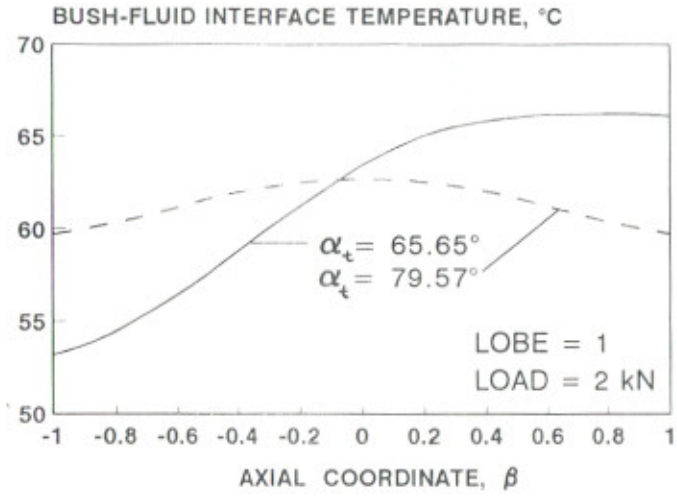

(b) SECTION AT B_2 - B_2

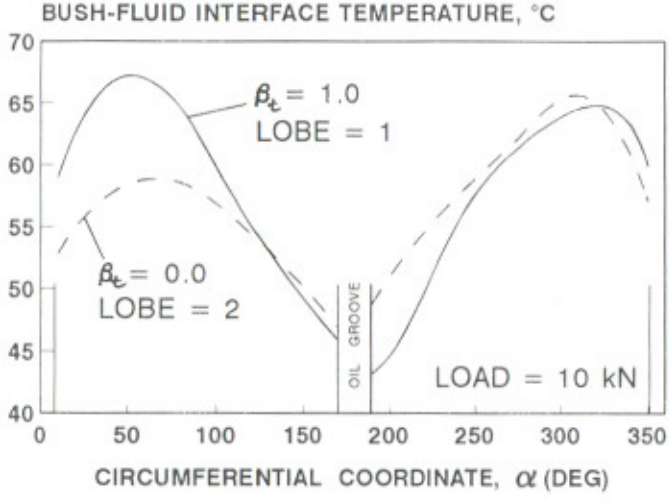

(c) SECTION AT A_2 - A_2

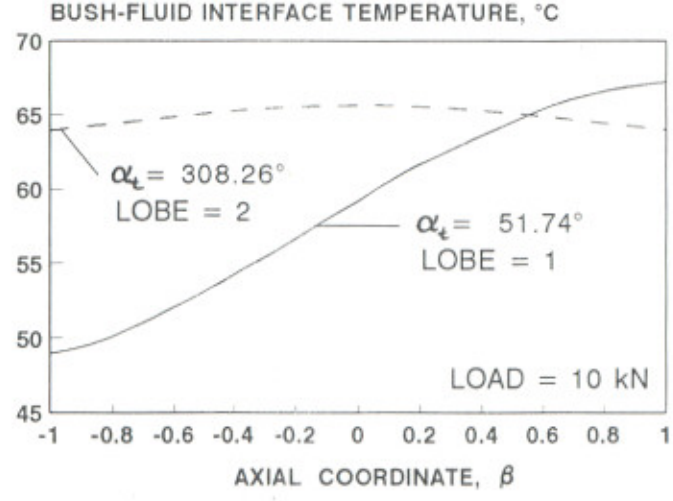

(d) SECTION AT B_2 - B_2

Fig. 5.69 ELLIPTICAL JOURNAL BEARING - TEMPERATURE PROFILES

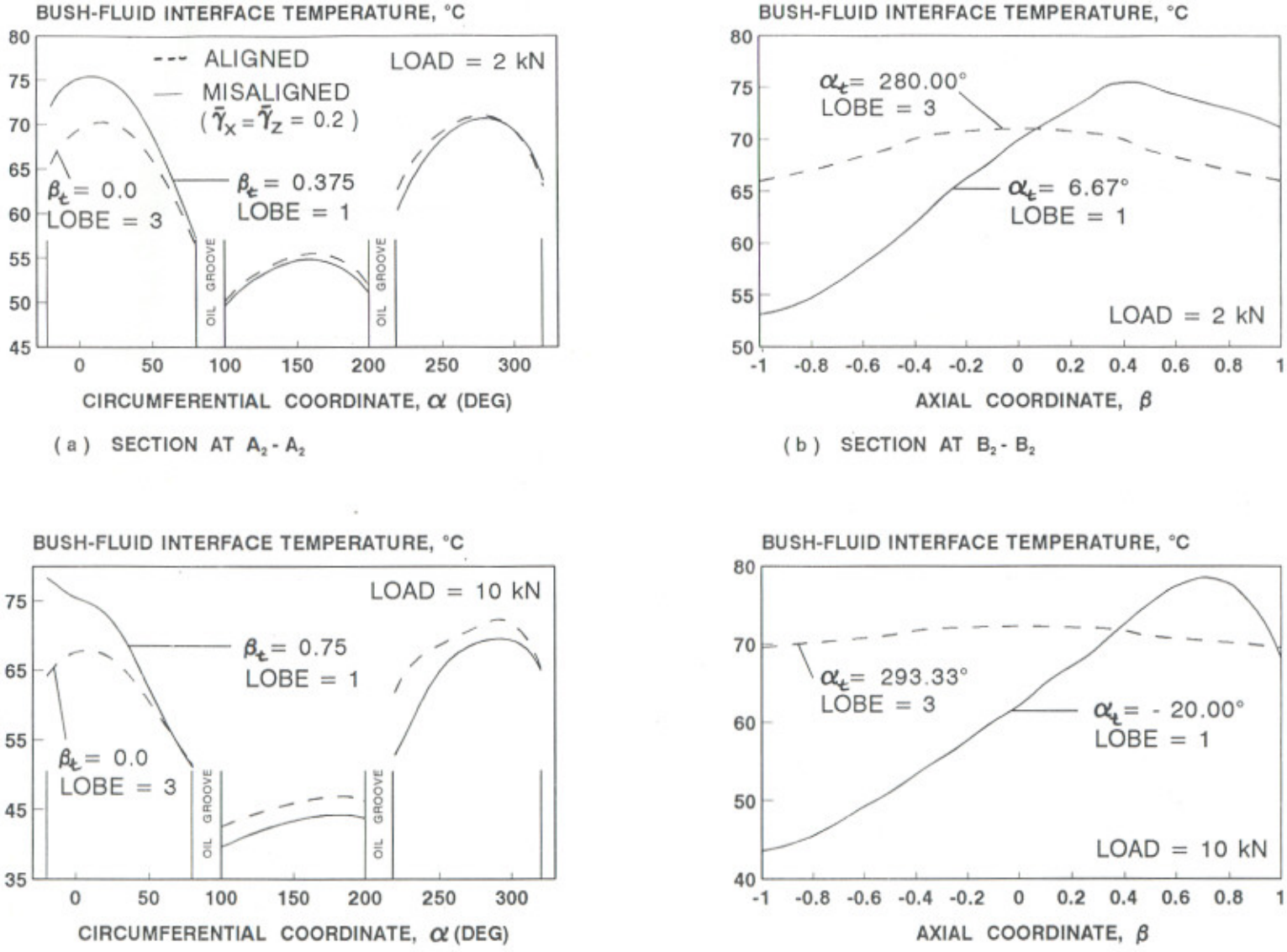

Fig. 5.70 THREE-LOBE JOURNAL BEARING - TEMPERATURE PROFILES

Table 5.11 Summary of Temperature Profiles

Type of Journal Bearing	Load, kN	Misalignment, $\bar{\gamma}_x = \bar{\gamma}_z$	Maximum Temperature, °C	Axial Temperature Difference, °C (Maximum)
Plain	2.0	0.0	56.9	0.4
		0.2	57.7	2.7
		0.4	60.0	7.3
	10	0.0	57.6	0.8
		0.2	58.8	3.2
	15	0.0	62.8	1.0
		0.4	70.2	12.7
Two-Axial-Groove	2.0	0.0	55.5	0.7
		0.2	59.3	7.0
		0.4	64.4	14.2
	10.0	0.0	63.7	1.3
		0.2	64.5	4.0
		0.4	69.6	11.3
Elliptical	2.0	0.0	62.7	3.0
		0.2	66.2	13.0
	10.0	0.0	65.6	1.7
		0.2	67.2	18.2
Three-lobe	2.0	0.0	71.0	5.0
		0.2	75.4	22.3
	10.0	0.0	72.3	2.7
		0.2	78.3	34.7

Figs. 5.71(a) and 5.71(b) show that the axial variation of journal temperature for a load of 10 kN and misalignment of $\bar{\gamma}_x = \bar{\gamma}_z = 0.2$ for the four bearing geometries studied. The figures clearly show that due to misalignment the journal temperature varies significantly along the axial length of the journal and the temperatures at the two ends of the journal are different. The difference between the maximum journal temperature and minimum journal temperature is more in the case of non-circular bearings{Fig. 5.71(b)} as compared to the circular bearings, Fig. 5.71(a). Hence, the journal cannot be assumed as a lumped thermal element in the analysis of misaligned bearings.

5.4 TRANSIENT MOTION TRAJECTORIES

In the present work, the effect of misalignment on the dynamic response of four journal bearing systems has been studied via the transient motion trajectories of journal-centre obtained using the linearised equations of motion for free translatory whirl.

In order to bring out the effect of misalignment clearly, the transient motion trajectories of journal-centre are drawn by keeping the value of journal mass, $\bar{M}_J$ same for the aligned and the misaligned journal bearings. For a given initial disturbance, trajectories have been traced until the final position of the journal centre reaches within specified distance from the static equilibrium position. The time taken during this period is recorded. A journal bearing system for which the journal centre after initial disturbance takes lesser time to reach desired position is relatively more stable than the one which takes more time. The trajectories so obtained are given in Figs. 5.72 to 5.79 for the four bearings. Table 5.12 gives the time recorded for each trajectory and the effect of misalignment is presented in terms of a parameter "% diff." defined below the table. It can be clearly seen that all bearings are relatively more stable when operating under misalignment. Also the relative stability is even better when the operating load is higher.

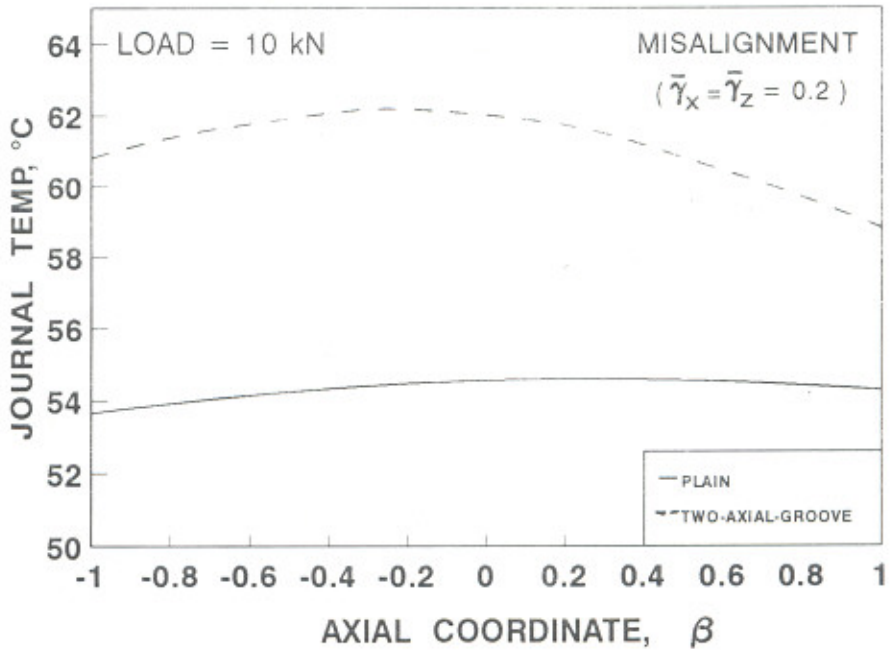

(a)

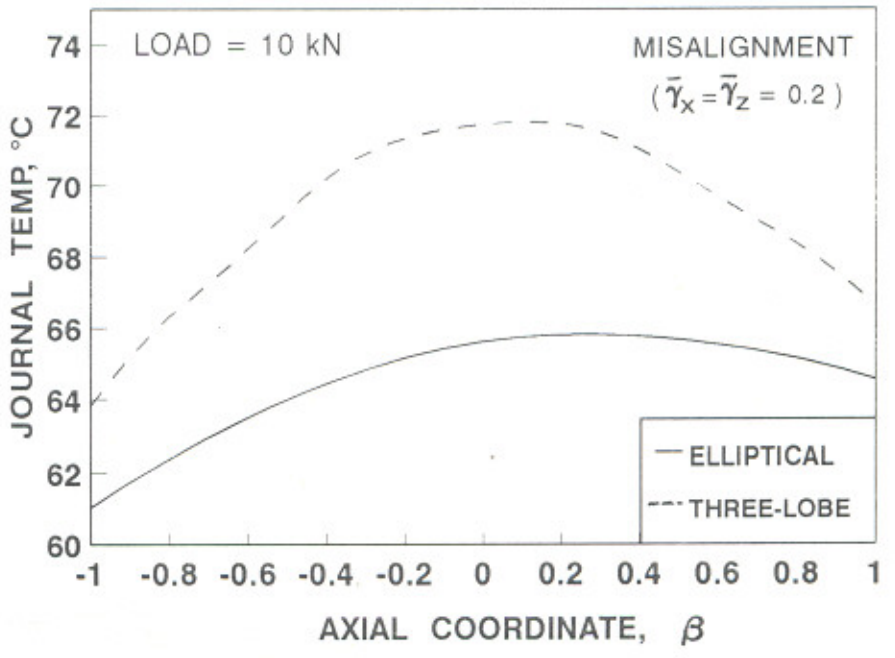

(b)

Fig. 5.71 JOURNAL TEMPERATURE PROFILES

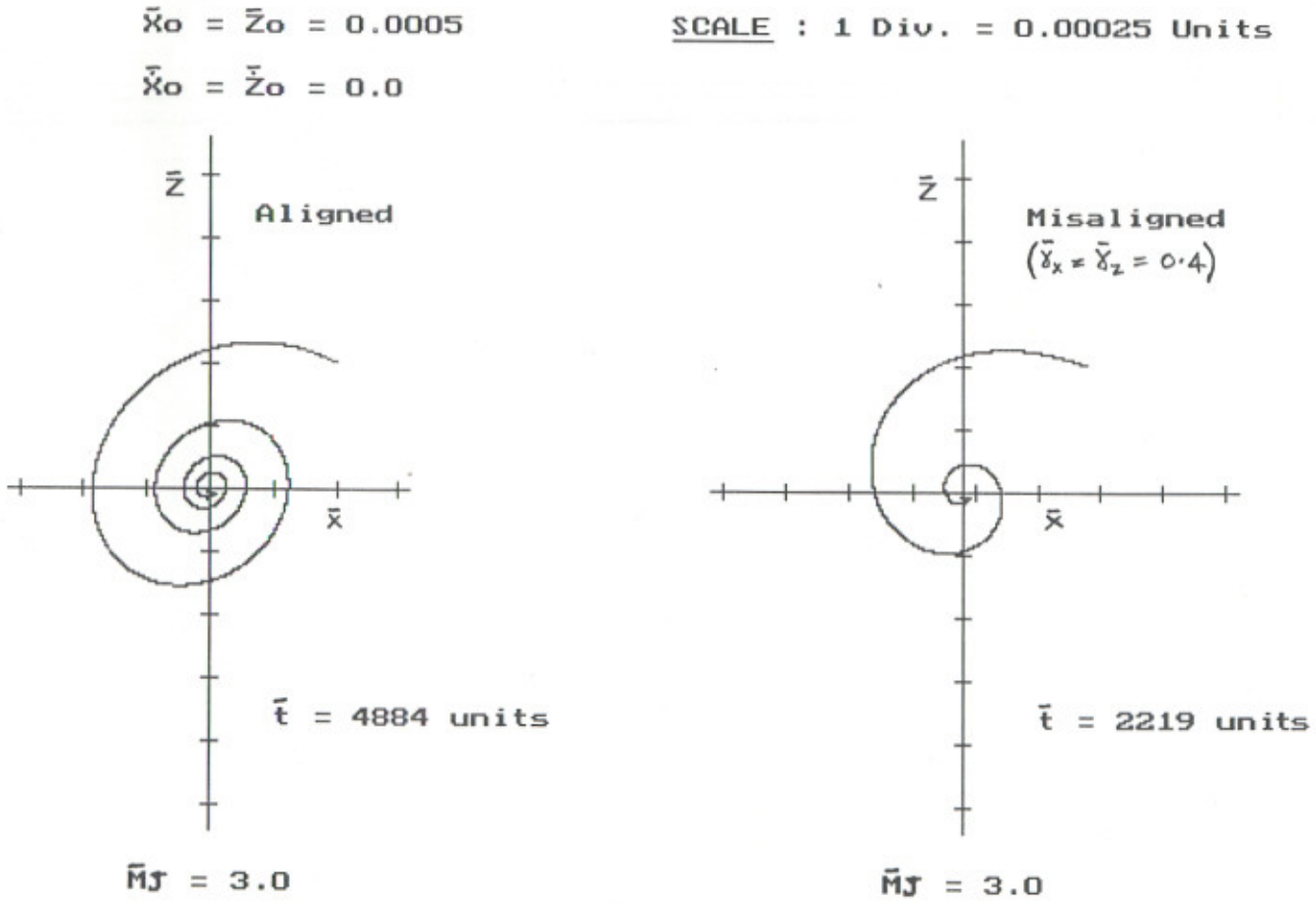

Fig. 5.72 : Linear Trajectories for Plain Journal Bearing – (Load = 2 kN)

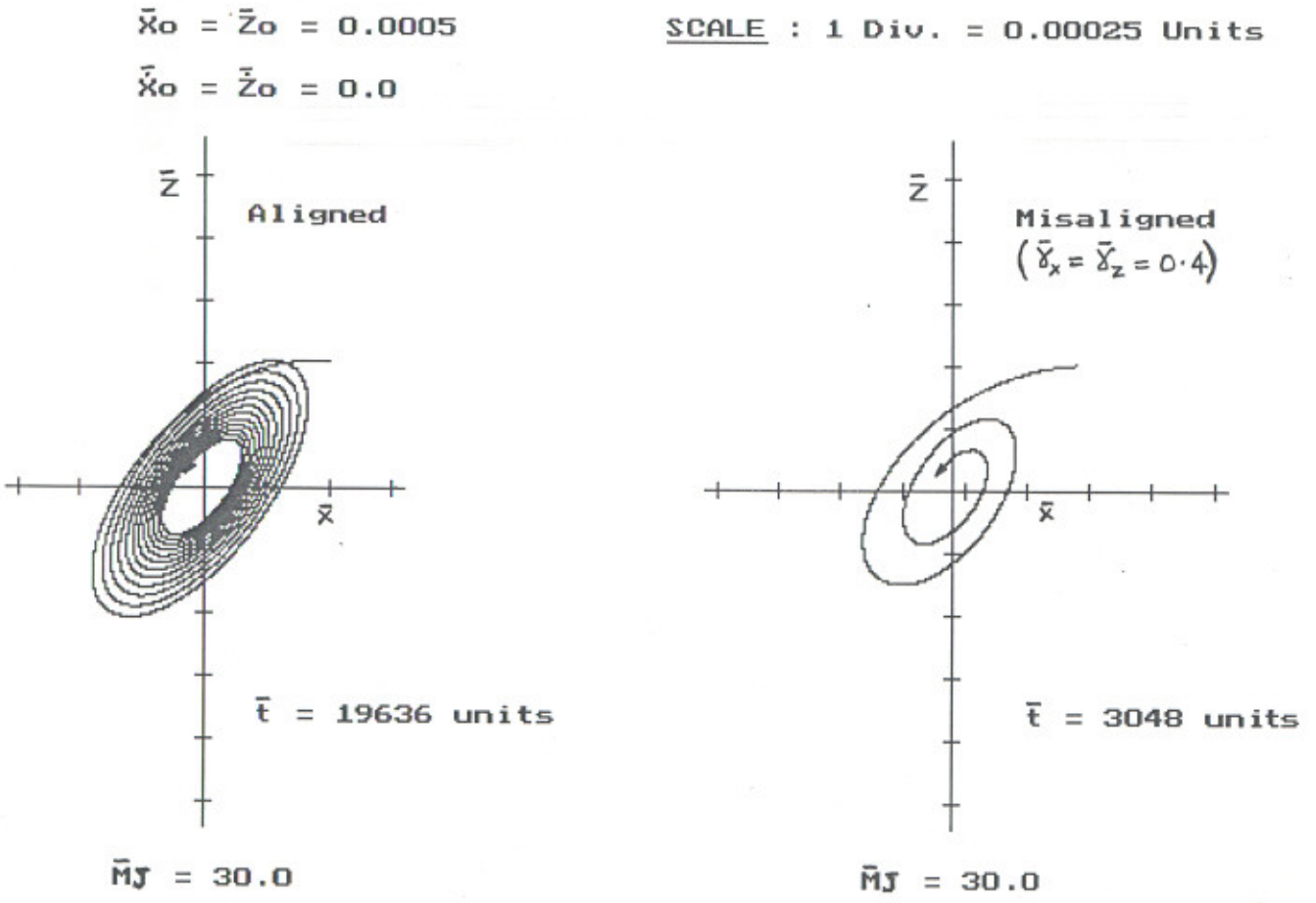

Fig. 5.73 : Linear Trajectories for Plain Journal Bearing – (Load = 10 kN)

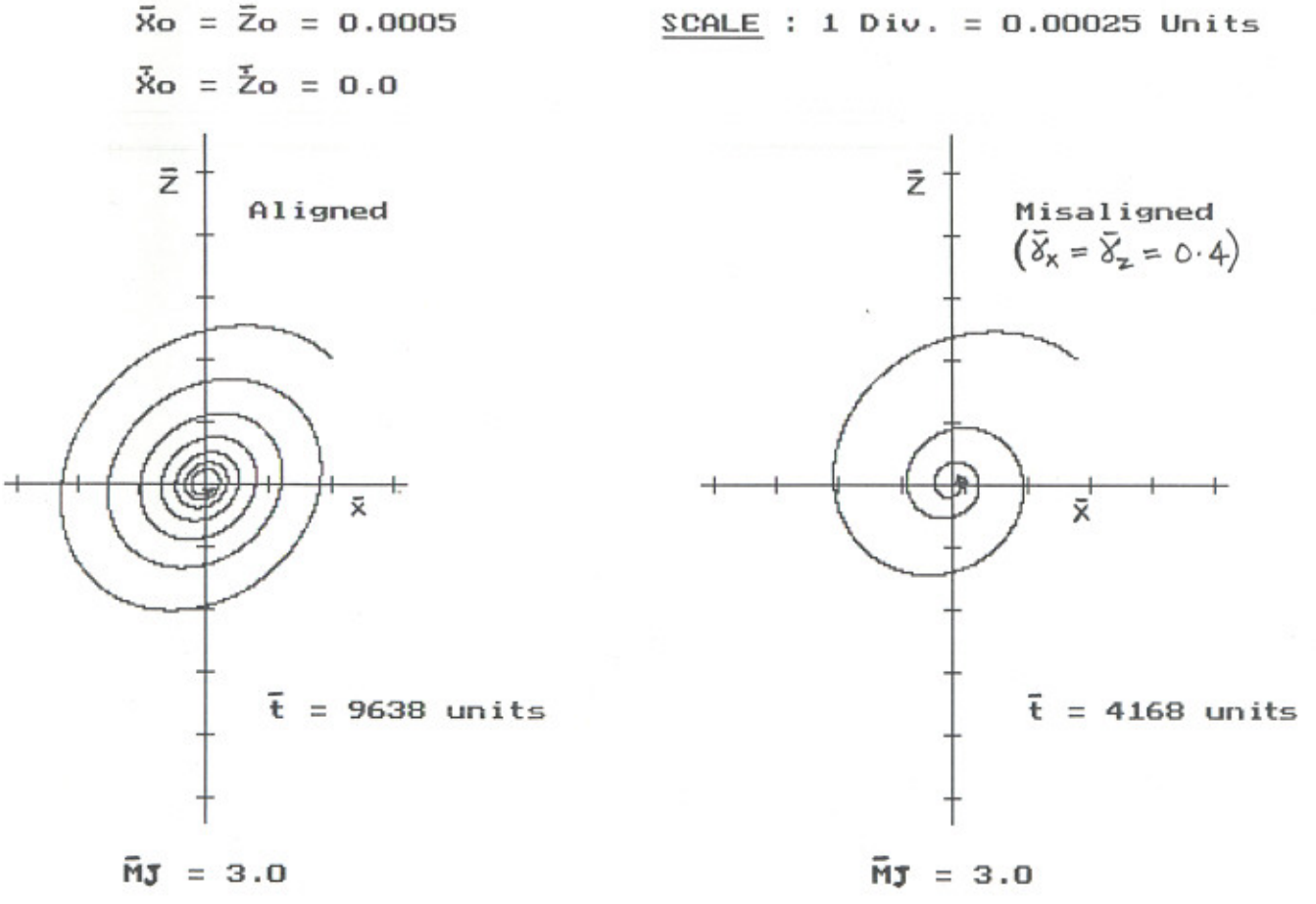

Fig. 5.74 : Linear Trajectories for Two-Axial-Groove Journal Bearing - (Load = 2 kN)

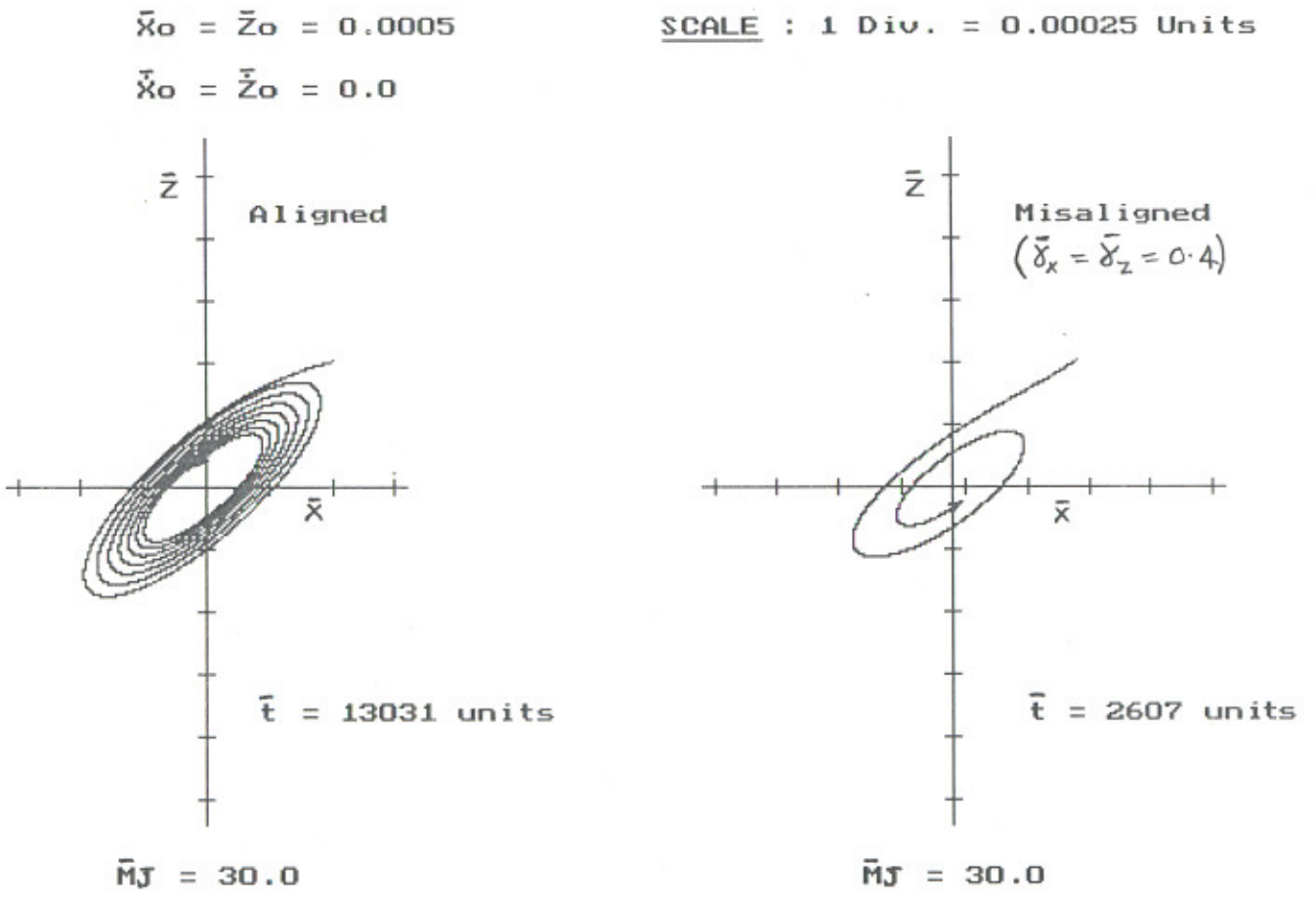

Fig. 5.75 : Linear Trajectories for Two–Axial–Groove Journal Bearing – (Load = 10 kN)

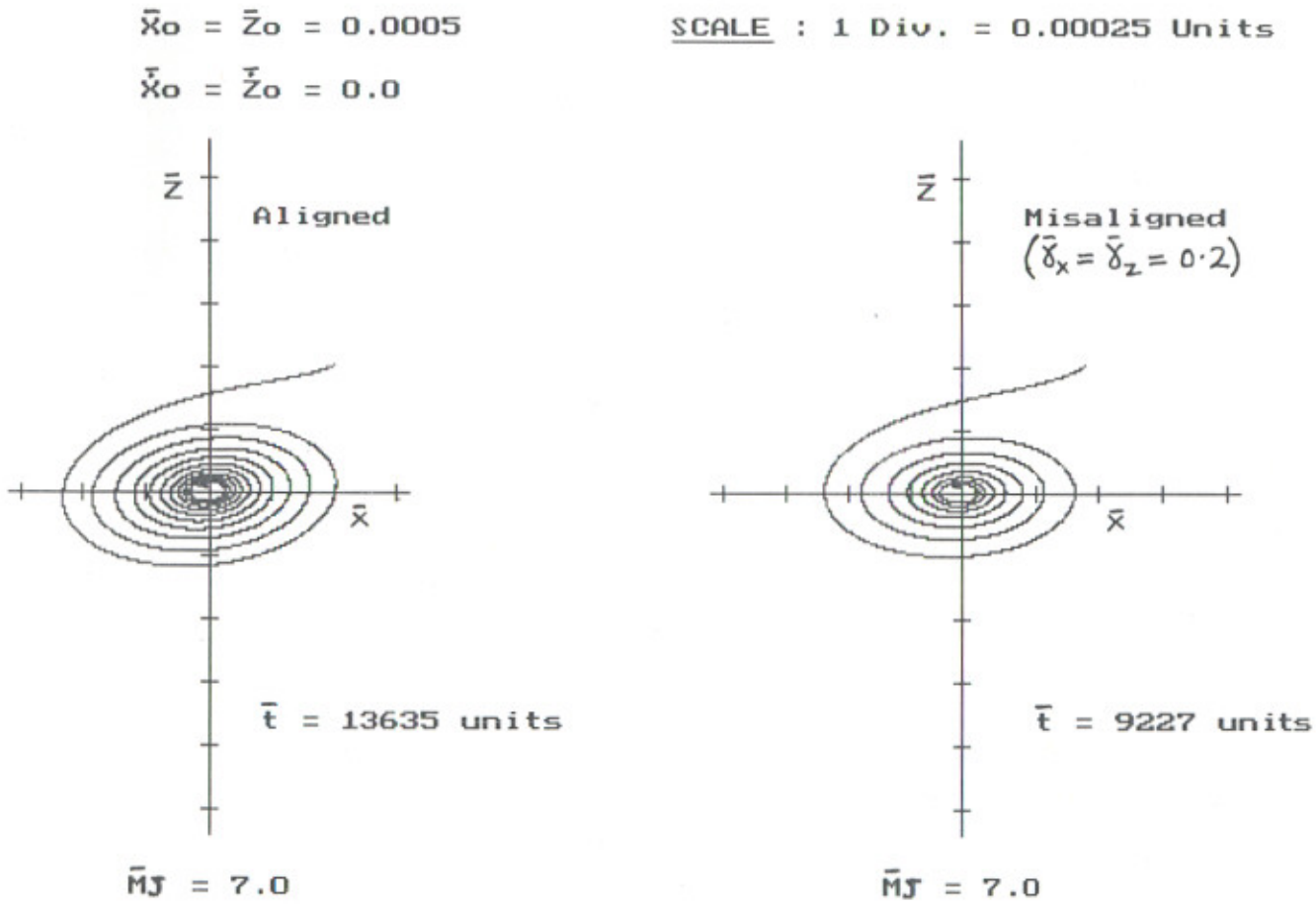

Fig. 5.76 : Linear Trajectories for Elliptical Journal Bearing – (Load = 2 kN)

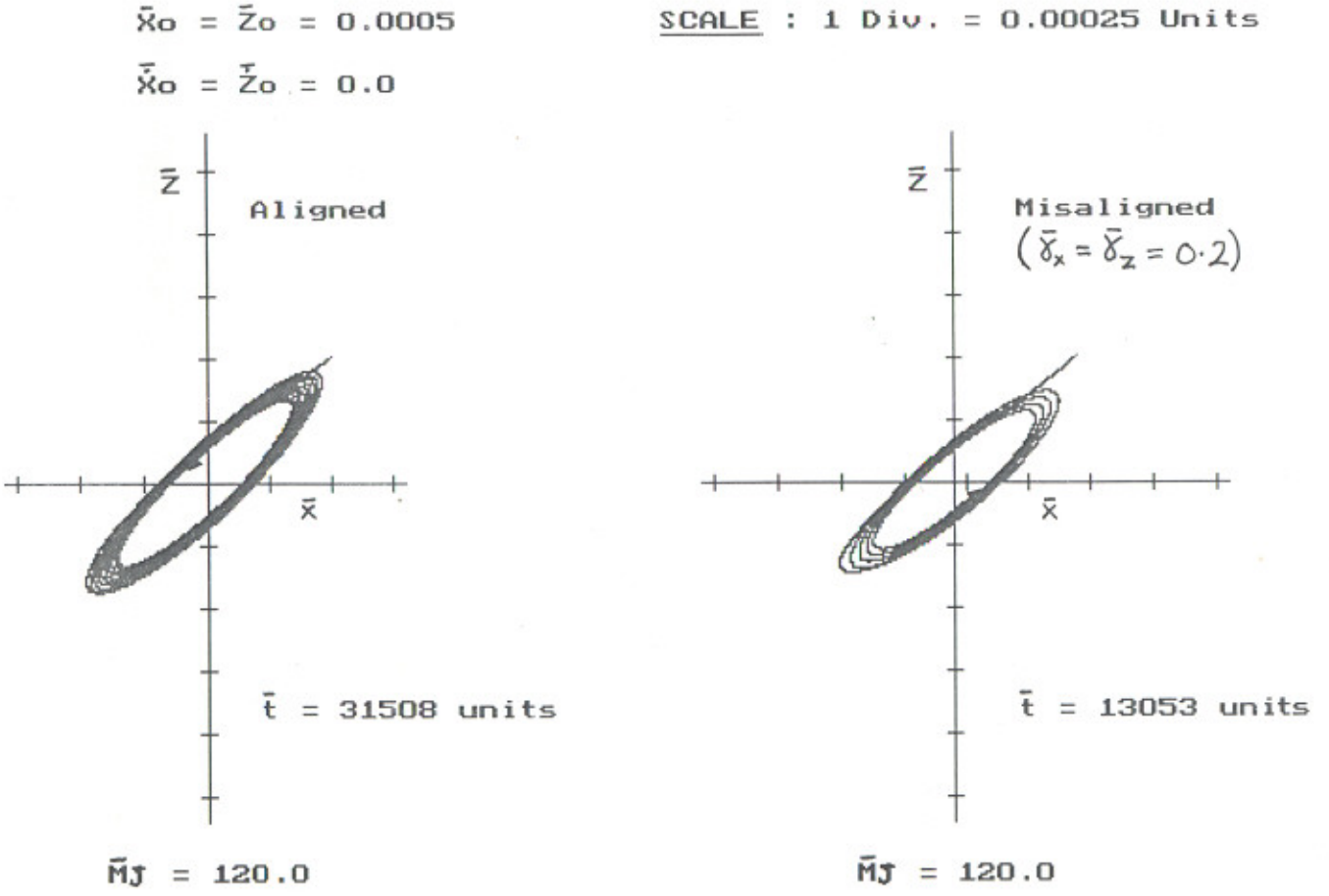

Fig. 5.77 : Linear Trajectories for Elliptical Journal Bearing – (Load = 10 kN)

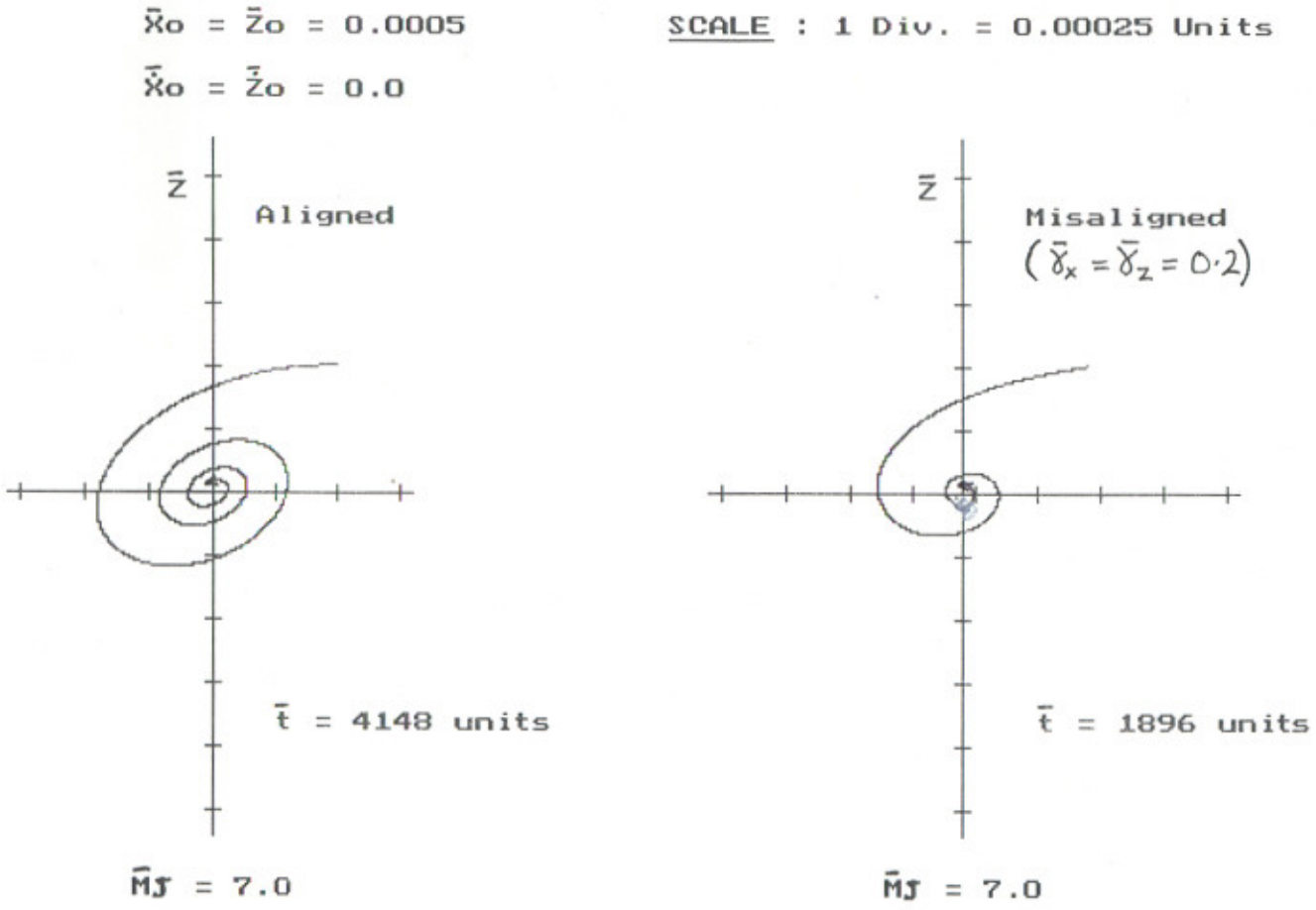

Fig. 5.78 : Linear Trajectories for Three-Lobe Journal Bearing – (Load = 2 kN)

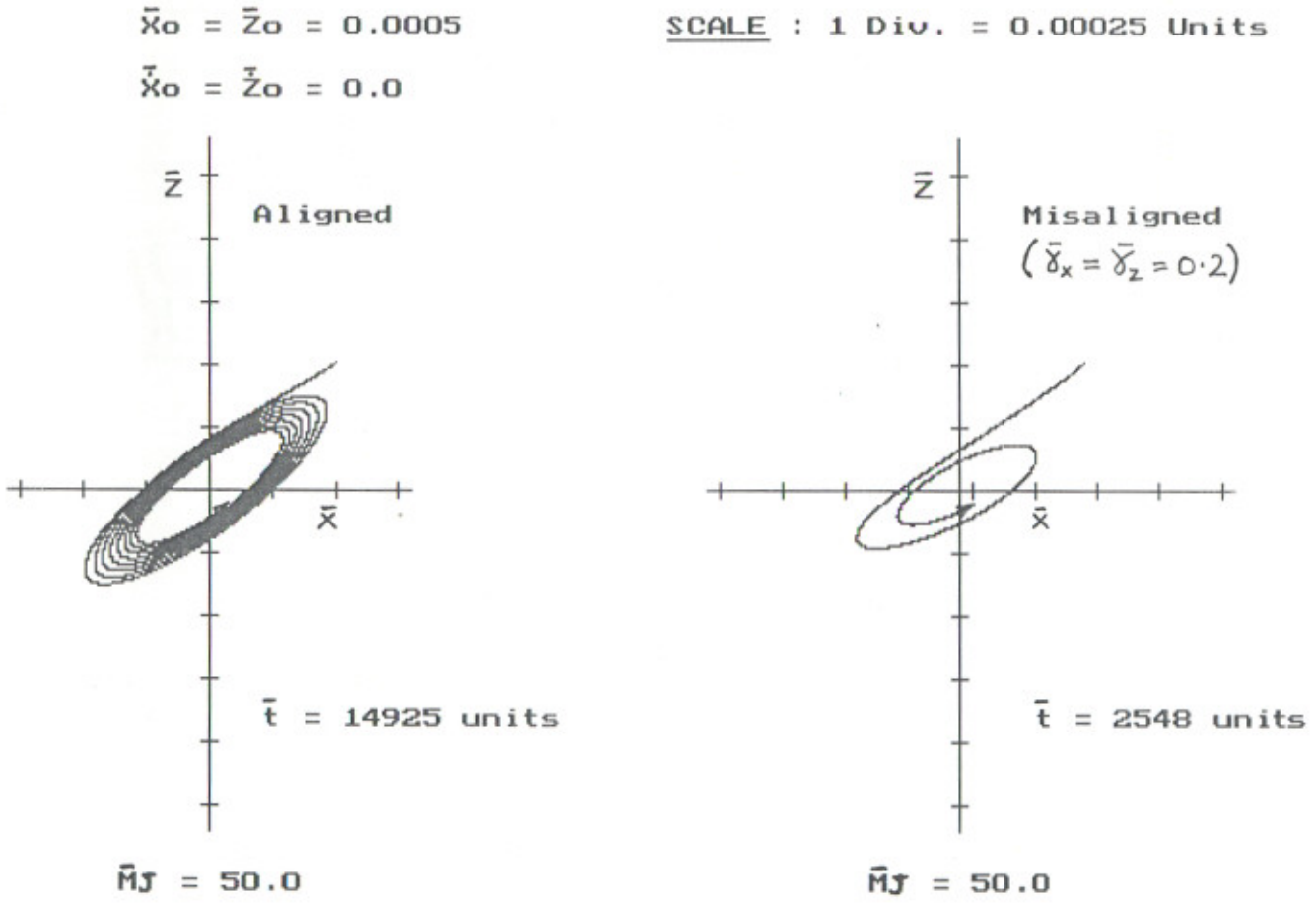

Fig. 5.79 : Linear Trajectories for Three-Lobe Journal Bearing - (Load = 10 kN)

Table 5.12 Comparison of Time Units Required for Reaching a Stable Position

$\bar{X} = \bar{Z} = 0.005$ $\dot{\bar{X}} = \dot{\bar{Z}} = 0.0$ $d\bar{t} = 0.01$

Type of Journal Bearing	Load, kN	Critical Mass, $\bar{M}_C$		Journal Mass, $\bar{M}_J$	Time (units)		% diff.*
		Aligned	Misaligned		Aligned	Misaligned	
Plain	2.0	4.91	7.73	3.0	4884	2219	54.57
	10.0	34.12	65.40	30.0	19636	3048	84.48
Two-Axial-Groove	2.0	4.03	5.53	3.0	9638	4168	56.75
	10.0	39.50	136.52	30.0	13031	2607	80.00
Elliptical	2.0	8.72	9.74	7.0	13635	9227	32.33
	10.0	148,08	180.17	120.0	31508	13053	58.57
Three-Lobe	2.0	12.00	19.46	7.0	4148	1896	54.29
	8.0	59.67	142.40	50.0	14925	2548	82.93

$$* \text{ \% dif.} = \frac{\text{time units for aligned bearing - time units for misaligned bearing}}{\text{time units for aligned bearing}} * 100$$

5.5 COMPARATIVE STUDY OF SOME VITAL PARAMETERS OF MISALIGNED JOURNAL BEARINGS

The failure of journal bearings generally occurs due to one or more of the following parameters reaching some critical values :

(i) Minimum fluid-film thickness (h_{min})

(ii) Stability parameters ($\bar{\Omega}$ and $\bar{\nu}$)

(iii) Bush and Journal Temperatures (T_b and T_j)

5.5.1 Minimum Fluid-Film Thickness (h_{min})

Table 5.13 shows the comparative values of minimum fluid-film thickness (h_{min}) for two values of load for the four types of journal bearings. It is observed that due to misalignment of $\bar{\gamma}_x = \bar{\gamma}_z = 0.2$, the minimum fluid-film thickness changes drastically. The % change in h_{min}, at light load is between 20 % to 30 % for plain journal bearing and two-axial groove journal bearing. At higher load values (20 kN), the % change in h_{min} is between 40 % and 60 % in case of plain journal bearing and two-axial groove journal bearing. For elliptical and three-lobe journal bearing, the % change in h_{min} is more than 50 % at the light load. At a heavy load, however, the % change in h_{min} decreases slightly in elliptical journal bearing but further increases in the three-lobe journal bearing.

5.5.2 Stability Parameters ($\bar{\Omega}$ and $\bar{\nu}$)

Table 5.14(a) shows the % change in the values of threshold speed ($\bar{\Omega}$) due to misalignment ($\bar{\gamma}_x = \bar{\gamma}_z = 0.2$) at various load capacities. At a light load, the increase in values of threshold speed ($\bar{\Omega}$) is about 5 % each for plain, two-axial-groove and elliptical journal bearings where as it is 27 % in the case of the three-lobe journal bearing. At higher load values, the % change in $\bar{\Omega}$ is on higher side as compared to the values at light load. The magnitude of change being more in case of three-lobe journal bearing.

The % change in the values of whirl frequency ratio, ($\bar{\nu}$) due to misalignment ($\bar{\gamma}_x = \bar{\gamma}_z = 0.2$) at various load values are shown in table 5.14 (b). It is observed from this table that the change in whirl frequency ratio due to misalignment is only marginal. It is seen that the whirl frequency ratio is reduced by the misalignment.

Table 5.13 Comparative Study of Minimum Film Thickness in Journal Bearings

Type of Journal Bearing	Load, kN	Minimum film thickness, in mm		% Change
		Aligned	Misaligned	
Plain	2	0.10690	0.07751	27.49
	10	0.05256	0.04005	23.80
	20	0.02729	0.01636	40.05
Two-Axial-Groove	2	0.10137	0.08068	20.41
	10	0.04276	0.03081	27.94
	20	0.02414	0.00971	59.77
Elliptical (Preload Factor = 0.5)	2	0.06794	0.03136	53.84
	10	0.04055	0.02335	42.42
Three-Lobe (Preload Factor = 0.5)	2	0.05730	0.02336	59.23
	10	0.02947	0.00868	70.54

Table 5.14 Comparative Study of Stability Parameters in Journal Bearings

(a) Threshold Speed, $\bar{\Omega}$

Type of Journal Bearing	Load, kN	Threshold Speed, $\bar{\Omega}$		% Change
		Aligned	Misaligned	
Plain	2	2.6178	2.7811	+ 6.23
	10	3.1110	3.4160	+ 9.80
	20	*	*	-
Two-Axial-Groove	2	2.3855	2.5006	+ 4.82
	10	3.2577	4.9228	+ 51.11
	20	*	*	-
Elliptical (Preload Factor = 0.5)	2	3.4818	3.6797	+ 5.68
	10	6.4166	7.0779	+ 10.31
Three-Lobe (Preload Factor = 0.5)	2	4.0834	5.2019	+ 27.39
	10	5.8491	22.6078	+ 286.52

(b) Whirl Frequency Ratio, $\bar{\nu}$

Type of Journal Bearing	Load, kN	Whirl Frequency Ratio, $\bar{\nu}$		% Change
		Aligned	Misaligned	
Plain	2	0.4836	0.4796	- 0.83
	10	0.4029	0.3855	- 4.32
	20	* *	* *	-
Two-Axial-Groove	2	0.4581	0.4506	- 1.64
	10	0.3464	0.3250	- 6.18
	20	* *	* *	-
Elliptical (Preload Factor = 0.5)	2	0.4782	0.4781	- 0.02
	10	0.2820	0.2671	- 5.32
Three-Lobe (Preload Factor = 0.5)	2	0.4553	0.4467	- 1.89
	10	0.2419	0.0921	- 61.92

* Negative critical mass - the bearing is stable under all conditions.

* * Negative value for $\bar{\nu}^2$ - absence of whirl under all conditions.

5.5.3 Bush and Journal Temperatures (T_b and T_j)

Table 5.15(a) shows the maximum temperature occurring in the bush and the axial temperature difference across the bush ends for both the aligned and misaligned ($\bar{\gamma}_x = \bar{\gamma}_z = 0.2$) bearings at different load values.

With the increase in load value, the maximum bush temperature increases both in the aligned and misaligned bearing. Due to the misalignment, there is a significant rise in maximum bush temperature in all the journal bearings studied. Higher load values further increases the bush temperature.

The axial temperature difference across the bush ends in misaligned bearings is more as compared to the aligned bearings. This difference is quite significant and it increases with the increase in load. Hence, the axial heat flow in bush cannot be neglected in misaligned journal bearings.

Table 5.15(b) shows the temperature change occurring in the values of mean journal temperature due to misalignment at different load values. It is observed that misalignment has little effect on mean journal temperature.

5.6 EFFECT OF OPERATING PARAMETERS ON STATIC AND DYNAMIC CHARACTERISTICS[2]

The most significant of all operating parameters affecting the bearing performance are found to be radial clearance, oil viscosity and rotating speed of the journal. This section presents the effect of these parameters on the performance characteristics of a plain journal bearing.

5.6.1 Static Performance Characteristics

The static performance characteristics have been obtained for a constant vertical load of 10 kN on the plain journal bearing. The operating conditions used are given in table 5.16.

5.6.1.1 Effect of Radial Clearance : The static performance characteristics of plain journal bearing for four different values of radial clearance ratio (0.001 to 0.004) and two lubricating oils (Oil 1 and Oil 2) are shown in Figs. 5.80(a) to 5.80(e). It is observed from Fig. 5.80(a) that as the radial clearance increases the eccentricity ratio also increases. This increase is quite high in lesser viscous lubricant (Oil 2).

---

[2] : Paper given at ref.[103] was published from this part of the work.

Table 5.15 Comparative Study of Temperature Variation in Different Bearings

(a) Bush

Type of Journal Bearing	Load, kN	Max. Temp. in Bush, °C		Temp. Variation, °C	Axial Temp. Diff. Across Bush Ends, °C		Temp. Variation °C
		Aligned	Misaligned		Aligned	Misaligned	
Plain	2	56.90	57.66	0.76	0.35	3.43	3.08
	10	57.59	58.78	1.19	0.78	4.37	3.59
	20	67.42	68.65	1.23	1.39	6.52	5.13
Two-Axial-Groove	2	55.50	59.30	3.8	0.74	9.34	8.6
	10	63.69	64.54	0.85	1.27	9.50	8.23
	20	69.86	72.60	2.74	1.68	11.19	9.51
Elliptical (Preload Factor = 0.5)	2	62.69	66.23	3.54	4.78	13.44	8.66
	10	65.64	67.20	1.56	4.08	18.76	14.68
Three-Lobe (Preload Factor = 0.5)	2	71.01	75.43	4.42	8.46	18.02	9.56
	10	72.28	78.33	6.05	7.76	25.61	17.85

(b) Journal

Type of Journal Bearing	Load, kN	Mean Journal Temp., °C		Temp. Variation, °C
		Aligned	Misaligned	
Plain	2	59.63	59.35	0.28
	10	54.06	54.56	0.50
	20	60.79	61.41	0.62
Two-Axial-Groove	2	61.97	63.18	1.21
	10	61.89	62.02	0.13
	20	64.13	65.20	1.07
Elliptical (Preload Factor = 0.5)	2	64.05	65.89	1.84
	10	64.17	65.62	1.45
Three-Lobe (Preload Factor = 0.5)	2	73.89	75.26	1.37
	10	70.51	71.75	1.24

Table 5.16 Operating Conditions

Journal Radius, R	= 0.05	m
External Bearing Radius, R_2	= 0.1	m
Bearing Length, L	= 0.08	m
Radial Clearance, CBAR	= 0.003	(for different N)
Speed of the Journal, N	= 3000	R.P.M. (for different CBAR)
Properties of Lubricants		
Oil 1 (SAE 30) :		
Kinematic Viscosity at 40 °C	= 0.08137	Pa.s
Kinematic Viscosity at 100 °C	= 0.00979	Pa.s
Density, ρ	= 840	Kg / m^3
Specific Heat, C_p	= 2083	J / Kg. °C
Thermal Conductivity, k_f	= 0.14	W / m °C
Oil 2 (ISO VG 32) :		
Kinematic Viscosity at 40 °C	= 0.0340	Pa.s
Kinematic Viscosity at 100 °C	= 0.0048	Pa.s
Density, ρ	= 846	Kg / m^3
Specific Heat, C_p	= 2000	J / Kg. °C
Thermal Conductivity, k_f	= 0.13	W / m °C
Bush-Housing Thermal Conductivity, k_b	= 250	W / m °C
Journal Thermal Conductivity, k_j	= 50	W / m °C
Convection Heat Transfer Coefficient, h_{ab}	= 80	W / m °C
Oil Groove Angle	= 20^0	
Inlet Lubricant Temperature, T_s	= 40	°C
Ambient Temperature, T_a	= 40	°C
Reference Temperature, T_r	= 40	°C

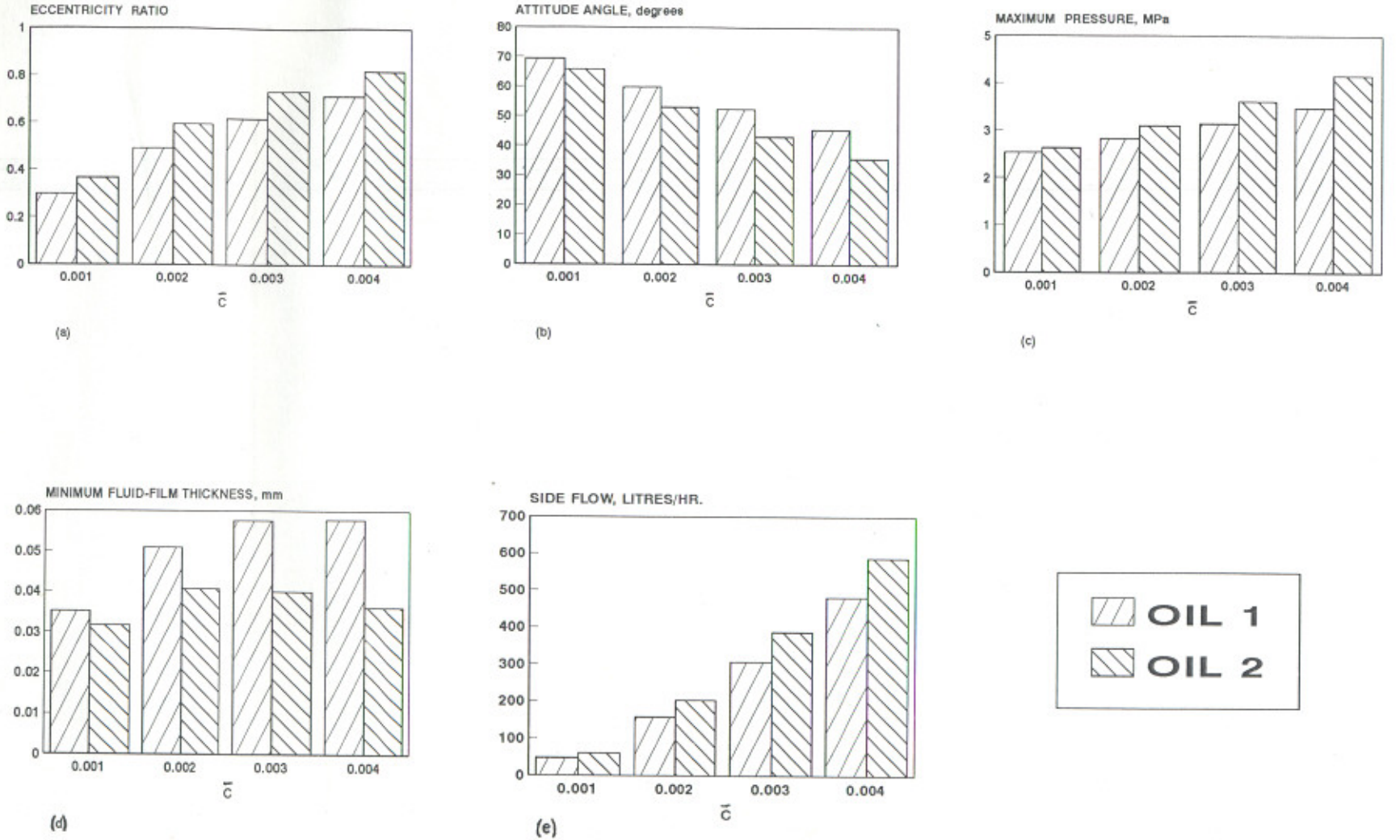

Fig. 5.80 PLAIN JOURNAL BEARING - STATIC PERFORMANCE CHARACTERISTICS WITH DIFFERENT $\bar{c}$ VALUES

Fig. 5.80(b) shows that the attitude angle decreases with the increase in radial clearance. For the same value of radial clearance, the higher the viscosity of the lubricant, higher is the attitude angle. This difference increases with the increase in radial clearance.

The maximum pressure rises as the radial clearance of the bearing increases, Fig. 5.80(c). At lower values of radial clearance, the difference between the maximum pressure for the two lubricants is not significant. At higher values of the radial clearance, however, the maximum pressure with lesser viscosity oil is significantly higher than that for the higher viscosity oil (Oil 1).

For oil 1 (more viscous), the value of minimum fluid-film thickness is found to be least when the value of radial clearance ratio($\bar{c}$) is 0.001 and it is found to increase as $\bar{c}$ is increased, Fig. 5.80(d). For oil 2 on the other hand, it is least when $\bar{c}$ = 0.001, becomes maximum with $\bar{c}$ = 0.002 and then decreases as $\bar{c}$ is further increased. Since it is always desirable to have as high a value of minimum fluid-film thickness as possible, the value for $\bar{c}$ may be selected between 0.002 and 0.003 for any type of oil.

Fig. 5.80(e) reveals that higher radial clearance leads to more side flow. However, higher is the value of viscosity, smaller is the side flow.

5.6.1.2 Effect of Journal Speed :The static performance characteristics of plain journal bearing for five values of journal speed (1000 r.p.m. to 5000 r.p.m.) and two lubricating oils are shown in Figs. 5.81(a) to 5.81(e). It is observed from Fig. 5.81(a) that as the journal speed increases the eccentricity ratio decreases. The reduction in eccentricity ratio is more in more viscous lubricant (Oil 1).

Fig. 5.81(b) shows that the attitude angle increases with the increase in journal speed. For the same value of journal speed, the attitude angle is higher when higher viscosity oil is used.

The maximum pressure decreases as the journal speed of the bearing increases, Fig. 5.81(c). Less viscous lubricant gives higher maximum pressure values.

The minimum fluid-film thickness increases as the journal speed increases, Fig. 5.81(d). For the same value of journal speed, the more viscous lubricant yields higher value of minimum fluid-film thickness.

Fig. 5.81(e) reveals that higher journal speed leads to more side flow. The side flow is, however, reduced with increase in viscosity.

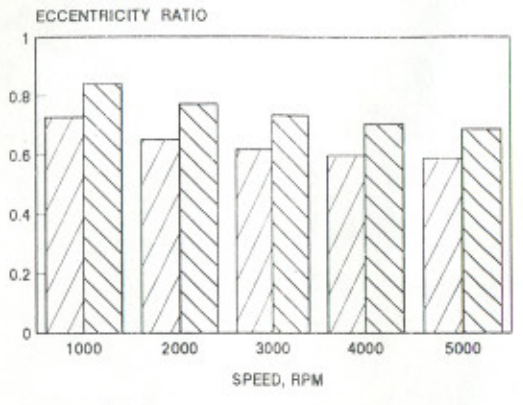

(a)

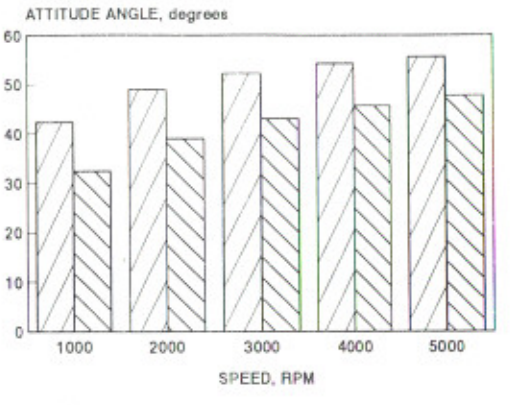

(b)

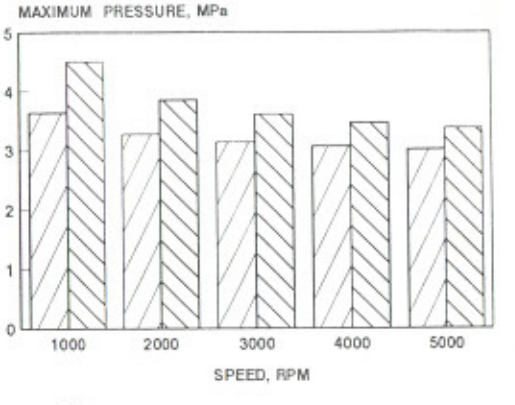

(c)

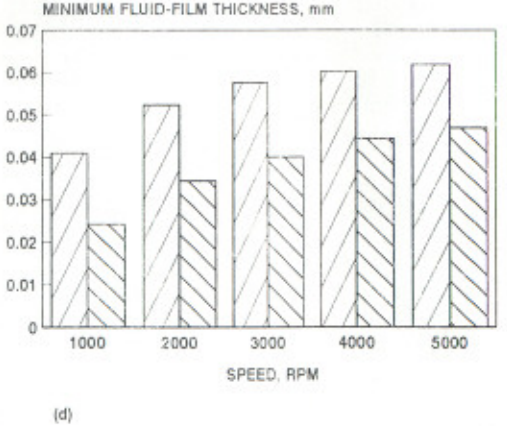

(d)

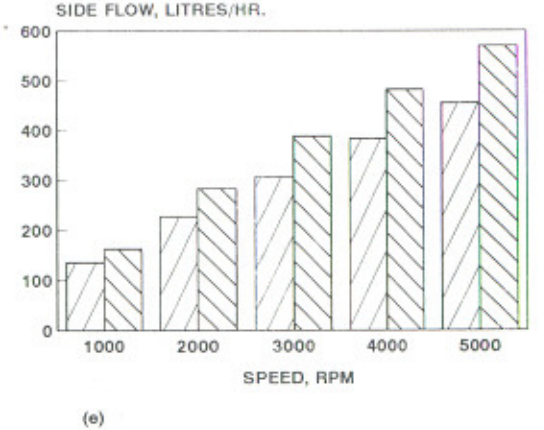

(e)

Fig. 5.81 PLAIN JOURNAL BEARING - STATIC PERFORMANCE CHARACTERISTICS WITH DIFFERENT JOURNAL SPEEDS

5.6.2 Dynamic Performance Characteristics

5.6.2.1 Stability Parameters : The stability parameters (instability threshold speed and whirl frequency ratio) of plain journal bearing with different values of radial clearance ($\bar{c}$) and two lubricating oils are shown in Figs. 5.82(a) - 5.82(b) and with different values of journal speed and two lubricating oils in Figs. 5.83(a) - 5.83(b).

Fig. 5.82(a) shows that stability improves on either side of a particular value of radial clearance for both oils. Also, whereas the instability threshold speed with both lubricating oils is practically the same at $\bar{c} = 0.001$, its value corresponding to lesser viscosity oil becomes infinity for $\bar{c} = 0.004$ while for the other oil it is much lower. Fig. 5.82(b) indicates reduction of whirl with the increase in the radial clearance for both oils.

Fig. 5.83(a) shows that the stability of the bearing system deteriorates as the speed is increased. Likewise, tendency to whirl also increases with the increase in speed.

5.6.3 Thermal Analysis

Figs. 5.84(a) - 5.84(b) shows the variation of bush and journal temperatures with radial clearance, respectively. Both these figures reveal that as the radial clearance increases, bush and journal temperatures are reduced. The same trend is exhibited by both oils used. The lower viscosity oil, however, results in marginally lower temperatures.

Figs. 5.85(a) - 5.85(b) shows the variation of bush and journal temperatures with speed, respectively. These figures show that the bush and the journal, both, run hotter as the speed of the journal is increased. Similar trend is obtained for the two oils. The lower viscosity oil, however, results in marginally lower temperatures.

Hence, the radial clearance ratio ($\bar{c}$) between 0.002 and 0.003 may be selected from the point of view of minimum fluid-film thickness. The stability of the journal bearing improves on either side of a particular value of radial clearance and the whirl frequency is reduced with the increase in the radial clearance. In general, low viscosity oil is good from stability and operating temperatures point of view but from the minimum fluid-film thickness criteria, a higher viscosity oil is desirable.

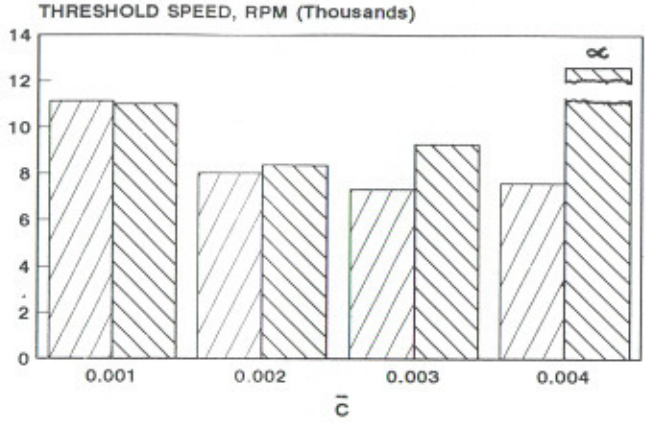

(a)

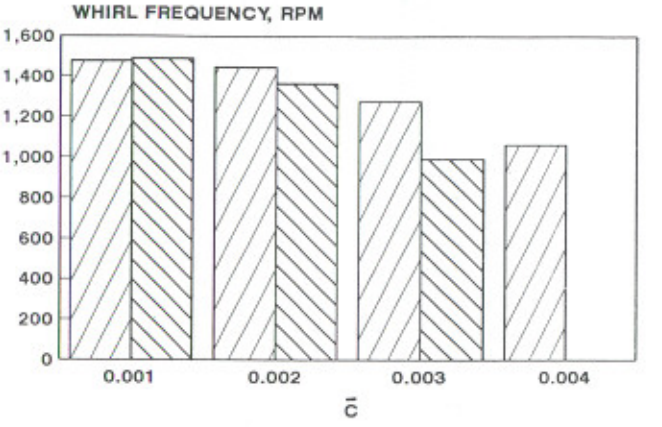

(b)

Fig. 5.82 PLAIN JOURNAL BEARING - STABILITY PARAMETERS WITH DIFFERENT $\bar{c}$ VALUES

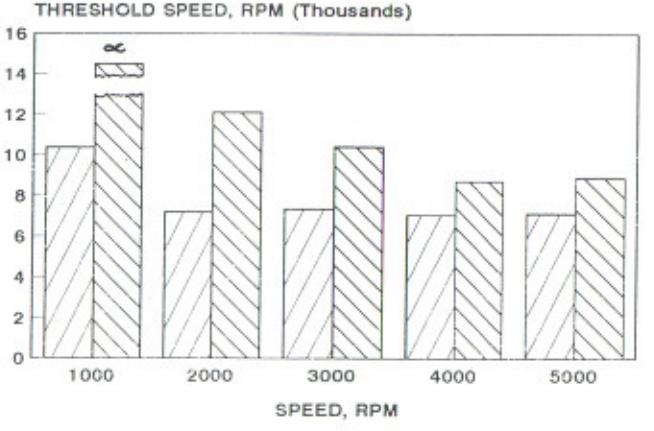

(a)

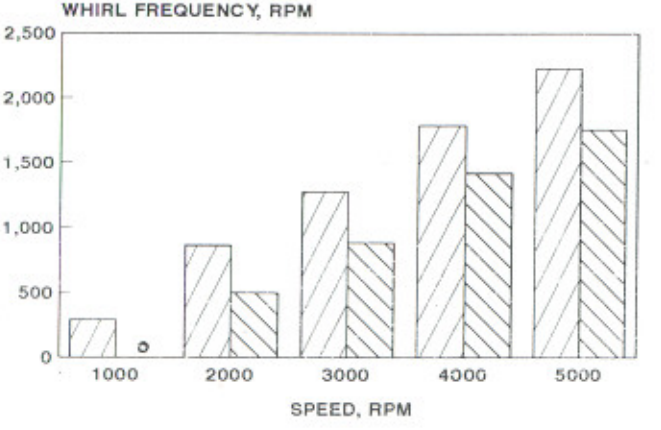

(b)

Fig. 5.83 PLAIN JOURNAL BEARING - STABILITY PARAMETERS WITH DIFFERENT JOURNAL SPEEDS

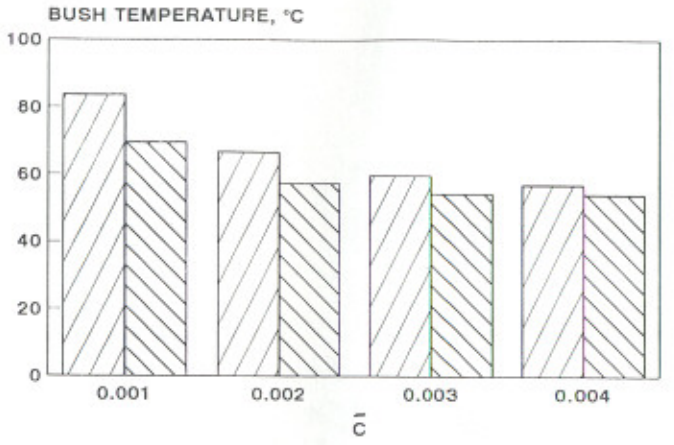

(a)

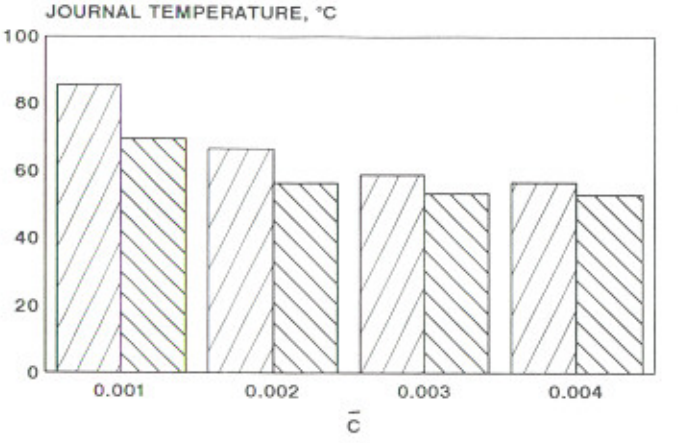

(b)

Fig. 5.84 PLAIN JOURNAL BEARING - VARIATION OF TEMPERATURES WITH DIFFERENT $\bar{c}$ VALUES

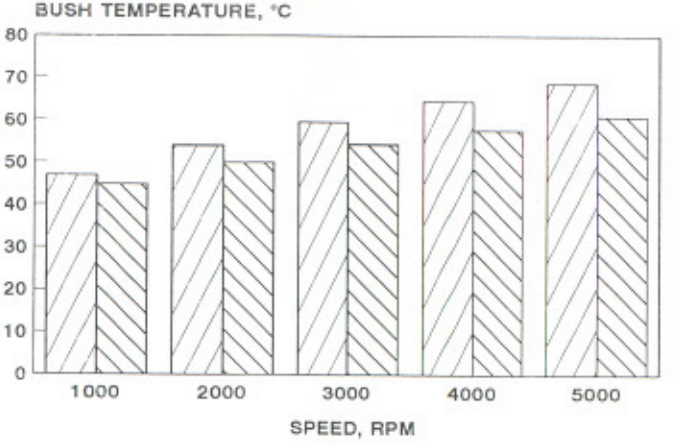

(a)

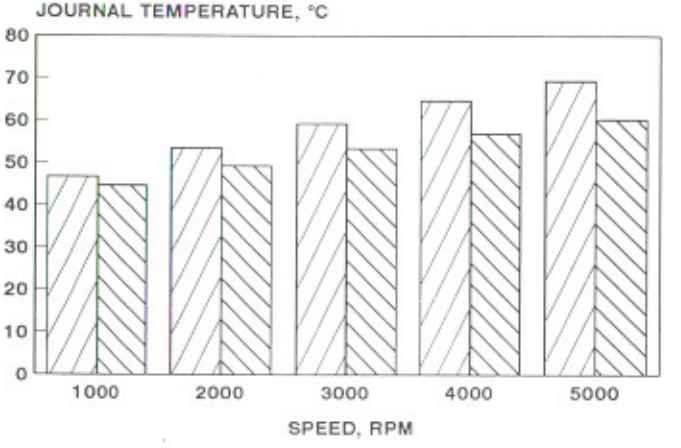

(b)

Fig. 5.85 PLAIN JOURNAL BEARING - VARIATION OF TEMPERATURES WITH DIFFERENT JOURNAL SPEEDS

CHAPTER - VI

CONCLUSIONS AND CLOSURE

6.1 CONCLUSIONS

Based on the results and discussion presented in the preceding chapter, the following conclusions can be drawn for the journal bearing configurations studied :

1. The boundary conditions defined as BC1 in this work are more appropriate.
2. Heat transfer from the oil in supply groove to solids and from solid to oil must be considered for more accurate simulation of the actual conditions.
3. In general, theory predicts less bush temperature than the experimental values especially when the thermohydrodynamic properties of bush / journal material are not exactly known.
4. The mid-plane eccentricity ratio decreases with the increase in misalignment at all load values for all the bearing systems.
5. The attitude angle decreases with the increase in misalignment for all the bearing systems. The effect is more pronounced at higher values of misalignment ratio.
6. In general, for all types of bearings, the maximum fluid-film pressure increases with the increase in misalignment.
7. For all the journal bearings, the minimum fluid-film thickness decreases as the misalignment is increased for all values of load. This may eventually lead to failure of the journal bearing systems due to metal-to-metal contact.
8. At light loads, the effect of increasing misalignment leads to increased side flow in all except elliptical bearings, whereas at higher load values, the trend is reversed. In elliptical journal bearing, increased misalignment leads to increased side flow at all load values.
9. An increase in the misalignment leads to higher mean journal temperature in all the bearing systems.

10. The maximum bush temperature increases with the increase in load for all bearing systems(for aligned as well as misaligned bearings). The maximum bush temperature further rises due to misalignment in all the journal bearings studied.
11. The misalignment significantly affects the magnitude of stiffness and damping coefficients.
12. The misalignment in bearings significantly improves the stability margin defined by the threshold speed.
13. In all bearing geometries operating with misalignment, bush temperature varies considerably along the axial length particularly in non-circular bearings and this variation further increases with the increase in load. Hence, a two-dimensional thermal analysis (ignoring axial variation of temperature) is not sufficient for the study of misaligned bearings. A complete three-dimensional analysis is suggested for this purpose.
14. The isotherms indicate that heat transfer takes place not only in radial direction in the bush but also in the circumferential and axial directions (Therefore, a three-dimensional analysis must be conducted).
15. The journal temperature varies significantly along the axial length of the journal and the temperatures at the two ends of the journal are different in the case of misaligned bearings. Hence, the journal cannot be assumed as a lumped thermal element in the analysis of misaligned bearings.
16. The transient motion trajectories of journal-centre show that all bearings are relatively more stable when operating under misalignment and the relative stability is even better when the operating load is higher.
17. The radial clearance ratio between 0.002 and 0.003 is recommended from the point of view of minimum fluid-film thickness.
18. In general, low viscosity oil is good from stability and operating temperatures point of view but from the minimum fluid-film thickness criteria, a higher viscosity oil is desirable.

6.2 CLOSURE

The THD investigations for misaligned journal bearings presented in this thesis indicates that bearing misalignment has an appreciable effect on static and dynamic

performance characteristics of plain, two-axial-groove, elliptical and three-lobe journal bearings.

Thermal / Elastic distortions of bush and journal may be vital in some cases for a more accurate modelling of journal bearing problem. This aspect has not been considered in the present work. However, there is a need for further work in this regard.

Further, only laminar flow conditions have been assumed in the present work. Since thermal effects are expected to be more pronounced with turbulent flow conditions, future investigations should include superlaminar flow conditions also.

The present work deals with the Newtonian lubricants. The nonlinear behaviour of non-Newtonian lubricants combined with the TEHD and misalignment effects would present an even more complex problem which could be a topic for future research.

There are many problems which are not fully understood and explained while accounting for the THD analysis; for example, the back flow of oil, mixing in oil grooves, dynamic response of the journal bearing system during starting and stopping with misalignment and non-linear behaviour of the journal bearing system during disturbance, to name a few. It is, therefore, expected that future investigations will be addressed more comprehensively at these problems.

****

REFERENCES

1. Petrov, N.P., "Friction in Machines and Effect of the Lubrication", Inzhenernii Zhurnal, St. Petersburg, Vol. 1, pp. 71-140; Vol. 2, pp. 227-279; Vol. 3, pp. 377-436; Vol. 4, pp. 435-464 (in Russian) (1883).

2. Tower, B., "First Report on Friction Experiments", Proc. Instn. Mech. Engg., Vol. 34, pp. 632-666 (1883).

3. Tower, B., "Second Report on Friction Experiments", Proc. Instn. Mech. Engg., Vol. 36, pp. 58-70 (1885).

4. Reynolds, O., "On the Theory at Lubrication and its Applications to Mr. Beauchamp Tower's Experiments including an Experimental Determination of the Viscosity of Olive Oil", Phil. Trans., Vol. 177(i), pp. 157-334 (1886).

5. Sommerfeld, A., "Zur Hydrodynamischen Theorie der Schmiermittelreibung", Z. Math. U. Phys., Vol. 150, p. 97 (1904).

6. Rayleigh, Lord, "Notes on The Theory of Lubrication", Phil. Magz., Vol. 35(1) (1918).

7. OcVirk, F. W., "Short Bearing Approximation for Full Journal Bearings", NACATN 2808 (1952).

8. Raimondi, A.A. and Boyd, J., "A Solution for the Finite Journal Bearings and its Applications to Analysis and Design, Parts I, II and III", ASLE Trans., Vol. 1, pp. 159-209 (1958).

9. Cole, J.A. and Hughes, C.J., "An Experimental Investigation of Temperature Effects in Journal Bearings", Proc. Instn. Mech. Engrs., Vol. 70, p.147 (1959).

10. Ng, C.W., and Pan, C.H.T., "A Linearized Lubrication Theory", Trans. ASME, Jr. of Lubr. Techn., Vol. 87, p. 675 (1965).

11. Constantinescu, V.N., "Theory of Turbulent Lubrication (in Romanian)", Publishing House of the Romanian Academy, Bucarest (1965), English translation (1968) : U.S. Atomic Energy Commission, Division of Technical Information, AEC-TR-6959, Washington, D.C.

12. Elrod, H.G. and Ng, C.W., "A Theory of Turbulent Fluid Film and its Application to Bearings", ASME Trans., Jr. Lubr. Tech., Series F, 89, 3, pp. 346-362 (1967).

13. Taylor, C.M. and Dowson, D., "Turbulent Lubrication Theory Application to Design", Trans. ASME, Jr. Lubr. Tech., Vol. 96, pp.36-47 (1974).

14. Singh, D.V., Sinhasan, R. and Kumar, A., "A Variational Solution of Two-Lobe Bearings", Mechanical and Machine Theory, Jr. IETOMM., Vol.12, p. 323 (1977).

15. Lund, J.W. and Thomsen, K.K., "A Calculation Method and Data for the Dynamic Coefficients of Oil Lubricated Journal Bearings, Topics in Fluid Film Bearing and Rotor Bearing System Design and Optimization", ASME Design Engg. Conf. Chicago, IL, pp. 1-29, ASME Publication 100118, New York (1978).

16. Malik, M., "A Comparative Study of Some Two-Lobed Journal Bearing Configurations", ASLE Trans., Vol. 26(1), pp. 118-124 (1981).

17. Flack, R.D. and Lanes R.F., "Effects of Three-Lobe Bearing Geometries on Rigid Rotor Stability", ASLE Trans., Vol. 25(2), pp. 221-228 (1982).

18. Lanes, R.F., Flack, R.D. and Lewis, D.W., "Experiments on the Stability and Response of a Flexible Rotor in Three Types of Journal bearings", ASLE Trans., Vol. 25(3), pp. 289-298 (1982).

19. Lanes, R.F. and Flack, R. D., "Effects of Three-Lobe Bearing Geometries on the Flexible Rotor Stability", ASLE Trans., Vol. 25 (3), pp. 377-385 (1982).

20. Chandrawat, H.N. and Sinhasan, R, "A Comparison Between Two Numerical Techniques for Hydrodynamic Journal Bearing Problems", Wear, Vol.127 pp. 78-87 (1987).

21. Choy, F.K., Braun, M.J., and Hu, Y., "Nonlinear Transient and Frequency Response Analysis of a Hydrodynamic Journal Bearing", Jr.of Trib., Trans. ASME, Vol. 114, pp. 448-454 (1992).

22. Kostrzewsky, G.J, Taylor, D.V., and Flack, R.D.; "Experimental Determination of the Dynamic Characteristics of a Two-Axial-Groove Journal Bearing", STLE Trans., Vol. 37(3), pp. 534-542 (1994).

23. Taylor, D.V., Kostrzewsky, G.J., Flack, R.D., and Barrett, L.E., "Measured Performance of a Highly Preloaded Three-Lobe Journal Bearing - Part I : Static Characteristics", STLE Trans., Vol. 38(3), pp. 507-516 (1995).

24. Taylor, D.V., Kostrzewsky, G.J., Barrett, L.E., and Flack, R.D., "Measured Performance of a Highly Preloaded Three-Lobe Journal Bearing - Part II : Dynamic Characteristics", STLE Trans., Vol. 38(3), pp. 707-713 (1995).

25. Elrod, H.G., and Vijayraghavan, D., "A Stability Analysis for Liquid-Lubricated Bearings Incorporating the Effects of Cavity Flow : Part II - Journal Bearing with Central Groove", Trans. ASME, Jr.of Trib., Vol. 117, pp. 365-367 (1995).

26. McKee, S.A. and McKee, T.R., "Pressure Distribution in Oil Films of Journal Bearings", Trans. ASME, Vol. 54, pp. 149 - 165 (1932).

27. Cowlin, F.J., "The Lubrication of Steam-Turbine Driven Electric Generators", Proc. Instn. Mech. Engrs., Vol. 143, pp. 83 -100 (1940).

28. Piggott, R.J.S., "Bearing and Lubrication Bearing Troubles Traceable to Design Can Be Avoided By Engineering Study", Mech. Eng. 64, pp. 259-269 (1942).

29. Buske, A. and Rolli, W., "Measurement of Oil-Film Pressure in Journal Bearings Under Constant and Variable Loads", NACA Tech. Mem. 1200 (1949).

30. Walther, A. Sessenfeld, H., "Pressure Distribution and Load in a 350 Bearing with an Inclined Shaft. Outline of Procedure with an Explanatory Example", Dept. of Scientific and Indl. Research, Sponsored Research(Germany), Report No.13, 1.P.M. Report No. 9 (1950).

31. Dubois, G.B., Mabie, H.H. and Ocvirk, F.W., "Experimental Investigation of Oil Film Pressure Distribution for Misaligned Plain Bearings", N.A.C.A. Tech. No. 2507 (1951).

32. Khrisanova, L.B. , "Analytical and Experimental Investigation of the Pressure in the Oil Film of a Journal. Bearing with Axes of Journal and Bushing Skewed", Frict. Wear Mach., Vol. 13, pp. 192 - 208 (1959).

33. Smalley, A.J. and McCallion, H., "The Effect of Journal Misalignment on the Performance of a Journal Bearing Under Steady Running Conditions", Proc. Instn. Mech. Engrs., Vol. 181, pt. 3B, p. 45 (1966-67).

34. Stokley, J.R. and Donaldson, P.P., "Misalignment Effects in 180° Partial Journal Bearings", ASLE Trans., Vol.12, pp. 216-226 (1969).

35. Asanabe, S., Akahosi, M., and Asai, R., "Theoretical and Experimental Investigation on Misaligned Journal Bearing Performance", Trib. Conv. 1971, Instn. Mech. Engrs., Vol. C36, pp. 1-8 (1971).

36. Bannister, R.H., "A Theoretical and Experimental Investigation Illustrating the Influence of Non-Linearity and Misalignment on the Eight Oil Film Force Coefficients", Proc. Instn. Mech. Engrs., Vol. C219 / 76, pp. 271-278 (1976).

37. Pinkus, O, and Bupara, S.S., "Analysis of Misaligned Grooved Journal Bearings", Trans. ASME, Jr. of Lubr. Tech., Vol. 101, pp. 503-509 (1979).

38. Pafelias, T.A. and Broniarek, C.A., "Bearing-System Dynamic with General Misalignment in the Journal Bearings", ASLE Trans., Vol. 29(4), pp. 441- 450 (1981).

39. Reason, B.R. and Siew, A.H., "A Numerical Solution for the Design and Performance Evaluation of Journal Bearings with Misalignment", Proc. Instn. Mech. Engrs., Vol. C9, pp.75-85 (1982).

40. Ikeuchi, K., Katsuse, S., Hamamura, K., and Mori, H., "Effects of Misalignment in Full Journal Bearing with Circumferential Oil Groove", Proc. of the JSLE Intern. Trib. Conf., Tokyo, pp. 67-72 (1985).

41. Buckholz, R.H., and Lin, J.F., "The Effect of Journal Bearing Misalignment on Load and Cavitation for Non-Newtonian Lubricants", Trans. ASME, Jr. of Trib., Vol. 108, pp. 645-654 (1986).

42. Jakeman, R.W., "Performance and Oil Film Dynamic Coefficients of a Misaligned Sterntube Bearing", ASLE Trans. ,Vol. 29(4), pp. 441-450 (1986).

43. Jakeman, R.W., "Non-linear Oil Film Response Model for the Dynamically Misaligned Sterntube Bearings", Trib. Int., Vol. 22(1), pp. 3-10 (1989).

44. Abdel-Latif, L.A. and Mokhtar, M.O.A., "Misalignment Effects on Hydrodynamically Lubricated Journal Bearings with Rough Surfaces", Wear, Vol. 128, pp. 225-237 (1988).

45. Vijayaraghavan, D. and Keith, T.G., Jr., "Effect of Cavitation on the Performance of a Grooved Misaligned Journal Bearing", Wear, Vol. 134, pp. 377-397 (1989).

46. Vijayaraghavan, D. and Keith, T.G., Jr., "Analysis of a Finite Grooved Misaligned ournal Bearing Considering Cavitation and Starvation Effects", Trans. ASME, Jr.of Trib., Vol. 112, pp. 60-67 (1990).

47. Choy, F.K., Braun, M.J., and Hu, Y., "Analytical and Numerical Study of a Misaligned Cavitating Hydrodynamic Cryogenic Journal Bearing", Trib. Int.,Vol. 25(1), pp.3-15 (1992).

48. Choy, F.K., Braun, M.J., and Hu, Y., "Nonlinear Study of a Misaligned Hydrodynamic Journal Bearing", STLE Trans., Vol. 36(3), pp. 421-431 (1993).

49. Sharda, H.B., Chandrawat, H.N., and Bahl, R.C., " EHD Analysis of a Misaligned Journal Bearing", Int. J. of Mech. Sci., Vol. 35(5), pp. 415-423 (1993).

50. Yu, Q., and Keith, T.G., " Prediction of Cavitation in Journal Bearings Using a Boundary Element Method", Trans. ASME, Jr. of Trib., Vol. 117, pp. 411- 421 (1995).

51. Qiu, Z.L., and Tieu, A.K., "Misalignment Effect on the Static and Dynamic Characteristics of Hydrodynamic Journal Bearings", Trans. ASME, Jr.of Trib., Vol. 117, pp. 717-723 (1995).

52. Kingsbury, A., "Heat Effects in Lubricating Films", Mech. Engg., Vol. 55, pp. 685 - 688 (1933).

53. Musket, M. and Morgan, F., "Temperature Behaviour of Journal Bearing System", J. Applied Physics, Vol. 14, pp. 214 (1941).

54. Hagg, A., "Heat Effects in Lubricating Films", Trans. ASME, 66, A72-A76 (1944).

55. Clayton, D. and Wilkie, M., "Temperature Distribution in the Bush of a Journal Bearings", Eng., Vol. 166, p. 49 (1948).

56. Hamilton, J., Burr. A. and Ocvirk, F., "Experimental Investigation of a Method of Predicting Heat Dissipation and Temperature of Plain Journal Bearings", Cornell University Programme Report No. 14, NACA Inthaca. NY (1955).

57. Cole, J. , "An Experimental Investigation of Temperature Effects in Journal Bearings", Proc. Conv. on Lubr. and Wear, Instn. Mech. Engrs. London, Vol. 111, pp. 111-117 (1957).

58. Burr, A., "The Effect of Shaft Rotation on Bearing Temperatures", ASLE Trans., pp. 235 -241 (1958).

59. Zienkiewicz, O., "Temperature Distribution Within Lubricating Film Between Parallel Bearing Surfaces and its Effects on the Pressure Development", Proc. Conf. Lubr. Wear, Instn. Mech. Engrs., Vol. 28, pp. 135 -141 (1958).

60. Tipei, N. and Nica, A., "Investigation on the Operating Conditions of Journal Bearings : I. Influence of Viscosity Variation", Revue de Mecanique Appliquee, Vol. 4, p. 4 (1959).

61. Dowson, D., Hudson, J. Hunter, B. and March, C., "An Experimental Investigation of the Thermal Equilibrium of Steadily Loaded Journal Bearing", Proc. Instn. Mech. Engrs. Vol. 101, Paper -3B, pp. 70 - 80 (1966-67).

62. Nica, A., "Thermal Behavior and Friction in Journal Bearing", ASME Trans., Jr. Lubr. Tech., pp. 373-380 (1970).

63. McCllion, H., Yousif, F. and Lloyd, T., "The Analysis of Thermal Effects in a Full Journal Bearing ", ASME Trans,. Jr. Lubr. Tech., Vol. 92, pp. 578 - 587 (1970).

64. Majumdar, B. and Saha, A., "Temperature Distribution in Oil Journal Bearings", Wear, Vol. 28, pp. 259 - 266 (1974).

65. Gardner, W. and Ulshmid J., "Turbulence Effects in Two Journal Bearing Applications", ASME Trans., Jr. Lubr. Tech. , Vol. 96, pp. 15-21 (1974).

66. Safar, Z., and Szeri, A., "Thermohydrodynamic Lubrication in Laminar and Turbulent Regimes", Trans. ASME, Jr. Lubr. Tech., Vol. 96, pp. 48-56 (1974).

67. Majumdar, B., "The Thermohydrodynamic Solution of Journal Bearings", Wear, Vol. 31, pp. 287-294 (1975).

68. Sugnami, T. and Szeri, A., "A Thermohydrodynamic Analysis of Journal Bearings", Trans. ASME, Jr. Lubr. Tech., Vol. 101, pp. 21-27 (1979).

69. Pinkus, O. and Bupara S.S., "Adiabatic Solutions for Finite Journal Bearings", Trans. ASME, Jr. Lubr. Tech., Vol. 101, pp. 492-496 (1979).

70. Boncompain, R., and Frene, J., "Thermodynamic Analysis of a Finite Journal Bearings Static and Dynamic Characteristics", Proc. 6th Leeds-Lyon Symp. on Thermal Effects in Tribology, Instn. Mech. Engrs., London, pp. 33-34 (1979).

71. Ferron, J., Frene, J. and Boncompain R., "A Study of Thermohydrodynamic Performance of a Plain Journal Bearings, Comparison between Theory and Experiments", Trans. ASME, Jr. Lubr. Tech., Vol. 105, pp. 422-428 (1983).

72. Mitsui, J. and Yamda, T., "A Study of the Lubricating Film Characteristics of Journal Bearings (Part I : A Thermohydrodynamic Analysis with Particular Reference to the Viscosity Variation Within Lubrication Film)", Bull. JSME, Vol. 22, pp. 492-496 (1979).

73. Tonnesen, J. and Hansen, P., "Some Experiments on the Steady-State Characteristics of a cylindrical Fluid Film Bearing Considering Thermal Effects", Trans. ASME, Jr. Lubr. Tech., Vol. 103, pp. 107-114 (1981).

74. Knight, J.D. and Barrett, L.E., "An Approximate Solution Technique for Multilobe Journal Bearings including Thermal Effects with Comparison to Experiment", ASLE Trans., Vol. 26(4), pp. 501- 508 (1983).

75. Knight, J.D. and Barrett, L.E., " Analysis of Axially Grooved Journal Bearings with Heat Transfer Effects", ASLE Trans., Vol. 30 (3), pp. 501-508 (1987).

76. Lund, J.W. and Hansen, P.K.., "An Approximate Analysis of the Temperature Conditions in a Journal Bearing, Part I : Theory", Trans. ASME, Jr. of Trib., Vol. 106, pp. 228-236 (1984).

77. Lund, J.W. and Tonnesen, J., "An Approximate Analysis of the Temperature Conditions in a Journal Bearing, Part II: Application", Trans. ASME, Jr. of Trib., Vol. 106, pp. 237-245 (1984).

78. Gethin, D.T. and Medwell, J. O., "An Experimental Investigation into the Thermohydrodynamic Behavior of a High Speed Cylindrical Bore Journal Bearing", Trans. ASME, Jr. of Trib., Vol. 107, pp. 538-543 (1985).

79. Gethin, D.T., " An Investigation into Plain Journal bearing Behavior Including Thermo-Elastic Deformation of the Bush", Proc. Instn. Mech. Engrs., Vol.199, No.C3, pp.215-223 (1985).

80. Boncompain, R., Fillon, M. and Frene, J., "Analysis of Thermal Effects in Hydrodynamic Bearings", Trans. ASME, Jr. of Trib., Vol. 108, pp. 219 - 224 (1986).

81. Khonsari, M.M. and Beaman, J.J., "Thermohydrodynamic Analysis of Laminar Incompressible Journal Bearings", ASLE Trans., Vol. 29 (2), pp. 141-150 (1986).

82. Heshmat, H. and Pinkus O., "Mixing Inlet Temperatures in Hydrodynamic Bearings", Trans. ASME, Jr. of Trib., Vol. 108, pp. 231-248 (1986).

83. Khonsari, M.M., " A Review of Thermal Effects in Hydrodynamic Bearings Part I : Slider and Thrust Bearings", ASLE Trans., Vol. 10 (1), pp. 19-25 (1987).

84. Khonsari, M.M., " A Review of Thermal Effects in Hydrodynamic Bearings, Part II : Journal Bearings", ASLE Trans., Vol. 30(1), pp. 26 - 33 (1987).

85. Braun, M.J., Wheeler III, R.L. and Hendricks, R.C., "Thermal Shaft Effects on Load-Carrying Capacity of a Fully Coupled, Variable-Properties Cryogenic Journal Bearing", ASLE Trans., Vol. 30(3), pp. 282-292 (1987).

86. Singh, D.V., Sinhasan, R. and Nair, K.P., " Elastothermohydrodynamic Effects in Elliptical Bearings", Trib. Int., Vol. 22(1) , pp. 43-49 (1989).

87. Sinhasan, R. and Chandrawat, H.N., "Analysis of a Two-Axial-Groove Journal Bearing Including Thermoelastohydrodynamic Effects", Trib. Int., Vol. 22(5), pp. 347-353 (1989).

88. Paranjpe, R.S. and Han, T., "A Study of the Thermohydrodynamic Performance of Steadily Loaded Journal Bearings", Jr.of Trib.,Trans. ASME, Vol.112, pp. 557-566 (1990).

89. Gethin, D.T., and El-Deihi, M.K.I., "Thermal Model for a Twin Axial Groove Bearing Subjected to a Varying Loading Direction and its Verification", Trib. Int., Vol. 24(3), pp. 131-136 (1991).

90. Tripp, H.A. and Melodick, T.E., "Journal Measurements Taken with Non-Newtonian Lubricants", STLE Trans., Vol. 35(1), pp. 149-155 (1992).

91. Sheeja, D., and Prabhu, B.S., "Thermal and Non-Newtonian Effects on the Steady State and Dynamic Characteristics of Hydrodynamic Journal Bearings - Theory and Experiments", STLE Trans., Vol. 35(3), pp. 441-446 (1992).

92. Fitzgerald, M.K. and Neal, P.B. "Temperature Distributions and Heat Transfer in Journal Bearings", Trans. ASME, Jr. of Trib., Vol. 114, pp. 122 -130 (1992).

93. Paranjpe, R.S. and Han, T., "A Finite Volume Analysis of the Thermohydrodynamic Performance of Finite Journal Bearings", STLE Trans.,Vol.37(4),pp. 679-690 (1994).

94. Paranjpe, R.S. and Han, T., "A Transient Thermohydrodynamic Analysis Including Mass Conserving Cavitation for Dynamically Loaded Journal Bearings", Trans. ASME, Jr.of Trib., Vol.117, pp. 369-378 (1995).

95. Gethin, D.T., "Modeling the Thermohydrodynamic Behaviour of High Speed Journal Bearings", Trib. Int., Vol. 29(7), pp. 579-596 (1996).

96. Braun, M.J., Mullen, R.L. and Hendricks, R.C., "An Analysis of Temperature Effect in a Finite Journal Bearing with Spatial Tilt and Viscous Dissipation", ASLE Trans., Vol. 27(4), pp. 405-412 (1984).

97. Safar, Z.S., Mohtar, M.O.A. and Peeken, H.J., "Thermal Characteristics of Misaligned Finite Journal Bearings", Trib. Int., Vol. 18(1), pp. 13-16 (1985).

98. Jang, Jin-Yuh, Chang and Chong-Ching, " Adiabatic Solutions for a Misaligned Journal Bearing with Non-Newtonian Lubricant", Trib. Int., Vol. 20 (5), pp. 267-275 (1987).

99. Chun, S.M. and Lalas, D.P., "Parametric Study of Inlet Oil Temperature and Pressure for a Half-circumferential Grooved Journal Bearing", STLE Trans., Vol. 35(2), pp. 213-224 (1992).

100. Huebner, K.H., " The Finite Element Method for Engineers, Wiley, New York (1995).

101. Banwait, S.S., Chandrawat, H.N., and Adithan, M., "Misalignment in Hydrodynamic Journal Bearings : The Problems", Proc. XI National Convention of Mechanical Engineers, 25-26 November, Bhopal (India), pp. T19-T24 (1995).

*102. Banwait, S.S., and Chandrawat, H.N., "Study of Thermal Boundary Conditions for a Plain Journal Bearing ", Trib. International, *Accepted for publication*, (1998).

*103. Banwait, S.S., Chandrawat, H.N., and Adithan, M., "Effect of Operating Parameters on Static and Dynamic Characterisitcs of Journal Bearing under Thermohydrodynamic Conditions", Proc. 8th International Conf. in Trib., NORDTRIB'98, 8-10 June, Ebeltoft, (Denmark), Vol. II, pp. 523 - 530 (1998).

*104. Banwait, S.S., Chandrawat, H.N., and Adithan, M., "Thermohydrodynamic Analysis of Misaligned Plain Journal Bearing", Proc. First Asia International Conf. on Trib., ASIATRIB'98, 12-15 October, Beijing, (China), *Accepted for presentation* (1998).

---

* Published / Presented from the present work.

APPENDIX - I

$\bar{B}_{xx}$ $\bar{B}_{xz}$ $\bar{B}_{zx}$ $\bar{B}_{zz}$	$(B_{xx}, B_{xz}, B_{zx}, B_{zz}) / 50570.37$
$\bar{B}_{x\gamma_x}$ $\bar{B}_{x\gamma_z}$ $\bar{B}_{z\gamma_x}$ $\bar{B}_{z\gamma_z}$	$(B_{x\gamma_x}, B_{x\gamma_z}, B_{z\gamma_x}, B_{z\gamma_z}) / 2528.5185$
$\bar{B}_{\gamma_x\gamma_x}$, $\bar{B}_{\gamma_x\gamma_z}$ $\bar{B}_{\gamma_z\gamma_x}$, $\bar{B}_{\gamma_z\gamma_z}$	$(B_{\gamma_x\gamma_x}, B_{\gamma_x\gamma_z}, B_{\gamma_z\gamma_x}, B_{\gamma_z\gamma_z}) / 126.4259$
$\bar{B}_{\gamma_x x}$, $\bar{B}_{\gamma_x z}$ $\bar{B}_{\gamma_z x}$, $\bar{B}_{\gamma_z z}$	$(B_{\gamma_x x}, B_{\gamma_x z}, B_{\gamma_z x}, B_{\gamma_z z}) / 2528.5185$
$\bar{c}$	$c / 0.05$
$\bar{\nu}$	$\nu / 366.5191$
$\bar{h}$	$h / 0.00015$
$\bar{M}_c$	$M_c / 137.9747$
$\bar{M}$, $\bar{M}_x$, $\bar{M}_z$	$(M, M_x, M_z) / 139.0126$
$\bar{p}$	$p / 1112100.40$
$\bar{Q}_s$	$Q_s / 3.4361 * 10^{-7}$
$\bar{r}$	$r / 0.05$
$\bar{R}_1$, $\bar{R}_2$	$R_1, R_2 / 0.05$
$\bar{S}_{xx}$, $\bar{S}_{xz}$ $\bar{S}_{zx}$, $\bar{S}_{zz}$	$(S_{xx}, S_{xz}, S_{zx}, S_{zz}) / 18535006.0$
$\bar{S}_{x\gamma_x}$, $\bar{S}_{x\gamma_z}$ $\bar{S}_{z\gamma_x}$, $\bar{S}_{z\gamma_z}$	$(S_{x\gamma_x}, S_{x\gamma_z}, S_{z\gamma_x}, S_{z\gamma_z}) / 926750.32$
$\bar{S}_{\gamma_x\gamma_x}$, $\bar{S}_{\gamma_x\gamma_z}$ $\bar{S}_{\gamma_z\gamma_x}$, $\bar{S}_{\gamma_z\gamma_z}$	$(S_{\gamma_x\gamma_x}, S_{\gamma_x\gamma_z}, S_{\gamma_z\gamma_x}, S_{\gamma_z\gamma_z}) / 46337.507$
$\bar{S}_{\gamma_x x}$, $\bar{S}_{\gamma_x z}$ $\bar{S}_{\gamma_z x}$, $\bar{S}_{\gamma_z z}$	$(S_{\gamma_x x}, S_{\gamma_x z}, S_{\gamma_z x}, S_{\gamma_z z}) / 926750.32$

$\bar{t}$	t * 366.5191
$\bar{T}_a$, $\bar{T}_b$, $\bar{T}_f$, $\bar{T}_j$, $\bar{T}_s$	(T_a, T_b, T_f, T_j, T_s) / 40.00
$\bar{u}$, $\bar{v}$, $\bar{w}$	u, v, w / 18.3260
$\bar{W}$, $\bar{W}_x$, $\bar{W}_z$	W, W_x, W_z / 2780.2510
$\bar{X}$, $\bar{Z}$, $\bar{X}_{jo}$, $\bar{Z}_{jo}$	(X, Z, X_{jo}, Z_{jo}) / 0.00015
$\bar{X}_{Li}$, $\bar{Z}_{li}$	X_{Li}, Z_{Li} / 0.00015
X, Z	(X, Z) / 0.0550
ε	e / 0.00015
$\bar{\mu}$	μ / 0.027308
λ	= ± 1.00
$\bar{\Omega}$	Ω / 255.7342
$\bar{\gamma}_x$, $\bar{\Delta\gamma}_x$ $\bar{\gamma}_z$, $\bar{\Delta\gamma}_z$	(γ_x, $\Delta\gamma_x$, γ_z, $\Delta\gamma_z$) / 0.003
$\bar{\Delta\dot{\gamma}}_x$, $\bar{\Delta\dot{\gamma}}_z$	($\Delta\dot{\gamma}_x$, $\Delta\dot{\gamma}_z$) / 1.0996

****

$\bar{t}$	t * 366.5191
$\bar{T}_a$, $\bar{T}_b$, $\bar{T}_f$, $\bar{T}_j$, $\bar{T}_s$	(T_a, T_b, T_f, T_j, T_s) / 40.00
$\bar{u}$, $\bar{v}$, $\bar{w}$	u, v, w / 18.3260
$\bar{W}$, $\bar{W}_x$, $\bar{W}_z$	W, W_x, W_z / 2780.2510
$\bar{X}$, $\bar{Z}$, $\bar{X}_{jo}$, $\bar{Z}_{jo}$	(X, Z, X_{jo}, Z_{jo}) / 0.00015
$\bar{X}_{Li}$, $\bar{Z}_{li}$	X_{Li}, Z_{Li} / 0.00015
X, Z	(X, Z) / 0.0550
ε	e / 0.00015
$\bar{\mu}$	μ / 0.027308
λ	= ± 1.00
$\bar{\Omega}$	Ω / 255.7342
$\bar{\gamma}_x$, $\bar{\Delta\gamma}_x$ $\bar{\gamma}_z$, $\bar{\Delta\gamma}_z$	(γ_x, $\Delta\gamma_x$, γ_z, $\Delta\gamma_z$) / 0.003
$\bar{\Delta\dot{\gamma}}_x$, $\bar{\Delta\dot{\gamma}}_z$	($\Delta\dot{\gamma}_x$, $\Delta\dot{\gamma}_z$) / 1.0996

****